THE DETERMINATION OF

SOIL PARAMETERS FOR DESIGN

FROM STRESS PATH TESTS

by

DAVID BRYAN CLINTON

A Thesis submitted for the degree of

Doctor of Philosophy

THE CITY UNIVERSITY

Civil Engineering Department

March 1987

CONTENTS

LIST OF TABLES

LIST OF FIGURES

ACKNOWLEDGEMENTS

The research was supported by the Science and Engineering research Council in collaboration with McClelland Limited.

My thanks and appreciation are due to Professor John Atkinson for his help and guidance throughout the project, and for the excellent facilities at The City University for which he is largely responsible. I would also like to thank my colleagues and the students in the Geotechnical Engineering Research Centre for the contributions that they have made.

The laboratory testing would not have been possible without Keith Osborne and his team of technicians. Lorraine Howell did a splendid job in typing this Thesis.

I am indebted to Mike Cooper of Southampton University for providing the soil samples.

DECLARATION

I grant powers of discretion to the University Librarian to allow this thesis to be copied in whole or in part without further reference to me. This permission covers only single copies made for study purposes, subject to normal conditions of acknowledgment.

ABSTRACT

The thesis concerns investigation and measurement of the elastic deformation properties of an anisotropic soil within the context of critical state soil mechanics. The soil tested is a heavily overconsolidated Gault Clay.

Laboratory triaxial testing on 38 mm and 100 mm diameter samples is used to measure soil stiffness. A microcomputer-based control system has been developed for use with hydraulically-operated triaxial cells to enable stress path testing, and this is described. The axial and radial stresses and the back pressure can be varied independently to produce any desired stress path.

A method of measurement of anisotropic stiffness is developed using various pairs of loading and unloading cycles, or stress path probes. Several alternatives are tried, with isotropic, undrained uniaxial and constant p' cycles proving to be of most use. For the soil tested, measured modulus values are found to be about 25% in error if anisotropy is neglected. Factors affecting stiffness measurements are assessed, including sample disturbance, soil structure, threshold and stress history effects, design of the apparatus and test procedure.

Elasticity theory for cross-anisotropic soils is reviewed, particularly as it relates to the triaxial apparatus. The way in which elasticity theory is incorporated in the critical state model is discussed.

Isotropic compression and swelling test results question the compression law usually used in the critical state model. Theoretical difficulties have been found with this law when formulating an elastic soil model within critical state theory. A series of stress probe tests is used to investigate the variation of elastic stiffness parameters with soil state. The results are compared with patterns of soil behaviour found from strain path tests.

NOTATION

D	Sample diameter
E	Young's modulus, total stresses
E'	Young's modulus, effective stresses
E_h'	Young's modulus in a horizontal direction
E_v'	Young's modulus in a vertical direction
G	Shear modulus, total stresses
G'	Shear modulus, effective stresses
G_a'	Anisotropic shear modulus
G_v'	Anisotropic shear modulus
H	Sample height
J'	Coupling modulus
J_1', J_2'	Coupling modulus
K'	Bulk modulus, effective stresses
K_a'	Anisotropic bulk modulus
K_o	Coefficient of earth pressure = σ_r'/σ_a'
L	Sample length
N	Intercept of normal consolidation line at p'=1
R	Overconsolidation ratio
$\bar{U}$	Degree of consolidation
V	Volume of sample
V_s	Solid volume of soil in sample
c'	Effective cohesion
c_v	Coefficient of consolidation
e	Voids ratio
k	Permeability. Other constant where defined
m_v	Coefficient of volume compressibility
p	Mean total stress
p'	Mean effective stress
p_c'	Preconsolidation pressure (see Fig 2.3)
p_e'	Equivalent mean effective stress (see Fig 2.3)
p_f'	Mean effective stress at failure
p_o'	Initial mean effective stress
q'	Effective deviator stress
q_o'	Initial deviator stress
t	Time
u	Pore water pressure
v	Specific volume
v_o	Initial specific volume
v_κ	Intercept of swelling line at p'=1
v_λ	Normalised specific volume
w	Moisture content
Γ	Intercept of critical state line at p'=1
Δ	Large increment
M	Ratio q'/p' at the critical state
M_c	Value of M in compression
M_e	Value of M in extension
$\gamma_{xy}, \gamma_{yz}, \gamma_{zx}$	Shear strain in general co-ordinate axes
γ_w	Unit weight of water

δ	Small increment
ε_a	Natural axial strain
ε_r	Natural radial strain
ε_s	Natural shear strain
ε_v	Natural volumetric strain
$\varepsilon_x, \varepsilon_y, \varepsilon_z$	Strains in general co-ordinate axes
ε_1	Principal strain
κ	Slope of swelling line in v:ln(p') space
κ^*	Slope of swelling line in ln(v):ln(p') space
λ	Slope of normal consolidation line in v:ln(p') space
λ^*	Slope of normal consolidation line in ln(v):ln(p') space
μ'	Ratio K'/3G'
ν'	Poisson's ratio, effective stresses
ν_{hh}'	Poisson's ratio: effect of horizontal strain on horizontal strain
ν_{vh}'	Poisson's ratio: effect of vertical strain on horizontal strain
ν_{hv}'	Poisson's ratio: effect of horizontal strain on vertical strain
σ	Total normal stress
σ'	Effective normal stress
σ_a'	Axial effective normal stress
σ_r'	Radial effective normal stress
$\sigma_x', \sigma_y', \sigma_z'$	Effective normal stresses in general co-ordinate axes
σ_1, σ_3	Major and minor total principal stresses
$\tau_{xy}, \tau_{yz}, \tau_{zx}$	Shear stresses in general co-ordinate axes
ϕ'	Angle of shearing resistance, effective stresses
ϕ_c'	Value of ϕ' for compression
ϕ_e'	Value of ϕ' for extension

CHAPTER 1

INTRODUCTION

1.1 INTRODUCTION

The triaxial test remains the most widely used laboratory method for the measurement of soil stiffness and strength. Most research work has concentrated on soil strength (eg Bishop, 1971), but there is an increasing need for reliable laboratory measurement of soil deformation parameters. In particular, computerised numerical methods used in solving boundary value problems call for accurate soil models.

There have been many recent advances in the design of triaxial test equipment. Control of the test has been improved by the introduction of the hydraulic triaxial cell (Bishop and Wesley, 1975). Electrical instrumentation has enabled reliable measurements to be made. Full automation is now possible using microcomputers.

In many heavily overconsolidated clays the soil behaviour may be regarded as elastic for stress levels well below failure (Henkel, 1971; Atkinson, 1973). These soils also display some degree of anisotropy (Atkinson, 1973).

This project examines the use of stress path tests in the triaxial apparatus to measure the anisotropic elastic behaviour of a heavily overconsolidated Gault clay.

1.2 THEORETICAL CONTEXT

The measurement of soil deformation parameters is examined within the context of the Critical State theory for soils (Schofield and Wroth, 1968; Atkinson and Bransby, 1978).

The critical state model embodies elastic deformations in the concept of an elastic wall in p':q':v space. Elastic compressibility is related to the critical state parameter κ, the slope of the isotropic swelling line in v:ln(p') space. For anisotropic soil behaviour, the elastic wall will be inclined. Shear deformation can be accommodated in the critical state model, but is not an essential feature of it.

1.3 ELASTIC DEFORMATION PARAMETERS

Elasticity theory has been widely used in the solution of boundary value problems in soil mechanics (eg Jurgensen, 1934; Newmark, 1942; Burminster, 1945; Poulos and Davis, 1974). This extends the ori ginal work of Boussinesq (1885). Analytical solutions are also available for the case of a cross-anisotropic continuum (eg Koning, 1957; De Urena et al., 1966; Gerrard and Harrison, 1970a and 1970b). The use of computers has enabled a wider range of problems to be tackled (eg Perloff et al., 1967).

Many soil models used in numerical computer techniques incorporate an elastic section.

Two elastic parameters are needed to describe the deformation behaviour of an isotropic soil. The Young's modulus and Poisson's ratio are frequently used, but in the critical state model the shear and bulk moduli are preferred. For cross-anisotropic soil five independent parameters are required. The bulk modulus is related to the slope of the swelling line in the critical state model.

1.4 SOIL STIFFNESS AND THE CRITICAL STATE MODEL

The compression law for swelling and recompression is a central part of the critical state model. The definition of the swelling line was challenged by Butterfield (1979) and is examined in detail in the present project. Load controlled isotropic swelling and compression tests have provided smooth stress-strain curves for several undisturbed samples of Gault clay.

1.5 MEASUREMENT OF ELASTIC PARAMETERS

Stiffness measurements derived from laboratory tests are often found to be much lower than those found from back-analysing field data (eg St John, 1980). There are two reasons for this. Firstly, the quality of many of the published laboratory measurements is in doubt (Wroth et al., 1979). Secondly, the results of triaxial tests are usually interpreted by obtaining a secant modulus at a deviator stress of one third or one half the failure value (eg Ward et al., 1959). Very little of the soil in situ reaches such a stress level. Careful measurements of small-strain parameters from triaxial tests show that modulus values can be obtained that are comparable with those found from back-analysis (eg Jardine et al., 1984).

The deformation of soil is stress path dependent. The need to determine deformation parameters from relevant stress paths has been demonstrated (Lambe, 1967; Som, 1969). Until recently only a limited number of stress paths have been possible in laboratory testing of soil.

The tests reported in Chapter 6 are interpreted using tangent stiffness values paying particular attention to the small strain range.

1.6 MEASUREMENT OF ANISOTROPIC ELASTIC PARAMETERS

Laboratory measurement of anisotropic stiffness parameters has generally focussed on triaxial tests on vertical and inclined specimens (eg Ward et al, 1959). However, a great deal of information can be obtained by testing vertical samples only, which is more suited to samples from routine site investigations. Two different stress paths are needed, from which three elastic parameters may be measured.

Graham and Houlsby (1983) tested several samples using different stress paths, and combined the results to obtain anisotropic elastic parameters. This has the disadvantage that natural variations between the samples will affect the results. The alternative approach examined in the present project is to carry out two different stress path probes on the same sample, from which the elastic parameters may then be obtained.

1.7 VARIATIONS OF STIFFNESS PARAMETERS

The values of the elastic stiffness parameters may be expected to vary inversely with the product vp'. Elasticity theory imposes conditions on the relative variation of the stiffness moduli.

There has been a little direct investigation of stiffness parameter variation (Houlsby, 1981). Other sets of data have provided further information (eg Wroth et al., 1979; Tavenas and Leroueil, 1979). In the present project, a series of stress probe tests is used to examine how the stiffness parameters may vary with soil state, augmenting data from isotropic compression and swelling tests.

An alternative approach to the investigation of parameter

variation is that adopted by Wroth and Loudon (1963). Contours of shear strain were drawn on undrained stress paths to reveal a pattern. This method has been adopted in other work (eg Balasubramaniam, 1969; Parry and Nadarajah, 1974; Lewin and Powell, 1985; Hight et al., 1985). In the present project, the versatility of the triaxial stress path apparatus has been used to obtain a complementary pattern. A sample was compressed under constant shear strain at several different values of shear strain, and contours of equal volumetric strain plotted on the stress paths.

1.8 THE TRIAXIAL STRESS PATH APPARATUS

The essential features of the triaxial cell have changed little since its introduction, but there have been significant advances in instrumentation, loading control and test procedure (eg Davis and Poulos, 1963; Lewin and Burland, 1970; Campanella and Vaid, 1972). The introduction of the hydraulic triaxial cell (Bishop and Wesley, 1975) made stress path testing possible. Recent advances in microcomputers have enabled automation and feedback control of triaxial tests (eg Menzies et al., 1977; Deveaux et al., 1981).

The main test series in the present project was carried out using hydraulic triaxial cells capable of testing samples up to 100mm diameter. A fully automated recording and control system was developed to enable stress path testing to be performed. Ancillary testing was carried out in Bishop and Wesley cells using The City University's multiple cell control system (Atkinson, Evans and Scott, 1985).

CHAPTER 2

BASIC THEORY

2.1 INTRODUCTION

In this chapter elasticity theory relevant to soil models is introduced. This is set in the context of critical state soil mechanics theory, and the elastic components of the critical state model are discussed. The basic theory for isotropic soils is extended to include anisotropy.

2.2 BASIC SOIL MECHANICS

2.2.1 Introduction

Later sections will examine in detail aspects of the stress-strain behaviour of soil. This must be viewed within the context of the overall theory of soil behaviour. The critical state theory of soil mechanics provides a conceptual model of soil behaviour. The basic features of the Modified Cam Clay model are described in the following sections.

The critical state theory was developed from the application of the principles of thermodynamics and plasticity theory to the observed behaviour of soils (Schofield and Wroth, 1968). The soil is assumed to be an isotropic continuum, and its behaviour is governed by the effective stresses.

Many refinements to the basic model are possible, but these are not discussed here. The conceptual model may be extended readily to a mathematical model, and some of the relevant formulae are given.

2.2.2 Soil Parameters

Soil behaviour is governed by effective stresses, defined as

$$\sigma' = \sigma - u \tag{2.1}$$

The state of soil may be described fully by the stresses acting on it and by its specific volume v. The stress state may be given by the general directional normal effective stresses σ'_x, σ'_y and σ'_z plus the shear stresses τ_{xy}, τ_{yz} and τ_{zx}. The critical state model was formulated in terms of the stress invariants p' and q' defined as follows:

$$p' = (\sigma'_x + \sigma'_y + \sigma'_z) / 3 \tag{2.2}$$

$$q' = \frac{1}{\sqrt{2}} \left[(\sigma'_x - \sigma'_y)^2 + (\sigma'_y - \sigma'_z)^2 + (\sigma'_z - \sigma'_x)^2 + 6(\tau_{xy}^2 + \tau_{yz}^2 + \tau_{zx}^2) \right]^{\frac{1}{2}} \tag{2.3}$$

In the triaxial apparatus where axial and radial directions are axes of principal stress, these reduce to

$$p' = (\sigma'_a + 2\sigma'_r) / 3 \tag{2.4}$$

$$q' = \sigma'_a - \sigma'_r \tag{2.5}$$

The corresponding strain invariants are

$$\delta\varepsilon_v = (\delta\varepsilon_x + \delta\varepsilon_y + \delta\varepsilon_z) / 3 \tag{2.6}$$

$$\delta\varepsilon_s = \frac{\sqrt{2}}{3} \left[(\delta\varepsilon_x - \delta\varepsilon_y)^2 + (\delta\varepsilon_y - \delta\varepsilon_z)^2 + (\delta\varepsilon_z - \delta\varepsilon_x)^2 + 3(\delta\gamma_{xy}^2 + \delta\gamma_{yz}^2 + \delta\gamma_{zx}^2)/2 \right]^{\frac{1}{2}} \tag{2.7}$$

reducing to

$$\delta\varepsilon_v = (\delta\varepsilon_a + 2\delta\varepsilon_r) / 3 \qquad (2.8)$$

$$\delta\varepsilon s = 2 (\delta\varepsilon_a - \delta\varepsilon_r) / 3 \qquad (2.9)$$

for the triaxial test configuration.

2.2.3 State Boundary Surface

The main feature of the critical state model is the state boundary surface. The state boundary surface represents a limit to all possible states for the soil. The form of the surface is shown in Figure 2.1.

For soil states beneath the state boundary surface the soil is assumed to behave elastically. Plastic flow occurs when the soil state lies on the surface.

The composition of the state boundary surface is illustrated on Figure 2.2. Figure 2.2(a) shows the projection of the state boundary surface on the q'=0 plane. Figure 2.2(b) is a section through the surface at constant specific volume. Isotropically normally consolidated soils lie at point D. Lightly overconsolidated soils lie to the right of point C, and heavily overconsolidated soils are located to the left. For normally consolidated and lightly overconsolidated soil the state boundary surface is curved and is called the Roscoe or Rendulic surface. Heavily overconsolidated soils lie beneath the Hvorslev surface. There is also a planar surface with a gradient of 3 representing the condition that soil cannot sustain tension (the tension cut-off).

2.2.4 Elastic Wall

Soil is assumed to deform plastically only when its state lies on the state boundary surface. For states beneath this surface, only elastic deformations can occur. This, in effect, limits the state of the soil beneath the state boundary surface to positions on or vertically above the current swelling line. This locus is termed the elastic wall. Soil can pass from one elastic wall to another only by sustaining some plastic deformation at a state on the state boundary surface.

Elastic soil behaviour beneath the state boundary surface will be examined in detail in later sections.

2.2.5 Yield and Plastic Strains

Yield represents the onset of plastic straining. For any soil, this will be at a state surface bounding the elastic region. In the critical state model, this coincides with the state boundary surface.

The directions of increments of plastic strain are governed by a flow rule. It is generally assumed that plastic flow is associated so that the yield surface is also a plastic potential. The direction of the plastic strain vector in $\varepsilon_s : \varepsilon_v$ space is normal to the yield surface in q':p' space at the point representing the state of the soil.

2.2.6 Failure

In the critical state model, ultimate failure occurs when the state of the soil reaches the critical state line. At this condition there can be continued deformation of the soil without change of state.

The locus of critical states for soil is found to project to a

straight line in q':p' space.

For heavily overconsolidated soil there is some local deformation as slip zones appear during the later stages of shearing. Soil in these slip zones will reach the critical state by dilating and taking in water from the surrounding material. This process is called strain softening. Measurements for a sample as a whole will not reflect this localised state, and the soil will appear to fail at some point on the Hvorslev surface. This measured failure state can also be represented well using the Mohr-Coulomb criterion.

2.2.7 Graphical and Mathematical Representation

It has been found experimentally that the shape of the state boundary surface remains the same at various sections of constant specific volume. A complete graphical representation of the surface can therefore be made by defining the shape and indicating how its scale varies with specific volume. As shown in Figure 2.3 a convenient scaling factor is provided by the normal consolidation line which has a slope of λ in v-ln(p') space and a specific volume of N at p'=1. The equivalent mean effective pressure p_e' representing the isotropic stress state of the soil at its normally consolidated state for a given specific volume may be used as a normalising parameter. In this way Figures 2.3 (a) and (b) can convey all the information needed for a conceptual view of the behaviour of the soil. If it is preferred to normalise a constant p' section through the surface, the normalised parameters shown in Figure 2.3(c) may be used.

A few simple equations define the basic soil parameters for the critical state model. The normal consolidation line is given by

$$v = N - \lambda \ln(p') \qquad (2.10)$$

and for swelling

$$v = v_\kappa - \kappa \ln(p') \tag{2.11}$$

where κ is the slope of the swelling line in v-ln(p') space, and v_κ is the intercept of this line at p'=1.

The projection of the critical state line is observed to be parallel to the normal consolidation line in v:ln(p') space, and is given by

$$v = \Gamma - \lambda \ln(p') \tag{2.12}$$

The projection of the critical state line in q':p' space is simply

$$q' = M\, p' \tag{2.13}$$

Equations for other aspects of the Cam Clay model can be deduced from those given above, and no further parameters are required. For Modified Cam Clay, the slope and intercept of the Hvorslev surface need to be specified.

2.3 THEORY OF ELASTICITY

2.3.1 Introduction

The theory of elasticity is based on Hooke's Law which requires that increments of stress are directly proportional to increments of strain. In addition, there must be no energy dissipated during straining so that elastic strains should be recoverable.

The equations of elasticity are given in incremental form in the following sections. The elastic parameters do not need to be constant over wider stress ranges. However, if they do vary then

there are restrictions in the relative variation of the parameters to conform with the strain energy requirement of the theory. If the parameters are constant (linear elasticity) then stresses and strains may be superposed and the incremental formulation is not needed.

2.3.2 Isotropic Elasticity

For an elastic material there is a linear relationship between increments of stress and increments of strain. The isotropic constitutive equations are as follows

$$\begin{Bmatrix} \delta\varepsilon_x \\ \delta\varepsilon_y \\ \delta\varepsilon_z \\ \delta\gamma_{xy} \\ \delta\gamma_{yz} \\ \delta\gamma_{zx} \end{Bmatrix} = \begin{bmatrix} \frac{1}{E'} & -\frac{\nu'}{E'} & -\frac{\nu'}{E'} & & & \\ -\frac{\nu'}{E'} & \frac{1}{E'} & -\frac{\nu'}{E'} & & & \\ -\frac{\nu'}{E'} & -\frac{\nu'}{E'} & \frac{1}{E'} & & & \\ & & & \frac{1}{G'} & & \\ & & & & \frac{1}{G'} & \\ & & & & & \frac{1}{G'} \end{bmatrix} \cdot \begin{Bmatrix} \delta\sigma'_x \\ \delta\sigma'_y \\ \delta\sigma'_z \\ \delta\tau_{xy} \\ \delta\tau_{yz} \\ \delta\tau_{zx} \end{Bmatrix} \qquad (2.14)$$

There are two independent elastic parameters, since it can be shown that

$$G' = E' \,/\, 2(\,1 + \nu'\,) \qquad (2.15)$$

In addition, the bulk modulus may be deduced as

$$K' = E' \,/\, 3(\,1 - 2\,\nu'\,) \qquad (2.16)$$

In critical state soil mechanics theory, it is preferred to use the stress invariants p' and q'. For the special case of axial symmetry, the equations may then be written as

$$\begin{Bmatrix} \delta\varepsilon_s \\ \delta\varepsilon_v \end{Bmatrix} = \begin{bmatrix} 1/3G' & 0 \\ 0 & 1/K' \end{bmatrix} \cdot \begin{Bmatrix} \delta q' \\ \delta p' \end{Bmatrix} \qquad (2.17)$$

and it can be seen that the shear and volumetric components are independent of each other.

2.3.3 Anisotropic Elasticity

Structural anisotropy in soils is caused by the process of sedimentation leading to particle alignment and layering. This creates a material that behaves differently in a vertical direction from a horizontal direction, but in which there is symmetry for rotation about a vertical axis. This is generally referred to as cross-anisotropy. It is elastically equivalent to crystals of the hexagonal system (Love, 1927).

Anisotropy may be induced by stress changes if the stress-strain behaviour of the soil is not linear. In particular, cross-anisotropy may be caused by the geological process of compression and swelling under conditions of zero lateral strain.

Five independent elastic parameters are required to describe the stress-strain behaviour of the material. The constitutive equations are given below, with the z-axis taken as vertical.

$$\begin{Bmatrix} \delta\varepsilon_x \\ \delta\varepsilon_y \\ \delta\varepsilon_z \\ \delta\gamma_{xy} \\ \delta\gamma_{yz} \\ \delta\gamma_{zx} \end{Bmatrix} = \begin{bmatrix} \frac{1}{E'_h} & \frac{-\nu'_{hh}}{E'_h} & \frac{-\nu'_{vh}}{E'_v} & & & \\ \frac{-\nu'_{hh}}{E'_h} & \frac{1}{E'_h} & \frac{-\nu'_{vh}}{E'_v} & & & \\ \frac{-\nu'_{hv}}{E'_h} & \frac{-\nu'_{hv}}{E'_h} & \frac{1}{E'_v} & & & \\ & & & \frac{2(1+\nu'_{hh})}{E'_h} & & \\ & & & & \frac{1}{G'_v} & \\ & & & & & \frac{1}{G'_v} \end{bmatrix} \cdot \begin{Bmatrix} \delta\sigma'_x \\ \delta\sigma'_y \\ \delta\sigma'_z \\ \delta\tau_{xy} \\ \delta\tau_{yz} \\ \delta\tau_{zx} \end{Bmatrix} \qquad (2.18)$$

The six elastic parameters shown in Equation 2.18 are not all independent, since it can be shown that $\nu'_{vh}E'_h=\nu'_{hv}E'_v$ (Barden, 1963).

The equations in terms of stress and strain invariants show that shear and volumetric components are coupled for anisotropic soil:

$$\begin{Bmatrix} \delta q' \\ \delta p' \end{Bmatrix} = \begin{bmatrix} 3G_a' & J' \\ J' & K_a' \end{bmatrix} \cdot \begin{Bmatrix} \delta\varepsilon_s \\ \delta\varepsilon_v \end{Bmatrix} \qquad (2.19)$$

The principle of conservation of elastic strain energy requires that the stiffness matrices in Equations 2.18 and 2.19 be symmetrical.

Bounds can be placed on the values of the parameters (Barden, 1963; Raymond, 1970; Pickering, 1970). The thermodynamics principle that the strain energy function cannot be negative requires all the elastic parameters to have positive values. In addition,

$$\nu'_{hh} + 2\nu'^{2}_{hv}E'_h/E'_v \leqslant 1 \qquad (2.20)$$

By requiring dilation to be the same sign as the applied stress,

$$\nu'_{hv} \leqslant \tfrac{1}{2} \qquad (2.21)$$

$$\nu'_{hh} + \nu'_{hv}E'_h/E'_v \leqslant 1 \qquad (2.22)$$

It follows from these that for zero dilation (incompressible material)

$$E'_h/E'_v \leqslant 2 \qquad (2.23)$$

Further results given by Pickering (1970) are not included here as they stem from the invalid assumption that an isotropic pressure increase will not produce any shear strains.

2.4 ELASTICITY IN THE CRITICAL STATE MODEL

2.4.1 Introduction

In the critical state model soil behaviour is elastic for states below the state boundary surface. The state of the soil lies on an elastic wall and the soil will deform elastically as the state moves along the wall. The soil state cannot move from one elastic wall to another unless some plastic deformation occurs at a soil state on the state boundary surface.

The elastic deformation behaviour on an elastic wall is discussed in the following sections.

2.4.2 Isotropic Elasticity

In an isotropic elastic soil the shear and volumetric components of stress and strain are decoupled. That is, changes in deviator stress will not cause any volumetric strain. Consequently, in the q'-p'-v space shown in Figure 2.1 the elastic wall is vertical above the elastic swelling line defined in Figure 2.3.

In the Cam Clay model the swelling line is given by

$$v = v_\kappa - \kappa \ln(p') \qquad (2.11 \text{ bis})$$

Differentiating this gives

$$dv/v = -\kappa\, dp'/vp' \qquad (2.24)$$

from which the bulk modulus may be derived as

$$K' = vp'/\kappa \qquad (2.25)$$

An alternative compression law was proposed by Butterfield (1979) giving linear behaviour in ln(v) - ln(p') space. Denoting the slope of the swelling line in this case as κ^*, the bulk modulus may be derived as

$$K' = p'/\kappa^* \qquad (2.26)$$

For both of the above cases the bulk modulus varies with soil state and is directly proportional to the mean effective stress. The dependence on specific volume in Equation 2.25 is small, but implies that soil becomes less stiff as it gets more dense, which is not intuitively correct. For constant p', a reduction in the specific volume also leads to a higher overconsolidation ratio. The stiffness of soil might also be expected intuitively to increase with increasing overconsolidation ratio. The

relationship between p', v and the overconsolidation ratio R is given by

$$v = N - (\lambda - \kappa)\ln(R) - \lambda \ln(p') \qquad (2.27)$$

In the original Cam Clay model elastic shear strains were assumed to be negligible. Later models incorporate elastic shear strains. The critical state model does not place any restrictions on the choice of values for the shear modulus, but its variation with soil state must be thermodynamically compatible with the definition used for the bulk modulus.

From Equations 2.15 and 2.16 it can be shown that

$$\frac{G'}{K'} = \frac{2(1+\nu')}{3(1-2\nu')} \qquad (2.28)$$

If K' varies with mean effective stress then either G' or ν' must vary. If ν' is constant, requiring $G' \propto p'$, then Zytynski et al. (1978) have shown that K' must also vary with the deviator stress. This leads to a warped elastic wall, and shear and volumetric components are no longer independent. Houlsby (1981) also examined this case, showing that contours of equal volume in q'-p' space form parabolas, and noting that it would be quite possible mathematically for these parabolas to intercept one another. The unrealistic situation then arises that undrained stress paths can cross. Zytynski et al. (1978) concluded that no sensible elastic model could be developed with $K' \propto p'$ without violating the principle of conservation of elastic strain energy.

2.4.3 Anisotropic Elasticity

For anisotropic soil the shear and volumetric components of elastic behaviour are coupled. This leads to an inclined elastic wall. The slope of the swelling line on the q'=0 plane may still

be defined by the parameter κ in v-ln(p') space or by κ^* in ln(v)-ln(p') space. From Equation 2.19,

$$\delta p'/\delta \varepsilon_v = K_a' + J'^2/3G_a' \qquad (2.29)$$

so the value of κ or κ^* can no longer be related directly to the bulk modulus.

In addition, the ratio G_a'/K_a' is a function of the anisotropic Young's moduli and Poisson's ratios, and cannot be regarded as constant with soil state.

2.4.4 Normalising

The critical state soil model predicts how deformation parameters vary with soil state, as discussed in the previous sections. It should therefore be possible to normalise these parameters, enabling comparison of soil behaviour from tests at different stress levels and easier application of the results.

The fundamental critical state parameter κ is independent of soil state. It may also be assumed from Equation 2.28 that the ratio G'/K' is approximately constant, writing

$$\mu' = K'/3G'. \qquad (2.30)$$

The stress-strain behaviour of the soil may then be written as

$$v\delta\varepsilon_s = \mu'\kappa \frac{\delta q'}{p'} \qquad (2.31)$$

$$v\delta\varepsilon_v = \kappa \frac{\delta p'}{p'} \qquad (2.32)$$

Hence, stress-strain behaviour may be normalised conveniently by

plotting stresses divided by p' and strains multiplied by v.

If the Butterfield compression law is used then the specific volume v may be omitted from the above equations, and strains do not have to be normalised.

2.5 SOIL MODELS

2.5.1 Introduction

A soil model is a means of describing the stress-strain behaviour of a soil and defining its failure condition. The use of a soil model is necessary in the solution of boundary value problems, using either analysis or a numerical method.

In analysis three sets of equations are used. The equations of equilibrium give the relationships between the various stresses or forces necessary at every point in a continuum. A similar set of equations relate the strains or displacements as the body must continue to fit together as it deforms. The third set of equations are provided by the soil model, relating the stresses to the strains.

There are several numerical methods which solve boundary value problems in a variety of ways, but all require some form of soil model. When computers are used, the soil model may be relatively complex.

The critical state model described in the previous sections is an example of a soil model combining elastic and plastic behaviour of the soil. This section gives a brief introduction to the main types of soil model commonly used in engineering design.

2.5.2 Elastic Models

Elastic soil models fall into two categories, differential or non-differential. The latter type link stress with accumulated strain. For example, the hyperbolic model uses the basic equation

$$\sigma_1 - \sigma_3 = \varepsilon_1 / (a + b \varepsilon_1) \qquad (2.33)$$

This formulation was originally adopted as a reasonable fit to triaxial stress-strain curves, and the constants a and b were chosen to obtain the best fit. Refinements are needed for purposes such as forcing conformity to a yield criterion, and this is generally done by redefining the parameters a and b as equations containing several constants.

In differential elastic models, increments of stress are related to increments of strain. Again, two basic parameters are usually required which are the elastic stiffness parameters. Any two may be used, such as E' and ν', but the models are often formulated in terms of stress and strain invariants. In this case, the moduli G' and K' are preferred, defined by

$$\delta q' = 3G' \delta \varepsilon_s \qquad (2.34)$$

$$\delta p' = K' \delta \varepsilon_v \qquad (2.35)$$

The parameters need not be constant. For example, in the K-G model

$$K = K_1 + \alpha_K p' \qquad (2.36)$$

$$G = G_1 + \alpha_G p' + \beta_G q' \qquad (2.37)$$

In this way a form of yielding can be built into the model by

reducing the shear modulus to a very low value at shear stresses above a certain level. At first sight the resulting stress-strain curve may appear to have a plastic region, but there are important differences regarding the direction of deformation.

Anisotropic elastic models have been used but are not very common (eg Raymond, 1972; Ballester and Sagaseta, 1979). Five basic elastic parameters are needed for a cross-anisotropic soil, leading to far more complexity.

2.5.3 Elasto-Plastic Models

The elastic part of these models follows one of the forms described in the previous section. Above a certain stress state an incremental plasticity model is used.

A yield criterion determines the stress state at which the soil behaviour becomes plastic. This is generally taken as a yield surface in stress space. The yield surface may be allowed to expand as plastic straining takes place by incorporating a hardening law.

The direction of plastic strain increments is governed by a flow rule. Often, this relates the direction of flow to the current position on the yield surface (associated flow). Based on thermodynamics principles, the normality condition should apply. This requires the vector of plastic strain increment in strain space to be perpendicular to the yield surface in the corresponding stress space.

Examples of elasto-plastic models include Cam Clay, Modified Cam Clay and the Drucker-Prager model.

2.5.4 Other Model Types

There are several other types of soil model which may have valid applications but which do not fall within the theoretical context of this dissertation. Examples of these are models assigning viscous parameters to the soil (e.g. elasto-visco-plastic models), and those based on endochronic theory. In addition, there are many models which have been designed for a specific application, such as shock loading, which do not have a general usefulness.

2.3.5 Soil Models Using The Stress Path Method

Lambe (1964 and 1967) proposed the use of stress path tests for prediction of soil deformation, although this was not actually used to formulate a model. The method uses the triaxial test to simulate the stress changes expected for a representative position in the ground beneath a structure. A sample is brought to the stress state thought to exist in the ground. Stress changes are imposed on the soil as predicted by elasticity theory, and the resulting strains are measured. These strains are then applied directly for prediction of soil deformation in the field.

Davis and Poulos (1963 and 1968) and Simons (1971) used triaxial stress path tests in a similar way to Lambe but then derived from the results elastic parameters which could be used as a soil model in design.

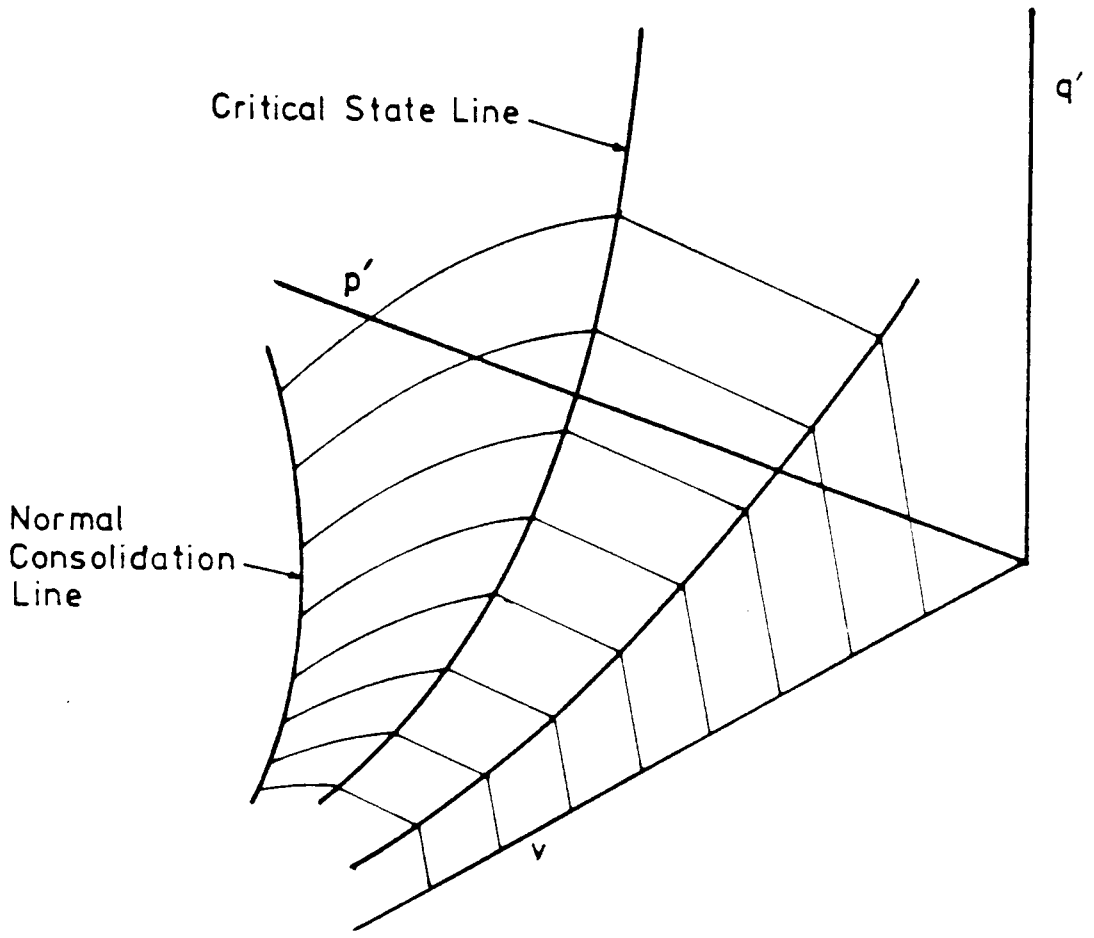

Fig 2.1 State boundary surface

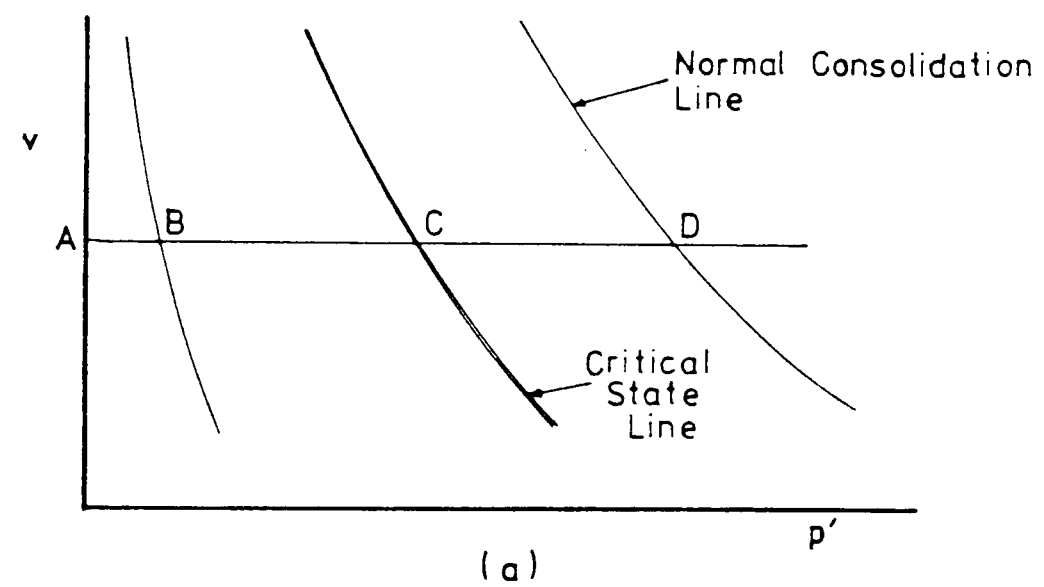

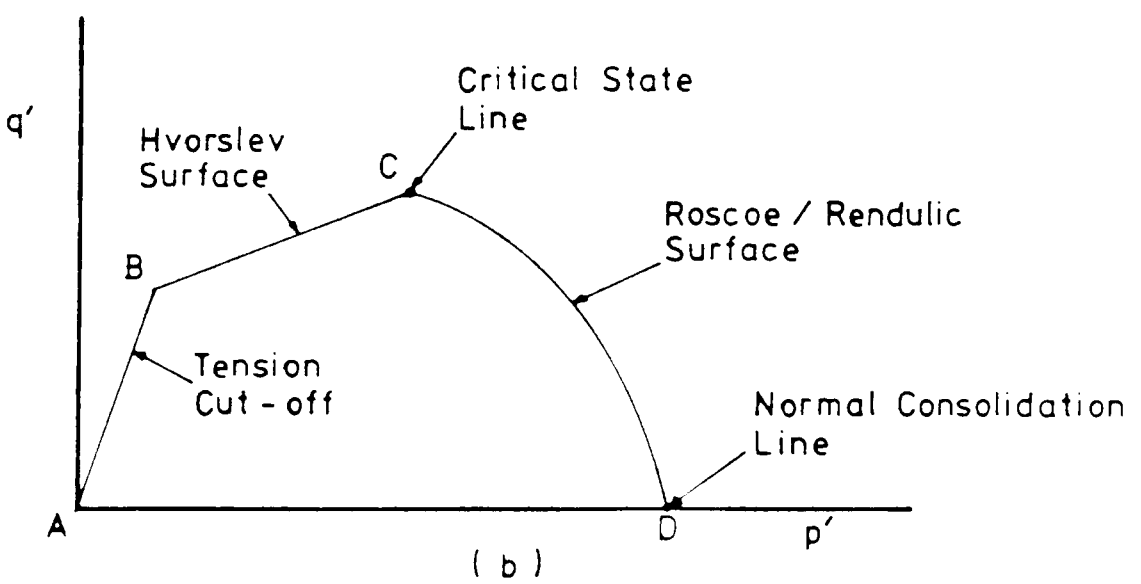

Fig 2.2 Composition of the state boundary surface

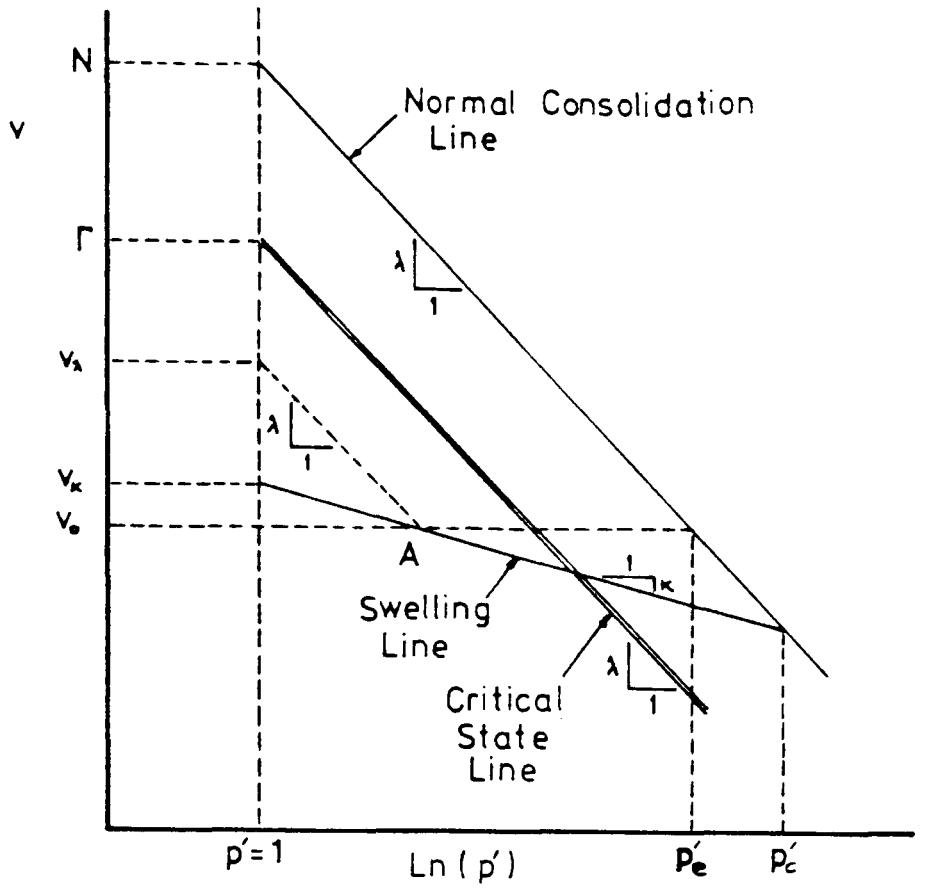

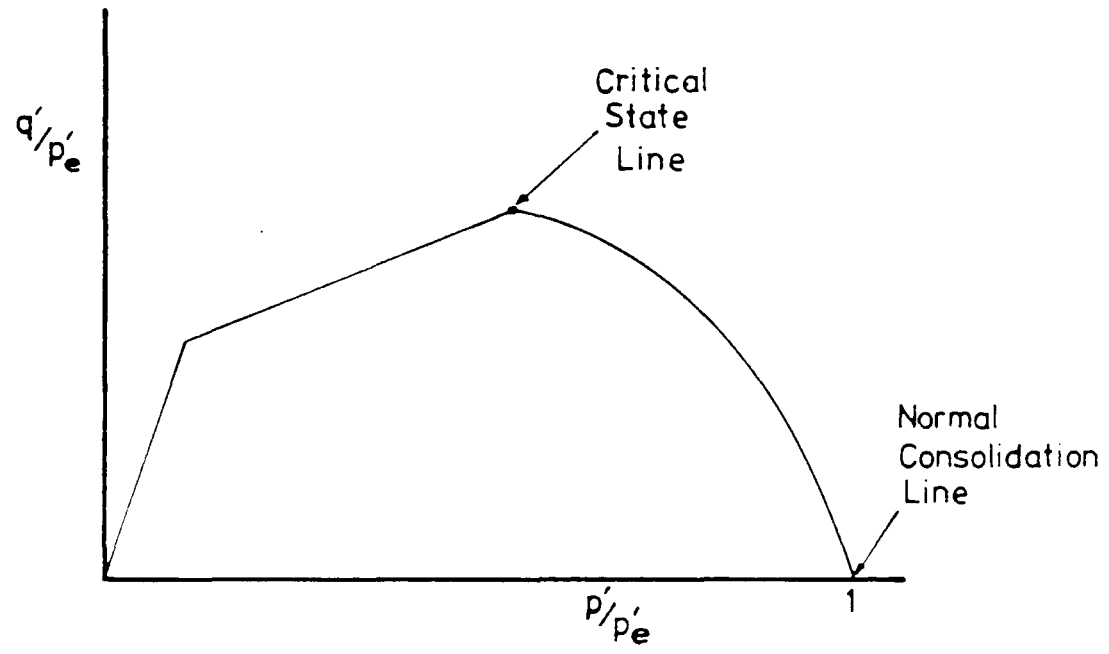

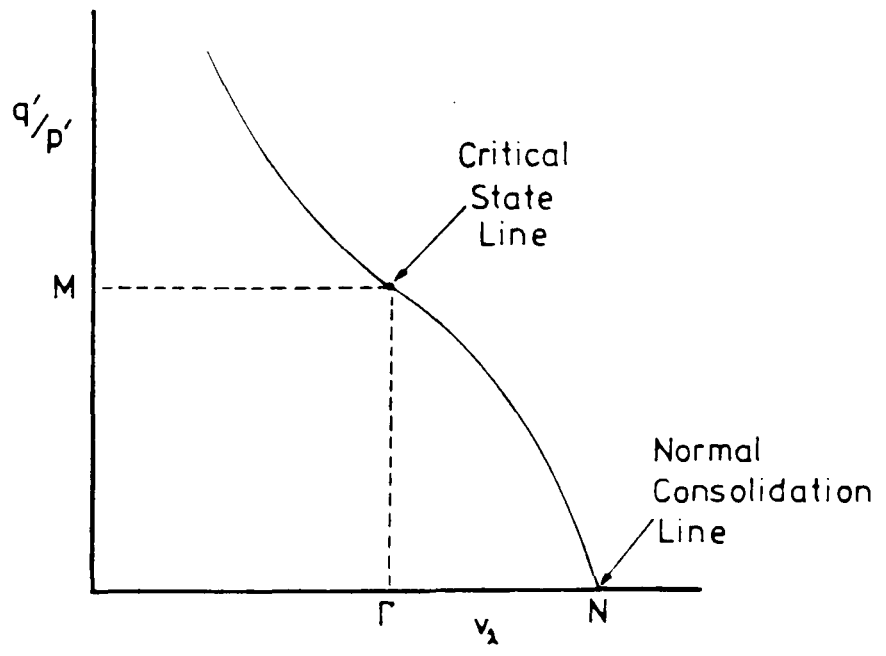

Fig 2.3 Graphical representation of the state boundary surface and normalising parameters

CHAPTER 3

SOIL STIFFNESS MEASUREMENTS IN THE TRIAXIAL APPARATUS

3.1 INTRODUCTION

This chapter deals with the use of the triaxial apparatus in measuring soil deformation parameters. The relevant elastic constitutive equations and parameters are first introduced, for both isotropic and anisotropic soil, and methods for deriving the parameters are discussed.

Factors such as sample disturbance and the threshold effect are discussed in the context of their effect on stiffness measurements. Problems associated with the triaxial apparatus and test procedure are described.

3.2 ELASTIC CONSTITUTIVE EQUATIONS

3.2.1 Isotropic Elasticity

For an isotropic soil the equations of elasticity relevant to the triaxial apparatus are

$$\begin{Bmatrix} \delta\varepsilon_a \\ \delta\varepsilon_r \end{Bmatrix} = \frac{1}{E'} \begin{bmatrix} 1 & -2\nu' \\ -\nu' & 1-\nu' \end{bmatrix} \begin{Bmatrix} \delta\sigma'_a \\ \delta\sigma'_r \end{Bmatrix} \qquad (3.1)$$

The alternative formulation in terms of stress and strain invariants is

$$\begin{Bmatrix} \delta\varepsilon_s \\ \delta\varepsilon_v \end{Bmatrix} = \begin{bmatrix} \frac{1}{3G'} & 0 \\ 0 & \frac{1}{K'} \end{bmatrix} \cdot \begin{Bmatrix} \delta q' \\ \delta p' \end{Bmatrix} \qquad (3.2)$$

The benefit of using invariants is obvious as shear and volumetric components are conveniently uncoupled.

For any general stress path the routine measurements enable both independent elastic parameters to be determined at any point.

The above equations are incremental in form. This means that the deformation moduli refer to the tangent values of stress-strain curve slopes. Secant values may be measured if desired, but unless the soil behaviour is approximately linearly elastic these may be used for specific applications only.

3.2.2 Anisotropic Elasticity

For cross-anisotropic soil the logical (and most practical) arrangement is to cut a cylindrical sample with the axis of symmetry along the axis of the specimen. The relevant equations of elasticity are then as follows.

$$\begin{Bmatrix} \delta\varepsilon_a \\ \delta\varepsilon_r \end{Bmatrix} = \begin{bmatrix} \frac{1}{E'_v} & \frac{-2\nu'_{hv}}{E'_v} \\ \frac{-\nu'_{hh}}{E'_h} & \frac{1-\nu'_{hv}}{E'_v} \end{bmatrix} \cdot \begin{Bmatrix} \delta\sigma'_a \\ \delta\sigma'_r \end{Bmatrix} \qquad (3.3)$$

It can be seen that only two parameters can be determined from these equations: E_v' and ν_{hv}'. In addition, the function $(1 - \nu_{hh}')/E_h'$ can be measured, but ν_{hh}' and E_h' cannot be determined separately. Further, it is not possible to measure the independent shear modulus G_v' in the triaxial apparatus.

It is still possible to formulate the elasticity equations in terms of invariants (Atkinson and Bransby, 1978):

$$\begin{Bmatrix} \delta\varepsilon_s \\ \delta\varepsilon_v \end{Bmatrix} = \begin{bmatrix} A & B \\ C & D \end{bmatrix} \begin{Bmatrix} \delta q' \\ \delta p' \end{Bmatrix} \tag{3.4}$$

In this case, the compliance matrix must be symmetric, so B = C. However, the shear and volumetric components are now coupled. There are three parameters in these equations, which is again less than the five required for a full description of the stress-strain behaviour of the soil. Since the behaviour of the soil is now directional, the physical significance of the parameters is not clear. By direct substitution, the following relationships may be found.

$$A = \frac{2}{9}\left[\frac{2(1+2\nu vh')}{Ev'} + \frac{1-\nu hh'}{Eh'}\right] \tag{3.5}$$

$$B = C = \frac{2}{3}\left[\frac{1-\nu vh'}{Ev'} - \frac{1-\nu hh'}{Eh'}\right] \tag{3.6}$$

$$D = \left[\frac{1-4\nu vh'}{Ev'} + \frac{2(1-\nu hh')}{Eh'}\right] \tag{3.7}$$

In numerical modelling applications, stiffness matrices are generally preferred to the compliances given above. The equations may then be written as

$$\begin{Bmatrix} \delta q' \\ \delta p' \end{Bmatrix} = \begin{bmatrix} 3G_a' & J' \\ J' & K_a' \end{bmatrix} \begin{Bmatrix} \delta\varepsilon_s \\ \delta\varepsilon_v \end{Bmatrix} \tag{3.8}$$

If the soil specimen is cut with the soil's axis of symmetry perpendicular to the axis of the cylindrical sample then the equations of elasticity become more complicated:

$$\begin{Bmatrix} \delta\varepsilon_a \\ \delta\varepsilon_r \end{Bmatrix} = \begin{bmatrix} \frac{1}{E'_h} & \frac{\nu'_{hh}}{E'_h} - \frac{\nu'_{vh}}{E'_v} \\ \frac{-\nu'_{hh} - \nu_{hv}}{2E'_h} & \frac{E'_v + E'_h}{2E'_v E'_h} - \frac{\nu'_{vh}}{E'_v} \end{bmatrix} \cdot \begin{Bmatrix} \delta\sigma'_a \\ \delta\sigma'_r \end{Bmatrix} \qquad (3.9)$$

The only useful item to arise from this is a possible direct measurement of E'_h.

If a triaxial specimen is cut with its axis at an angle θ to the plane of symmetry, then the apparent undrained modulus will be given by the following equation (Gibson, 1974).

$$\frac{1}{E_\theta} = \left(\frac{1}{G_v} - \frac{1}{E_v}\right) \mathrm{Sin}^2\theta\ \mathrm{Cos}^2\theta + \frac{1}{E_v}\mathrm{Sin}^4\theta + \frac{1}{E_h}\mathrm{Cos}^4\theta \qquad (3.10)$$

The influence of the independent shear modulus G_v is strong, and this provides a means of making an approximate measurement of this parameter. It must be noted that the moduli E_v and E_h in the above equation are now undrained values, and the parameter G_v is assumed to be the same for both the drained and the undrained case.

3.3 DERIVING STIFFNESS PARAMETERS FROM TEST DATA

Measurements made in the triaxial test are axial and radial total stress, the pore pressure, and axial and volumetric strains. The radial strain is generally calculated from the axial and volumetric strain measurements assuming the specimen to deform as a right circular cylinder. From these measurements the effective axial and radial stresses may be calculated readily, and the values of stress and strain invariants found using the equations given in Section 2.2.2.

Because soil is not in general linearly elastic, the constitutive equations must be used in incremental form. The stiffness parameters relate to slopes of stress-strain curves, and the incremental formulation dictates that the tangent slope of a curve must be used for deriving the parameters.

For isotropic soil, any general stress path followed in a triaxial test will provide sufficient information to enable the two independent stiffness parameters to be found. In Equation 3.1 the two parameters are E' and ν'. There are two Equations linking the axial and radial strains to the axial and radial stresses, and these can be solved directly. A particularly useful test is the drained compression or extension test, where $\delta\sigma_r'=0$ and E' is found directly as the tangent slope of the axial stress - axial strain curve. In an isotropic compression and swelling test, the parameters E' and ν' cannot be determined separately, but only as the function $E'/(1-2\nu')$ which is the bulk modulus.

Using stress and strain invariants the shear and volumetric components are decoupled for isotropic soil, as shown in Equation 3.2. The stiffness parameters G' and K' may therefore be found directly from any stress path as the tangent slopes of the $q':\varepsilon_s$ and $p':\varepsilon_v$ curves respectively. Both parameters may be found from any general stress path except the special cases of constant p' tests and constant q' tests. The best measurement of K' will be

from a constant q' path, and for G' a constant p' path will give the best resolution.

For anistropic soil there are three stiffness parameters which can be found in the triaxial apparatus with a vertical specimen. From Equation 3.3, these are E_v', ν_{hv}' and the function $E_h'/(1-\nu_{hh}')$, and in terms of invariants (Equation 3.8) the parameters are G_a', K_a' and J'. Hence, two different stress path tests are required to determine the three parameters.

Referring to Equation 3.3, it can be seen that the drained uniaxial test is again very useful, with $\delta\sigma_r'=0$. E_v' may be derived directly as the tangent slope of the axial stress - axial strain curve, and the function $E_h'/(1-\nu_{hh}')$ is given by the slope of the axial stress - radial strain curve. Any other stress path will give an equation relating the axial strain to the stress increments, and ν_{hv}' may be found by substituting the value of E_v' already derived.

In general, any two stress paths may be used, but the best resolution will be obtained if they are approximately at right angles to each other in stress space. Since there are only three parameters to be found, and effectively four equations from two different stress paths, there is a redundancy in the data which may be used to check the consistency of the results. The stiffness equations in terms of invariants may be writen as

$$\begin{Bmatrix} \delta q' \\ \delta p' \end{Bmatrix} = \begin{bmatrix} 3G_a' & J_1' \\ J_2' & K_a' \end{bmatrix} \begin{Bmatrix} \delta\varepsilon_s \\ \delta\varepsilon_v \end{Bmatrix} \qquad (3.11)$$

Theoretically, $J_1' = J_2'$, and this criterion may be used in assessing the consistency of the data.

The stiffness parameters may be measured directly for tests with certain strain paths. The undrained test ($\delta\varepsilon_v=0$) enables direct

measurement of $3G_a'$ as the tangent slope of the $q':\varepsilon_s$ curve, and J_2' is found as the slope of the $p':\varepsilon_s$ curve. The constant shear strain test would give similar measurements for J_1' and K_a', but this is not a common test.

For stress path tests (as opposed to strain path tests) it is more convenient to derive the compliance matrix of Equation 3.4. An isotropic test ($\delta q'=0$) will give B and D directly as the tangent slopes of the $p':\varepsilon_s$ and $p':\varepsilon_v$ curves respectively, and a constant p' test will give similar measurements for A and C. It is then a simple matter of matrix inversion to obtain G_a', K_a' J_1' and J_2'. For other pairs of stress paths, simultaneous equations may be set up and solved in a straightforward way. However, from a practical point of view, there is generally a better accuracy if parameters can be measured directly wherever possible. In Appendix A procedures for solving the stress-strain equations are given for the various pairs of stress path probes which will be used in Chapter 7, based on the principle of using direct measurements as much as possible.

3.4 SOIL PROPERTIES AFFECTING STIFFNESS MEASUREMENTS

3.4.1 Fissures and Bedding Planes

Many papers have been written on the effect of fissuring and bedding on the strength of soil, but there is little evidence of the effect on deformation. Several researchers have measured a reduced soil strength on fissures and bedding planes in the laboratory (eg Skempton et al., 1979; Simons, 1971). There is also some field evidence for this, particularly for failure along bedding planes beneath embankments (eg Rivard and Lu, 1978).

In situ tests by Marsland (1971) attributed anomalies in stiffness measurements partly to fissuring. However, several factors were involved in these tests and differences in scale and

rate of test mean that other effects such as threshold and partial drainage would be more important. Certainly, fissuring does not affect the stiffness as much as the strength (Simpson et al., 1979).

Both in the ground and in laboratory tests the effective stress across a fissure is the same as that in the main soil body. In most situations this would be enough to keep the fissure closed. It is probable that compressibility of the closed fissure may still be greater than that of the intact soil, but the very small thickness of the fissure zone means that this contribution to the overall soil stiffness would be small. Similarly, shear stresses across a fissure would cause a negligible additional shear deformation due to the thinness of the softer zone.

One mechanism which would affect a significantly large proportion of the soil is the possibility of stress concentration at the edges of fissures. The scale and significance of any such effect is not known.

Where bedding planes are closely spaced their reduced stiffness may have a significant effect on the overall properties of the soil. This would contribute to the apparent anisotropy.

3.4.2 Threshold, Aging and Stress History

The effect of aging on oedometer samples was investigated by Bjerrum (1967). Secondary compression was found to decrease the volume compressibility of soil. The amount of secondary compression was proportional to the logarithm of elapsed time. A similar stiffening effect takes place for aging prior to shearing (Ladd et al., 1977; d'Appolonia and Lambe, 1970).

The immediate stress history of the soil has also been found to affect its stiffness (eg Gens, 1982). In a series of tests on slate dust, Lewin (1978) measured the change in strain increment

direction for different stress histories. In general, a change in stress path direction will increase the apparent stiffness of soil.

More recently, a threshold effect has been defined which is associated with aging and stress history (Simpson et al., 1979; Richardson, 1986). The stress state of the soil can be regarded as being in a zone surrounded by a threshold state. For stress paths within this zone the stress-strain response is governed by aging and stress history, and in general this soil is very stiff. When the stress path crosses the threshold the immediate stress history and aging are no longer significant. Data confirming this were published by Hight et al. (1985). Simpson (1986) used a soil model including a threshold zone with a radius of one tenth of the current effective stress in the soil, and found that this gave good results in a finite element back-analysis.

3.4.3 Other Factors

Other aspects of the physical properties of soil affecting stiffness measurements include cementing, particle crushing and thixotropy. These factors may cause the stress-strain behaviour to be stress path dependent and irreversible.

3.5 SAMPLE DISTURBANCE AND SOIL STIFFNESS

Disturbance during sampling is inevitable. Mechanical disturbance can be reduced with care and good equipment design, but relief of the stresses on the sample cannot be avoided.

Hvorslev (1949) found moisture content and density changes due to sampling, disturbance to the soil structure, and chemical changes. The chemical changes included oxidation, drilling fluid ingress, reaction with the sample tube metal, and fungus growth. For overconsolidated clays mechanical disturbance was found to

decrease the density and pore pressures, with the opposite effect for normally consolidated clays. There was generally a loss of undrained strength, although Skempton and Sowa (1963) found that ϕ' was not affected. The stiffness of the soil was reduced. McGown et al. (1974) found that disturbance increases the coefficient of consolidation in a soft clay. Maguire (1975) showed that suction in the soil caused by stress relief was reduced by disturbance. Kirkpatrick and Khan (1984) found that stress relief alone could cause a change in the effective stress state of the soil.

Baligh (1984; reported by Hight et al., 1985) explained the mechanism of mechanical disturbance at the perimeter of tube samples in terms of the strain paths of the soil. This work showed that the badly disturbed zone is a function of the thickness of the tube wall, which agrees well with Hvorslev's experimental results. A conclusion is that for a given tube thickness, larger diameter samples will contain a much smaller proportion of badly disturbed soil. Apted (1978) showed that dilation or compression within the outer, badly disturbed zone would cause a redistribution of moisture contents throughout the sample.

The overall effect of sample disturbance on the stress-strain behaviour of soil is a reduction in the stiffness (Hight, 1983).

3.6 APPARATUS CONSTRAINTS FOR STIFFNESS MEASUREMENTS

The stiffness of soil measured in the triaxial apparatus is affected by instrument accuracy and apparatus compliance. In addition, the apparatus will partly affect the measurements being made.

Errors due to apparatus compliance were discussed by Jardine et al. (1984). Sources of error include load cell deflection,

loading system deflection and top cap to sample reorientation or misalignment. Sample preparation is also very important. Errors arise due to non-uniformity of the ends of the sample, non-parallel ends and lack of squareness of the specimen.

Many published test results show an initial slackness in the measured stress-strain response for compression (eg Ward et al., 1959) and this is attributed to bedding errors. Bedding errors are generally considered to occur between the platens and the sample (Jardine at al., 1984). Costa Filho (1985) included bedding within the apparatus in this category. Undoubtedly there will be some initial seating when the sample and platen are first brought together. Most of this seating could be expected to occur when pressures are first imposed on the specimen, generally during an initial consolidation stage. As the contact pressure between the soil and the platen (the axial effective stress) is increased so bedding will increase also, but the amount is likely to be very small after the initial stages. It is therefore unlikely that sample to platen bedding will account for a significant proportion of the observed initial slackness on compression loading.

Costa Filho (1985) used measurements at points on the side of a triaxial test specimen to quantify the bedding errors. Bedding errors were in fact measured. However, on examining his data more carefully, it can be seen that, at the bottom platen where only soil to platen bedding can occur, the error measurements are insignificant. Most of the bedding was measured at the top platen where bedding within the top cap and load cell assembly would be included.

The problem of end restraint affecting both stiffness and strength measurement has been well recognised (eg Rowe and Barden,1964). The cause is friction between the end platens and the soil which increases the mean total stress locally in compression tests, and reduces it in extension tests.

Two alternatives are used to minimise the errors. The first possibility is to attempt to eliminate friction at the platens. Many methods have been tried, and most succeed to a degree, at least initially. However, some form of grease is often used, and there is some doubt about how long the system will remain efficient as the grease is gradually squeezed out. The end lubrication arrangement itself may well deform, affecting axial strain measurements.

The alternative to using lubricated ends is to use a sample with a minimum height to diameter ratio of two. The middle section of the sample is then relatively unaffected by end restraint. This works well for strength measurement in compression tests, since platen friction increases the stresses near the ends, so that failure will occur in the weaker, more uniform middle section. For extension tests the sample ends will be at a lower stress level due to end restraint. Failure is often observed near the sample ends for extension tests. Stiffness measurements for the whole sample will be affected by end restraint whatever the sample dimensions. There is still advantage in using a longer sample, since the proportion of affected soil reduces as the height to diameter ratio increases.

Costa Filho (1985) reviewed data on the stiffening effect of end restraint. He found that the error in stiffness modulus increases as Poisson's ratio increases, up to a maximum value of about ten per cent.

Jardine et al. (1984) partly overcame the problem of end restraint by measuring deformation over the middle section of the sample. This was achieved using electrolevel gauges inside the cell mounted on a frame attached to the rubber membrane at two gauge points.

The rubber membrane used in triaxial tests will affect the stress

state of the soil. Generally, for stiff soils at low strain levels the error is thought to be negligible. For softer soils the effect can be significant. Henkel and Gilbert (1952) produced a means of correcting the axial stresses for membrane stiffness. Their approach may be modified to correct for induced radial stresses where this is more appropriate (Clinton and Ng, 1984). The rubber membrane is generally assumed to be unstressed at the start of a test.

3.7 TEST PROCEDURES AFFECTING STIFFNESS MEASUREMENTS

3.7.1 Rate of Test

It is well recognised that the measured undrained soil strength is affected by the rate of loading in the triaxial test (eg Taylor, 1948; Bishop and Henkel, 1962). Measured strength decreases as the duration of the test increases. This phenomenon is due to local drainage within the sample, associated with the formation of a slip zone. In slow tests, soil within a slip zone can dilate by taking in water from the surrounding soil. The slip zone becomes weaker as its moisture content increases, thus reducing the measured strength for the sample as a whole. In fast tests, the amount of dilation possible within a slip zone is limited by the rate of flow of the water through the surrounding soil, and higher strengths can thus be achieved.

For stiffness measurements below failure, slip zones are not important. Internal drainage is, however, still a factor. Because of lateral restraint by the platens on the ends of the triaxial sample, the stress distribution within the sample will not be entirely uniform. There will be different pore pressures set up at different parts of the sample by any loading increment. The degree of equalisation of these excess pore pressures will affect the measured stress-strain response.

For very slow rates of loading, the stress-strain behaviour of the soil will be affected by creep.

For pore-pressure related effects, the significant rate is the rate of loading, and not the rate of straining. Conventional triaxial test apparatus applies loading by advancing the loading ram mechanically. This is strain controlled loading. For very stiff soil, this can lead to a very high rate of stress loading. For example, the triaxial tests reported by Houlsby (1985) were carried out with an axial rate of strain of 5% per hour. For an average test the shear modulus was quoted as 12,200 kPa. This results in a stress loading rate of 1,830 kPa per hour. Among the slowest strain controlled tests reported in the literature are those by Jardine et al. (1984). From their data, the average rate of loading during the first 0.1 per cent strain may be calculated as 84 kPa per hour, with the maximum 251 kPa per hour. It is evident that more consistent testing can be achieved using stress controlled tests.

3.7.2 Loading Control

In addition to the differences discussed in the previous section between stress control and strain controlled loading, the method of applying stress controlled loading can also affect stiffness behaviour. Ideally, loading should be smooth, with the sample in equilibrium at all times. If the loading is applied in steps then two inaccuracies may arise. The first is that consolidation drainage may occur setting up large pore pressure gradients within the sample. This causes a lack of uniformity within the specimen (Atkinson, Evans and Ho, 1985). The second problem is that the actual effective stress path followed by the soil during consolidation is not known. If the soil stress-strain behaviour is non-linear then results for stepped loading will differ from those for smooth loading.

3.7.3 Stress Path Probing

In section 3.4.2 the importance of stress history on soil deformation was discussed. In tests where short or discontinuous stress paths are used, full account must be taken of threshold and stress history effects.

CHAPTER 4

CURRENT KNOWLEDGE

4.1 INTRODUCTION

The published data is reviewed for measurement of anisotropic stiffness parameters on soils. The current knowledge on the variation of stiffness parameters with soil state is also presented. These are set in the context of the application of elasticity theory to soils, in particular through the critical state model.

4.2 BASIC ELASTICITY THEORY

The basic equations of elasticity are well established, both for isotropy and for cross-anisotropy (eg Hearmon, 1961; Lekhnitskii, 1963). The application of linear elasticity in the analytical solution of boundary value problems has been used widely (eg Gibson, 1974) and in some cases anisotropy has been taken into account (eg Barden, 1963).

The use of the elastic constitutive equations as the basis for a soil deformation model is common in computer analysis.

4.3 ELASTICITY IN THE CRITICAL STATE MODEL

In the critical state model elastic soil behaviour takes place for soil states below the state boundary surface. The state of the soil is confined to an elastic wall, and the position of this is governed by the swelling line. Elastic compression therefore depends entirely on the definition used for the swelling line.

It has been a basic assumption in the formulation of critical state theory that

$$\delta\varepsilon_v = \frac{\kappa}{vp'}\,\delta p' \qquad (4.1)$$

(Roscoe and Schofield, 1963; Calladine, 1963), which is the requirement for the swelling line to be straight in v-ln(p') space.

Parry and Amerasinghe (1969) used the equation

$$\delta\varepsilon_v = \frac{(1-\nu')e}{kp'}\,\delta p' \qquad (4.2)$$

where e is the voids ratio and k is a constant. They pointed out that changes in e and v are very small such that the two equations are almost identical. An important qualification, also relevant to Equation 4.1, is that this refers to the initial slope of the swelling line only.

Butterfield (1979) challenged the assumption of Equation 4.1, pointing out some practical and theoretical disadvantages. He proposed the revised expression

$$\delta\varepsilon_v = \frac{\kappa^*}{p'}\,\delta p' \qquad (4.3)$$

In Section 2.4.2 it was shown that for all of these cases it is implied that the bulk modulus is proportional to the mean effective stress, and that this gives rise to theoretical difficulties in formulating a consistent elastic model.

The value of the shear modulus is not dictated by the critical state model, but must be consistent with the values used for the bulk modulus.

4.4 NORMALISING ELASTIC STIFFNESS PARAMETERS

In section 2.4.4 normalising parameters were derived from the requirements of the critical state model. A suitable normalising procedure would be to multiply strains by the specific volume and divide stresses by the mean effective stress. Hence, stiffness parameters may be normalised by dividing by vp'. If Butterfield's (1979) compression law is used, then stiffness parameters may be divided by p' alone in normalising.

Several different normalising parameters have been used in published data, not all of which can be justified in critical state theory. The most commonly used are the undrained shear strength, the initial mean effective stress and the preconsolidation pressure. Of these, the undrained shear strength is the most often used, despite the wide scatter typical of undrained shear strength results in overconsolidated clays. The scatter is caused by several factors such as sample disturbance, shear zone formation and rate of test.

A comparison of data by Jardine et al., (1984) showed that it is preferable to use the initial mean effective stress rather than the undrained shear strength as a normalising parameter for stiffness values. This also agrees with the findings of Wroth et al. (1979) in a review of shear modulus data.

4.5 PREVIOUS STIFFNESS MEASUREMENTS

4.5.1 Introduction

The quality of most published stiffness data is very low (Wroth et al., 1979). Stiffness values are frequently quoted from the results of the standard unconsolidated undrained test carried out at a strain rate of 2% per minute, which involves a very high rate of loading initially if the soil is at all stiff. As discussed in Section 3.7.1, very few strain controlled tests have been carried out slowly enough to enable a sufficiently low initial rate of stress loading. Stress controlled tests have only occasionally reported. Some of these are step-loaded (eg Graham and Houlsby, 1983) and suffer from difficulties with non-uniformity and non-linear stress-strain, as discussed in Section 3.7.2.

Published stiffness parameters are generally secant values. The range over which the secant was taken is not always reported, and frequently "bedding" in the apparatus affects the measurements quoted. In addition, corrections for apparatus compliance are not usually mentioned and it can frequently be assumed that no account has been taken of this. For these reasons, previous measurements of isotropic stiffness parameters will not be reviewed here. Such reviews are available elsewhere (Butler, 1975; St John, 1980; Wroth et al., 1979; Ladd et al., 1977). Very few measurements of anisotropic stress-strain behaviour have been found in the literature, and these are reviewed in the following section.

Measurements frequently refer to the undrained Young's modulus E which is related to the drained parameters by the equation

$$E = 3E' / 2(1+\nu') = 3G' \qquad (4.4)$$

It is worthwhile to compare previous measurements of stiffness

modulus with those measured in this project. Tests on North Sea Clay and London Clay reported by Jardine et al. (1984) using very slow strain-controlled tests with internal measurement of axial strain gave undrained Young's modulus values of between 32 and 170 MPa (for a secant at 0.1% strain), with values of E/p_o' generally between 200 and 360. The corresponding moduli for Gault Clay reported in Chapter 7 range from 39 to 150 MPa, with $3G'/p_o'$ between 90 and 390.

4.5.2 Anisotropic Stiffness Measurements

There is limited published data on the anisotropic stiffness of soil. Much of this work has centred on London Clay. Ward et al. (1959) carried out a large series of triaxial tests on vertical, horizontal and inclined specimens and deduced values for the ratio E_h/E_v between 1.1 and 2.0. The results for initial loading, unloading and reloading gave very consistent values for this ratio, despite different absolute stiffness measurements for each stage. Henkel (1971) reported $E_h'/E_v' = 1.6$ for a similar set of tests. Tan (1961) stated that for most Chinese overconsolidated clays E_h/E_v was less than three.

Atkinson (1973; 1975) used the slope of the undrained compression stress path to estimate values of E_h'/E_v' between 1.6 and 2.0 for London Clay.

4.5.3 Anisotropic Stiffness Parameters From Stress Path Tests

Graham and Houlsby (1983) used triaxial stress path tests with step loading to measure the anisotropic deformation parameters for Canadian Winnipeg Clay. Groups of samples were tested using different load-controlled stress paths, and anisotropic stiffness parameters were deduced by combining the results. The ratio E_h'/E_v' was found to range from 1.31 to 2.45. The authors reported a good consistency within the results.

4.6 VARIATIONS OF ELASTIC MODULI

4.6.1 Bulk Modulus

A series of tests by Houlsby (1981) investigated directly the variation of the bulk modulus. The best fit to the data was found to be log (K') proportional to log (p').

Tavenas and Leroueil (1979) found that the bulk modulus was a function of the preconsolidation pressure. This is also implied in the SHANSEP model (Ladd and Foott, 1974).

4.6.2 Shear Modulus

The original Cam Clay model (Schofield and Wroth, 1968) neglected elastic shear strains. However, more recent soil models have recognised the importance of including a realistic elastic shear modulus. Although a reasonable amount of data is available in the literature, the quality of much of it is doubtful (Wroth et al., 1979).

Tests by Namy reviewed by Houlsby (1981) suggested that the shear modulus is proportional to the mean effective stress. Data from Wroth and Loudon (1967), Lambe (1964), and Houlsby (1985) support this for heavily overconsolidated soils. Wroth (1971), Simons and Som (1970), Wroth et al. (1979) and Gens and Hight (1979) found a dependence on p_o', which is much the same thing.

Tavenas and Leroueil (1979) and Ladd and Foott (1974) found that the shear modulus is proportional to the preconsolidation pressure. Atkinson (1973), Wroth et al. (1979) and Houlsby (1985) also found a strong connection with this parameter.

An uncertain dependence on the overconsolidation ratio is demonstrated by several sets of data (Atkinson, 1973; Wroth,

1971; Ladd, 1964; Wroth et al., 1979; Jardine et al., 1984).

Houlsby (1981) investigated the variation of the shear modulus with mean effective stress and found a linear relationship between log (G') and log (p').

4.6.3 Patterns of Stress-Strain Behaviour

A qualitative view of variations in elastic moduli can be obtained by plotting patterns of soil behaviour. In particular, attempts have been made to plot "contours" of equal strain on stress path graphs.

Wroth and Loudon (1967) plotted contours of equal axial strain on stress paths of undrained compression tests on kaolin. Their results are illustrated on Figure 4.1. For heavily overconsolidated soils the results support a linear variation of the shear modulus with mean effective stress. A similar pattern was obtained by Balasubramaniam (1969) and Parry and Nadarajah (1974). The results of Lewin and Powell (1985) showed the same trend for Cowden Till, as shown on Figure 4.2.

For anisotropically consolidated samples a similar pattern has been observed. Results for kaolin from Parry and Nadarajah (1974) are shown on Figure 4.3, and strain contours for London Clay from Hight et al. (1985) are presented on Figure 4.4, and for North Sea Clay on Figure 4.5.

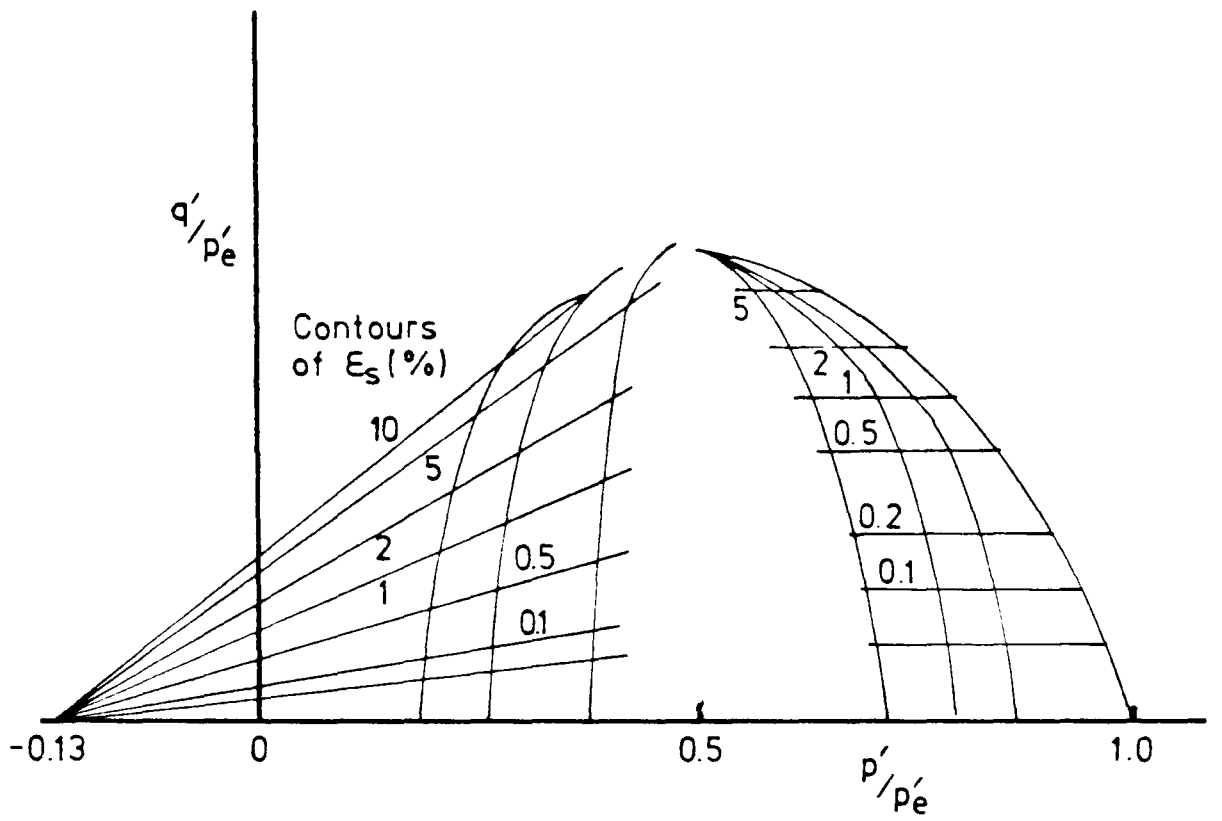

Fig 4.1 Pattern of stress-strain behaviour. After Wroth and Loudon (1967)

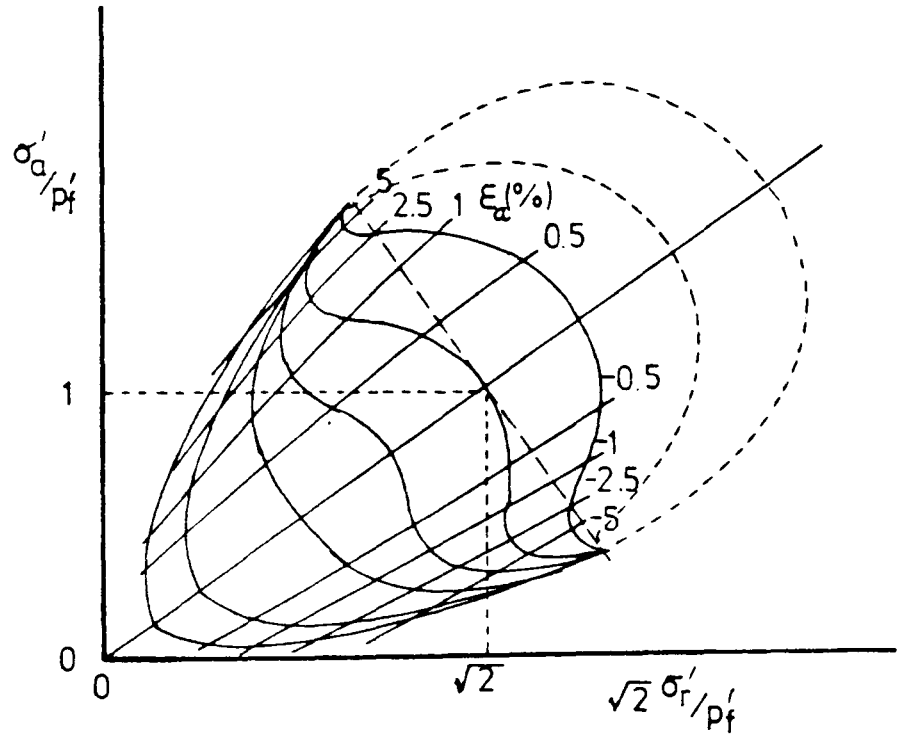

Fig 4.2 Pattern of undrained behaviour for Cowden Till. After Lewin and Powell (1986)

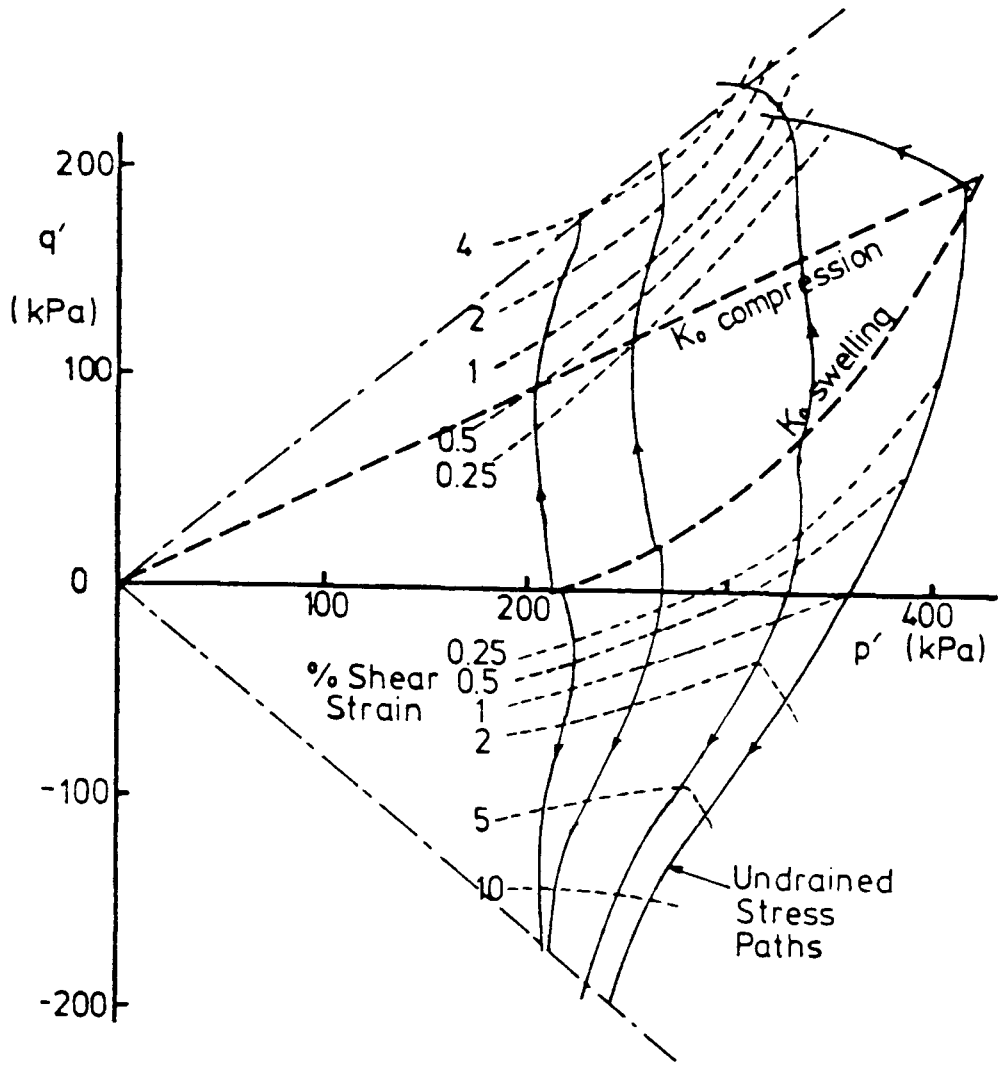

Fig 4.3 Shear strain contours for anisotropically consolidated specimens of kaolin. After Parry and Nadarajah (1974)

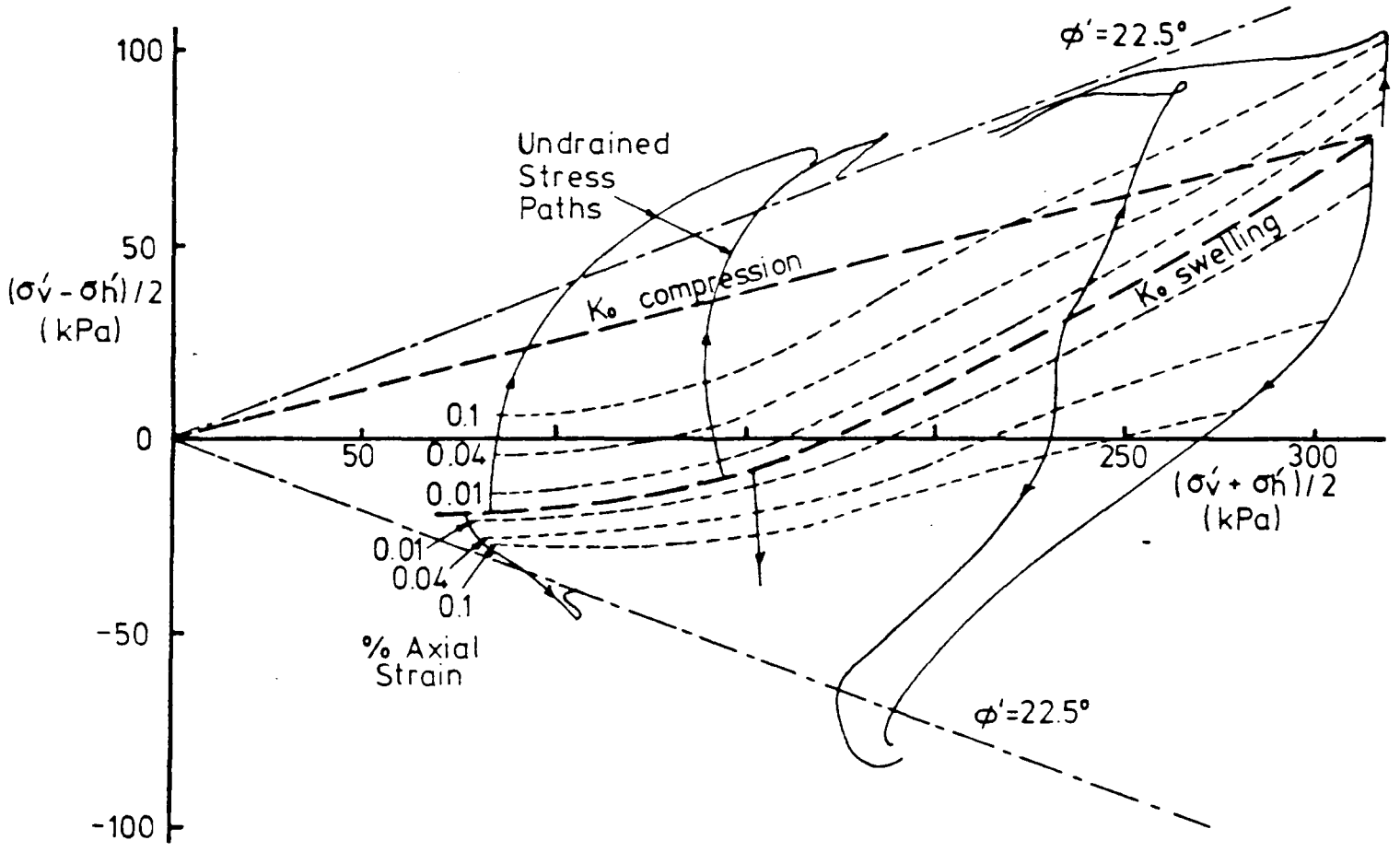

Fig 4.4 Pattern of undrained behaviour for reconstituted London Clay. After Hight et al. (1985)

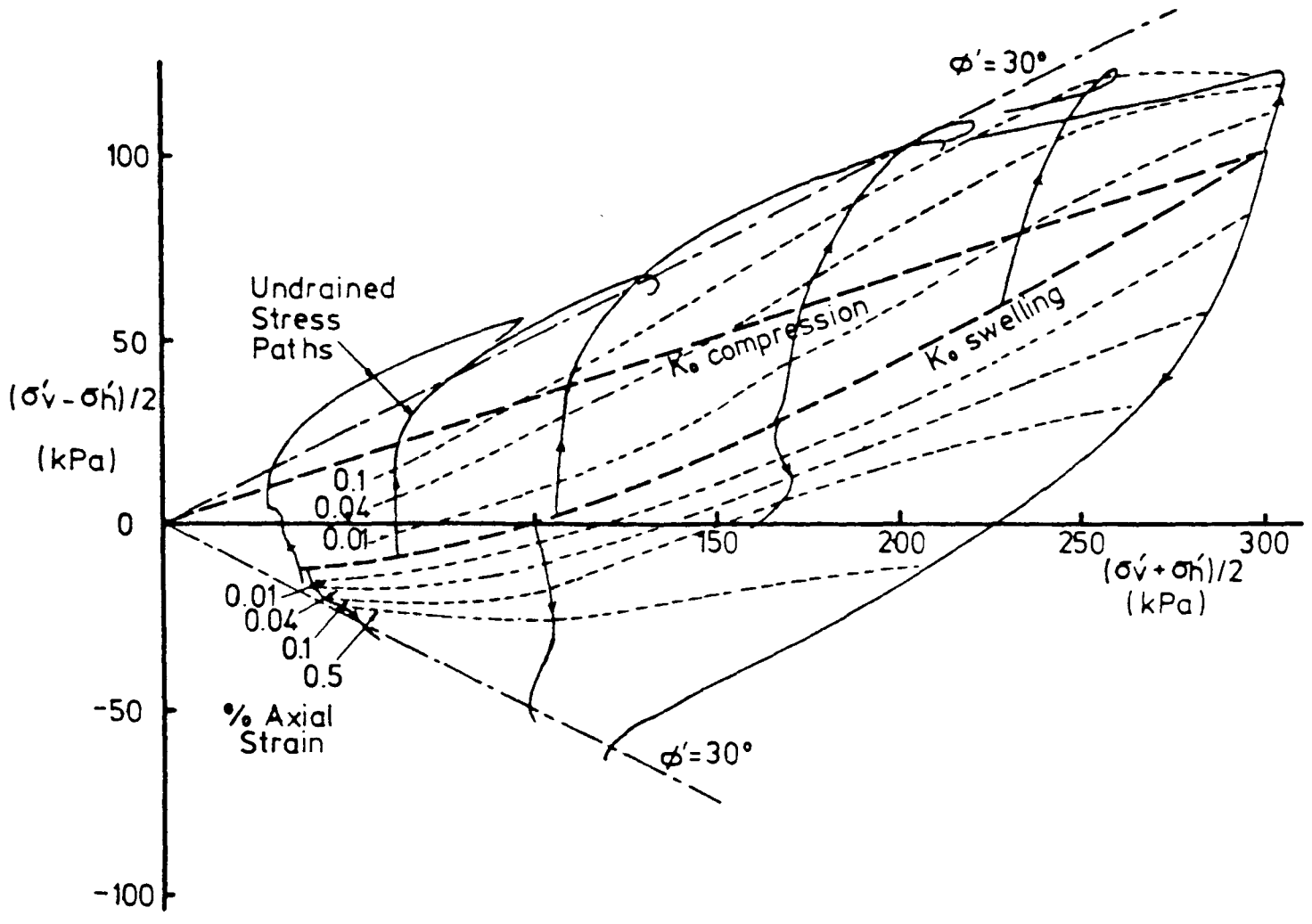

Fig 4.5 Pattern of undrained behaviour for reconstituted North Sea Clay. After Hight et al. (1985)

CHAPTER 5

THE TRIAXIAL STRESS PATH APPARATUS AND TEST PROCEDURE

5.1 INTRODUCTION

The stress path testing for the present project was carried out on 100mm diameter samples in a large triaxial cell developed at The City University. The recording and control system for this apparatus was developed as part of the project. The equipment and test procedure are described in detail.

The ancillary testing was carried out in Bishop and Wesley cells (Bishop and Wesley, 1975) on 38mm diameter samples. These cells were part of the stress path system described by Atkinson, Evans and Scott (1985). A brief description of this system is given, paying particular attention to any differences between the two sets of apparatus.

5.2 THE STRESS PATH APPARATUS FOR 100mm SAMPLES

5.2.1 General Description

The triaxial cell and its recording and control system are illustrated on Figure 5.1. The pressures were applied hydraulically. Air pressure from a compressor at about 800 kPa was stepped down using electromanostats, and applied to the cell through air-water interfaces. The electromanostats were controlled by relay switches operated by a microcomputer.

Electrical instrumentation was used to measure the pressures on the sample and resulting strains. The electrical signals were converted to digital form in an interface unit and transmitted to

the microcomputer. A comprehensive recording and control program made the system completely automatic.

The components of the apparatus are described fully in the following sections.

5.2.2 The Triaxial Cell

The principles of the design of the conventional triaxial apparatus were described fully by Bishop and Henkel (1962). A more versatile hydraulically operated cell was introduced by Bishop and Wesley (1975). The larger triaxial apparatus used for the present project was similar in principle to the Bishop and Wesley cell, but was capable of testing samples up to 100mm diameter. It is illustrated in Figure 5.2 and is described below.

The soil sample was subject to the conventional triaxial system of pressures: an all-round pressure was applied by containing it in a water-filled pressure vessel, and a deviatoric load imposed through the end platens. A back pressure was applied to the pore fluid through a porous stone at the base of the specimen.

The pressure vessel comprised an aluminium cylinder 12.5mm thick of 280mm internal diameter. Round plates formed the ends of the pressure cell and these were sealed against the cylinder with o-rings. Reaction against the fluid pressure on these plates was provided by three tension bars of 36.5mm diameter located within the cell. The bars also provided the reaction for axial load on the sample.

An axial load was applied to the specimen by a 102mm diameter piston through the base of the cell. A rolling bellofram formed a seal with the bottom plate of the cell. Reaction to the axial load was transferred to the top plate through an internal load cell.

The force on the axial piston was provided hydraulically through a second rolling bellofram at its base. As well as applying a deviatoric load to the sample, the force on the piston had also to act against the cell pressure. To achieve the necessary loading capability either a higher fluid pressure was needed at the base or the area of the base must be increased. As with the Bishop and Wesley cell, the latter design was chosen. Initially, an area ratio of four to one was tried. This allowed the total axial stress in the sample to be up to four times the maximum total radial stress. However, it was found that control of the axial stress was not very sensitive with this arrangement and the ratio was subsequently reduced to about 1.9 to one. The arrangement shown in Figure 5.2 incorporates an adaptation of the original design to accommodate a smaller lower bellofram diameter. If future projects require high axial pressures the equipment may be readily changed back to the former arrangement.

The pedestal for the sample was bolted to the top of the axial ram piston and could be removed easily. This allowed different size pedestals to be fitted quickly in order to test various sizes of soil sample, if desired. Two drainage leads to the pedestal connected to separate holes on top of it at some distance apart along a diameter. One lead provided drainage to the volume gauge, the other led to the pore pressure transducer. Water could be supplied or drawn out through both leads enabling flushing of the porous stone at the base of the sample in order to remove any trapped air.

Measurements of stresses and deformation of the specimen were made as close to the soil as possible. The cell pressure was monitored by a pressure transducer at the base of the cell, and the deviator load was measured through a load cell within the pressure vessel attached to the top platen. A second pressure transducer was mounted in a block on the base plate and measured the pore pressure at the base of the sample, connected by a short

lead to the pedestal.

Drainage from the sample flowed through a second tube from the pedestal to a volume gauge adjacent to the cell. The axial deformation of the sample was measured by monitoring the upward movement of the axial ram piston using a displacement transducer. The volume gauge and measurement instruments are described more fully in the following sections.

5.2.3 Electrical Instrumentation

All the electrical instrumentation was based on the full Wheatstone Bridge arrangement of strain gauges with a maximum nominal input voltage of 10 volts. The actual input voltage was generally in the range 7 to 10 volts.

The pressure transducers used were Druck Ltd. type PDCR 10-15 bar or Wykeham Farrance Ltd. type WF 17060 10kg/sq.cm. Both types comprised a silicon gauge bridge diffused in a single crystal silicon diaphragm. The maximum pressure was 1000kPa and the sensitivity nominally 0.1 mV/kPa. A typical calibration is shown in Figure 5.3. Errors due to noise and drift in the transducers were found to be less than the resolution of the measuring system (see section 5.2.6) over a period of a few days.

Linear displacement transducers used for axial and volumetric strain measurement were types LSC-HS50B and LSC-HS25B respectively, manufactured by MPE Transducers Limited. The non-linearity specification was $\pm$0.1% of full scale, and measurement of the linearity is shown in Figure 5.4. Noise and drift of the instruments were found to be less than than the resolution of the measuring system over a period of a few days.

The 2700kg Imperial College load cell was used, consisting of a machined loading column fitted with strain gauges. A description was given by Bishop et al. (1975). A typical calibration is shown

in Figure 5.5 and the load-deflection behaviour is plotted in Figure 5.6. Noise and drift of the instrument readings were found to be less than the resolution of the measurement system over a period of a few days. A little hysteresis was noted in the load cell response, but the error involved was found to amount to less than 1 kPa for the range of stress cycles carried out in the laboratory testing programme.

5.2.4 Volume Gauge

The volume gauge used was the Imperial College type of 100ml capacity marketed by Wykeham Farrance Limited. This comprised a freely moving piston within a cylindrical vessel. The piston was sealed at both ends with rolling belloframs. An air pressure could be applied at one end of the piston causing an equal pressure in the pore water system at the other end. The piston moved freely as water flowed into or out of the gauge, and the change in volume of water in the gauge was monitored by measuring the movement of the piston with a displacement transducer.

A typical calibration of the volume gauge is shown in Figure 5.7. There was a little inaccuracy in the gauge when the direction of volume change was reversed, taking the form of hysteresis, and this amounts to an error of about $\pm$ 0.001% of the volume of a 100mm diameter sample. The gauge was subject to expansion when the back pressure changed causing some movement of the piston. This could be measured and the appropriate correction applied. The gauge was found to be unreliable for back pressures below about 50kPa.

5.2.5 The Control System

In the hydraulic triaxial cell the following functions may be controlled:

1. Water pressure in the cell
2. Pressure on the lower bellofram of the axial ram
3. Back pressure to the base of the sample
4. Volume flow of fluid into the lower bellofram of the axial ram
5. Volume flow of water into the cell

For the axial ram and the cell either pressure or volume may be controlled, but not both; otherwise, each function may be controlled independently of the others.

Pressures were supplied from a central air compressor operating at about 800kPa. The supply pressure was stepped down to the required value using an electromanostat valve, and this lower pressure was transferred to the apparatus through an air-water interface. The electromanostats were manufactured by John Watson and Smith Limited and were operated by electric stepper motors acting through a gear box. Rotation of the motors was controlled simply by opening and closing switches: opening and closing a switch once would turn the motor through one "step" of a fixed value, and a second switch controlled the direction of turn. Each step corresponded to a pressure change of about 0.4kPa. Some slackness in the gear box could cause problems in the control when the motor changed direction, as illustrated in Figure 5.8, but this was corrected by adding a weak spring on the manostat side of the gear box.

Operation of an electromanostat controlled the cell pressure directly through an air-water interface, and using feedback (see section 5.2.6) the pressure was controlled easily to $\pm$1kPa. The back pressure was also controlled faithfully, with little

interference measurable from the volume gauge. The axial load on the sample was, however, controlled less perfectly for two reasons. Firstly, the area ratio between the lower bellofram and the sample amplified any pressure changes. Secondly, some friction existed in the bearing of the ram. This was most evident on changing direction. In Figure 5.8(a) the pressure in the bellofram was measured by the force of the ram against a relatively inflexible load cell. In Figure 5.8(b) a flexible load measurement system was used inducing larger movements of the ram. Comparing the responses shown in the two diagrams indicates the nature and extent of the friction. Nevertheless, even with the larger size lower bellofram the axial stress in the sample was controlled to $\pm$2kPa (including the effect of variation of cell pressure), and this could be improved if the reversal of pressure increments could be avoided.

The displacement of the axial ram piston (and thus axial strain of the sample) could be controlled by forcing fluid into or out of the lower bellofram chamber. Two methods were tried using either a small positive-displacement pump or a Bishop ram. The latter device was found more successful. The Bishop ram was linked into the hydraulic system as shown in Figure 5.1. When the valve to the air-water interface was closed, screwing the Bishop ram in or out would directly raise or lower the axial ram piston. The Bishop ram was turned by a stepper motor acting through a gear box.

Axial strain control has been little used so far on the larger triaxial apparatus and the performance of the Bishop ram system has not yet been fully assessed.

It is also possible to control the volume of water in the cell itself in a similar manner to that described above for the axial ram. Since the diameters of the axial piston and the sample are nominally the same (for a 100mm diameter sample) then controlling the volume of the cell should theoretically control the radial

size of the sample directly (subject to expansion of the cell vessel). This is the principle behind some developments of K_o consolidation cells (eg. Campanella and Vaid, 1972). This arrangement has not yet, however, been tried. At present the radial strain of the sample is controlled indirectly by raising or lowering the cell pressure.

5.2.6 The Microcomputer and Interface System

This section covers the microprocessor, its peripherals and the interface unit (A/D and D/A conversion).

The microcomputer at the centre of the system was the Acorn BBC Model B equipped with a 32k Solidisk Technology Limited sideways RAM extension. The computer controlled taking instrument readings, converting them to engineering units, recording them at appropriate intervals, calculating the corrections or control increments required and operating the relevant switches. In addition, other ancillary functions were performed such as accepting test data through the keyboard. The control program is covered in more detail in the next section.

The computer peripherals included a monchrome screen, an Epson RX80-FT dot-matrix printer and a Cumana 80-track disc drive.

The microcomputer communicated through an RS423 serial bus with an interface unit providing analogue to digital and digital to analogue conversion. The interface unit used was the Spectra Micro-ms manufactured by Intercole Systems Limited. Details of this are given in the Spectra Micro-ms Handbook (Intercole Systems Limited, 1985).

Each electrical measurement instrument was connected to an input channel of the interface unit. The gain of the channel was selected automatically to enable maximum resolution of the signal. The analogue signal was then converted to digital form

with 12-bit accuracy, giving a resolution of one four-thousandth of full range, and passed to the microcomputer.

On command from the microcomputer, the interface unit operated a separate relay box (CM62, made by Intercole Systems Limited). The relay switches gave direct control of the stepper motors.

The interface unit contained a real-time clock which could be read by the computer. However, during control of tests the computer used its own internal clock for elapsed time readings.

The choice of interface unit was an important part of the design of the apparatus, as it controls the accuracy and resolution of the measurement system. The manufacturer quotes the accuracy of the Spectra Micro-ms as better than 0.01% of full scale. The resolution depends on the number of bits used in the analogue to digital converter. In general, the cost increases considerably for instruments with finer resolution. The 12-bit resolution of the system chosen is thought to be adequate when combined with a variable gain. The resolution in engineering units for each parameter measured in a typical apparatus is given in Table 5.1. This represents the worst resolution for readings at the upper end of the normal range. For smaller readings a more sensitive gain would be selected automatically and the resolution would be improved by a factor of at least two.

The microcomputer and interface unit were the most complicated and vulnerable parts of the entire apparatus, and a high standard of reliability was essential. The equipment used proved to be reliable, but was susceptible to external interference from peripheral devices, and in particular from the mains power supply. It was found necessary to isolate the computer and interface using filters in the power line. In addition, the precaution was taken of protecting the apparatus against power failure using an uninterruptable power supply to the essential items (computer, interface and the power supply to the

transducers) with a back-up generator.

5.2.7 The Control Program

Full details of the control program are given elsewhere (Clinton, 1986) and the salient features are described below.

The main function of the control program was to take instrument readings and control the test. At a predetermined interval, typically every ten seconds, each measurement instrument was read together with the supply voltage. Because the instruments consisted of full resistance bridges variations in the supply voltage would affect the instrument signal, and in order to correct for any fluctuations, the instrument readings were divided by the supply voltage reading. The reference (zero) values of the readings were then subtracted and a calibration factor applied to convert to engineering units. Appropriate adjustments were made to correct for current sample area and system compliance. The values were stored in the sideways RAM periodically, typically every hour.

For each function being controlled, the required value was calculated and the difference between the required and actual values determined. The relevant system calibration factor was applied to find the number of relay operations required to effect the correction or increment, and the relay was then activitated. The current state of the sample was subsequently displayed on the screen.

The control loop of the program could be interrupted by pressing a switch sending a signal through the interface unit to the computer. While control was suspended the stored records could be displayed on the screen or dumped to disc. Alternatively a printout of the stored records could be obtained. The printing process could take some time, so the program enabled control of the test to be continued at intervals during the printing.

Interruption of the control loop also enabled a test stage to be ended. A full printout was made and the records dumped to disc. The menu was then displayed so that further data could be input or other action made.

While setting up a test and between test stages a menu of options was displayed.

5.2.8 Accuracy

The accuracy of the measurement system was quoted by the manufacturer as better than 0.01% of full scale. The accuracy of the instrumentation is a function of the calibration and the repeatability of the readings.

Table 5.2 gives an estimate of the accuracy of the measurements, based on observations made during calibration. This includes systematic errors such as zeroing errors.

5.3 THE STRESS PATH APPARATUS FOR 38mm SAMPLES

5.3.1 Introduction

The stress path testing system for 38mm diameter samples was described by Atkinson et al. (1985). It formed the basis for the design of the apparatus described in the preceeding sections, and was similar in principle and in most details.

5.3.2 General Description

The overall system was the same as that shown in Figure 5.1 except that six Bishop and Wesley Cells were controlled by a single microcomputer. The instrumentation to the cells was the same as that described in Section 5.2 except that the volume

gauge capacity was only 50ml and a more sensitive load cell was used.

5.3.3 The Control System

Air pressures to the Bishop and Wesley cells were controlled by manostats which were turned by small direct current motors acting through a gear box. The rate of operation, about 40 kPa per hour, was sufficiently slow that effective control could be achieved by simply switching the motors on or off as appropriate every ten seconds.

5.3.4 The Microcomputer and Interface System

Logging and test control was carried out by a Spectra microcomputer with a Spectra MB interface unit manufactured by Intercole Systems Limited. A second microcomputer, an Epson QX10, was linked to the system to assist with data handling.

5.3.5 The Control Program

The recording and control program was similar to that described in Section 5.2. Because several cells were controlled by a single microcomputer there was a little less flexibility. The control time interval was fixed at ten seconds, and readings were recorded every hour.

5.4 COMPLIANCE OF THE APPARATUS

In order to apply pressures to a sample of soil, similar pressures must be generated within the apparatus. The apparatus will therefore deform at least a little. When taking measurements of sample deformation it is necessary to correct for any compliance in the system which might affect the measurements. The way in which corrections were calculated and applied is

covered in the section on calibration. The factors affecting this calibration for the larger apparatus are discussed below.

Axial strain was measured using a linear transducer in a housing on the side of the lower bellofram chamber, measuring to an arm attached to the axial ram piston. On application of an axial load the axial ram piston would be compressed and its entire housing put into tension. The load was transferred to the top plate through tension in the three internal bars in the cell, and the top plate would undergo bending and shear to supply reaction to the load cell. The load cell itself would compress. Apart from the small strains in the lower bellofram housing below the point of attachement of the transducer, each deformation in the system (although small) would add to the error in the displacement measurement. However, the apparatus was designed to accommodate the largest forces likely to occur in the system, and under normal working loads its deflection was negligible.

The load cell itself was the least stiff part of the system. A typical stress-strain measurement for a load cell is shown in Figure 5.6. With little inaccuracy this can be approximated to a bi-linear stress-strain response coupled with a translation as the load passes through zero.

Changes in the cell pressure would extend or compress the three tension bars and deform the top plate affecting the axial strain measurement. The compliance in respect of cell pressure changes was measured as 0.04mm per 100kPa and its effect on measurement is considered to be not very significant. However, strain readings were corrected for this compliance.

The other deformation measurement affected by system compliance was that of volume change of the sample. The main factor involved was expansion of the volume gauge as the back pressure varied. Expansion of the leads to the sample would also contribute a small volume change. A short length of tube passed

through the pressure vessel to the sample pedestal, and there would be some contraction of this section as the effective radial pressure was increased.

In addition to the compliance of the system discussed above, measurements of deformation would be affected by changes in temperature. To overcome this factor, the apparatus was located in a temperature controlled laboratory.

5.5 APPARATUS CALIBRATION

5.5.1 Introduction

The recording and control program incorporated linear calibration factors for all measurements. This was found to be adequate for all control purposes. The methods used to obtain these calibration factors are set out below. For the load cell there was a small non-linearity in the calibration which was accounted for when processing the data, as discussed in Section 5.6.

In all cases the calibration measurements were made using the main control program with the whole apparatus working. The calibrations therefore account for the response of the entire system and not just individual instruments.

5.5.2 Load Cell

The load cell measured the deviator load which could be tensile or compressive, and a different calibration factor was used for each. For lighter loads in both compression and tension the calibration procedure comprised using dead weight on or suspended from the instrument. A known weight was applied and the equivalent stress calculated using the sample diameter entered into the computer as data. This was compared with the axial stress displayed on the screen by the control program. A series

of weights was used, and the results plotted as actual reading against applied loading. A typical calibration plot is shown in Figure 5.4. If the best fit straight line through the points was not at 45 degrees then the calibration factor was corrected and the procedure repeated.

To apply higher loads a modified oedometer frame was used.

5.5.3 Water Pressure Transducers

The pressure transducers were calibrated using a Budenberg apparatus. This applied a known hydraulic pressure by supporting weights on a piston of known diameter. The piston was rotated to eliminate friction. The transducer was mounted in a block in the calibration apparatus and a zero reading taken with the hydraulic system open to atmosphere. In practice, this was not truly zero, but the small head of water present corresponded to about 2kPa and was allowed for. Experiments indicated that this did not affect the calibration. The hydraulic system was then closed to atmosphere and pressurised using successive weights on the rotating piston. The pressure at the transducer was calculated as the pressure applied by the weights at the piston less the head of water between the piston and the mounting block. The calculated pressure was then compared with the pressure displayed on the screen by the control program.

The calibration factor was adjusted to give the best correspondence between the applied pressure and the reading displayed. The transducer response was generally very linear so that an almost exact correspondence between the displayed and imposed pressures could be seen at all stages.

5.5.4 Volume Gauge

The volume gauge was calibrated using a Bishop ram connected to the outlet at the top of the gauge. Each turn of the screw drive of the Bishop ram forced a known volume of water into or out of the gauge. The percentage volume strain was calculated for each increment of volume change, based on the sample dimensions entered as data to the computer. The volume change was then compared directly with the volume strain reading shown on the computer screen. A typical calibration plot of volume strain reading against volume flow / calculated volume strain is shown in Figure 5.7.

5.5.5 Axial Strain Transducer

The linear displacement transducer was mounted in a block incorporating a micrometer screw gauge. In this way a known displacement could be applied accurately to the transducer. The applied displacement was divided by the specimen length input as data to the computer to give a strain, and this was compared directly with the strain value displayed on the screen. In practice, it was possible to adjust the calibration factor until an exact correspondence to two decimal places of percentage strain was found over the whole length of the micrometer travel.

5.5.6 Axial Compliance

The control program for the single cell system corrected the axial strain measurement automatically for apparatus compliance. The correction was calculated from the load cell reading multiplied by a calibration factor.

The compliance factor was calibrated directly using the main control program. A block of aluminium was set up in place of a soil sample. The calibration factor was checked by applying an axial load to the dummy sample. With the correct factor, the

axial strain measurement displayed on the screen would not change.

Nearly all the axial compliance was caused by the load cell. Since the axial compliance was approximately bi-linear (see Figure 5.6) the application of a single calibration factor was not adequate for the whole range of axial stress normally used. In practice, it was found to be sufficient to apply the calibration factor relevant to the lower stress range, and to correct the higher range results at a later time if the error was considered significant.

5.5.7 Volume Gauge Expansion

The volumetric strain measurement was corrected automatically in the control program for the single cell system for expansion of the volume gauge as the back pressure changed. The compliance factor could be calibrated directly using the control program.

The volume gauge expansion was calibrated with the piston at about the mid-point of its travel and the valve to the pedestal closed. Expansion of the gauge could be observed as a change in the volume strain reading as the back pressure was increased. Changing the pore pressure reading (for example, by applying a pressure to the transducer using the Budenberg calibrater) would cause the computer program to correct the volumetric strain reading in proportion to the measured change in pressure. The calibration factor was correct if the volume strain reading remained unchanged when the applied back pressure increment corresponded to the measured pore pressure change.

5.6 TEST PROCEDURE

5.6.1 Setting Up The Specimen

(a) 100mm Samples

The soil samples of nominal 100mm diameter were extruded from the sample tube and trimmed to a suitable length in a conventional cradle using a sharp knife and a stout straight edge. Particular attention was paid to obtaining flat, smooth ends which were parallel to each other and orthogonal to the axis of the specimen. Moisture content samples were taken from the trimmings, and the specimen was weighed.

The sample was set up on a saturated, de-aired porous stone upon the pedestal of the triaxial cell, with a soaked filter paper disc between the soil and the stone to prevent clogging. A similar filter paper disc was placed on top of the specimen and the top platen was positioned.

Soaked filter paper side drains were then wrapped around the soil to overlap the porous stone at the bottom. These were either standard vertical strip drains or, if axial extension was anticipated, a "fishnet" arrangement cut from a single piece of filter paper.

Where possible, two rubber membranes were used because tests on the larger diameter samples typically last for several weeks, and it is important to ensure that as little leakage as possible occurs. The inside membrane only was sealed to the pedestal and top platen using pairs of o-rings.

With the soil sample set up, the axial ram piston was raised to a suitable starting position and the valve to the lower bellofram was closed, locking the ram in this position. The load cell was then screwed down to just touch the top platen, and the two were

rigidly connected with bolts. The cell body could then be positioned and the apparatus filled with de-aired water.

Because of the bolted connection between the top platen and the load cell, some care was needed when commencing loading. A suitable procedure was to raise the cell pressure to a small value of about 30kPa while the axial piston was locked stationary. A small pressure was then applied to the line to the lower bellofram which was expected to produce a total axial stress equal to the cell pressure. The valve to the lower bellofram was eased open while observing the axial strain dial gauge. If the gauge showed a sudden movement the valve was quickly closed again. This indicated that the bellofram pressure was wrong, and should be corrected. Any small deviator stress applied accidentally to the specimen could be relieved by adjusting the screw mounting of the load cell, and the new axial dial gauge reading noted. This procedure was repeated until no significant movement of the dial gauge was noticed on opening the bellofram valve, and the valve could be left open. This procedure was thought to cause minimal disturbance to the sample.

Once the sample was installed as described above then control could be given to the computer.

(b) 38mm Samples

The U100 samples were extruded directly into a cluster of three thin walled tubes of 38mm internal diameter. Any samples which could not be tested immediately were sealed using wax. The 38mm diameter samples were extruded onto a cradle for trimming.

The specimens were set up in a similar way to the 100mm samples. Only a single membrane was used for these tests. The rubber was examined visually for flaws beforehand. A period of rest was allowed in the preliminary stages of the test program to check for any leakage through or past the membrane.

In the Bishop and Wesley cell, the top platen was not connected to the load cell immediately. This allowed preliminary isotropic pressures to be applied by manual adjustment of the manostats. A rubber suction cap was fitted to the top platen which would connect to the load cell as shown in Figure 5.9. To make the connection, the pressure in the lower bellofram was adjusted until it just balanced the cell pressure and the axial ram could "float". The ram was suitably positioned and the load cell screwed down to make light contact. A Bishop ram was then used to draw water from the load cell connector. This brought the top platen into firm contact with the connector with the suction cap forming a seal. The Bishop ram was removed, and the lead was left vented to atmosphere. This procedure needed to be followed with great care to avoid disturbing the sample.

(c) Reconstituted Samples

Reconstituted samples were made with the soil from Borehole 7 at 4.5m depth (see Section 6.1). This soil was air-dried and ground to a powder. It was then stored in a plastic bag.

Specimens were made individually when required. About 120g of the dried, ground soil was mixed with distilled, de-aired water to a moisture content of about 90 per cent (approximately one and a quarter times the liquid limit). The mixture was left for an hour or two to ensure complete wetting of the soil particles, and then spooned carefully into a press.

The press consisted of a 200mm long perspex tube of 38mm internal diameter. Close-fitting pistons were able to move freely at either end of the tube. The face of each piston was set with a porous stone, and a drainage hole connected this to the free face of the piston. Filter paper discs prevented clogging of the porous stones.

The soil soup in the press was tapped gently to bring any trapped air bubbles to the surface. The top piston was then installed and the soil compressed using weights acting on the pistons. Initially, a 200g weight was placed directly on the top piston, with the tube vertical and resting on the bottom piston. After about an hour, larger weights were imposed using a hanger arrangement. Each weight was left on for about an hour, allowing time for consolidation before adding further weight. In this way the weight was increased in four or five stages to 8kg. The specimen was left overnight under this weight.

The quantity of soil used was found to produce a finished specimen of between 75mm and 80mm length. This was extruded into a cradle and installed in the triaxial cell directly, as described in the previous section.

5.6.2 Conduct of the Test

Once the sample was installed, conduct of the test was straightforward using the microcomputer control. The sample dimensions were entered through the keyboard, together with the parameters for the required stress path. Control of the test and all the measurements were then carried out automatically.

The tests on 100mm diameter samples were carried out using stress controlled loading throughout, except for the one specimen compressed with zero lateral strain. The tests in the smaller apparatus used both stress and strain control. These were the "standard" uniaxial compression and extension tests. All the tests were carried out with stress control initially, but at a suitable time before failure was reached they were changed to strain control. This enabled the peak and post-peak behaviour of the soil to be tested.

In determining the rate of loading, the methods proposed by Atkinson (1984a) were used as a guideline. In the larger

apparatus the typical rate used for drained loading was 3kPa per hour on the deviator stress. For undrained loading this was increased to 50 kPa per hour. Isotropic compression was initially carried out at 2kPa per hour. In later tests this was reduced to 1kPa per hour.

The loading rate of 2kPa per hour for isotropic compression was checked by stopping a test part way through the compression stage and immediately closing the drainage valve. After several hours the observed excess pore pressure was about 10 kPa, which agreed well with the value predicted from measurements of the coefficient of consolidation. This was thought to be acceptable for general compression and swelling stages, but for subesquent stress path probing the rate of loading was reduced to 1 kPa per hour.

In the Bishop and Wesley cell the smaller specimen size enabled faster loading rates. Typical values were 8kPa per hour for drained and undrained loading, and 5 kPa per hour for isotropic compression.

5.6.3 Ending a Test

The sample was removed from the apparatus as soon as possible after the end of the test. The sample was immediately weighed and, when not totally deformed, it was measured. The larger samples were cut up and moisture content specimens were taken from at least six representative locations within the specimen, away from the edges and outside any failure zone. The final moisture content of the sample was taken to be the average of these moisture content measurements. This procedure was checked successfully by measuring the moisture content of the whole sample for one of the tests. For the 38mm diameter samples, the moisture content of the whole specimen was measured for every test.

5.7 DATA PROCESSING

The specific volume was calculated from the moisture content measurements as

$$v = 1 + 2.73\ w \tag{5.1}$$

which uses a measured value for the specific gravity. The solid volume of the soil was calculated using

$$V_s = V/v \tag{5.2}$$

for both the initial and final test measurements.

For each stage of the test the specific volume was then calculated as

$$v = V/V_s \tag{5.3}$$

For the larger samples a good agreement was generally obtained between the two. The 38mm diameter samples produced a discrepancy amounting to an inaccuracy in the specific volume of about $\pm$ 0.02. This was probably due to the sensitivity of the volume change measurements, unrepresentative moisture contents found from the soil trimmings, and change of the final moisture content by the sample taking in water from the porous stone while the apparatus was being dismantled. For consistency, the final moisture content was preferred in specific volume calculations.

The test data was stored on a floppy disc and could be processed readily by microcomputer.

The first stage in processing this data was to make corrections for slight non-linearity in the load cell calibration. This was followed by adjusting strain measurement to take account of

system compliance not catered for by the control program. The data could then be easily analysed and plotted automatically.

Automatic data analysis was straightforward. The corrected data was read from disc into the microcomputer. The relevant initial value of specific volume was entered through the keyboard. The computer then calculated selected functions, such as p' or q', and provided a printout of their values.

Many of the required graphs were plotted manually using the computer-analysed data. Some of the routine graphs were plotted automatically on the computer using high a resolution graphics mode with a screen dump facility to a dot-matrix printer. Frequent manual checks were made on the plots.

Tangent slopes were taken from graphs manually on a drawing board. A large number of sampling points were used to compensate for any inaccuracies of judgement.

Slopes for stress path probe data were calculated on a microcomputer using the least squares fitting method. The data was first displayed graphically to the required axes. The section of the graph to be fitted was then selected, and any anomalous data points deleted. The best straight line fit was drawn through the data points and the parameters of the line were output to the printer.

5.8 DEVELOPMENT AND ASSESSMENT OF THE APPARATUS

5.8.1 Introduction

The design of the large triaxial stress path apparatus for 100mm samples was based on the existing stress path system using Bishop and Wesley cells (Atkinson et al., 1985). The triaxial cell itself, capable of testing samples up to 100mm diameter, had not

previously been used to any degree. The measurement and control system was developed for specific use with the triaxial cell during the present project. Assessment of the system was made during preliminary trials and during the progress of the testing reported in the next chapter.

In the following sections, some of the criteria behind the design are discussed and experience gained during development is presented.

5.8.2 The Triaxial Cell

The design of the triaxial cell was based on that of the smaller Bishop and Wesley (1975) cell, and the principle of the design was therefore well established. The cell performed well and was found to be easy to use. Of particular note is the ability to make a sound connection between the top platen and the load cell before the cell body is installed, preventing a possible cause of sample disturbance encountered when using the Bishop and Wesley cell.

The design of the lower bellofram was modified during the test series. Initially, the lower bellofram had a diameter of 200mm giving approximately a four to one area ratio on the sample. This enabled high axial stresses to be achieved, but made the axial pressure control on the sample very sensitive. A reduction of the bellofram size to 135mm was found to be an improvement.

5.8.3 Instrumentation

The choice of electrical instrumentation for the large cell was based on that for the smaller Bishop and Wesley cells already in use, and was known to be reliable.

Measurements were found to be very good, with the large sample size making resolution and accuracy much better than for the 38mm

diameter apparatus. This was particularly apparent in the volume measurements. Measurement of axial ram movement were also very good, but the high compliance of the load cell made axial strain measurements less precise. Although a reasonable repeatability was found in axial compliance tests, this is apparently not always found for the load cells used (Hight, 1986). The method adopted for checking the compliance was to install a machined aluminium sample in the apparatus. This kept the load cell properly aligned and free from eccentric loading, which may not be the case when testing soil. This aspect needs further investigation.

5.8.4 The Control System

The electromanostats manufactured by John Watson and Smith Limited proved to provide a convenient means of controlling stresses. They were easy to install and simple to use. Problems were encountered with loose grub screw linkages to the manostat and they had to be checked regularly. Failure of the linkage was not always disastrous, since the output pressure remained approximately constant if this error occurred.

Slackness in the gear box driving the manostat caused some difficulty with pressure control using feedback during preliminary tests. This can be seen in Figure 5.8. The problem was overcome using a weak spring (a rubber band) on the manostat side of the gear box.

Axial strain in Bishop and Wesley cells was controlled using a Bishop ram. Transferring this system to the larger cell presented some difficulties as the area ratio between the lower bellofram and the Bishop ram piston was very big. The full stroke of the Bishop ram available commercially would only produce about 1.5 per cent axial strain in a 200mm long sample. When the size of the lower bellofram was reduced, this figure was increased to 2.5 per cent which was considered to be usable but not ideal. The

alternative of manufacturing a Bishop ram with a larger piston diameter was considered, but preliminary calculations showed that friction in the screw mechanism would be excessive, requiring either a very powerful stepper motor or a very high gear ratio.

A small positive-displacement pump was considered as an alternative. Rotary pumps available commercially were found to be very expensive, so a small piston pump was designed and built. Each stroke delivered about 1 cc of water to the lower bellofram, and trials showed that this gave acceptable control of the axial strain. However, the pump was very susceptible to interference from air drawn into the system, and proved to be unreliable. A further disadvantage with using pumps is that they cannot usually be reversed, so two pumps working in opposite directions would need to be combined for full automatic feedback control of axial strain.

5.8.5 The Interface Unit

The interface was required to provide accurate analogue to digital conversion with an appropriate signal amplification to a 12-bit A/D converter. Since tests were expected to last for several weeks a high degree of stability and reliability was essential. The prototype unit was designed to suit this application by Digital Design and Development Limited. Two further units were built to different designs with a greater number of input channels and incorporating a programmable gain. The latter unit was rejected when interference was detected between the different input channels. The other two tended to be unreliable. Eventually the unit described in Section 5.2.6 marketed by Intercole Systems Limited was purchased, and found to be far superior, both in its facility for automatic gain control and in its reliability. The cost was about 75 per cent more than for the purpose-built units, but this was justified by its performance.

Few problems were encountered with the relay units. Some initial experimentation was necessary to find how fast the relays and stepper motors could operate, since the mechanical side of the system was much slower in response than the electrical side.

5.8.6 The Microcomputer

The prototype system used a 3D09 computer manufactured by Digital Design and Development Limited. This was adequate, but the relatively small 16K RAM was found to be only just large enough to accommodate the control program, and test data had to be dumped to disc regularly. The latter operation was found to be the cause of some unreliability. In redesigning the system, the Acorn BBC Model B microcomputer was chosen on grounds of cost and by its reputation for reliability, and the 32K RAM was expected to be large enough to accommodate the control program comfortably. A further 32K of sideways RAM was fitted using the system marketed by Solidisc Technology Limited, and this was used for data storage to avoid regular dumping to the disc storage.

5.8.7 The Control Program

The BASIC recording and control program was adapted from that used in the multiple cell system (Atkinson et al., 1985). It was restructured to make the best use of Acorn BASIC and modified to provide the flexibility of operation of which the single cell system was capable.

The program was continually developed throughout the project as possible improvements were recognised. These included more convenient monitoring of the test's progress, the use of the automatic gain control facility of the interface unit, and storage of zero readings on disc to enable tests to be restarted after a shut-down.

5.8.8 Reliability

The measurement and control system was found to be susceptible to interference from many sources, particularly from appliances drawing power from the same mains circuit. Most of these problems were overcome by incorporating filters in the power supplies to the microcomputer and interface unit. Eventually an uninterruptible power-pack supply was installed for the computer, interface unit and instrumentation.

The use of a serial RS423 buss connector between the computer and interface unit was found to be more reliable than a parallel ribbon cable.

5.8.9 Operation

In order to check the operation of the stress path system and to develop the procedures for using the apparatus, some preliminary testing was carried out on samples of remoulded kaolin. When a suitable procedure had been established, a series of tests was made on kaolin samples to demonstrate the ability of the apparatus to control tests following stress paths commonly found in engineering design problems. The results of these tests were reported by Atkinson and Clinton (1984).

Measurement	Instrument	Working Range	Signal Range	Channel Range	Resolution
Cell & pore pressure	)Pressure)Transducer	0-800kPa	0-80mV	±80mV	0.10kPa
Axial load*	Load cell	±800kPa*	±40mV	±40mV	0.39kPa
Axial strain	Linear Transducer	0-25%	0-36mV	±40mV	0.014%
Vol. strain	Linear Transducer	0-6%	0-60mV	±80mV	0.004%

* Based on a sample of 100mm diameter

Table 5.1 Measurement of System Resolution for a Typical Apparatus

Measurement	Accuracy
Cell and Pore pressure	1 kPa
Deviator stress	1.5 kPa
Axial strain	0.01 %
Volume strain	0.01%

Table 5.2 Measurement Accuracy

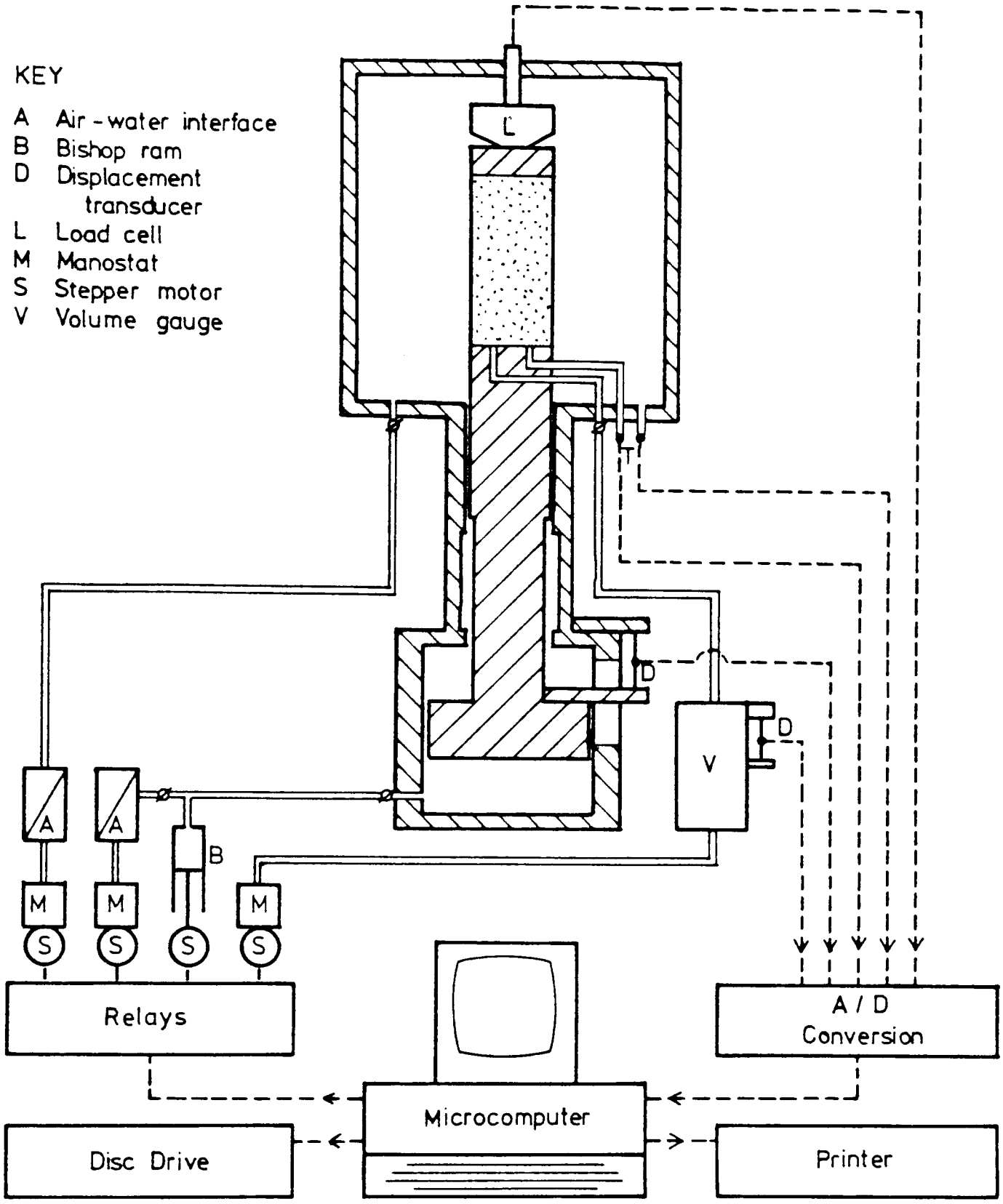

Fig 5.1 Triaxial stress path apparatus control system

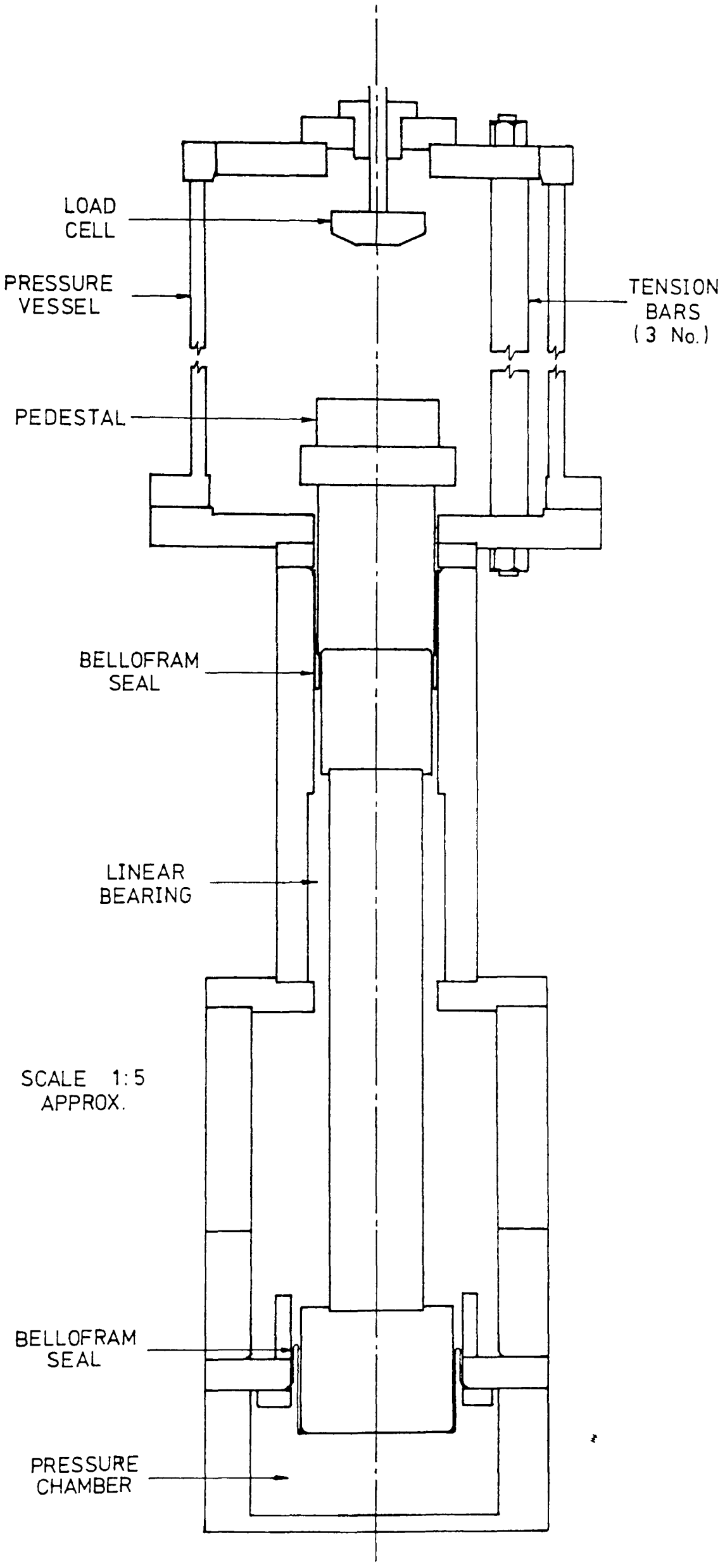

Fig 5.2 Hydraulic triaxial cell for samples up to 100mm diameter

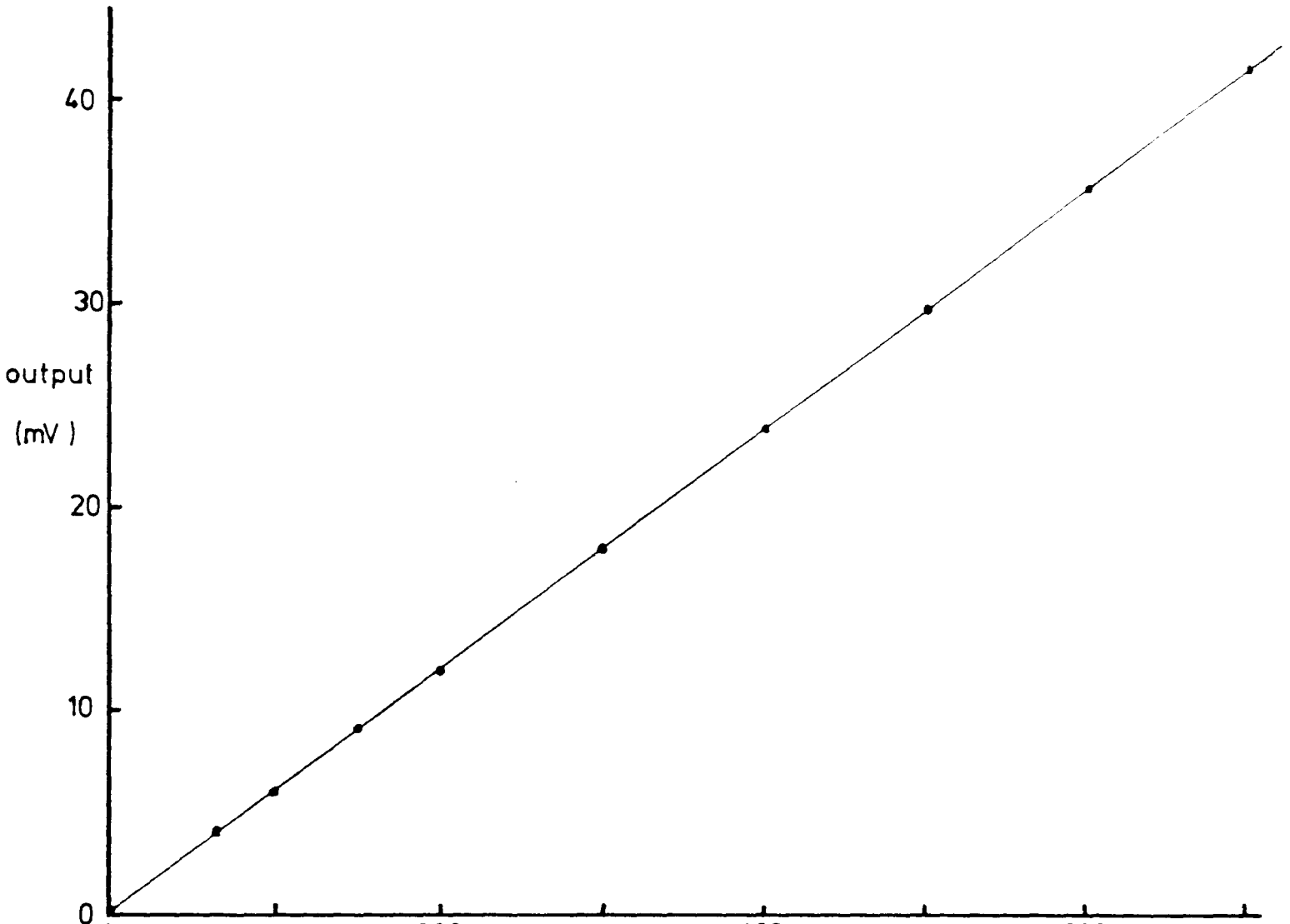

Fig 5.3 Typical pressure transducer calibration

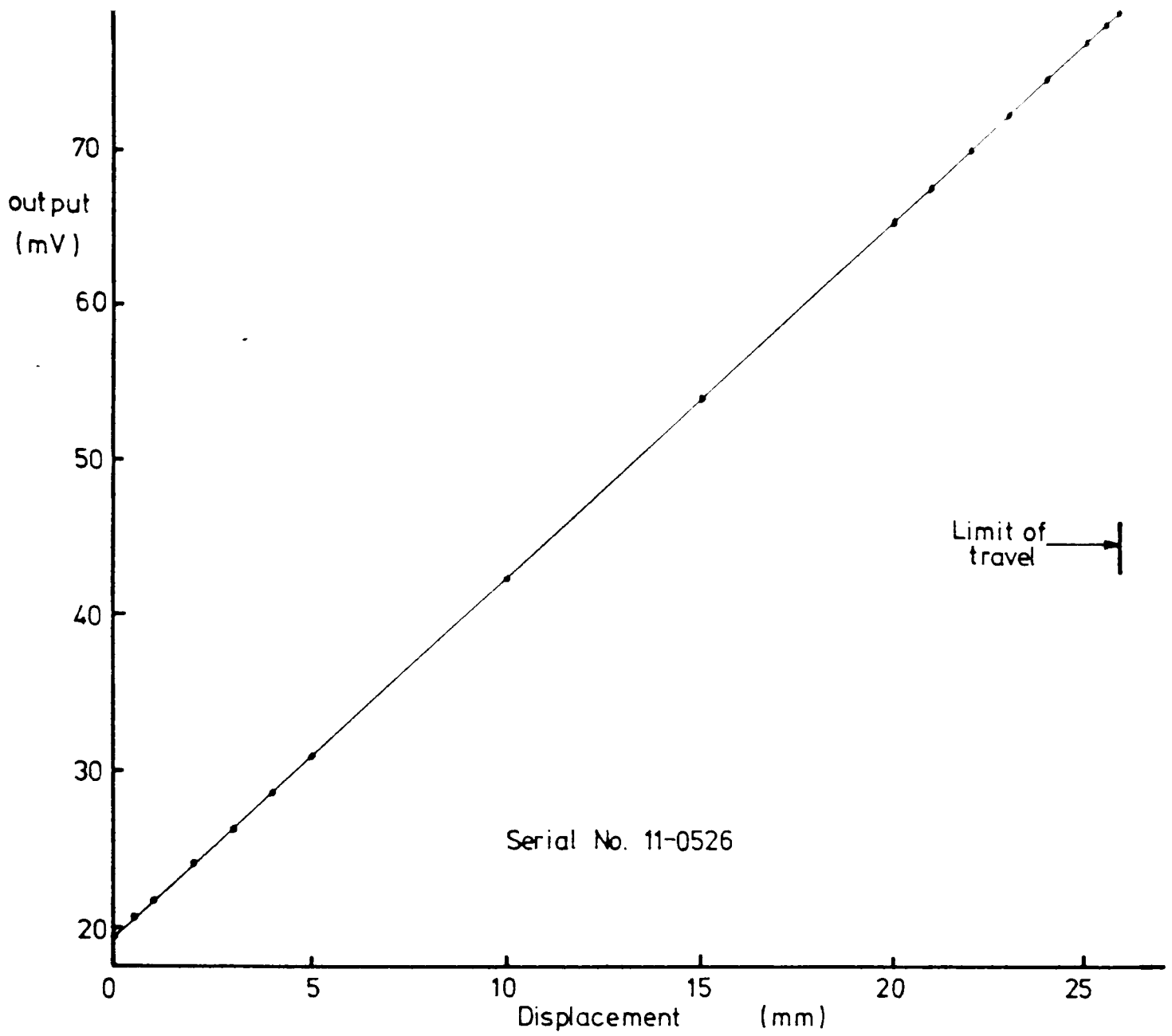

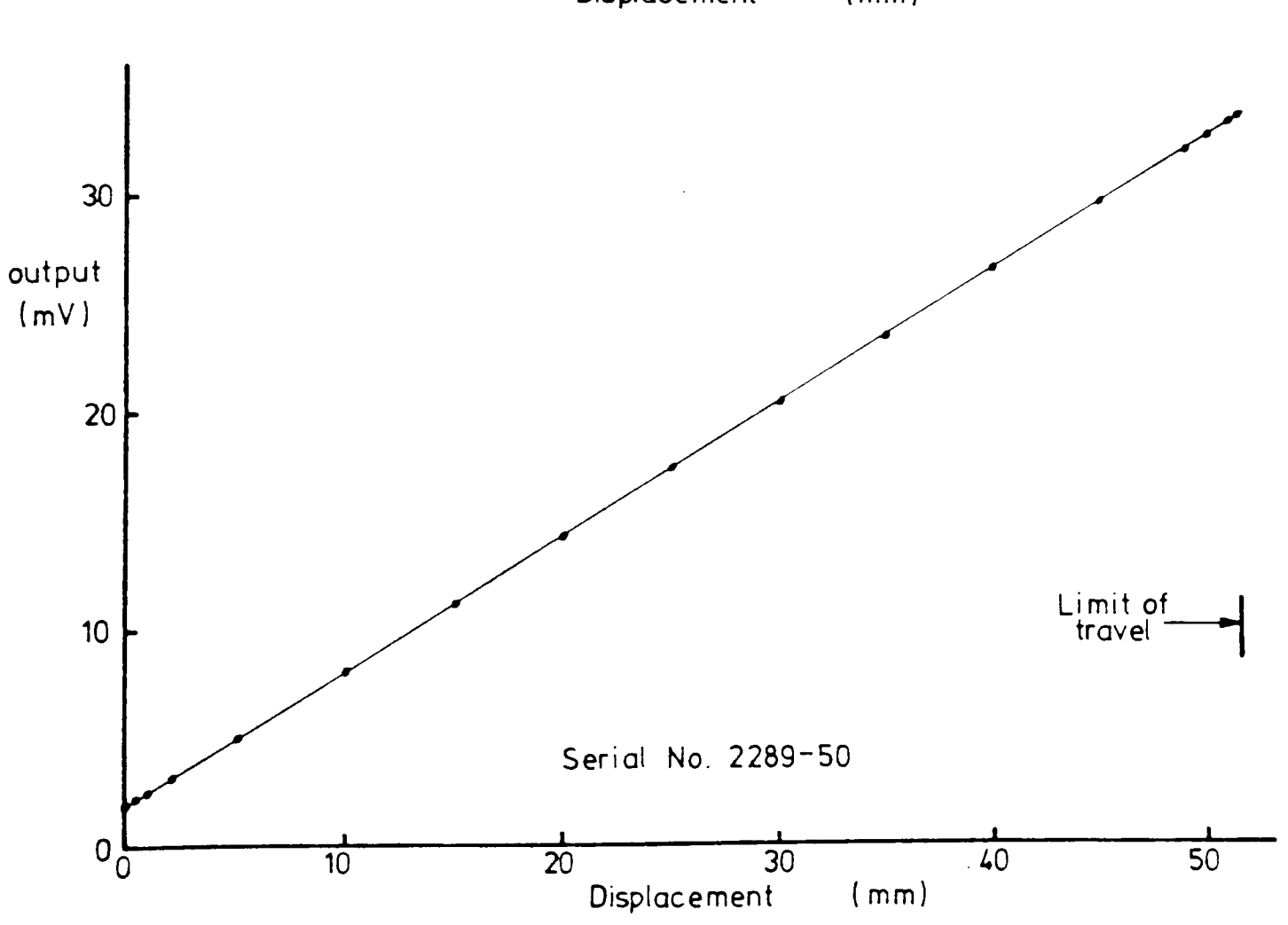

Fig 5.4 Linearity and typical calibration for displacement transducers

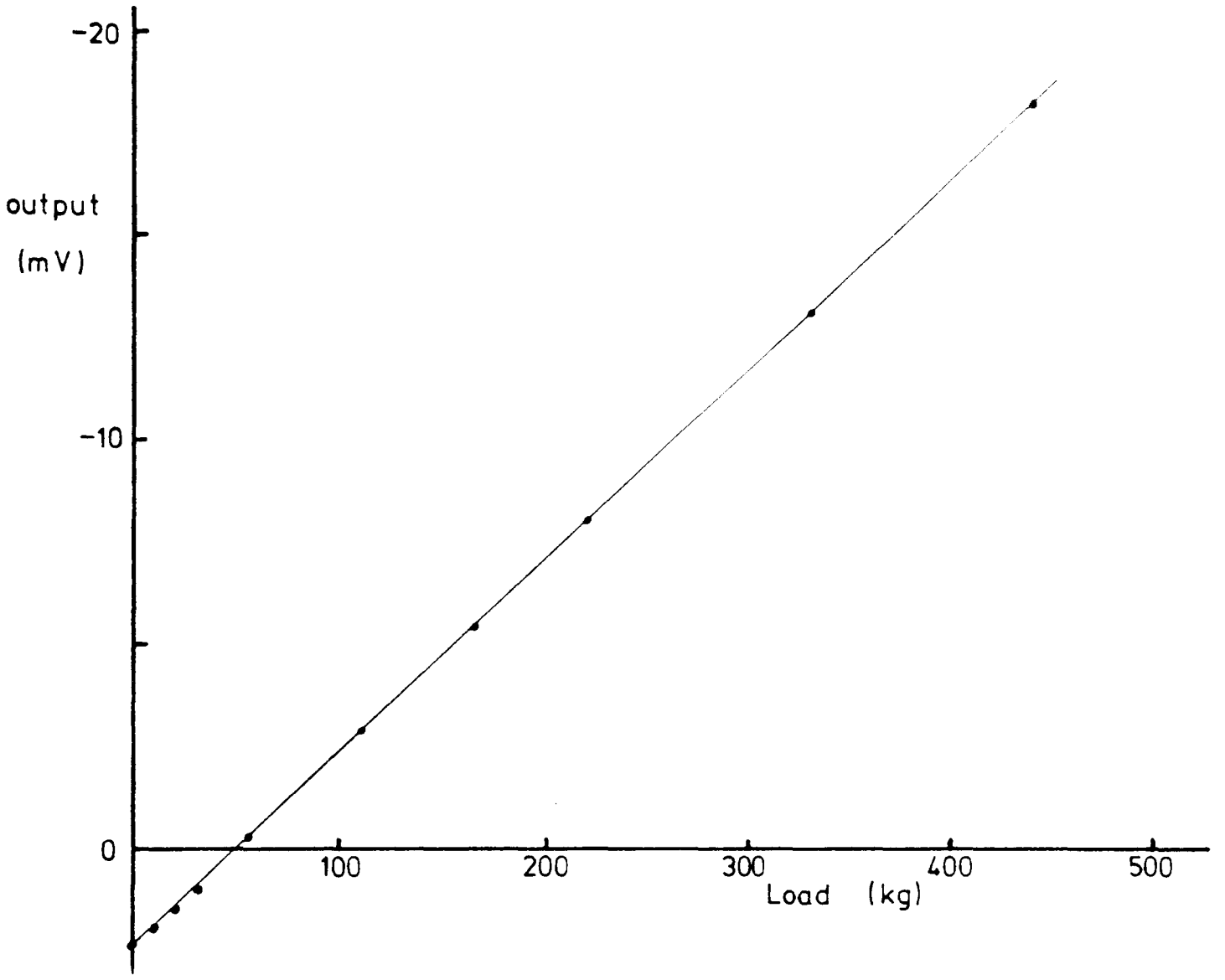

Fig 5.5 Typical load cell calibration

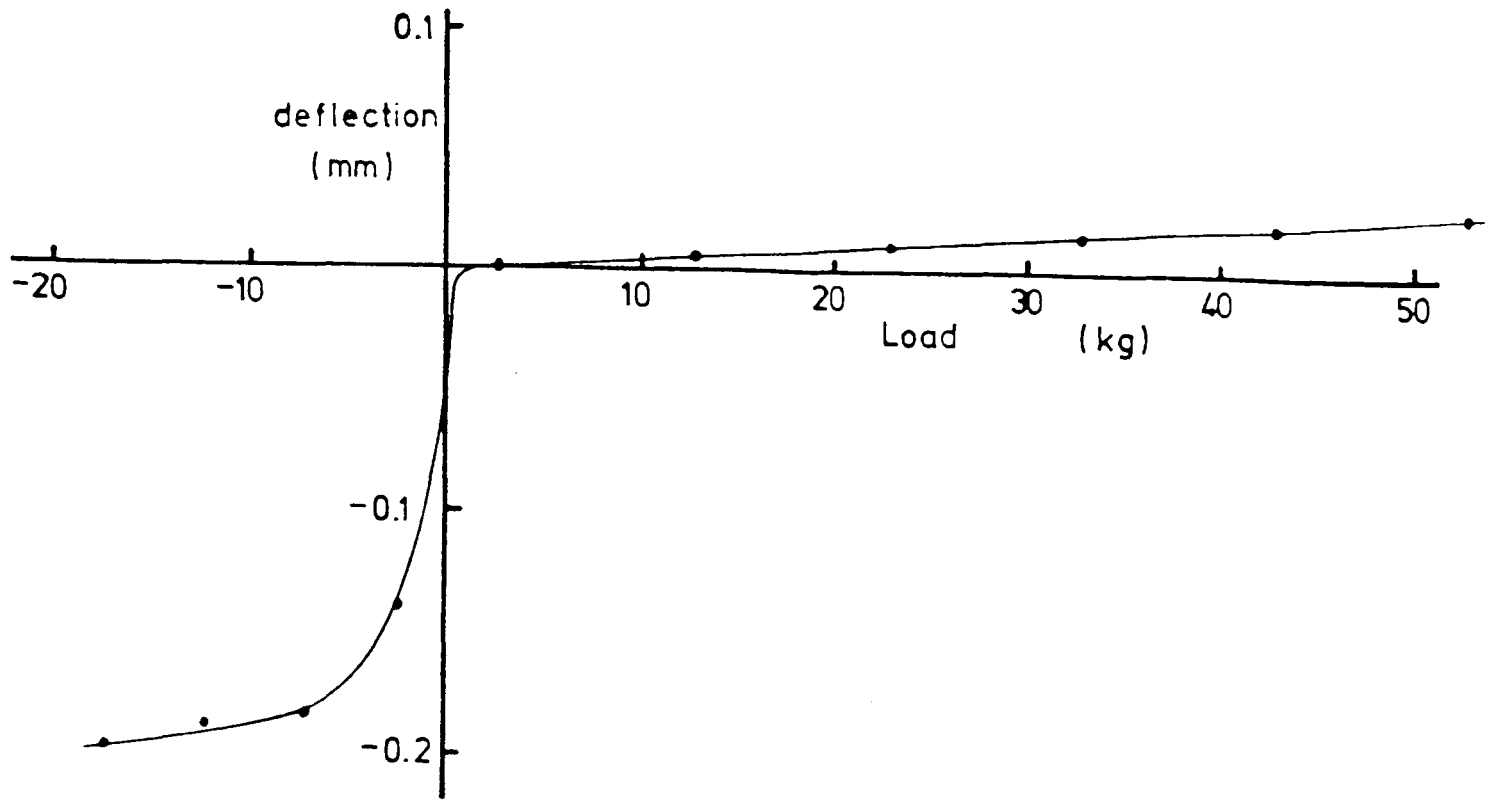

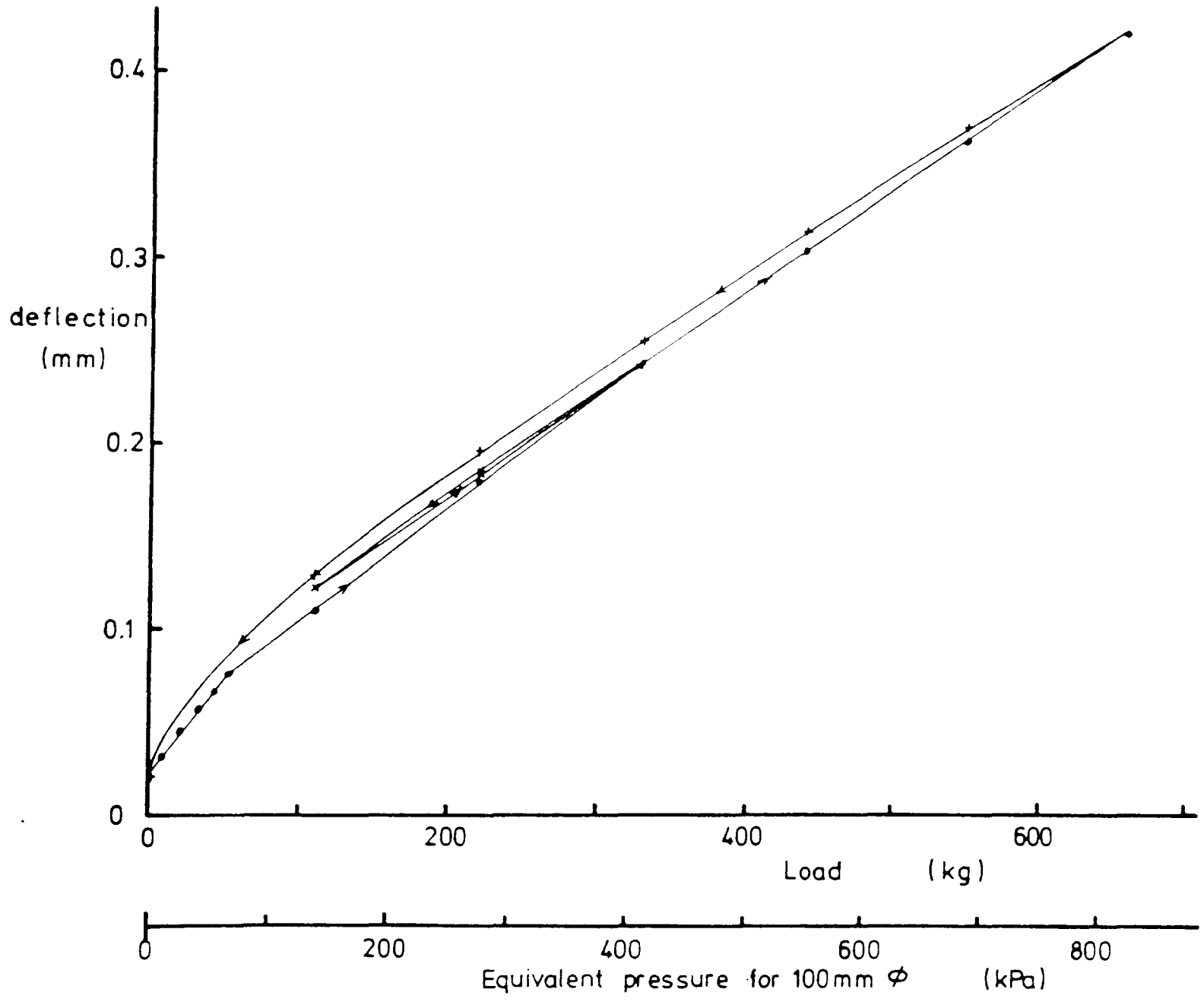

Fig 5.6 Typical load - deflection characteristics for a load cell

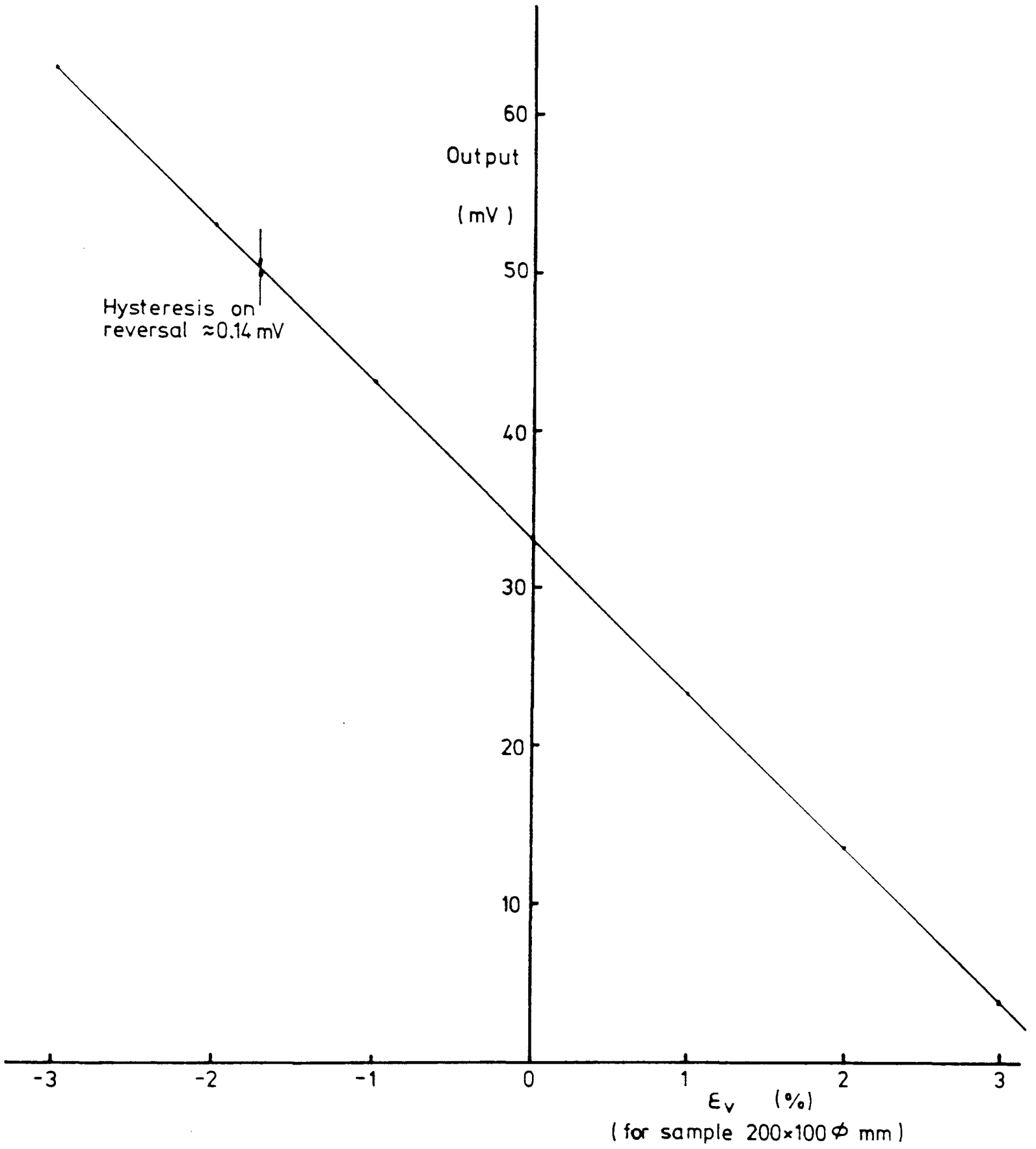

Fig 5.7 Typical volume gauge calibration

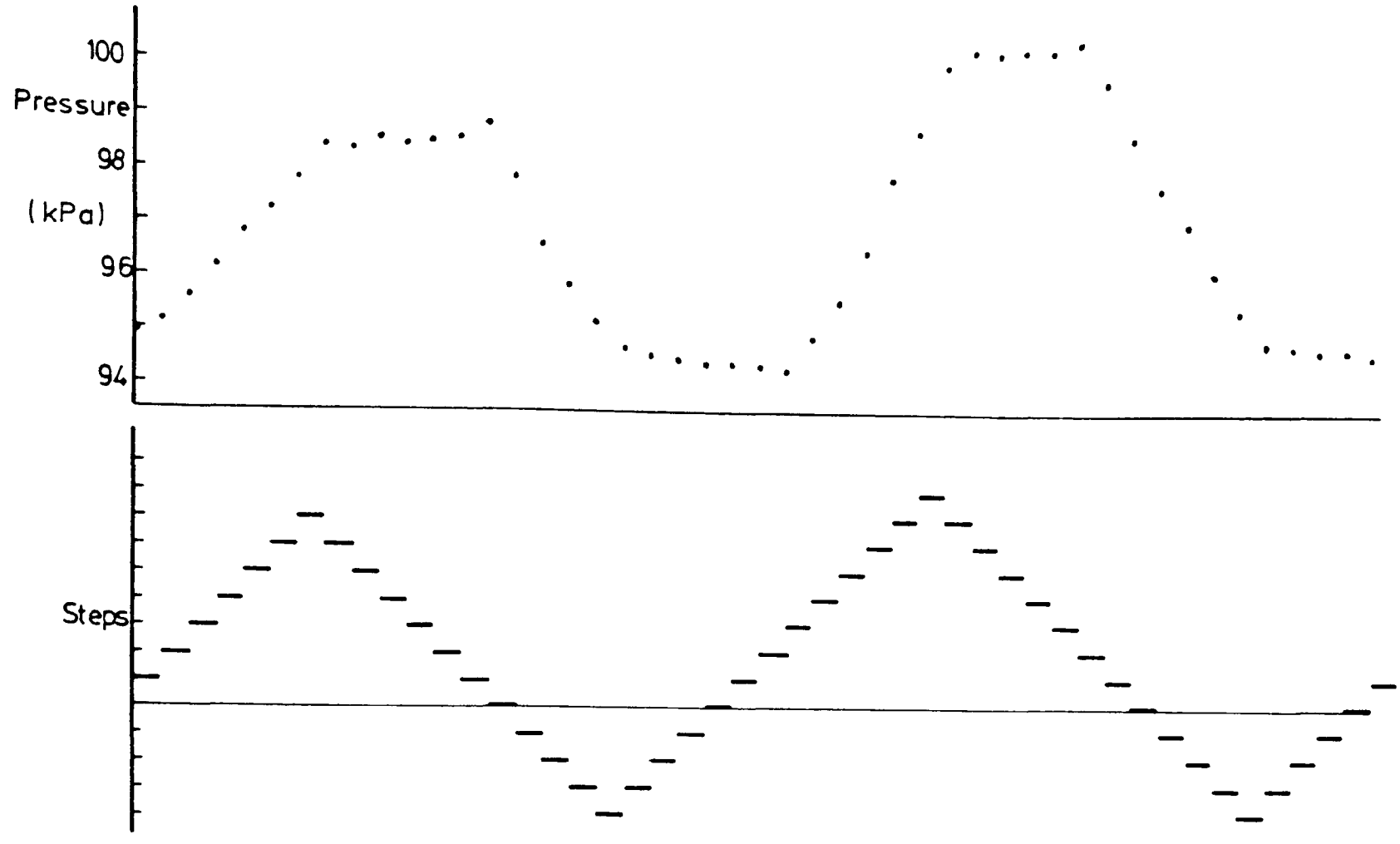

Fig 5.8 Electromanostat control using stepper motors

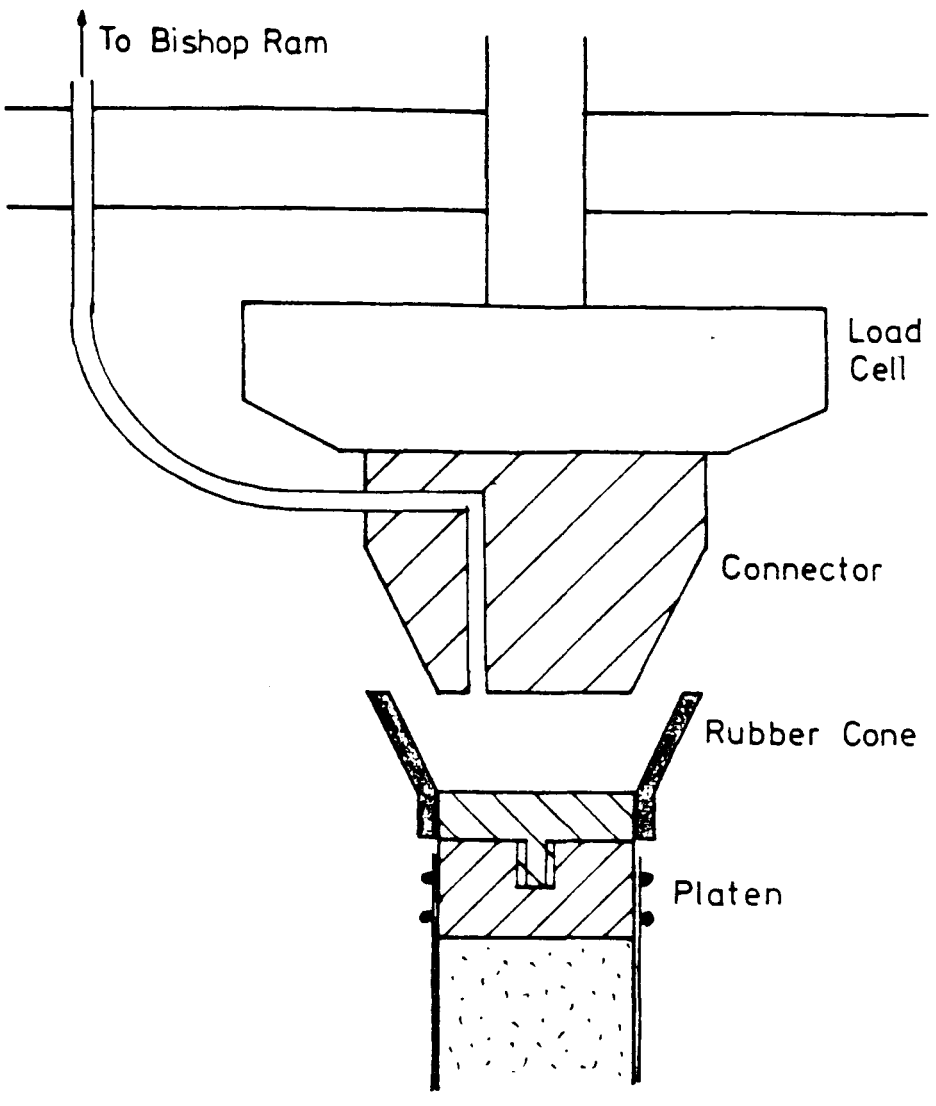

Fig 5.9 Top platen and suction cap fitting arrangement

CHAPTER 6

LABORATORY TESTING AND RESULTS

6.1 THE SOIL

The soil tested was a heavily overconsolidated Gault Clay from Selborne, Hampshire. A site at Selborne Brick Works was investigated by Southampton University as a possible test bed site. A standard site investigation was carried out, comprising eight cable percussion boreholes located at various positions on a recently excavated slope. The location of the site is shown on Figure 6.1, and a borehole plan is given on Figure 6.2. The soil samples were obtained using standard U100 thin walled open driven tube samplers of 100mm diameter.

The Gault Clay tested was found to be very uniform and consisted of stiff becoming very stiff, dark grey, fissured, silty clay containing gypsum in places, with traces of fossils. It dates from the Cretaceous period and is very heavily overconsolidated. The clay pit at the brick works penetrated the Gault Clay near its base, and the transition to the underlying Lower Greensand was located in the boreholes. Further information on the geology of the site was given by Cooper (1986), and a cross-section through the boreholes is reproduced as Figure 6.3.

Tests on typical samples gave liquid and plastic limits of 73 per cent and 26 per cent respectively, with a specific gravity of 2.73. A particle size distribution determined by the hydrometer method (BS 1377: 1975 Test 7D) is shown in Figure 6.4. The moisture contents and densities of the samples tested are given on Table 6.1.

6.2 DATA PRESENTATION

All the triaxial test data presented in the following sections are the product of the automatic recording and control systems described in the previous chapter. Data was recorded continually throughout each test stage at frequent intervals, with up to 150 records per stage. The close spacing of these points on graphs enables good definition of the line drawn through the points. For this reason, the results are presented as lines on graphs and individual data points are omitted for clarity.

The strains used throughout this thesis are natural strains.

6.3 RECONSTITUTED SAMPLES

6.3.1 Compression and Swelling

One reconstituted sample was compressed isotropically to p'=600kPa and swelled back to p'=50kPa. A second reconstituted sample underwent K_o compression and swelling. In addition, four further specimens were compressed isotropically to p'=200kPa prior to shearing. All the tests were on 38mm diameter samples. Details are given on the schedule in Table 6.2, and the test results are plotted on Figure 6.5. The stress path for K_o compression and swelling (Test R2) is shown on Figure 6.6.

6.3.2. Compression and Extension

Uniaxial compression and extension tests were performed on four reconstituted 38mm diameter specimens. Each test was commenced at an isotropic stress state of p'=200kPa. Two of the tests were undrained, one in compression and the other in extension. The remaining two tests were drained, in compression and extension. Details are given in the schedule on Table 6.2. The basic test data is plotted on Figure 6.7. Volume change in the drained tests

is shown on Figure 6.8, and the undrained stress paths are given on Figure 6.9. Figure 6.10 shows the stress-strain curves.

6.4 UNDISTURBED SAMPLES, BASIC TESTS

6.4.1 Compression and Swelling

Several triaxial compression and swelling tests were made on undisturbed samples as detailed on Table 6.3. These were generally carried out as initial or intermediate stages for shearing or stress probe tests.

The results are plotted as v-ln(p') curves on Figure 6.11. Figure 6.12 shows the stress-strain curves for the compression tests, with the anisotropic strain response plotted on Figure 6.13. The corresponding data for the swelling tests is given on Figures 6.14 and 6.15.

In Test C6 the sample was compressed isotropically to p'=300kPa, followed by compression and swelling under conditions of zero lateral strain. The stress path for this test is included on Figure 6.6.

6.4.2 Oedometer Compression

Two oedometer tests were carried out on undisturbed samples in accordance with BS1377:1975 Test 17. Details are given on Table 6.4, and the compression curves are plotted on Figure 6.16.

6.4.3 Consolidation

Triaxial consolidation tests, numbered D1 to D3, were carried out subsequent to compression tests C2, C5 and C6. Details are given on Table 6.5. The results are presented as consolidation curves on Figures 6.17 to 6.19.

Consolidation curves from the two oedometer tests are plotted on Figures 6.20 and 6.21.

6.4.4. Compression and Extension Tests

Six uniaxial triaxial compression and extension tests were carried out on undisturbed samples of 38mm diameter, as detailed on Table 6.6. Undrained compression and extension tests were conducted on four of the specimens consolidated to p'=100kPa and p'=300kPa. The remaining two tests were drained compression and extension tests from p'=300kPa. The basic test data is given on Figure 6.22. Volume change in the drained tests is shown on Figure 6.23, and the undrained stress paths are plotted on Figure 6.24. Figure 6.25 shows the stress-strain curves.

6.5 STRESS PROBE TESTS

6.5.1 Introduction

Eight tests, numbered P1 to P8, were carried out on undisturbed samples of 100mm diameter. Each test comprised a series of stress probes at various stress levels. A summary of the tests is given on Table 6.8, and a schedule is presented on Table 6.8. Further details of each stage of the tests is given in Appendix B.

For each probe, stresses were cycled about the initial stress state. Measurements were made of the stress-strain behaviour and undrained stress path, where appropriate. The objective of the stress probing was to study the soil deformation parameters. The slope of the relevant stress-strain curves will therefore be reported. Typical plots of the stress-strain data are shown in Figures 6.26 to 6.28 for Cycles 4 (constant p'), 6 (undrained) and 12 (isotropic) of Test P1. It can be seen that the stress-strain behaviour was found to be approximately linear for each

section of the cycle. The data was therefore processed on a microcomputer to determine the best straight line fit by the least squares method.

Particular attention was paid to the stress history of the soil prior to the first measurements during loading. On unloading or reloading, the data for the first half of the stress path was discounted as being subject to threshold effects, and with the pore pressures possibly not in equilibrium. The stress-strain slope was measured for the section of the stress probe after the initial stress state had been passed.

6.5.2 Test P1

A variety of stress path probes was carried out on a single sample based on an isotropic stress state of p'=300 kPa. The probes are detailed on Table 6.9 and illustrated on Figure 6.29. The resulting measurements are given in Table 6.10.

Each probe had a similar stress history, with the initial stress state being approached from below the p' axis on a constant p' path or the undrained effective stress path. In addition, a further cycle was made for stage 12 (numbered 12* in the results) in which the stress history was continuous with the isotropic stress probe followed.

6.5.3 Tests P2 and P3

A series of stress path probes was carried out at various values of mean effective stress. The probes comprised undrained cycles and isotropic stages. In addition, constant p' probes were made in Test P2. The results are given in Tables 6.11 to 6.13.

In Test P2 the stress history for each probe was continuous with the stress probe being followed. For Test P3 the start positions were approached on an isotropic stress path.

6.5.4 Tests P4 to P8

A series of stress path probes was carried out at different initial stress states. These comprised constant p' and constant q' probes as illustrated on Figure 6.30. The results are given in Tables 6.14 to 6.19.

For these tests the stress history was continuous with the stress probe direction.

6.6 CONSTANT p' TESTS TO FAILURE

Compression and extension at constant mean effective stress was carried out between stress probes in Tests P4 to P8. The samples were subsequently brought to failure at constant p', as indicated in the schedule in Table 6.8.

The basic test data for the constant p' sections of the stress probe tests are given on Figure 6.31. Figure 6.32 shows the stress-strain curves.

6.7 CONSTANT SHEAR STRAIN TESTS

A short series of constant shear strain tests was carried out on a single undisturbed sample of 38mm diameter. The specimen was first swelled isotropically to p'=100 kPa. Maintaining a constant back pressure the axial strain was increased very slowly. The radial strain was controlled to obtain a constant shear strain by using feedback control on the cell pressure.

At the end of the strain path, the sample was returned to an isotropic stress state and swelled back to p'=100 kPa. Undrained compression or extension was used to bring the specimen to a

different state of shear strain. The constant shear strain test was then repeated at this new value of ε_s. Five such strain paths were completed.

The stress-strain behaviour of the soil is shown in Figure 6.33 and the resulting stress paths are plotted on Figure 6.34.

Borehole	Depth (m)	Moisture Content (%)	Bulk Density (Mg/m^3)	Tests
4	4.6	22.1	2.09	C1,P2,P4
5	3.0	23.7	2.05	U6,C4
	3.0	23.5	2.06	U5,C3
	3.0	25.6	2.03	C2,D1,P3
6	4.5	20.5	2.10	O2
	4.5	20.9	2.10	P1,P5
	7.5	23.3	2.05	P8
	7.5	25.6	2.05	U3
7	4.5	22.5	2.09	C5,D2,R1-R6
8	3.5	26.9	2.01	C6,D3
	3.5	25.5	2.01	C8,U1
	3.5	25.8	2.01	U2
	3.5	25.4	2.01	C7
	6.2	27.5	1.99	C9
	8.3	22.5	2.09	O1
	8.3	23.5	2.05	C10,P7
	9.0	18.9	2.23	U4
	12.0	21.2	2.09	C11,P6

Table 6.1 Moisture Contents and Densities of Samples Tested

Test	Stage	Start p' (kPa)	Start v	End p' (kPa)	End v	Description
R1	1	4	2.543	600	1.834	Isotropic Compression
	2	600	1.834	50	1.988	Isotropic Swelling
R2	1	12	2.502	15	2.496	Raise σ'_a to K_o = 0.6
	2	15	2.496	393	1.880	K_o Compression
	3	393	1.880	44	2.059	K_o Swelling
R3	1	14	2.541	200	2.080	Isotropic Compression
	2	200	2.080	282	1.932	Drained Compression
R4	1	12	2.451	200	2.068	Isotropic Compression
	2	200	2.068	158	2.044	Drained Extension
R5	1	14	2.410	200	2.047	Isotropic Compression
	2	200	2.047	118	2.047	Undrained Compression
R6	1	15	2.432	200	2.062	Isotropic Compression
	2	200	2.062	122	2.062	Undrained Extension

Table 6.2 Schedule of Triaxial Tests for Reconstituted Samples

Test	Stage	Start p' (kPa)	Start v	End p' (kPa)	End v	Nominal Sample Diameter (mm)	Compression or Swelling
C1	1	500	1.593	300	1.606	100	S
C2	1	278	1.692	300	1.690	100	C
	2	289	1.690	400	1.677	100	C
	3	374	1.677	500	1.661	100	C
	4	477	1.661	400	1.666	100	S
	5	413	1.666	300	1.677	100	S
	6	312	1.677	200	1.694	100	S
C3	1	200	1.715	100	1.750	38	S
C4	1	202	1.734	300	1.721	38	C
C5	1	193	1.673	600	1.627	100	C
	2	600	1.627	310	1.646	100	S
	3	330	1.646	100	1.685	100	S
C6	1	150	1.708	300	1.680	100	C
	2	300	1.680	497	1.644	100	CK_o
	3	497	1.644	300	1.611	100	SK_o
C7	1	227	1.732	100	1.732	138	S
C8	1	212	1.738	300	1.724	38	C
C9	1	106	1.749	300	1.711	100	C
	2	300	1.709	200	1.720	100	S
C10	1	358	1.637	260	1.645	100	S
C11	1	405	1.582	260	1.595	100	S
	2	205	1.594	540	1.578	100	C

Table 6.3 Schedule of Triaxial Compression and Swelling Tests for Undisturbed Samples.

Test	Stage	Start		End	
		σ_v' (kPa)	v	σ_v' (kPa)	v
01	1	321	1.676	428	1.670
	2	428	1.670	856	1.638
	3	856	1.638	1712	1.603
	4	1712	1.603	3424	1.545
02	1	321	1.631	428	1.626
	2	428	1.626	856	1.602
	3	856	1.602	1712	1.568
	4	1712	1.568	3424	1.515

Table 6.4 Schedule of Oedometer Tests, Undisturbed Samples.

Test	Stage	Start		End		Description
		p' (kPa)	v	p' (kPa)	v	
D1	1	128	1.685	200	1.674	Consolidation
	2	200	1.674	400	1.660	Consolidation
	3	400	1.660	600	1.637	Consolidation
D2	1	300	1.663	400	1.653	Consolidation
	2	395	1.653	600	1.635	Consolidation
D3	1	212	1.694	400	1.670	Consolidation

Table 6.5 Schedule of Triaxial Consolidation Tests Undisturbed Samples.

Test	Stage	Start p' (kPa)	Start v	End p' (kPa)	End v	Description
U1	1	212	1.738	300	1.724	Isotropic Compression
	2	300	1.724	415	1.693	Drained Compression
U2	1	206	1.732	300	1.713	Isotropic Compression
	2	300	1.713	236	1.744	Drained Extension
U3	1	122	1.747	100	1.755	Isotropic Swelling
	2	100	1.755	147	1.755	Undrained Compression
U4	1	210	1.582	300	1.567	Isotropic Compression
	2	300	1.567	307	1.567	Undrained Compression
U5	1	200	1.715	100	1.750	Isotropic Swelling
	2	100	1.750	211	1.750	Undrained Extension
U6	1	202	1.734	300	1.721	Isotropic Compression
	2	300	1.721	341	1.721	Undrained Extension

Table 6.6 Schedule of Basic Tests for Undisturbed Samples

Test	Borehole	Depth (m)	Description
P1*	6	4.5	Various stress paths at p_o'=300, q_o'=0
P2*	4	4.6	Const. q' and const. p' probes and undrained probes at different values of p'
P3	5	3.0	Undrained probes at different values of p'
P4*	4	4.6	Const. q' and const. p' probes p_o'=100, q_o'=0 & 100
P5*	6	4.5	Const. q' and const. p' probes p_o'=300, q_o'=0, 100, 200, 300
P6	8	12.0	Const. q' and const. p' probes p_o'=500, q_o'=0, 200, 400
P7	8	8.3	Const. q' and const. p' probes p_o'=300, q_o'=0, -100, -200
P8	6	7.5	Const. q' and const. p' probes p_o'=500, q_o'=0 & -200
All	-	-	All tests have const. q' and const. p' probes at p_o'=300, q_o'=0

* Notes: Tests P1 & P5 were conducted consecutively on the same sample
Tests P2 & P4 were conducted consecutively on the same sample

Table 6.7 Summary of Stress Probe Tests

Test	Stage	p_o' (kPa)	q_o' (kPa)	v_o	Description
P1	1	300	0	1.576	Undr. Uniaxial probe
	2	300	0	1.577	Undr. uniaxial probe
	3	300	0	1.577	Undr. $\Delta q=-\Delta p$ probe
	4	300	0	1.577	Const. p' probe
	5	300	0	1.577	$\Delta q'=\Delta p'$ probe
	6	300	0	1.578	Undr. uniaxial probe
	7	300	0	1.578	Undr. $\Delta q = \Delta p$ probe
	8	300	0	1.578	$\Delta q'=-\Delta p'$ probe
	9	300	0	1.577	Undr. uniaxial probe
	10	300	0	1.577	Drained uniaxial probe
	11	300	0	1.577	Const. p' probe
	12	300	0	1.577	Isotropic probe
	13	300	0	1.577	Undr. uniaxial probe
P2	1	500	0	1.596	Undr. Uniaxial probe
	2	500	0	1.596	Const. p' probe
	3	500	0	1.595	Undr. uniaxial probe
	4	500	0	1.595	Const q' probe
	5	500	0	1.593	Isot. swelling to p'=300
	6	300	0	1.606	Undr. uniaxial probe
	7	300	0	1.607	Const. p' probe
	8	300	0	1.608	Undr. uniaxial probe
	9	300	0	1.608	Isotropic probe
	10	300	0	1.608	Isot. swelling to p'=100
	11	100	0	1.675	Undr. uniaxial probe
	12	100	0	1.675	Const p' probe
	13	100	0	1.676	Undr. uniaxial probe
	14	100	0	1.676	Isotropic probe
P3	1	374	0	1.677	Isot. compression
	2	500	0	1.661	Undr. uniaxial probe
	3	477	0	1.661	Isot. swelling
	4	400	0	1.666	Undr. uniaxial probe
	5	413	0	1.666	Isot. swelling
	6	300	0	1.677	Undr. uniaxial probe
	7	312	0	1.677	Isot. swelling
	8	200	0	1.694	Undr. uniaxial probe
P4	1	100	0	1.675	Undr. uniaxial probe
	2	100	0	1.675	Const. p' probe
	3	100	0	1.676	Undr. uniaxial probe
	4	100	0	1.676	Isotropic probe
	5	100	0	1.677	Undr. uniaxial probe
	6	100	0	1.677	Const. p' loading
	7	100	100	1.675	Const q' probe
	8	100	100	1.673	Const p' load to failure

Table 6.8 Schedule of Stress Probe Tests

Cont'd/-

Test	Stage	p_o' (kPa)	q_o' (kPa)	v_o	Description
P5	1	300	0	1.577	Const p' probe
	2	300	0	1.577	Isotropic probe
	3	300	0	1.577	Undr. uniaxial probe
	4	303	0	1.577	Const. p' loading
	5	303	100	1.575	Const. q' probe
	6	300	100	1.575	Const. p' loading
	7	300	200	1.574	Const. q' probe
	8	300	200	1.573	Const p' loading
	9	300	300	1.573	Const q' probe
	10	300	300	1.573	Const p' load to failure
P6	1	300	0	1.582	Isotropic probe
	2	300	0	1.593	Undr. uniaxial probe
	3	305	0	1.593	Const. p' probe
	4	305	0	1.594	Isotropic compression
	5	500	0	1.579	Isotropic probe
	6	500	0	1.578	Const p' probe
	7	500	0	1.578	Const p' loading
	8	500	200	1.573	Isotropic probe
	9	500	200	1.574	Const. p' probe
	10	500	200	1.574	Const. p' loading
	11	500	400	1.571	Const. q' probe
	12	500	400	1.571	Const. p' probe
	13	500	400	1.571	Const. p' load to failure
P7	1	300	0	1.643	Isotropic probe
	2	300	0	1.643	Undr. uniaxial probe
	3	305	0	1.643	Const. p' probe
	4	305	0	1.643	Const. p' unloading
	5	300	-100	1.647	Const. q' probe
	6	300	-100	1.647	Const. p' probe
	7	300	-100	1.647	Const. p' unloading
	8	300	-200	1.656	Const. q' probe
	9	300	-200	1.656	Const. p' probe
	10	300	-200	1.656	Const. p' unload to fail
P8	1	300	0	1.645	Isotropic probe
	2	300	0	1.645	Const. p' probe
	3	350	0	1.641	Isotropic compression
	4	500	0	1.631	Isotropic probe
	5	500	0	1.631	Const. p' probe
	6	500	0	1.631	Const. p' unloading
	7	500	-200	1.633	Const. q' probe
	8	500	-200	1.633	Const. p' probe
	9	500	-200	1.633	Const p' unload to fail

Table 6.8 (Cont'd) Schedule of Stress Probe Tests

Cycle	Stress path probes	
	Undrained	Drained
1	Uniaxial	
2	Uniaxial	
3	$\Delta q = -\Delta p$	
4		Const. p'
5		$\Delta q' = \Delta p'$
6	Uniaxial	
7	$\Delta q = \Delta p$	
8		$\Delta q' = -\Delta p'$
9	Uniaxial	
10		Uniaxial
11		Const. p'
12		Const. q'
13	Uniaxial	

Table 6.9 Stress Path Probes for Test P1 at $p_o' = 300$, $q_o' = 0$

Cycle	v_o	Slopes (MPa)				Slope
		$q':\varepsilon_s$	$q':\varepsilon_v$	$p':\varepsilon_s$	$p':\varepsilon_v$	$q':p'$
1	1.576	76	-	-18	-	-4.6
2	1.577	82	-	-14	-	-6.0
3	1.577	78	-	-16	-	-5.1
4	1.577	60	190	-	-	
5	1.577	32	22	31	22	
6	1.578	64	-	-17	-	-3.9
7	1.578	61	-	-13	-	-4.8
8	1.578	88	40	-86	40	
9	1.577	67	-	-10	-	-6.3
10	1.577	53	73	18	26	
11	1.577	55	84	-	-	
12	1.577	-	-	69	32	
12*	1.577	-	-	64	23	
13	1.577	97	-	-18	-	-5.3

* No change in stress path direction

Table 6.10(a) Stress-Strain and Undrained Stress Path Slopes - Loading
Test P1
Various Stress Path Probes at $p_o'=300$, $q_o'=0$

Cycle	v_o	Slopes (MPa)				Slope
		$q':\varepsilon_s$	$q':\varepsilon_v$	$p':\varepsilon_s$	$p':\varepsilon_v$	$q':p'$
1	1.576	66	-	-17	-	-4.2
2	1.577	58	-	-16	-	-4.2
3	1.577	74	-	-19	-	-3.5
4	1.577	50	94	-	-	
5	1.577	25	17	27	17	
6	1.578	87	-	-24	-	-3.6
7	1.578	100	-	-18	-	-3.5
8	1.578	230	-30	-550	30	
9	1.577	105	-	-26	-	-4.3
10	1.577	38	40	13	13	
11	1.577	58	88	-	-	
12	1.577	-	-	75	26	
13	1.577	89	-	-25	-	-3.5

Table 6.10(b) Stress-Strain and Undrained Stress Path Slopes - Unloading
Test P1
Various Stress Path Probes at $p_o'=300$, $q_o'=0$

Cycles	p_o'	q_o'	v_o	Slopes (MPa)			
				$q':\varepsilon_s$	$q':\varepsilon_v$	$p':\varepsilon_s$	$p':\varepsilon_v$
12,14	100	0	1.675	35	105	49*	14*
7,9	300	0	1.607	62	-370	105*	38*
2,4	500	0	1.596	60	120	180	43

* First Loading

(a) Loading

Cycles	p_o'	q_o'	v_o	Slopes (MPa)			
				$q':\varepsilon_s$	$q':\varepsilon_v$	$p':\varepsilon_s$	$p':\varepsilon_v$
12,14	100	0	1.675	16	74	67	16
7	300	0	1.607	19	93	-	-
2,4	500	0	1.596	39	120	110	34

(b) Unloading

Table 6.11 Stress-Strain Slopes
Test P2
Constant p' and Constant q' Probes

Cycle	p_o'	q_o'	v_o	Slopes (MPa)		Slope
				$q':\varepsilon_s$	$p':\varepsilon_s$	$q':p'$
13	100	0	1.676	39	-4	-9.6
8	300	0	1.608	96	-16	-5.4
3	500	0	1.595	150	-27	-5.2

(a) Loading

Cycle	p_o'	q_o'	v_o	Slopes (MPa)		Slope
				$q':\varepsilon_s$	$p':\varepsilon_s$	$q':p'$
13	100	0	1.676	18	-8	-7.2
8	300	0	1.608	40	-12	-4.4
3	500	0	1.595	68	-14	-4.6

(b) Unloading

Table 6.12 Stress-Strain and Undrained Stress Path Slopes
Test P2
Undrained Cycles

Cycles	p_o'	q_o'	v_o	Slopes (MPa)		Slope
				$q':\varepsilon_s$	$p':\varepsilon_s$	$q':p'$
8	200	0	1.694	57	-5	-9.6
6	300	0	1.677	59	-11	-4.0
4	400	0	1.666	140	-14	-15.9
2	500	0	1.661	70	-25	-2.8

(a) Loading

Cycles	p_o'	q_o'	v_o	Slopes (MPa)		Slope
				$q':\varepsilon_s$	$p':\varepsilon_s$	$q':p'$
8	200	0	1.694	31	-8	-4.8
6	300	0	1.677	34	-11	-3.4
4	400	0	1.666	36	-13	-2.8
2	500	0	1.661	41	-10	-4.1

(b) Unloading

Table 6.13 Stress-Strain and Undrained Stress Path Slopes
Test P3
Undrained Cycles

Cycles	p_o'	q_o'	v_o	Slopes (MPa)			
				$q':\varepsilon_s$	$q':\varepsilon_v$	$p':\varepsilon_s$	$p':\varepsilon_v$
2,4	100	0	1.675	34	105	53	14
7,8	100	100	1.677	25	100	38*	14*

* First Loading

(a) Loading

Cycles	p_o'	q_o'	v_o	Slopes (MPa)			
				$q':\varepsilon_s$	$q':\varepsilon_v$	$p':\varepsilon_s$	$p':\varepsilon_v$
2,4	100	0	1.675	26	78	67	17
7	100	100	1.677	-	-	350	41

(b) Unloading

Table 6.14 Stress-Strain Slopes
Test P4
Constant p' and Constant q' Probes

Cycles	p_o'	q_o'	v_o	Slopes (MPa)			
				$q':\varepsilon_s$	$q':\varepsilon_v$	$p':\varepsilon_s$	$p':\varepsilon_v$
1,2	300	0	1.577	60	190	64	23
5,6	300	100	1.575	30	290	50	33
7,8	300	200	1.574	48	-510	46	32
9,10	300	300	1.573	18	-66	32	37

(a) Loading

Cycles	p_o'	q_o'	v_o	Slopes (MPa)			
				$q':\varepsilon_s$	$q':\varepsilon_v$	$p':\varepsilon_s$	$p':\varepsilon_v$
1,2	300	0	1.577	50	94	75	26
5	300	100	1.575	-	-	590	46
7	300	200	1.574	-	-	900	39
9	300	300	1.573	-	-	-180	36

(b) Unloading

Table 6.15 Stress-Strain Slopes
Test P5
Constant p' and Constant q' Probes

Cycles	p_o'	q_o'	v_o	Slopes (MPa)			
				$q':\varepsilon_s$	$q':\varepsilon_v$	$p':\varepsilon_s$	$p':\varepsilon_v$
5,6	500	0	1.579	105	140	100	27
8,9	500	200	1.575	120	250	170	53
11,12	500	400	1.571	51	470	120	84

(a) Loading

Cycles	p_o'	q_o'	v_o	Slopes (MPa)			
				$q':\varepsilon_s$	$q':\varepsilon_v$	$p':\varepsilon_s$	$p':\varepsilon_v$
5,6	500	0	1.579	75	340	150	44
8,9	500	200	1.575	190	1100	200	68
11,12	500	400	1.571	220	∞	280	105

(b) Unloading

Table 6.16 Stress-Strain Slopes
Test P6
Constant p' and Constant q' Probes

Cycles	p_o'	q_o'	v_o	Slopes (MPa)			
				$q':\varepsilon_s$	$q':\varepsilon_v$	$p':\varepsilon_s$	$p':\varepsilon_v$
1,3	300	0	1.643	57	76	58	20
5,6	300	-100	1.647	50	45	47	18
8,9	300	-200	1.656	46	47	47	16

(a) Loading

Cycles	p_o'	q_o'	v_o	Slopes (MPa)			
				$q':\varepsilon_s$	$q':\varepsilon_v$	$p':\varepsilon_s$	$p':\varepsilon_v$
1,3	300	0	1.643	41	67	45	16
5,6	300	-100	1.647	47	58	48	17
8,9	300	-200	1.656	55	63	48	17

(b) Unloading

Table 6.17 Stress-Strain Slopes
Test P7
Constant p' and Constant q' Probes

Cycles	p_o'	q_o'	v_o	Slopes (MPa)			
				$q':\varepsilon_s$	$q':\varepsilon_v$	$p':\varepsilon_s$	$p':\varepsilon_v$
4,5	500	0	1.631	40	130	98	36
7,8	500	-200	1.633	220	220	74	34

(a) Loading

Cycles	p_o'	q_o'	v_o	Slopes (MPa)			
				$q':\varepsilon_s$	$q':\varepsilon_v$	$p':\varepsilon_s$	$p':\varepsilon_v$
4,5	500	0	1.631	69	160	105	42
7,8	500	-200	1.633	95	260	105	42

(b) Unloading

Table 6.18 Stress-Strain Slopes
Test P8
Constant p' and Constant q' Probes

Test	Cycles	v_o	Slopes (MPa)			
			$q':\varepsilon_s$	$q':\varepsilon_v$	$p':\varepsilon_s$	$p':\varepsilon_v$
P1	4,12*	1.577	60	190	64	23
P2	7,9	1.607	62	-370	105$	38$
P3	7	1.690	-	-	33	15
P4			As Test P2			
P5			As Test P1			
P6	1,3	1.594	61	98	105	28
P7	1,3	1.643	57	76	58	20
P8	1,2	1.645	45	73	66	23

$ First loading

(a) Loading

Test	Cycles	v_o	Slopes (MPa)			
			$q':\varepsilon_s$	$q':\varepsilon_v$	$p':\varepsilon_s$	$p':\varepsilon_v$
P1	11,12*	1.577	50	94	75	26
P2	7,9	1.607	19	93	-	-
P3	7	1.677	-	-	49	13
P4			As Test P2			
P5			As Test P1			
P6	1,3	1.594	53	105	64	15
P7	1,3	1.643	41	67	45	16
P8	1,2	1.645	34	88	57	21

(b) Unloading

Table 6.19 Stress-Strain Slopes
All Tests at $p_o'=300$, $q_o'=0$
Constant p' and Constant q' Probes

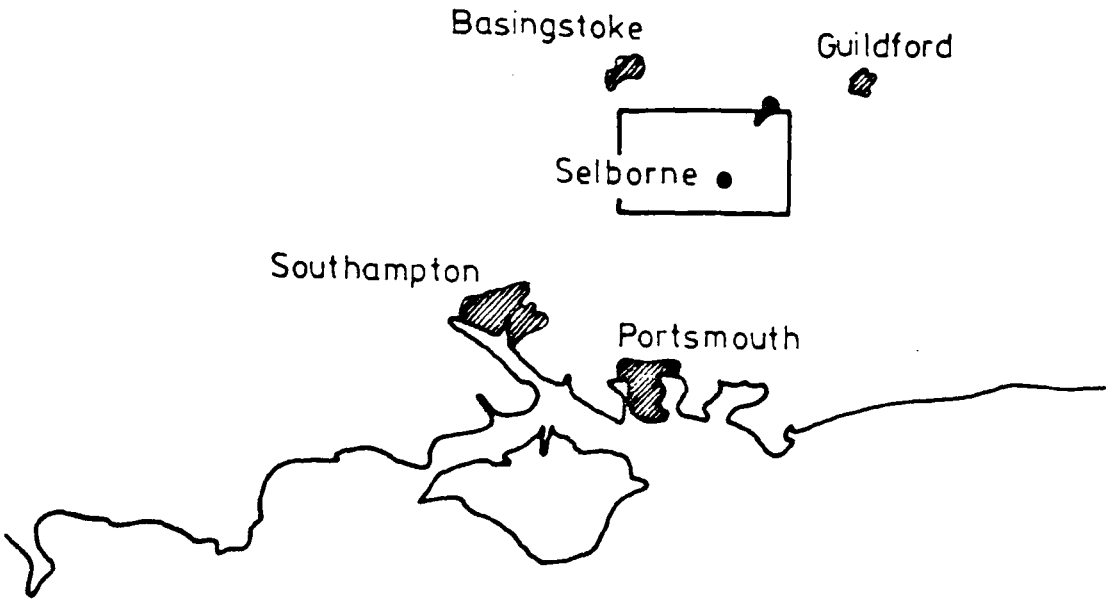

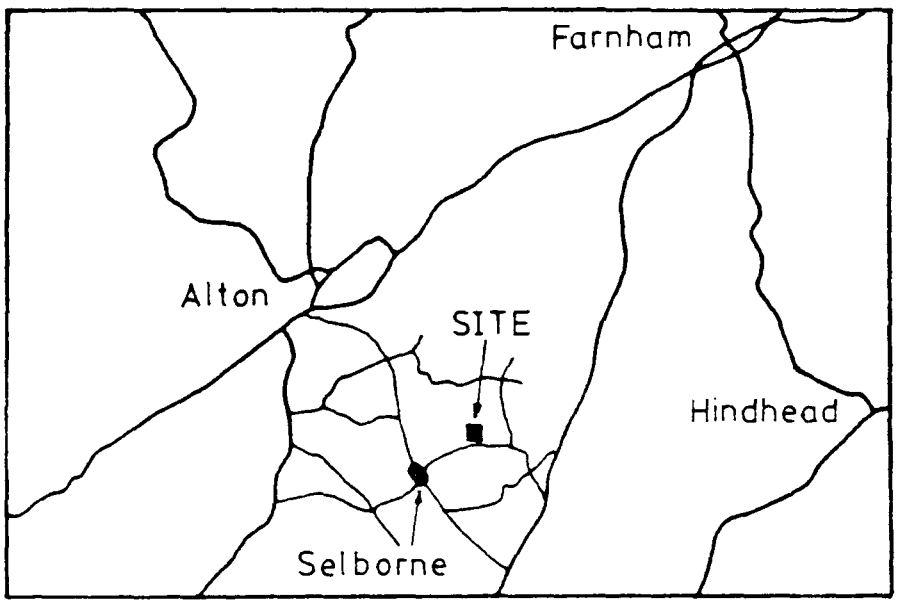

Fig 6.1 Site location

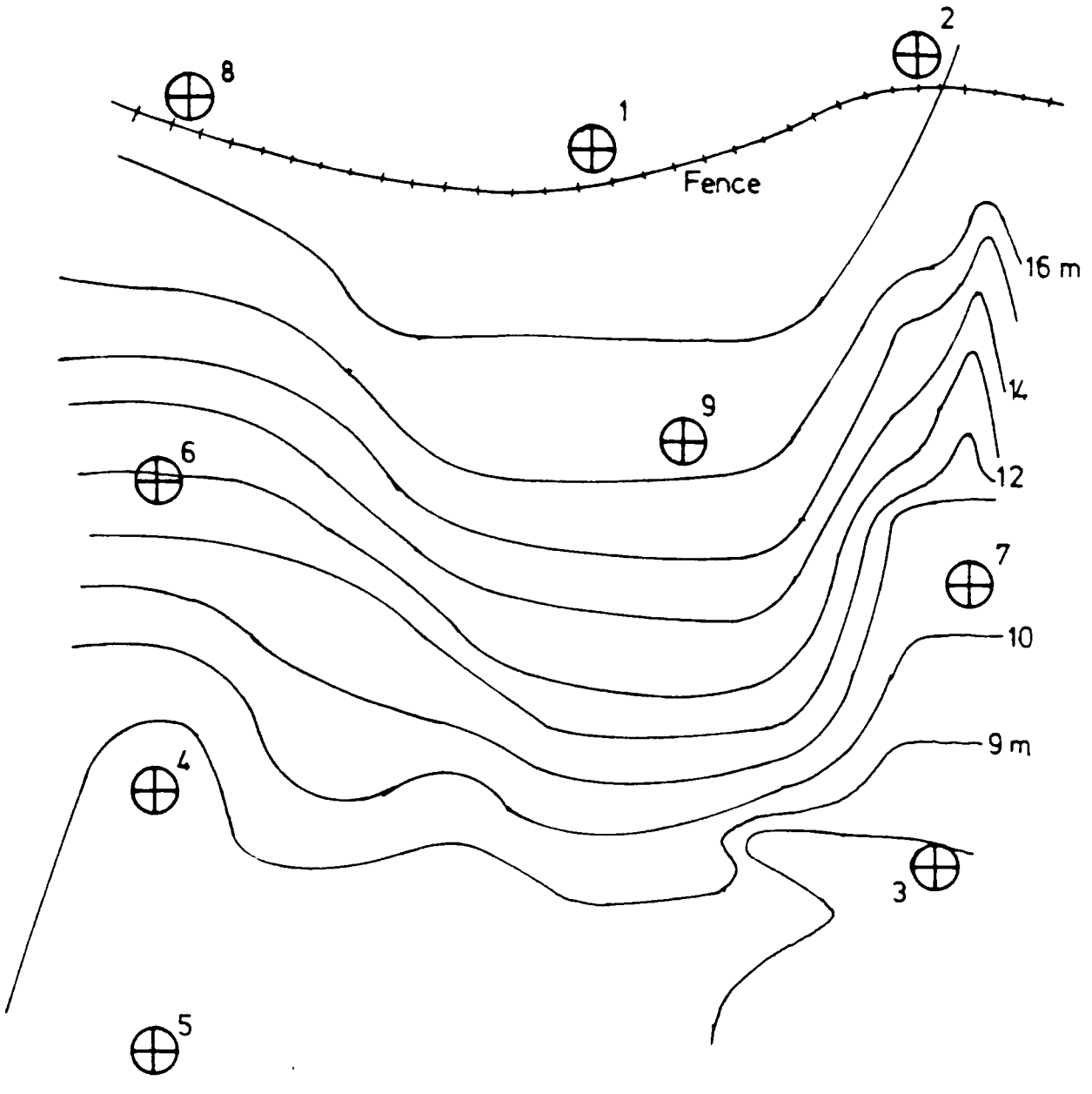

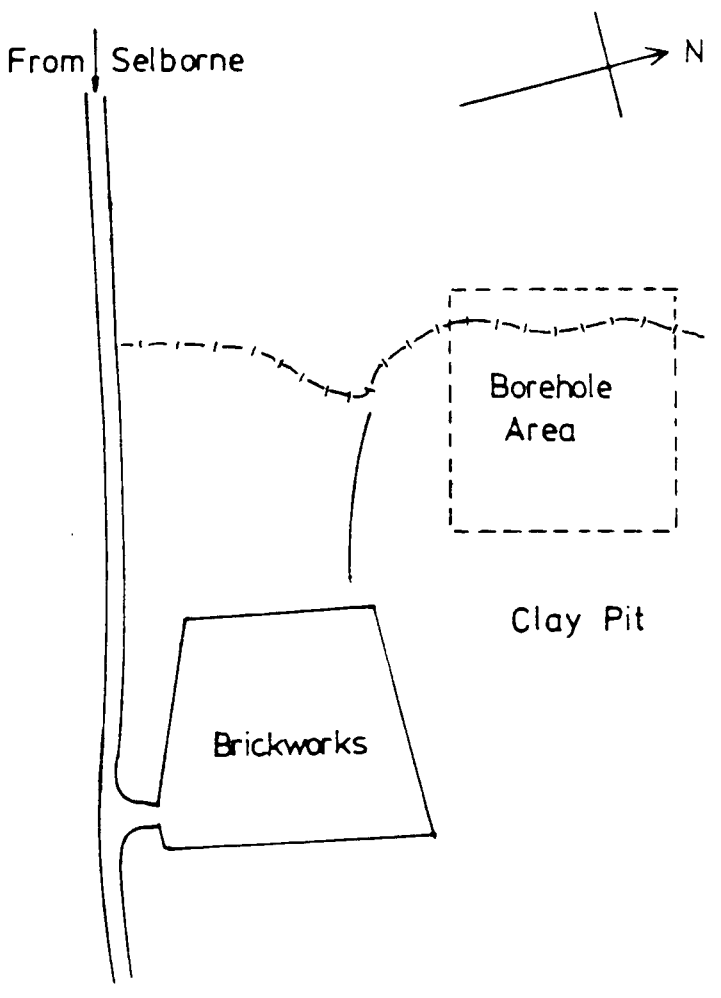

Fig 6.2 Borehole location plan

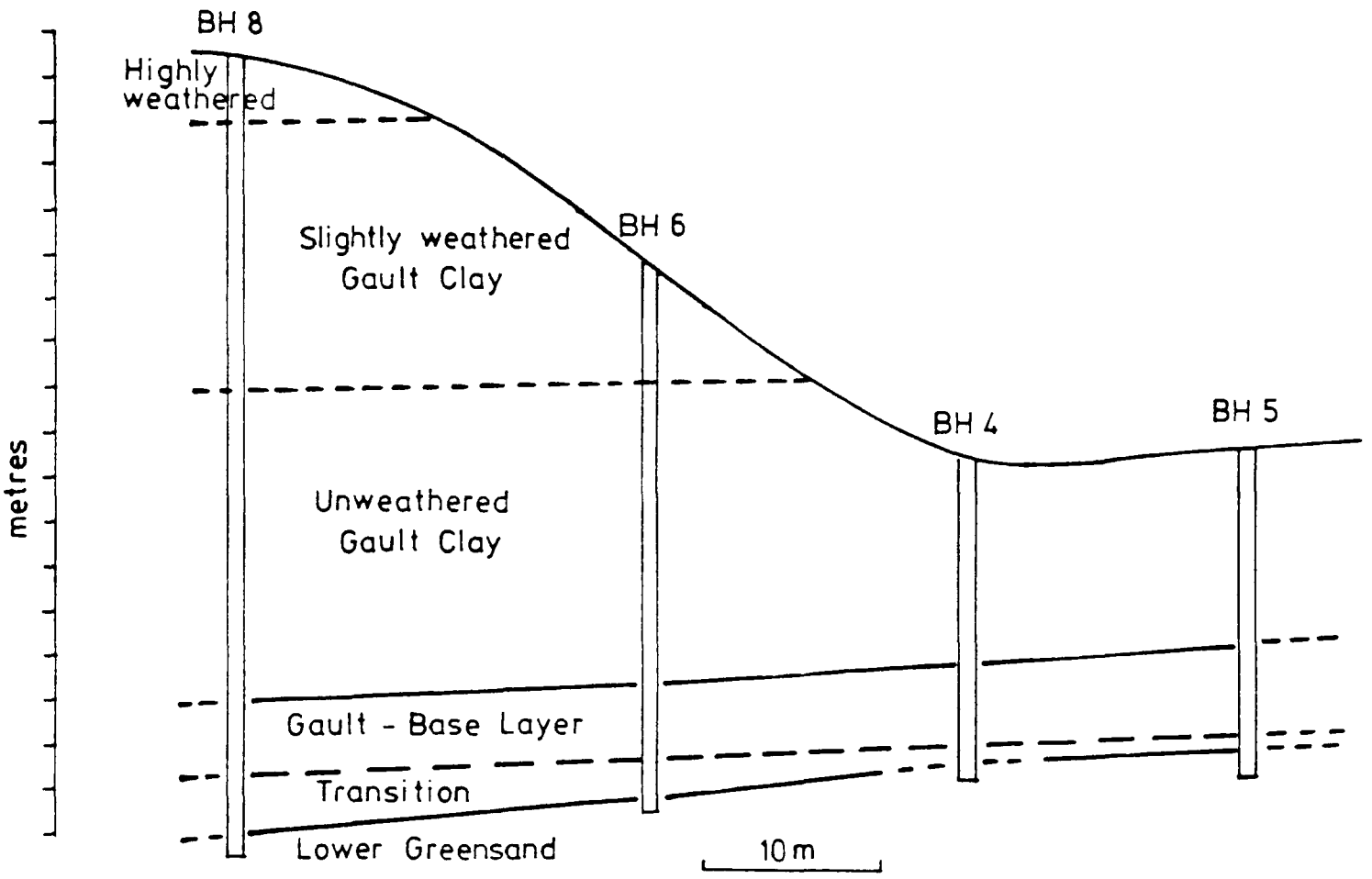

Fig 6.3 Borehole cross - section

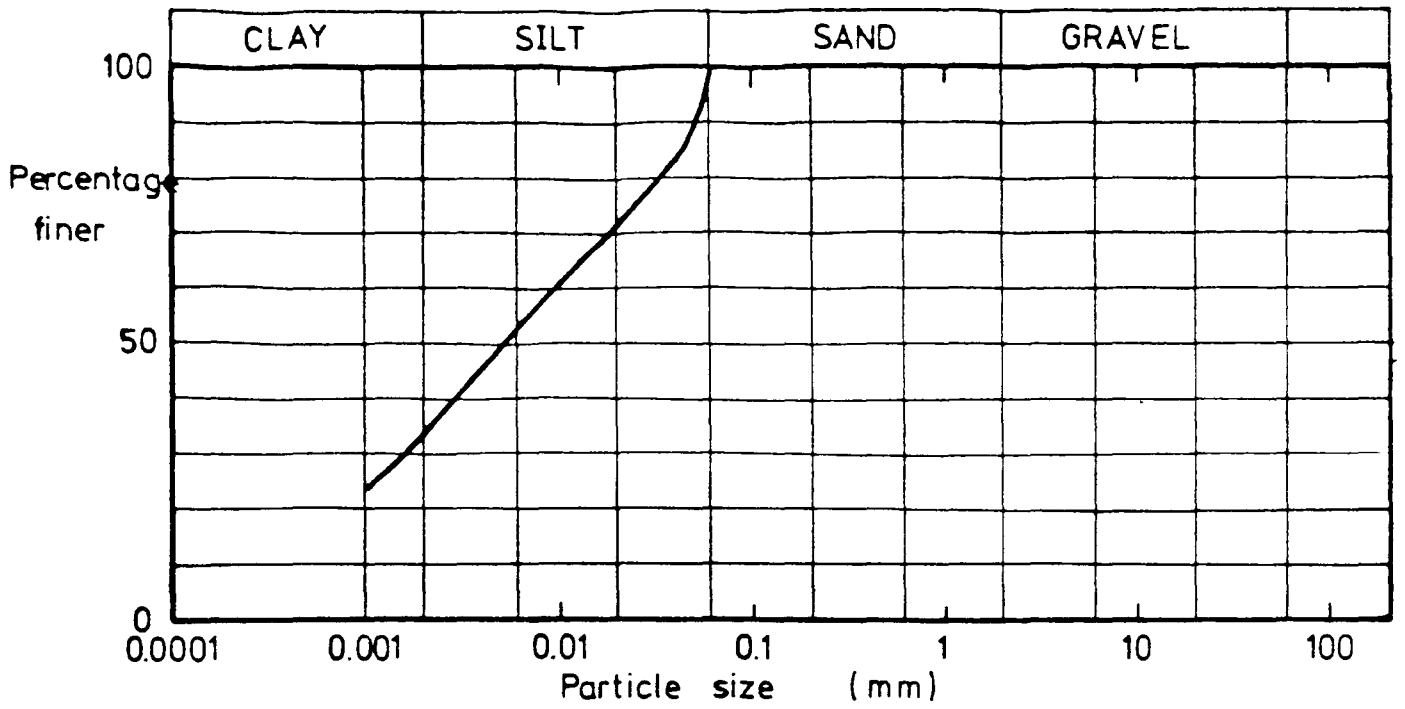

Fig 6.4 Typical particle size distribution

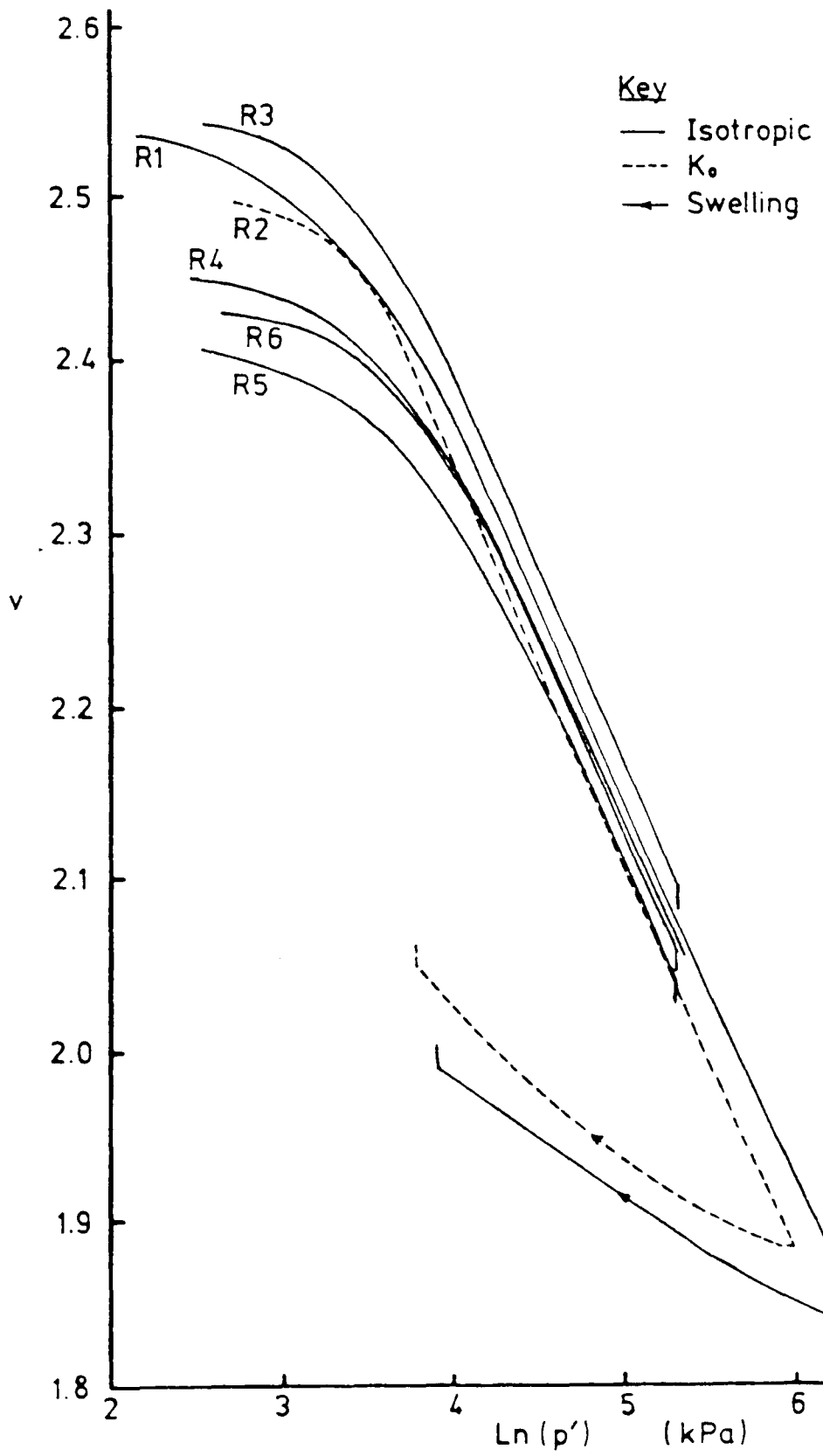

Fig 6.5 Compression and swelling test results, reconstituted samples

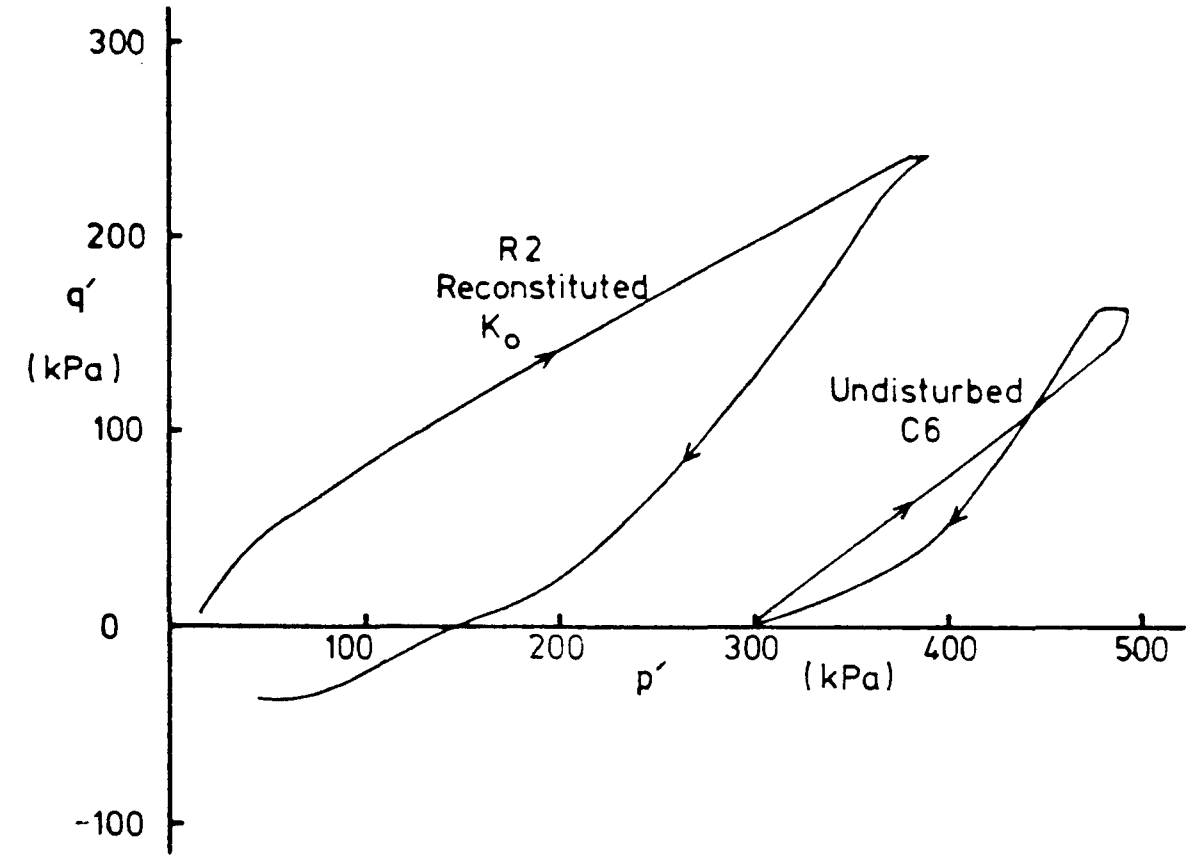

Fig 6.6 Stress paths for anisotropic compression and swelling

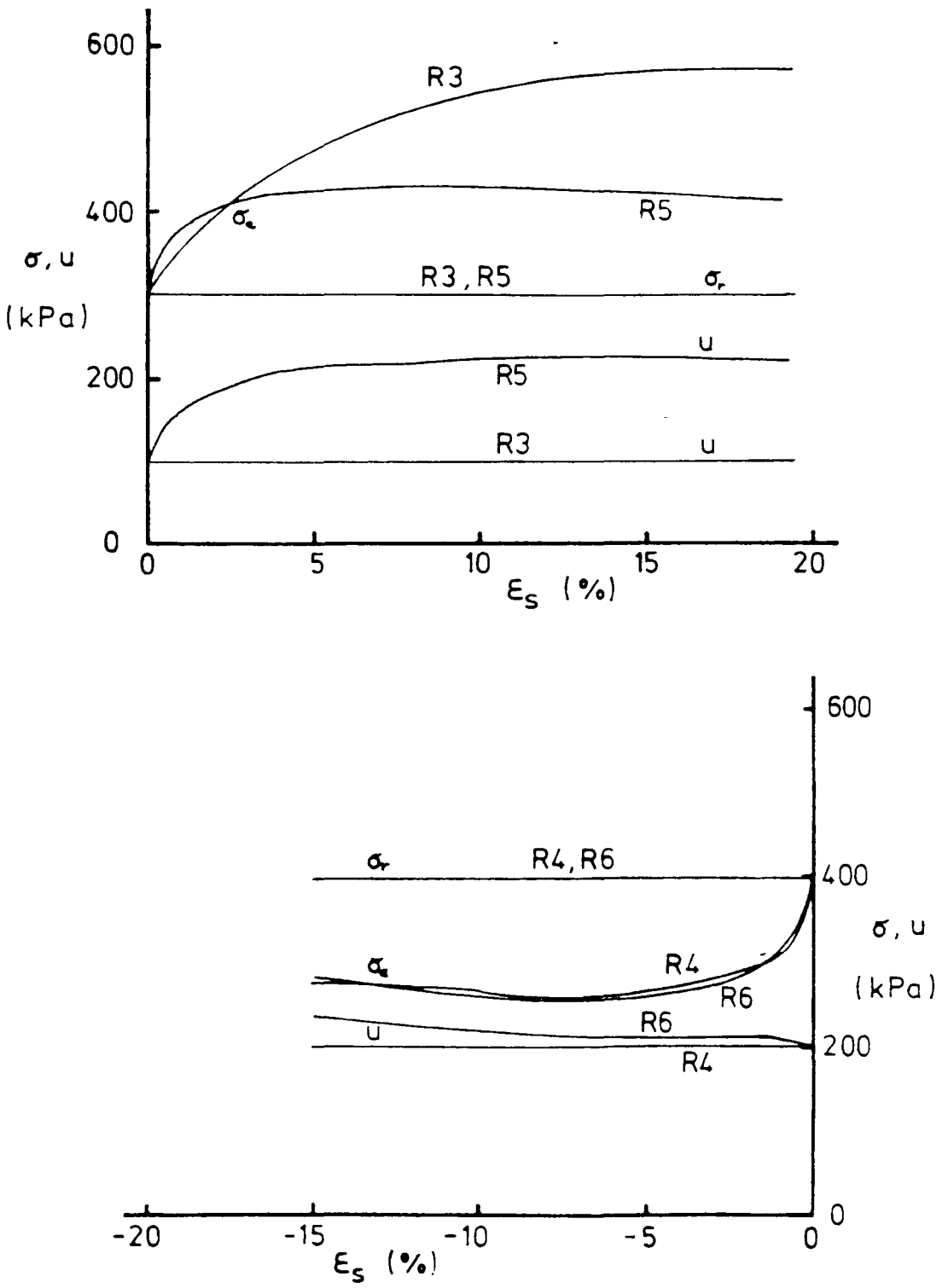

Fig 6.7 Basic test data for compression and extension tests, reconstituted samples

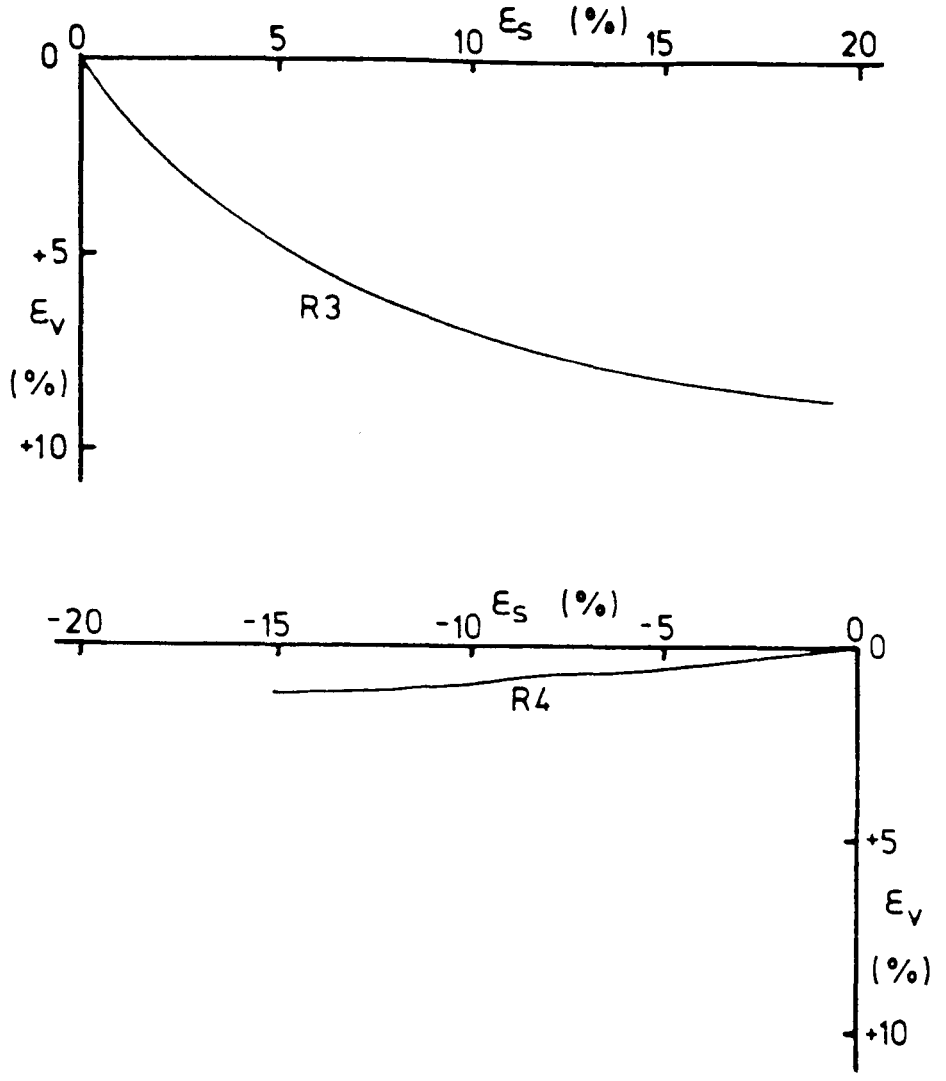

Fig 6.8 Volume change in drained tests, reconstituted samples

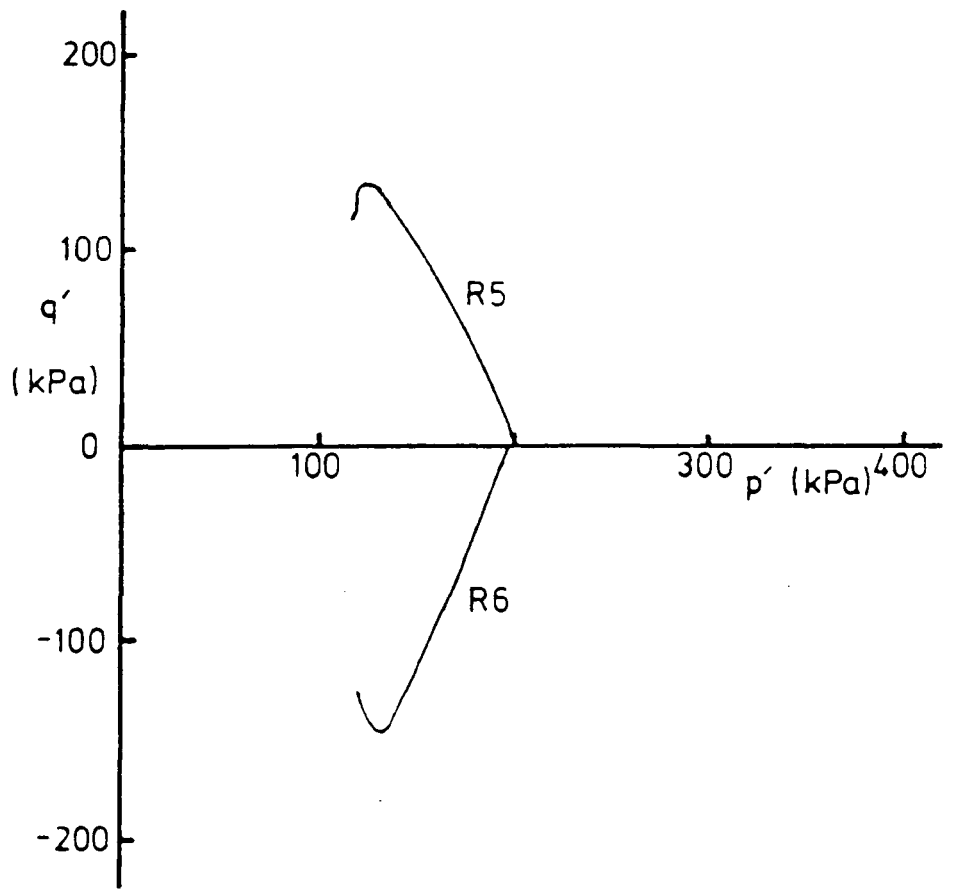

Fig 6.9 Undrained stress paths, reconstituted samples

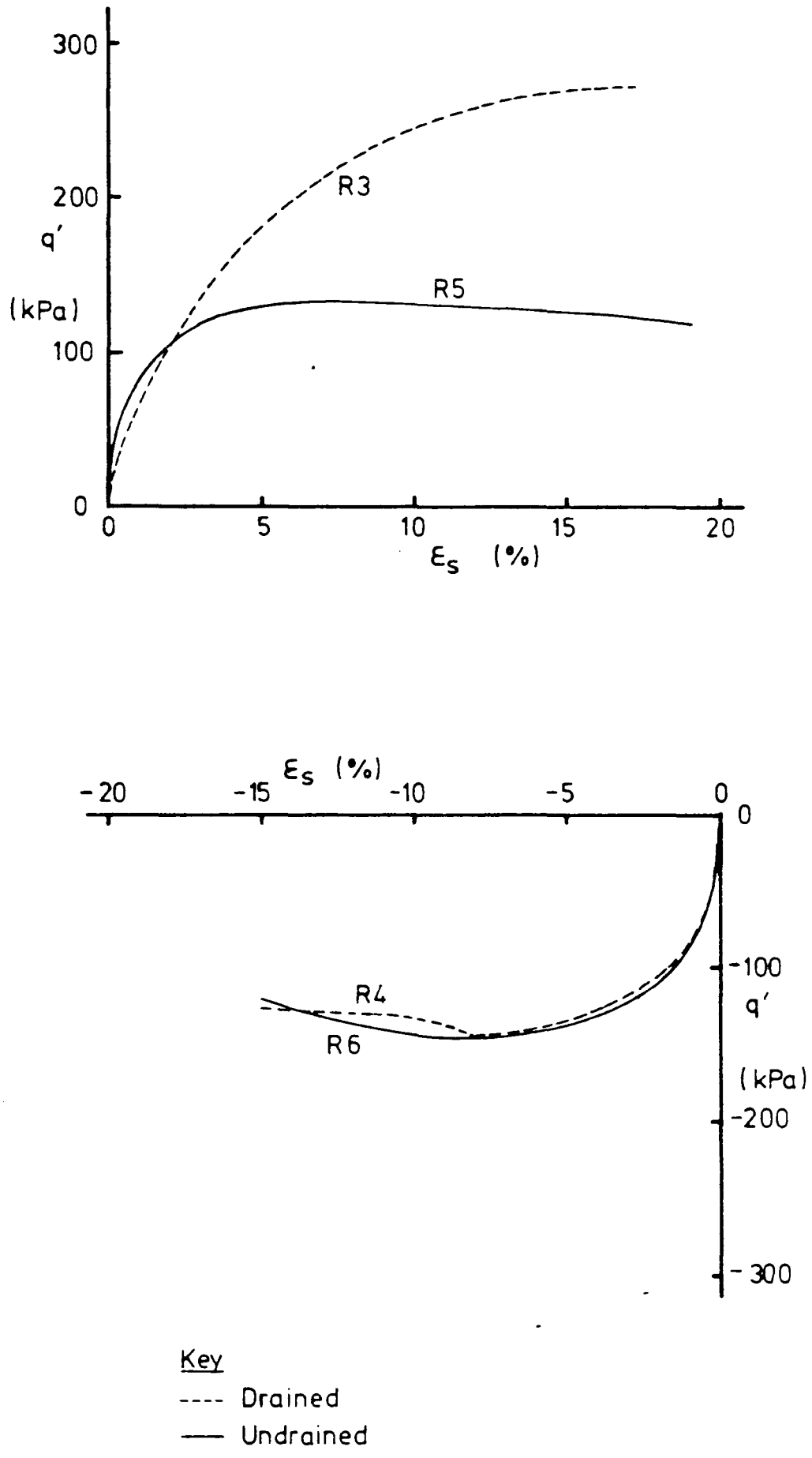

Fig 6.10 Stress - strain curves for compression and extension tests, reconstituted samples

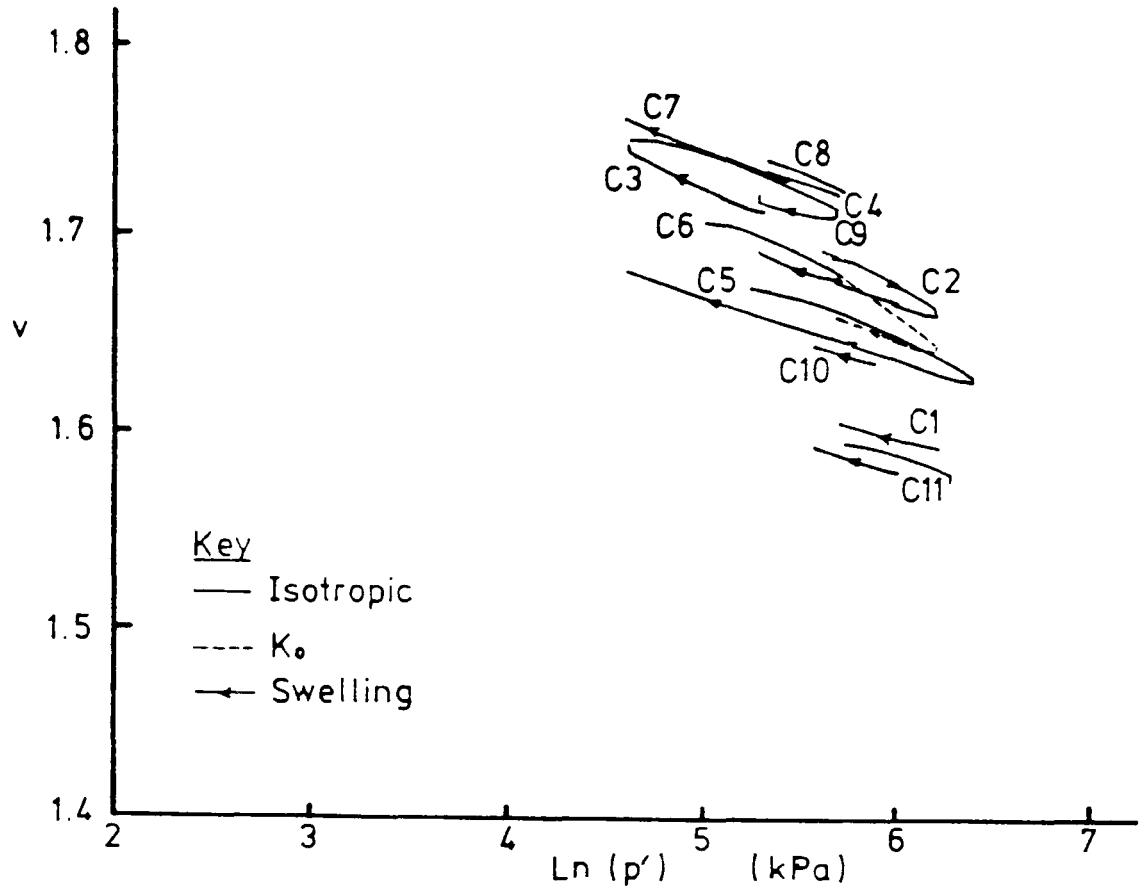

Fig 6.11 Compression and swelling test results, undisturbed samples

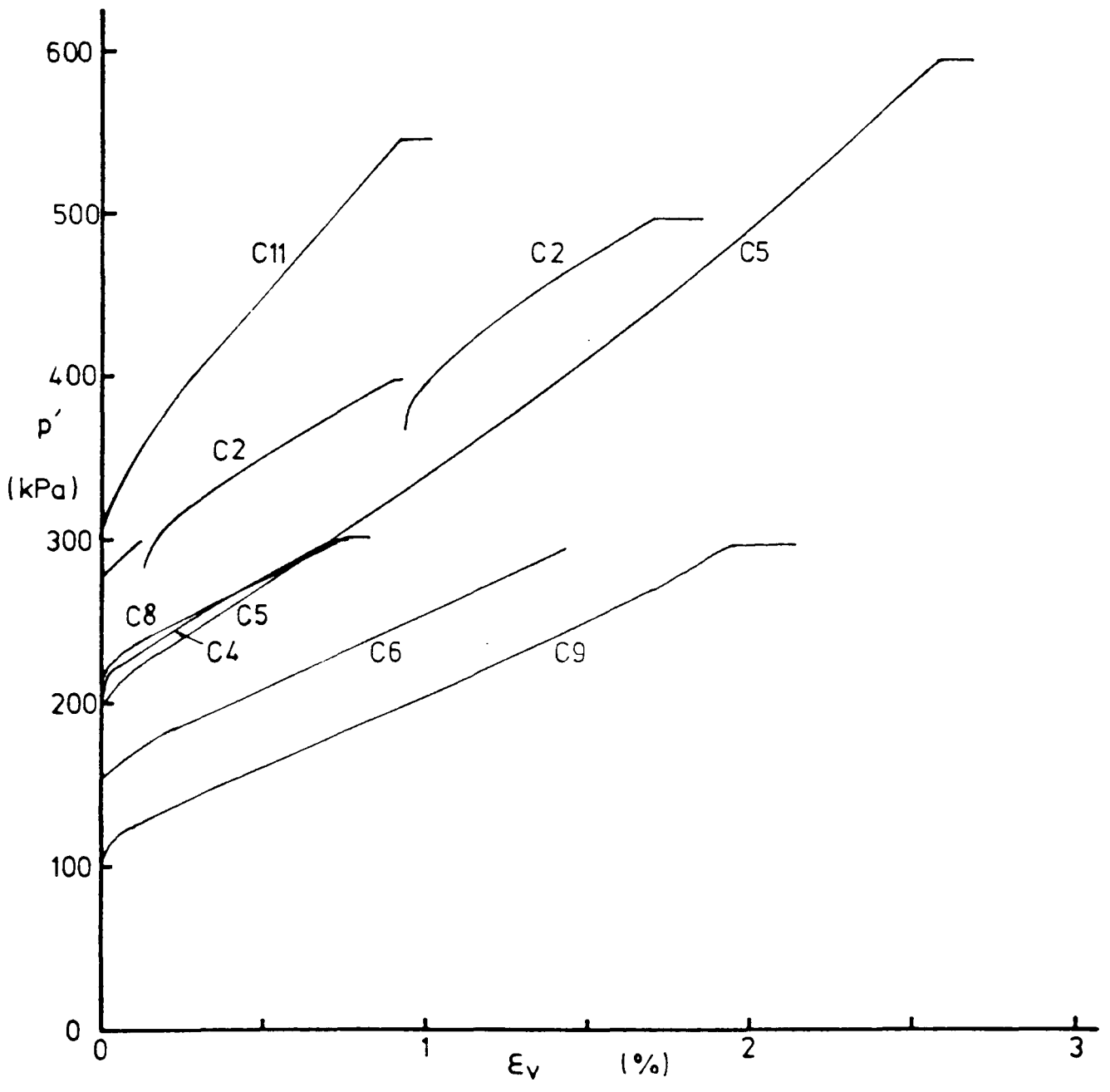

Fig 6.12 Stress - strain curves for isotropic compression tests, undisturbed samples

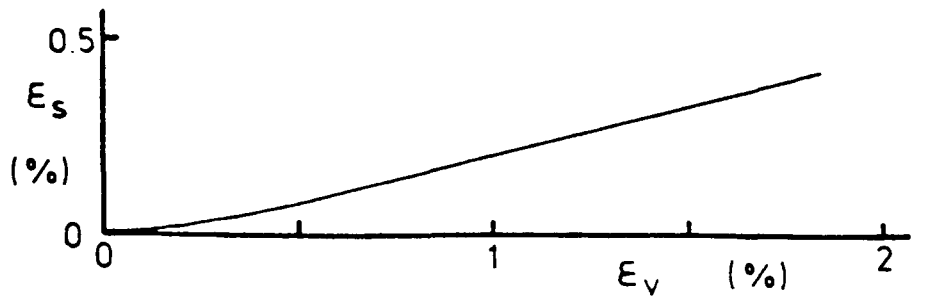

Test C2

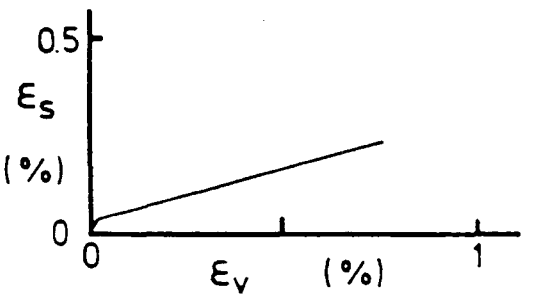

Test C4

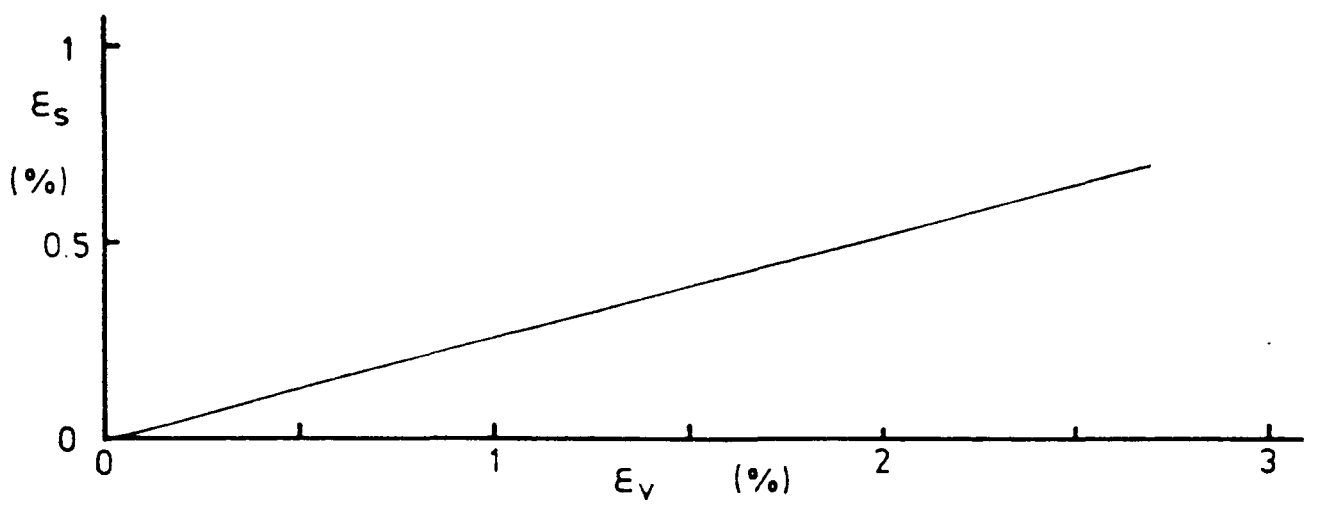

Test C5

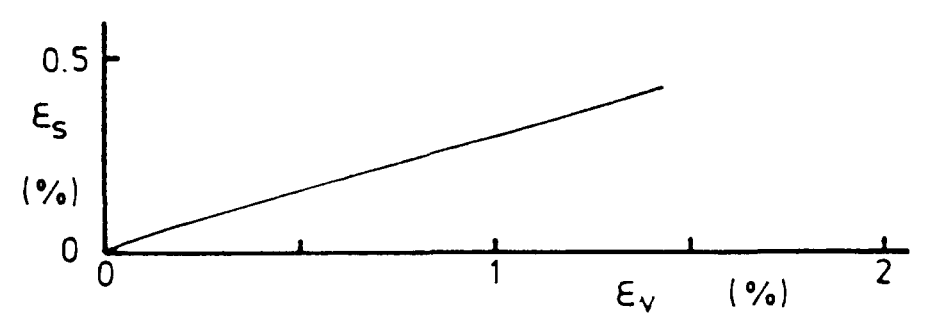

Test C6

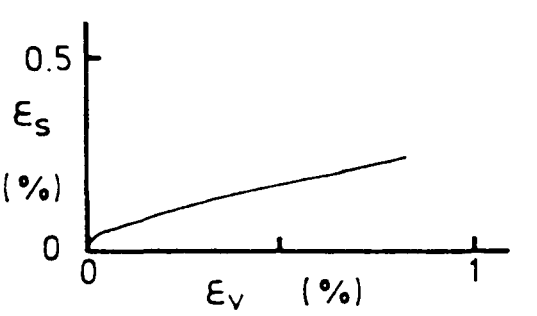

Test C8

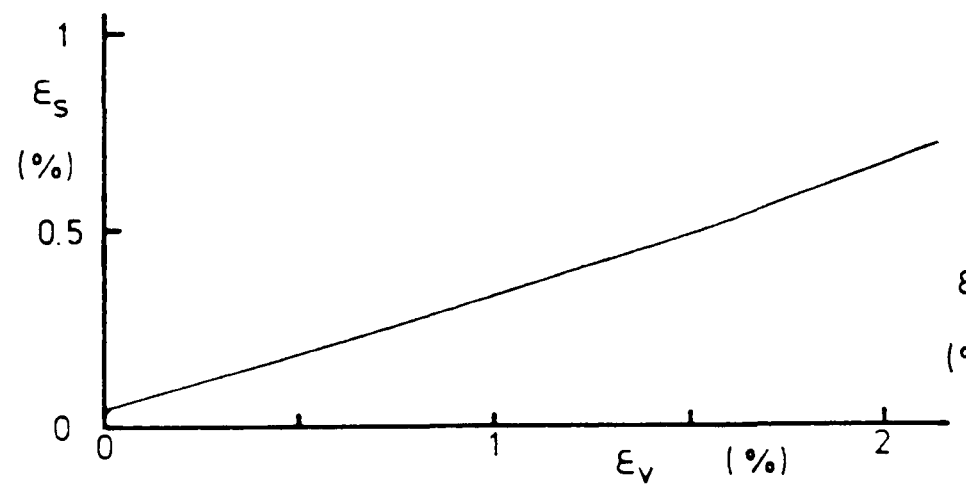

Test C9

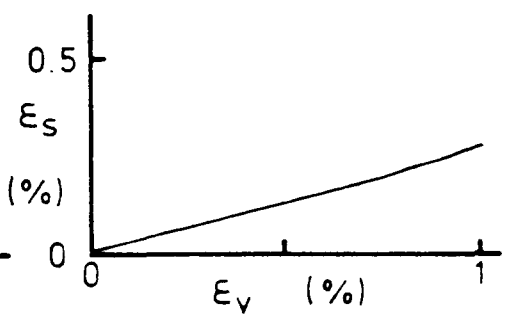

Test C11

Fig 6.13 Shear strain response in isotropic compression tests, undisturbed samples

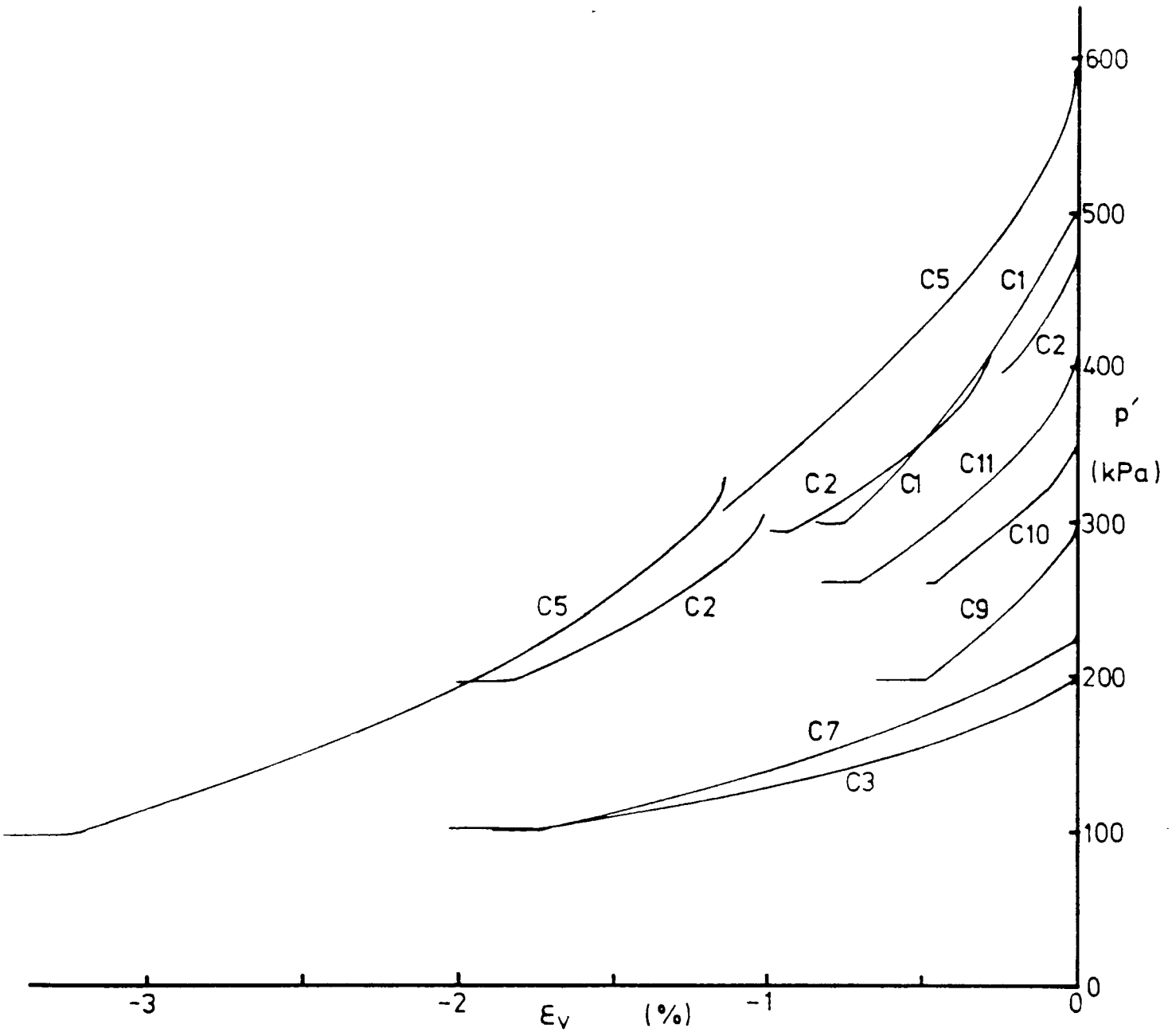

Fig 6.14 Stress - strain curves for isotropic swelling tests, undisturbed samples

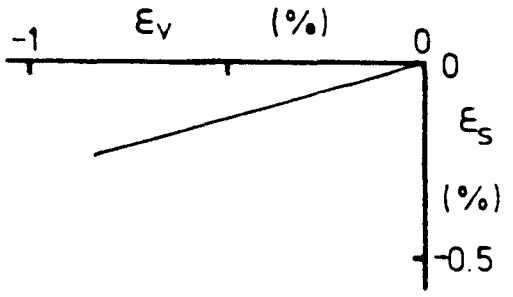

Test C1

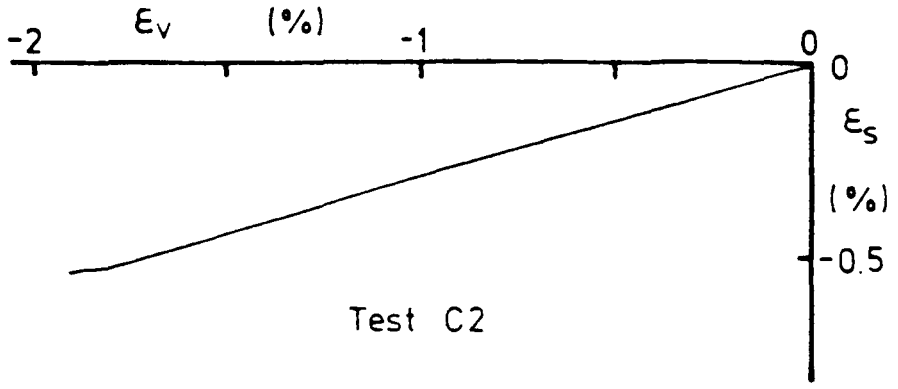

Test C2

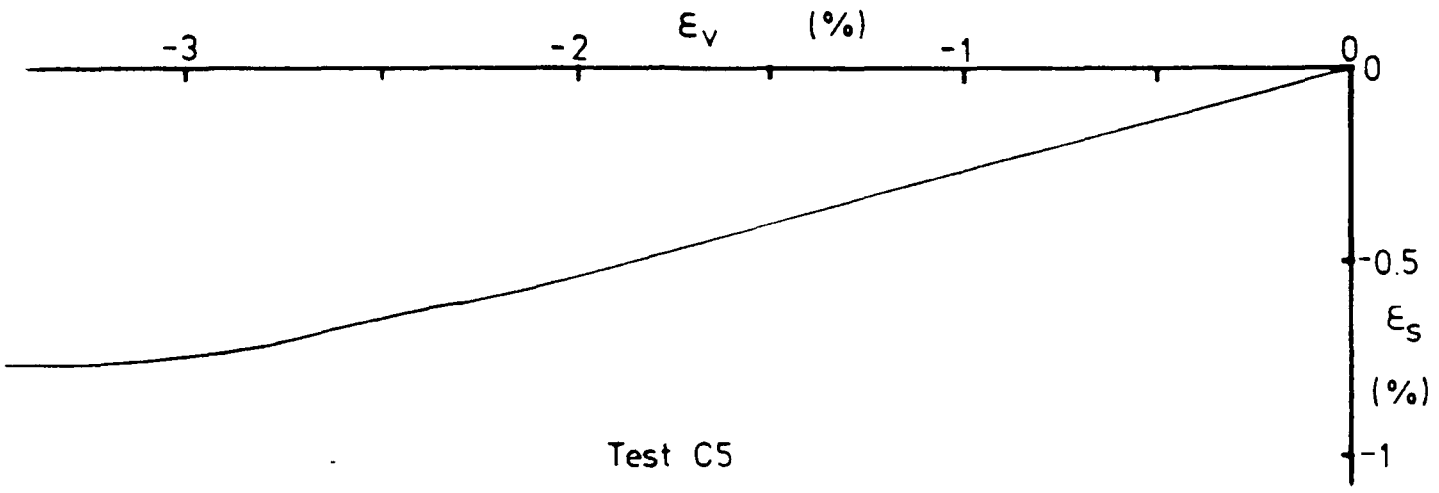

Test C5

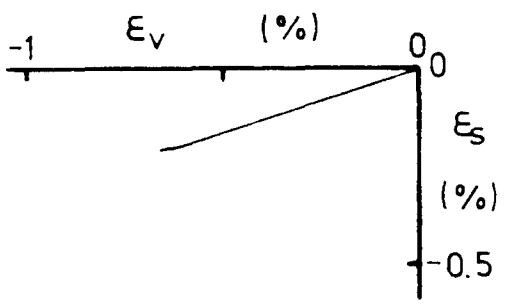

Test C9

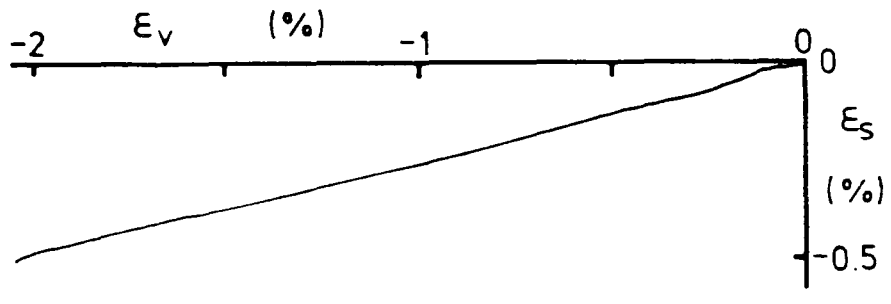

Test C3

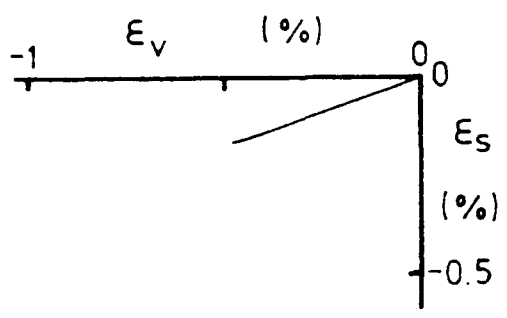

Test C10

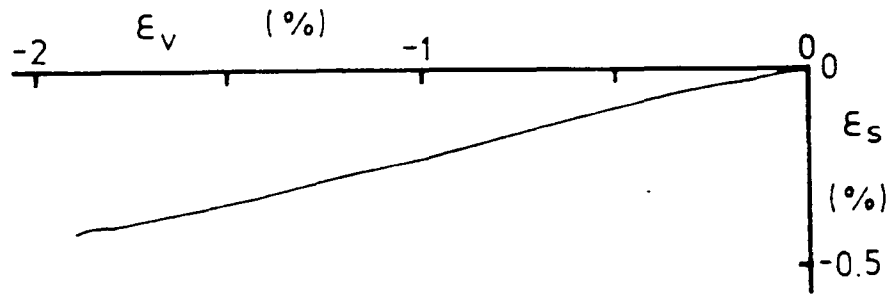

Test C7

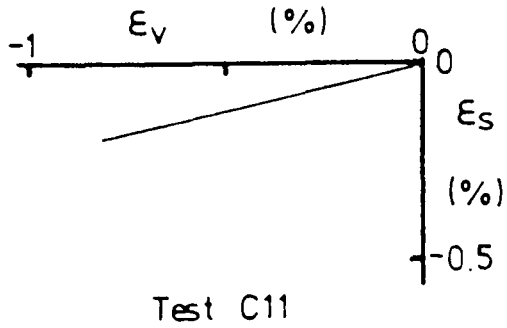

Test C11

Fig 6.15 Shear strain response in isotropic swelling tests, undisturbed samples

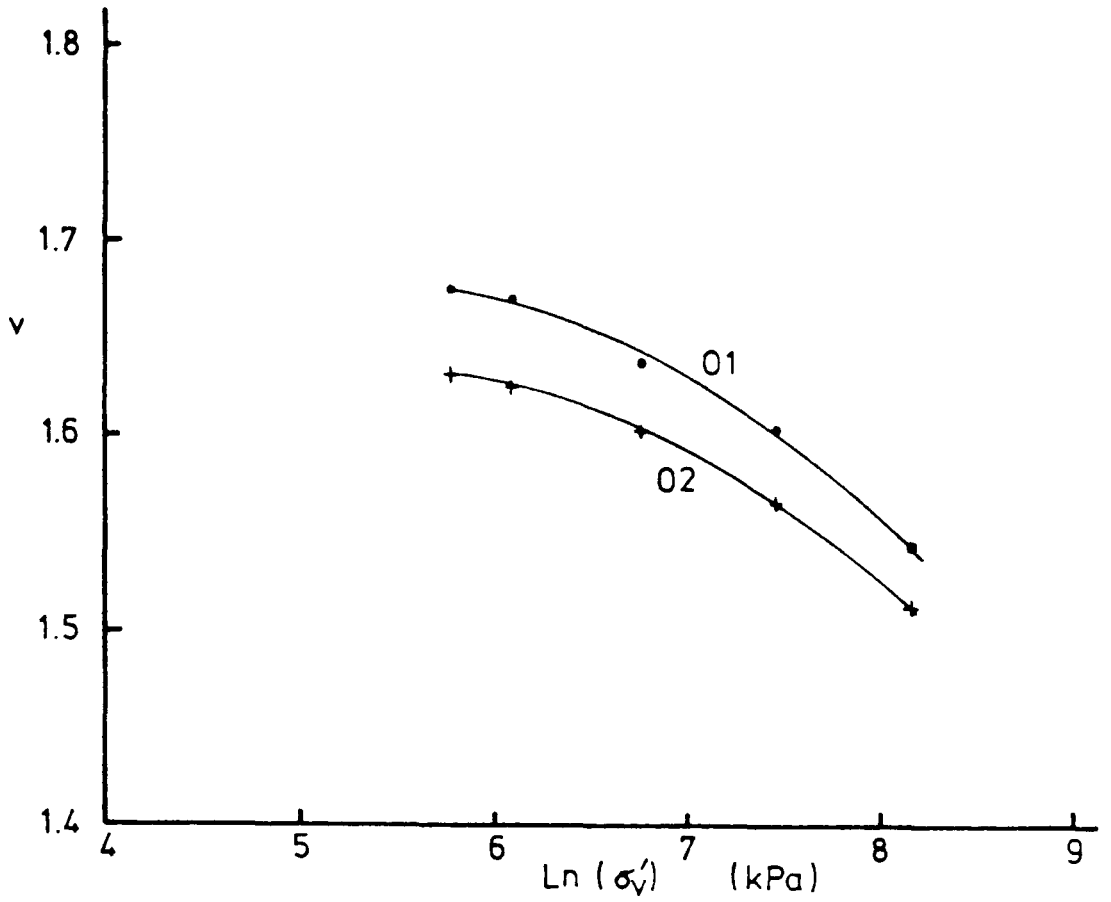

Fig 6.16 Oedometer compression curves

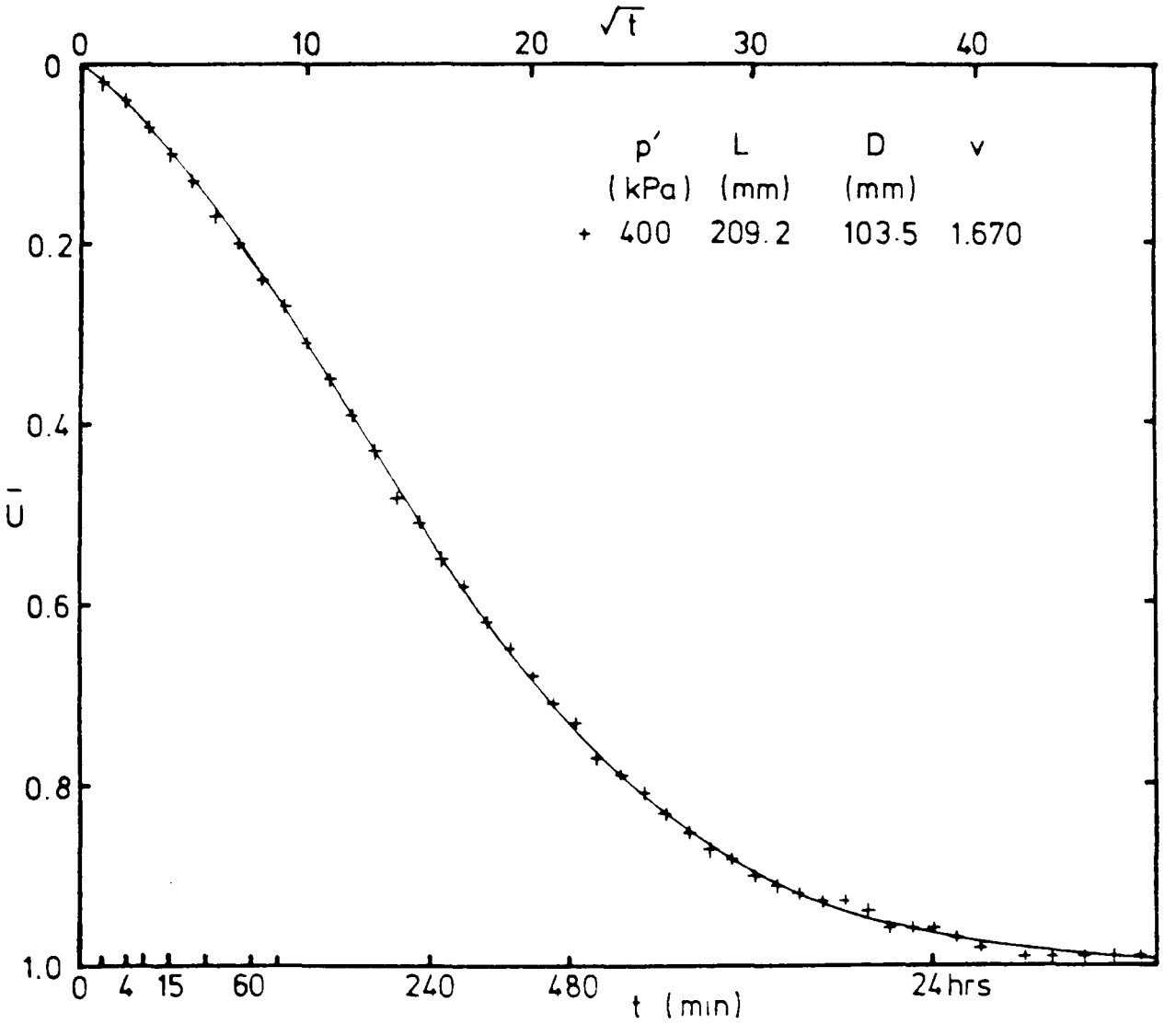

Fig 6.17 Triaxial consolidation test results, Test D1

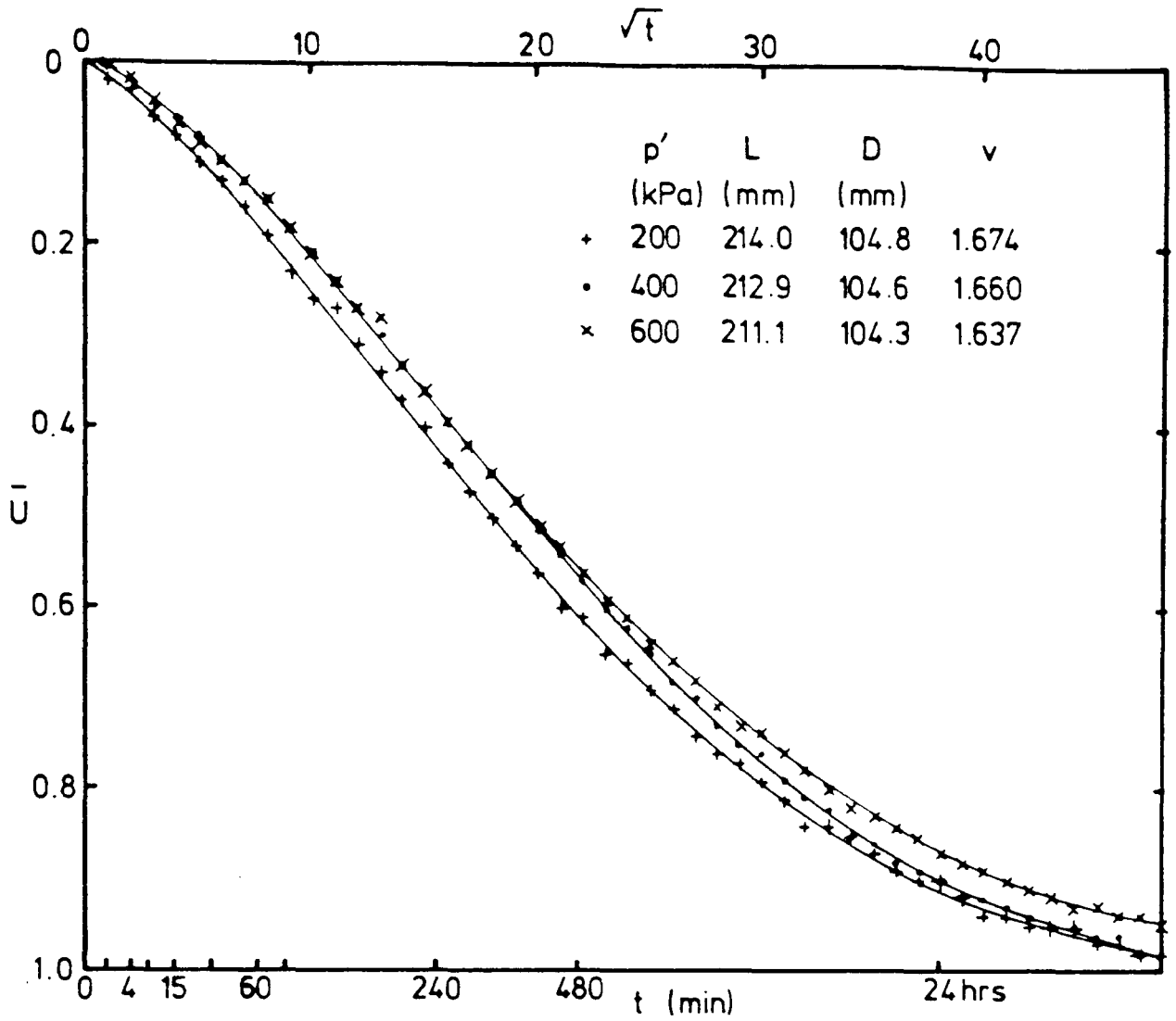

Fig 6.18 Triaxial consolidation test results, Test D2

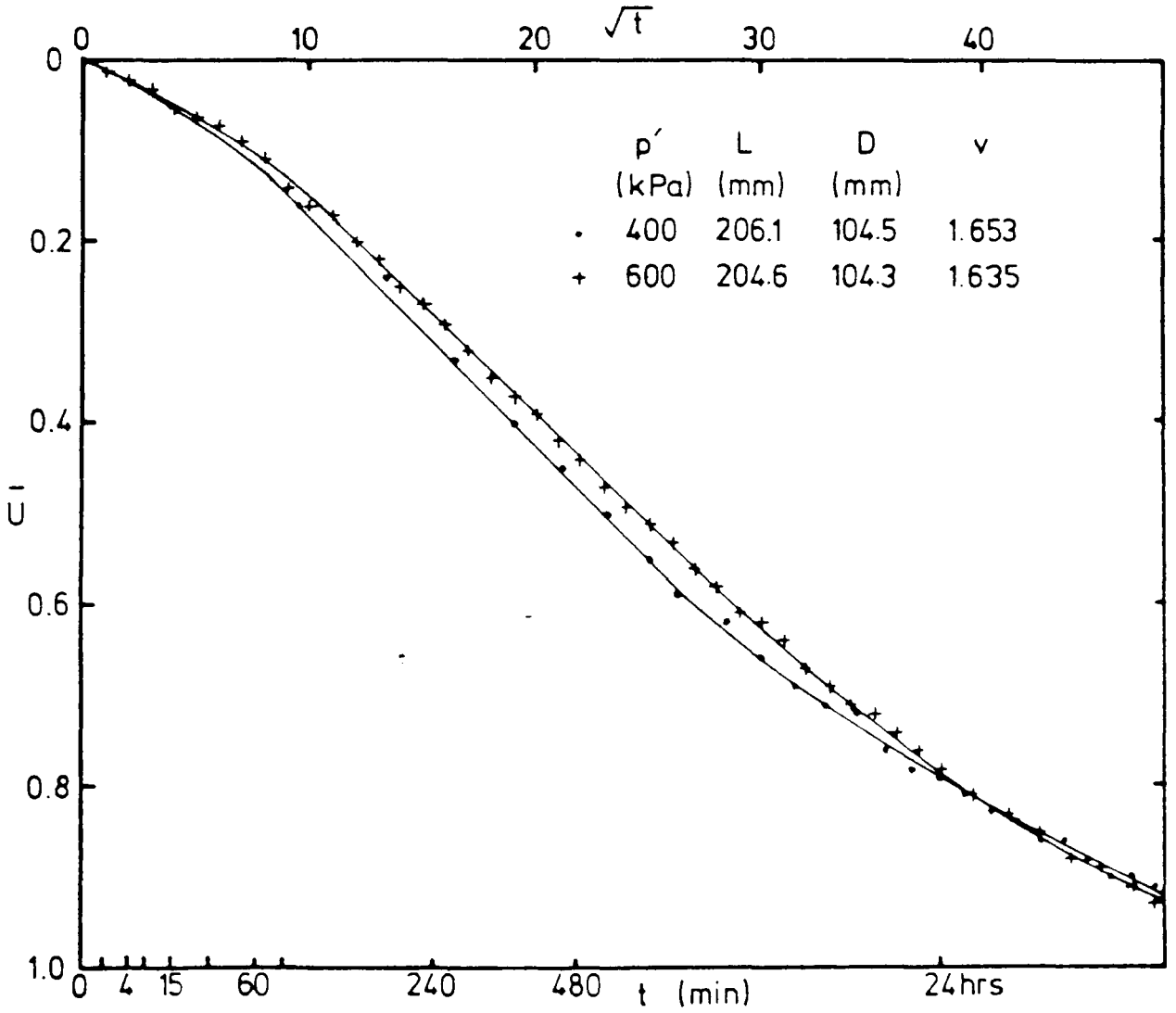

Fig 6.19 Triaxial consolidation test results, Test D3

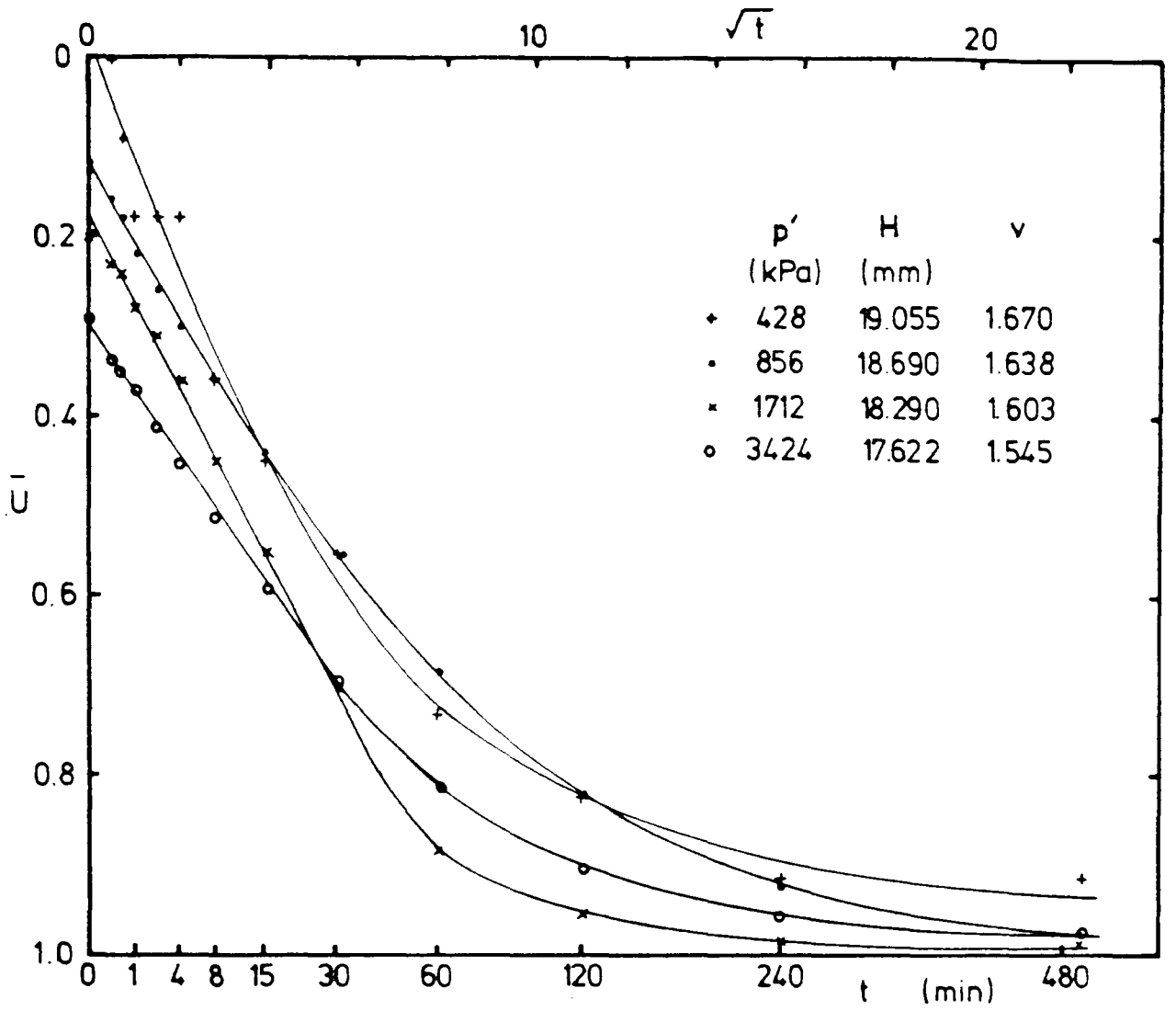

Fig 6.20 Oedometer consolidation, Test 01

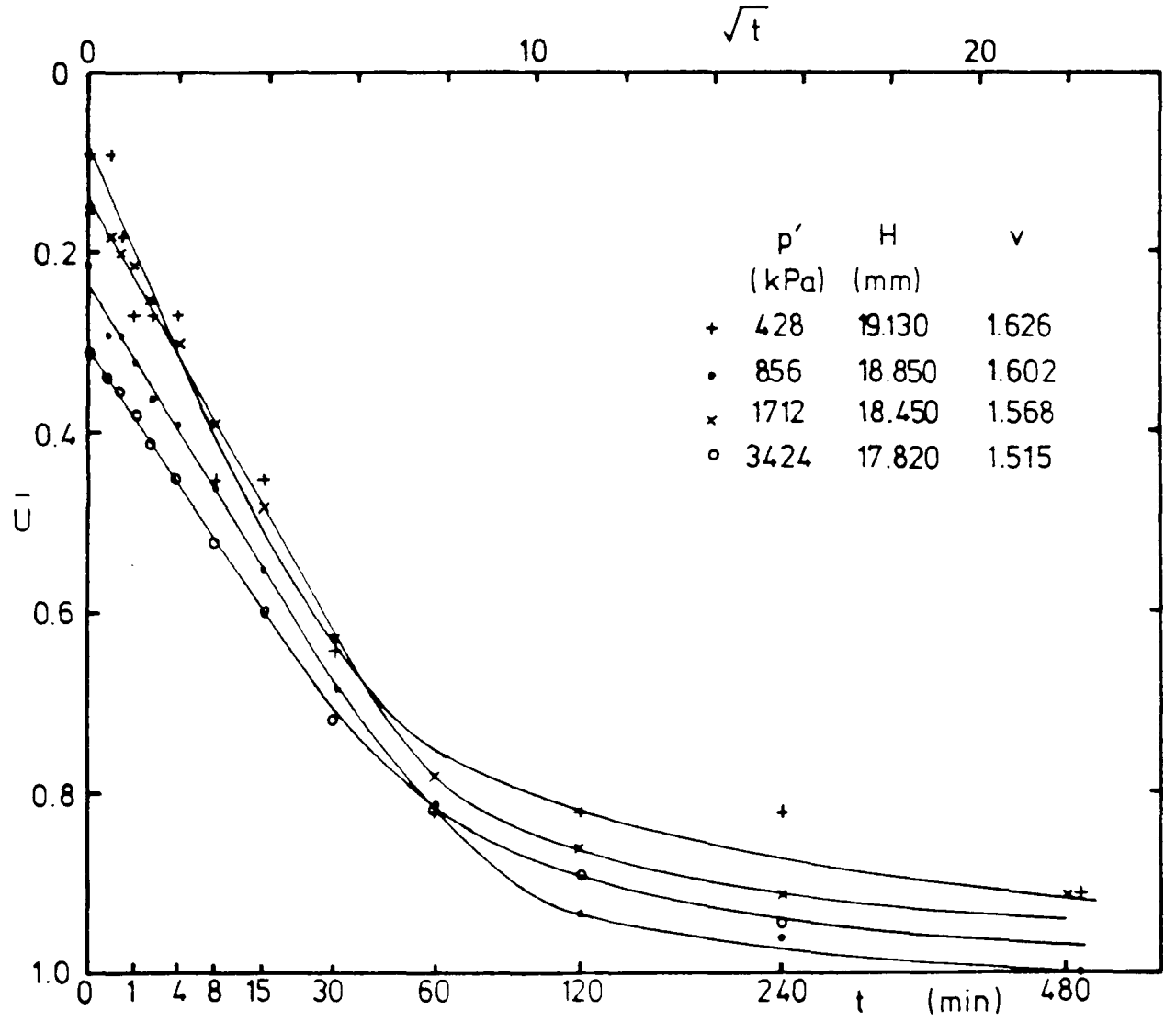

Fig 6.21 Oedometer consolidation, Test 02

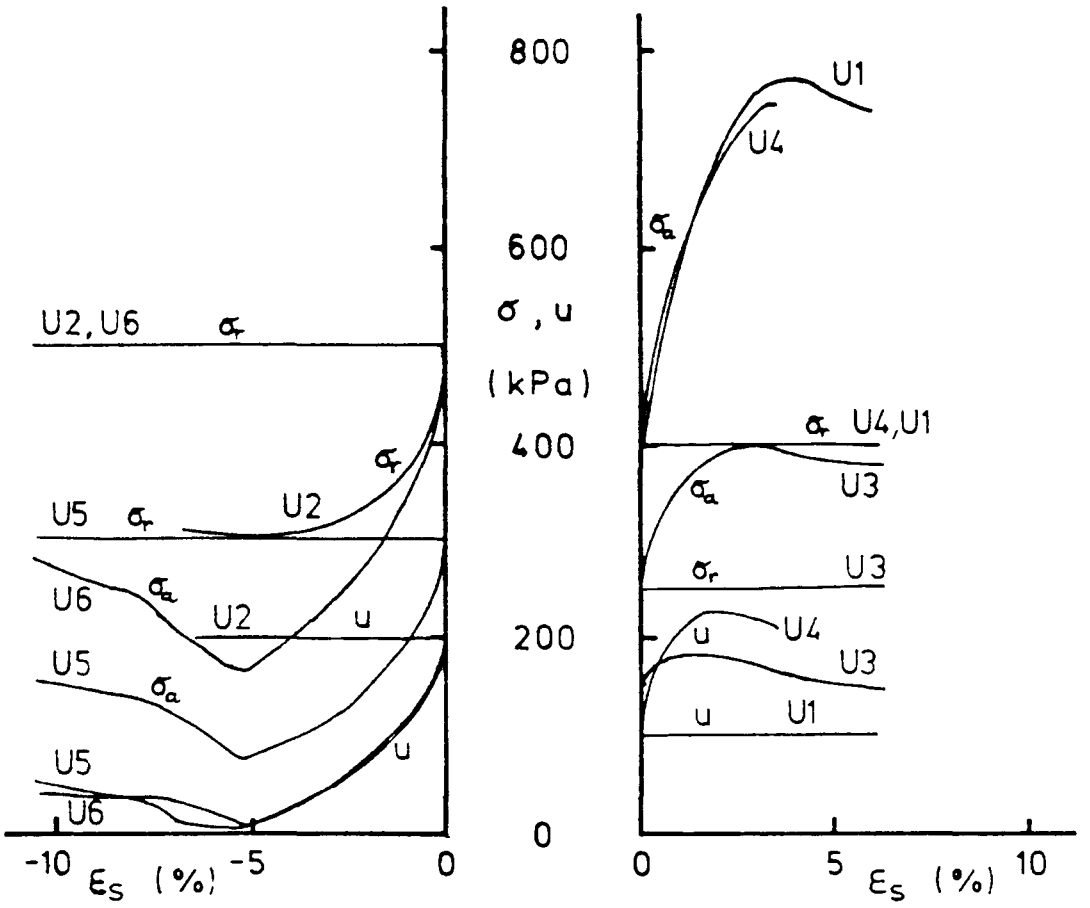

Fig 6.22 Basic test data for compression and extension tests, undisturbed samples

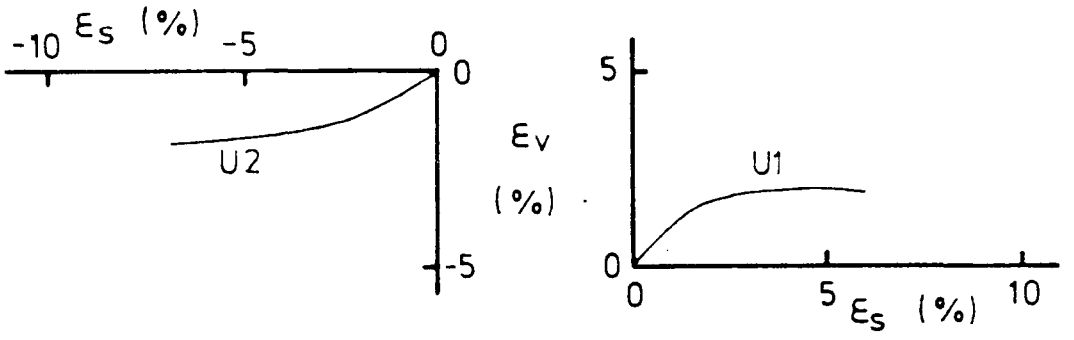

Fig 6.23 Volume change in drained tests, undisturbed samples

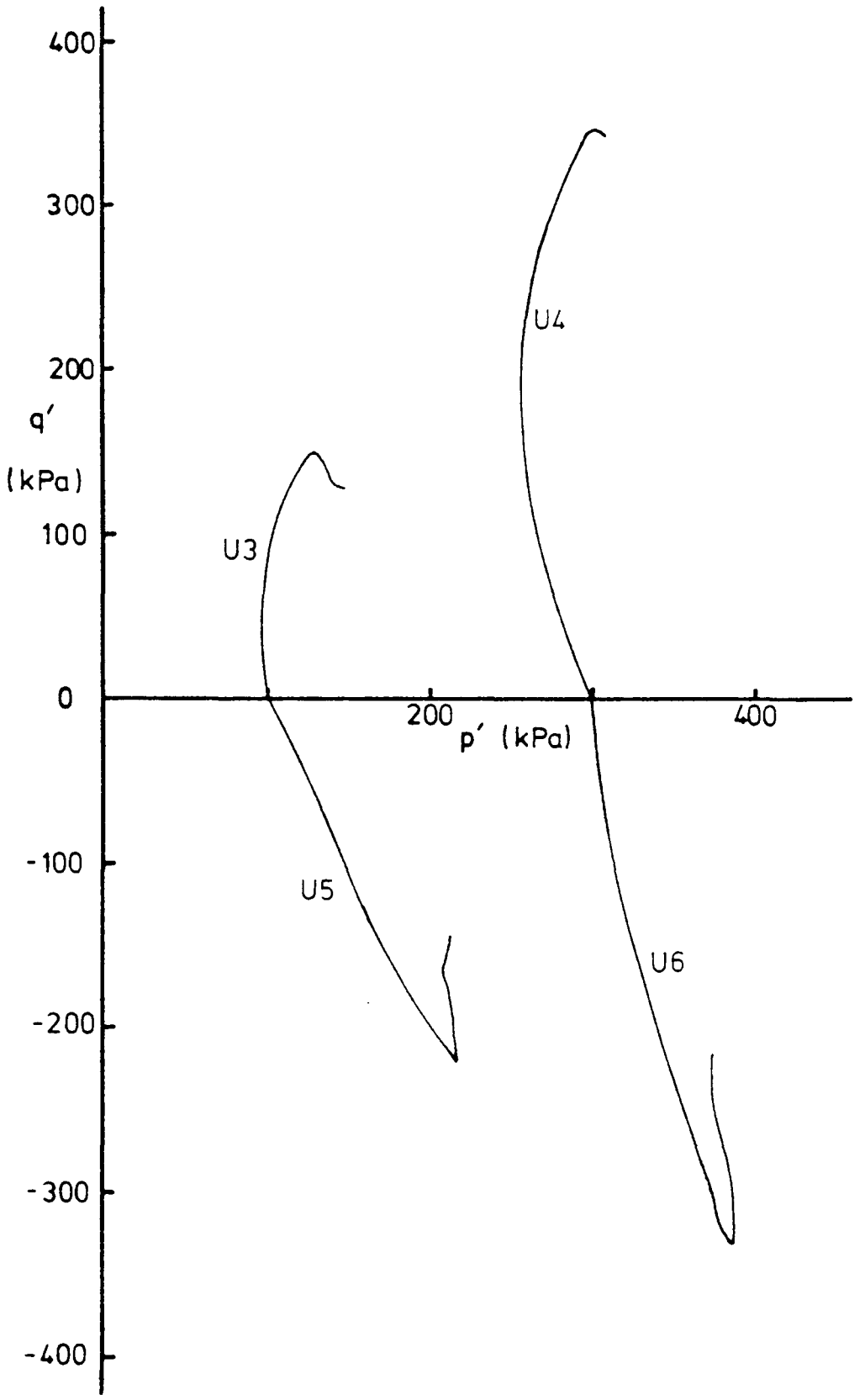

Fig 6.24 Undrained stress paths, undisturbed samples

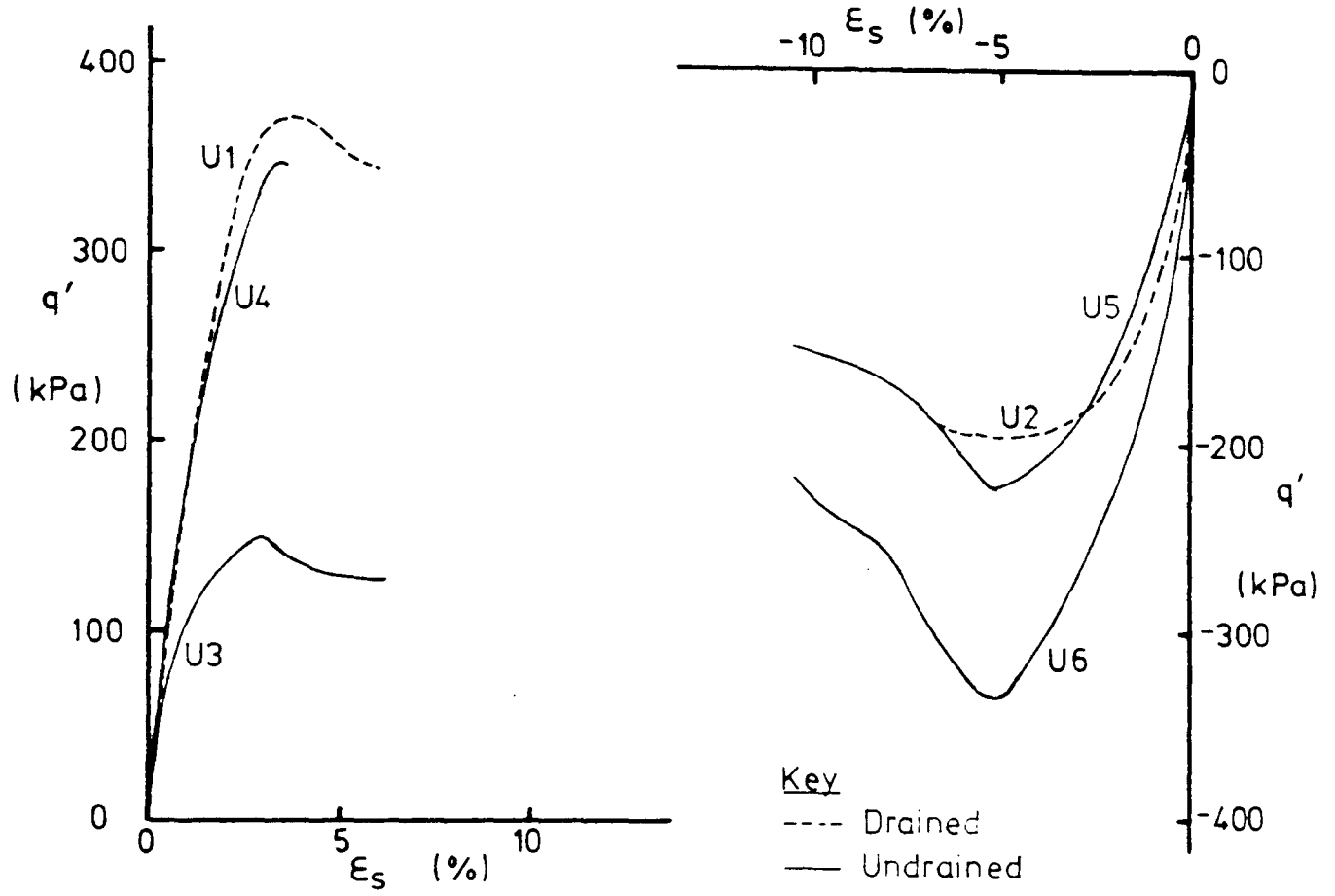

Fig 6.25 Stress - strain curves for compression and extension tests, undisturbed samples

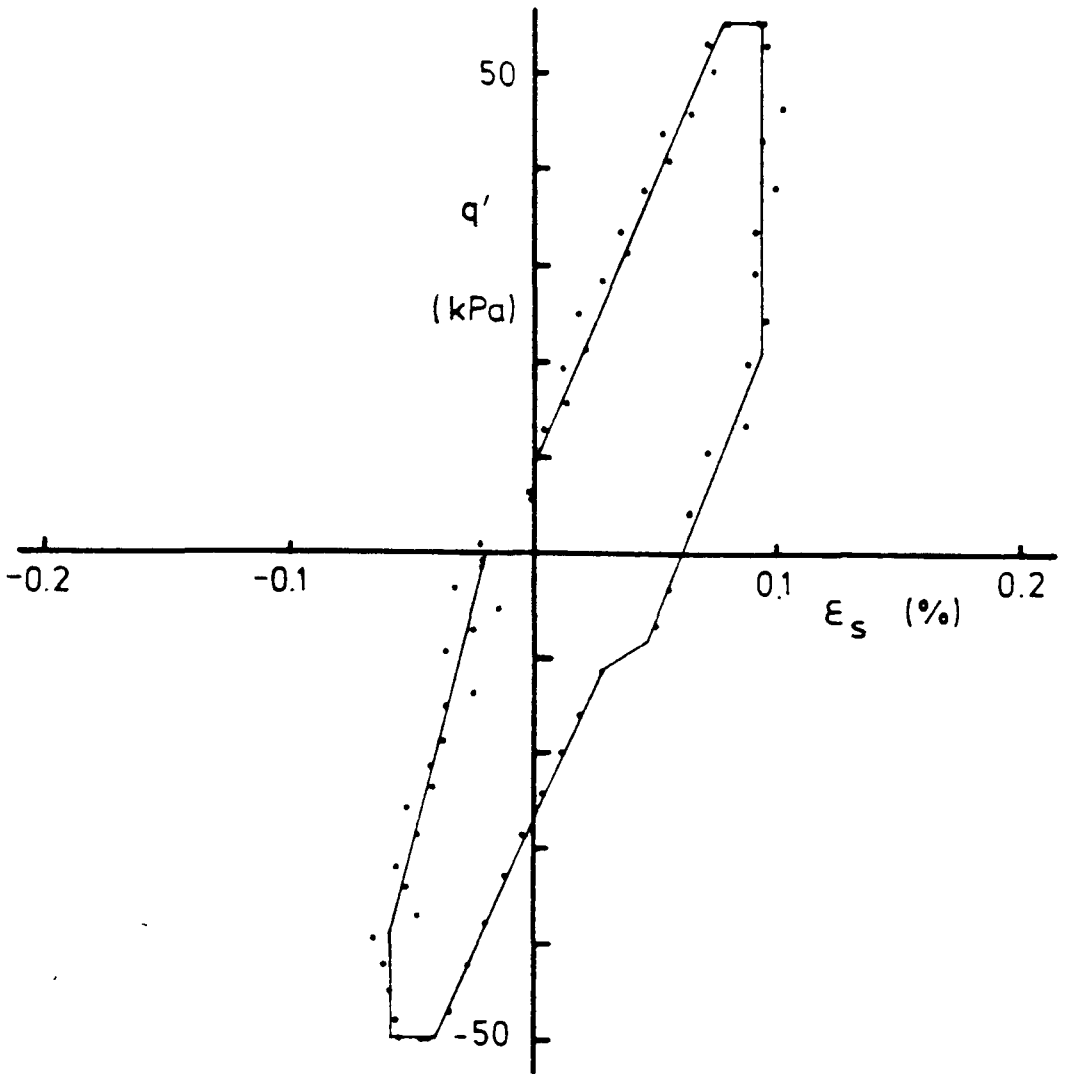

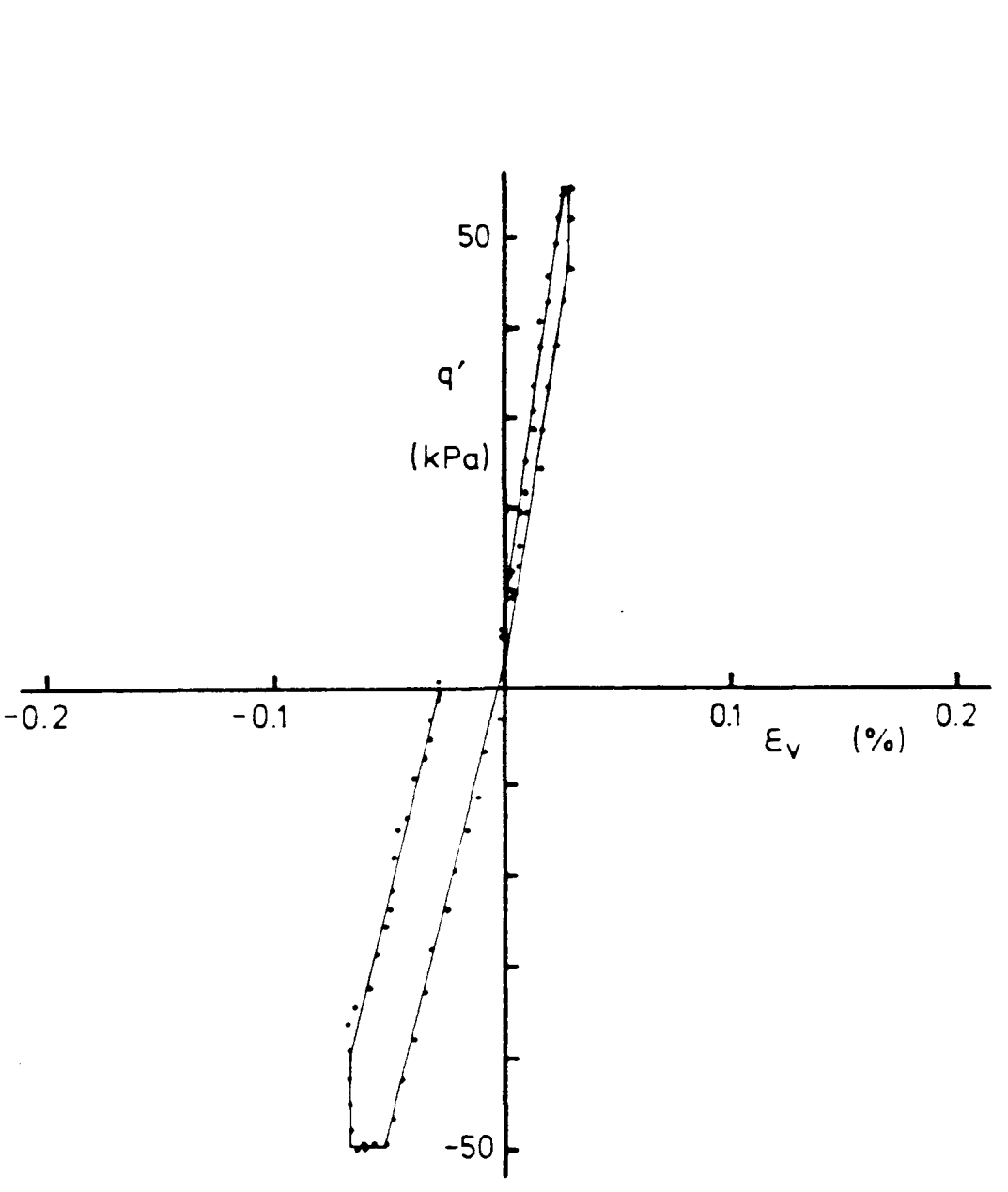

Fig 6.26 Stress - strain curves for constant p' probe, Test P1 Cycle 4

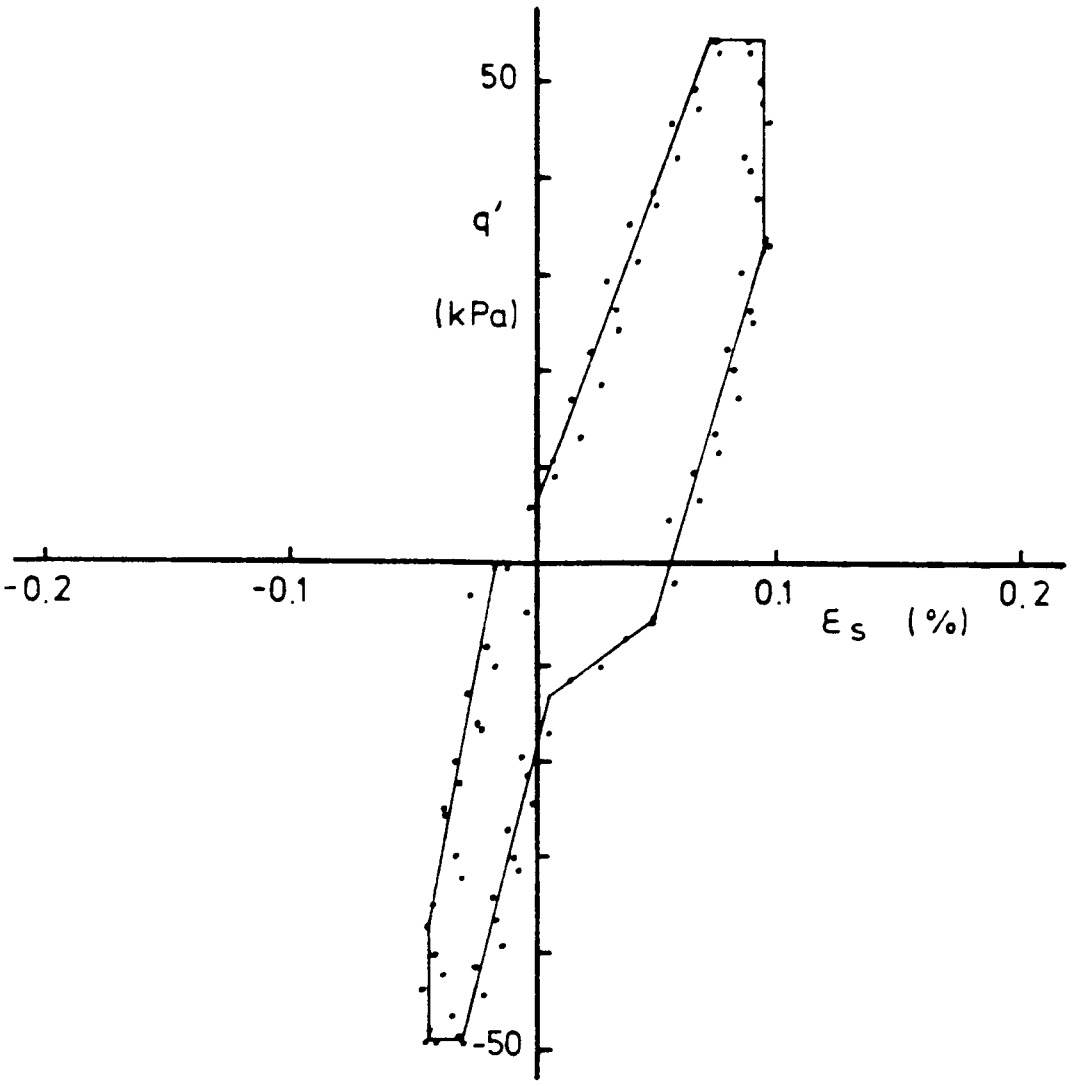

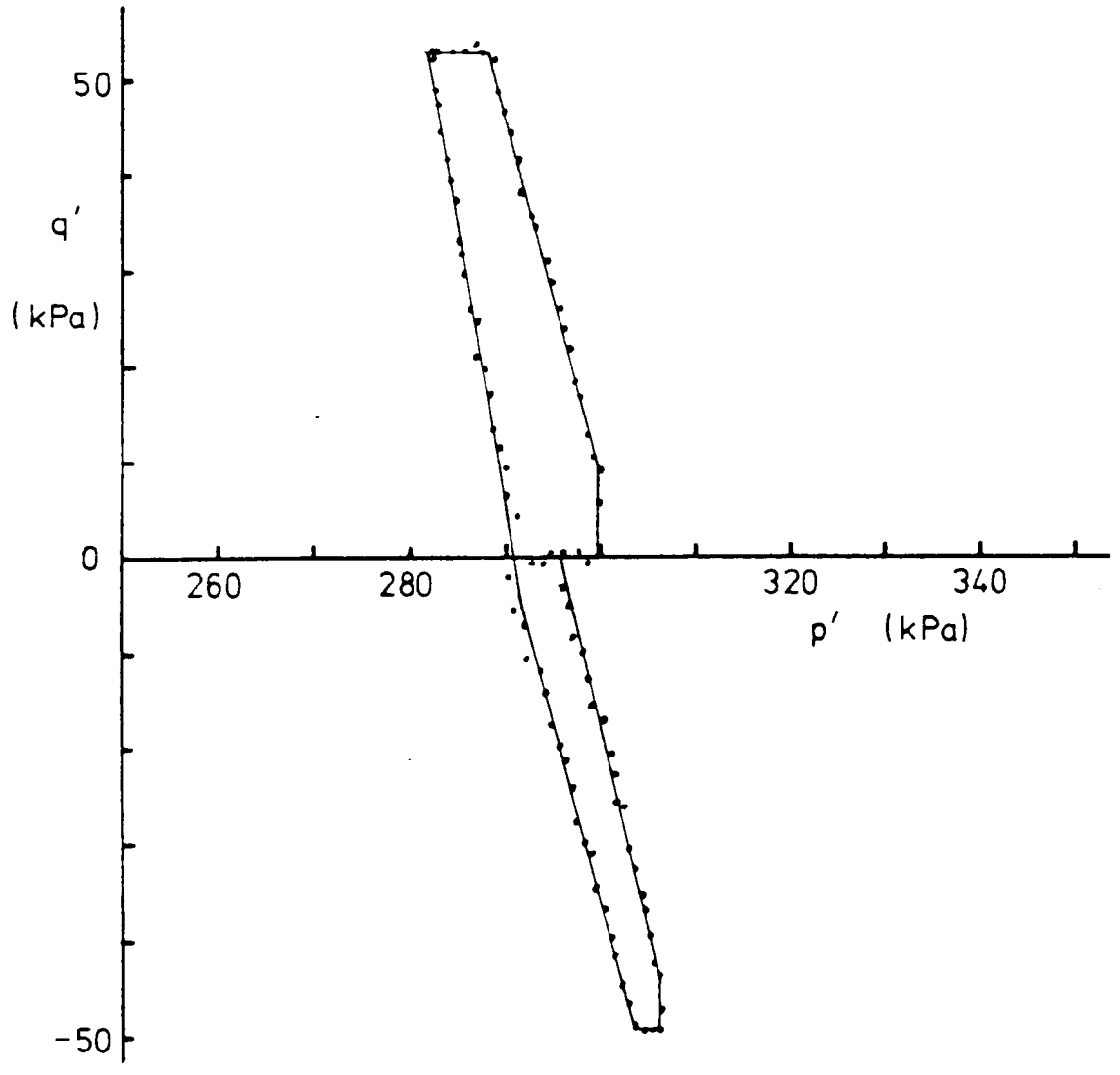

Fig 6.27 Stress - strain curves and undrained stress path for undrained uniaxial probe, Test P1 Cycle 6

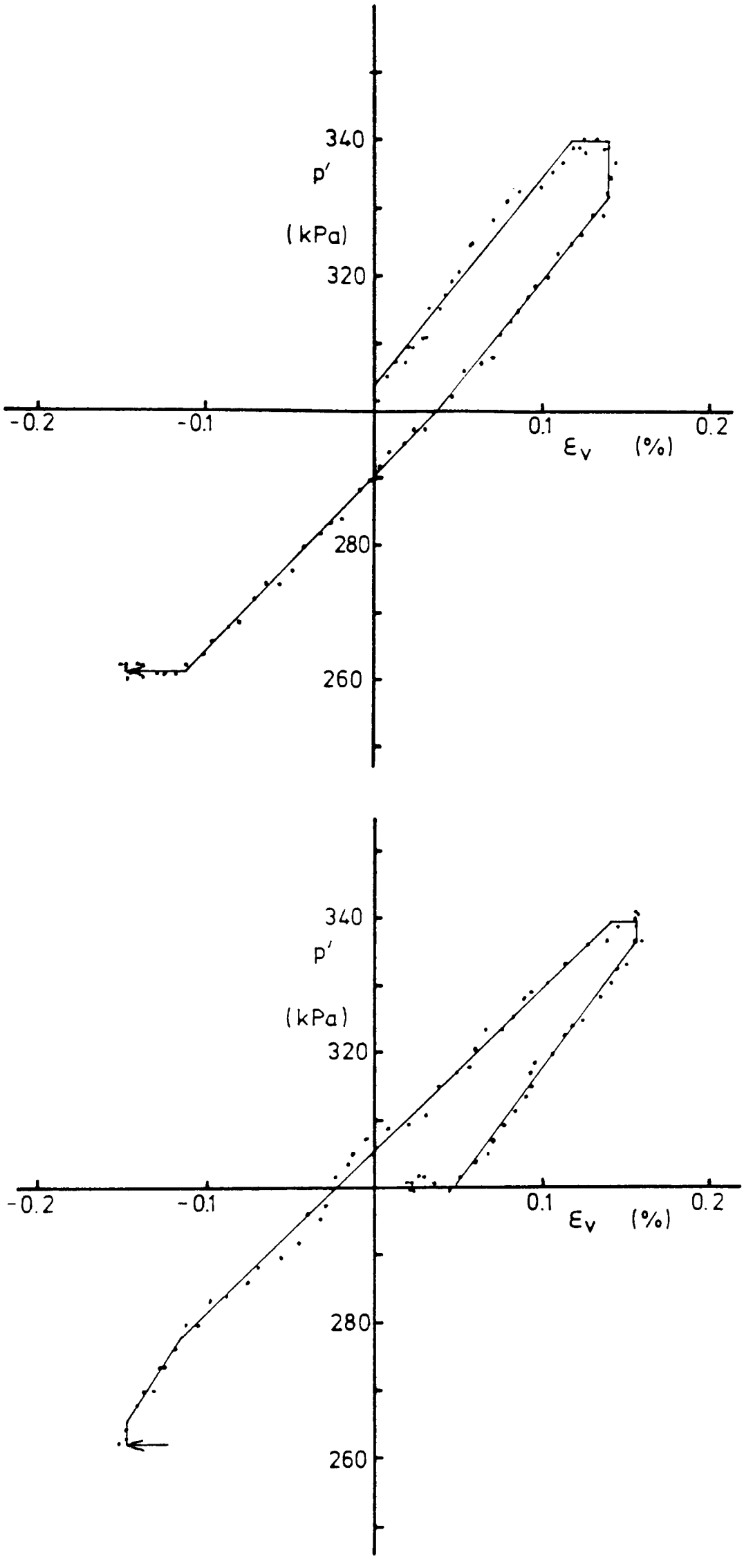

Fig 6.28 Stress - strain curves for isotropic probe, Test P1 Cycle 12

Cont'd/-

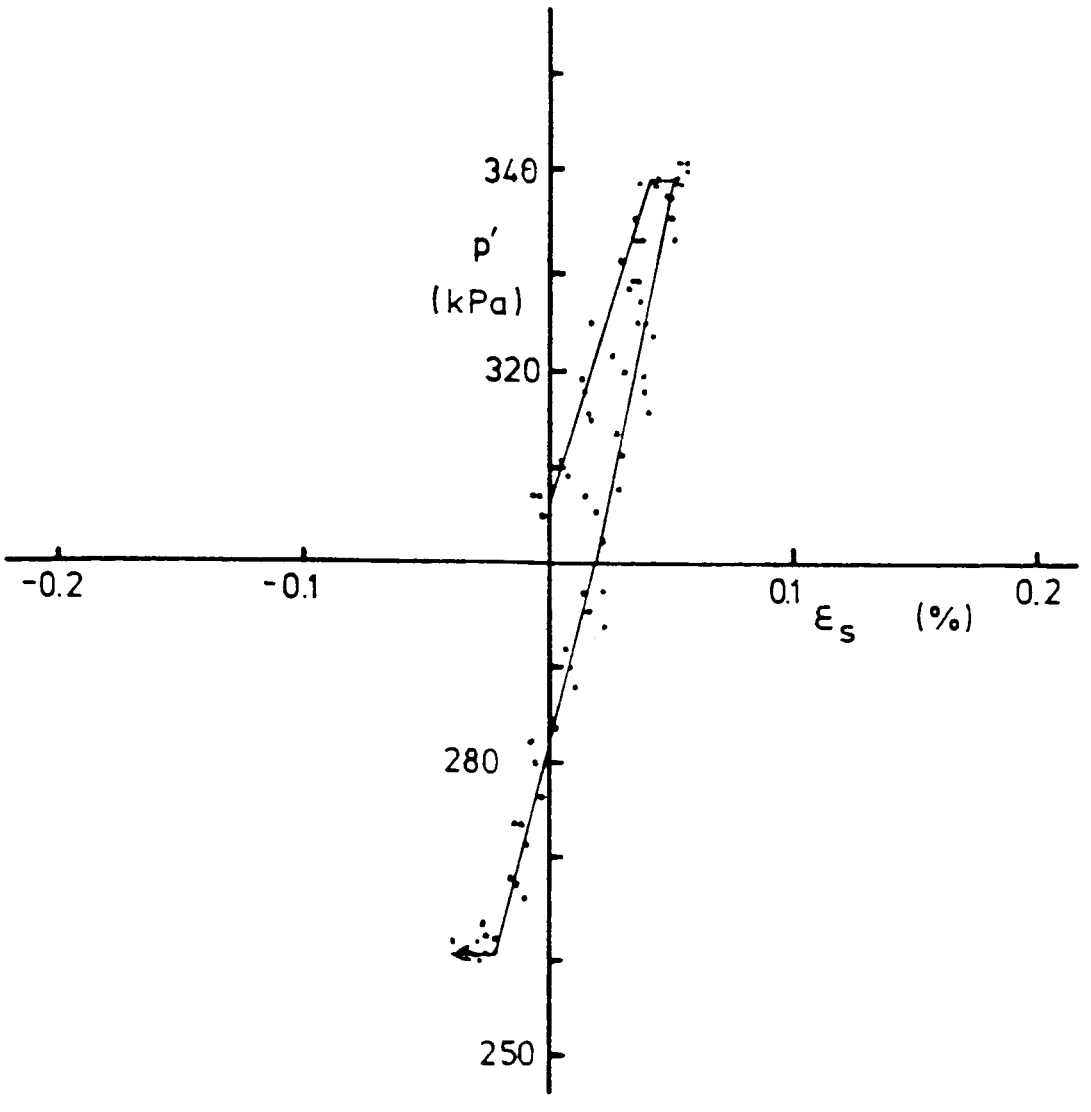

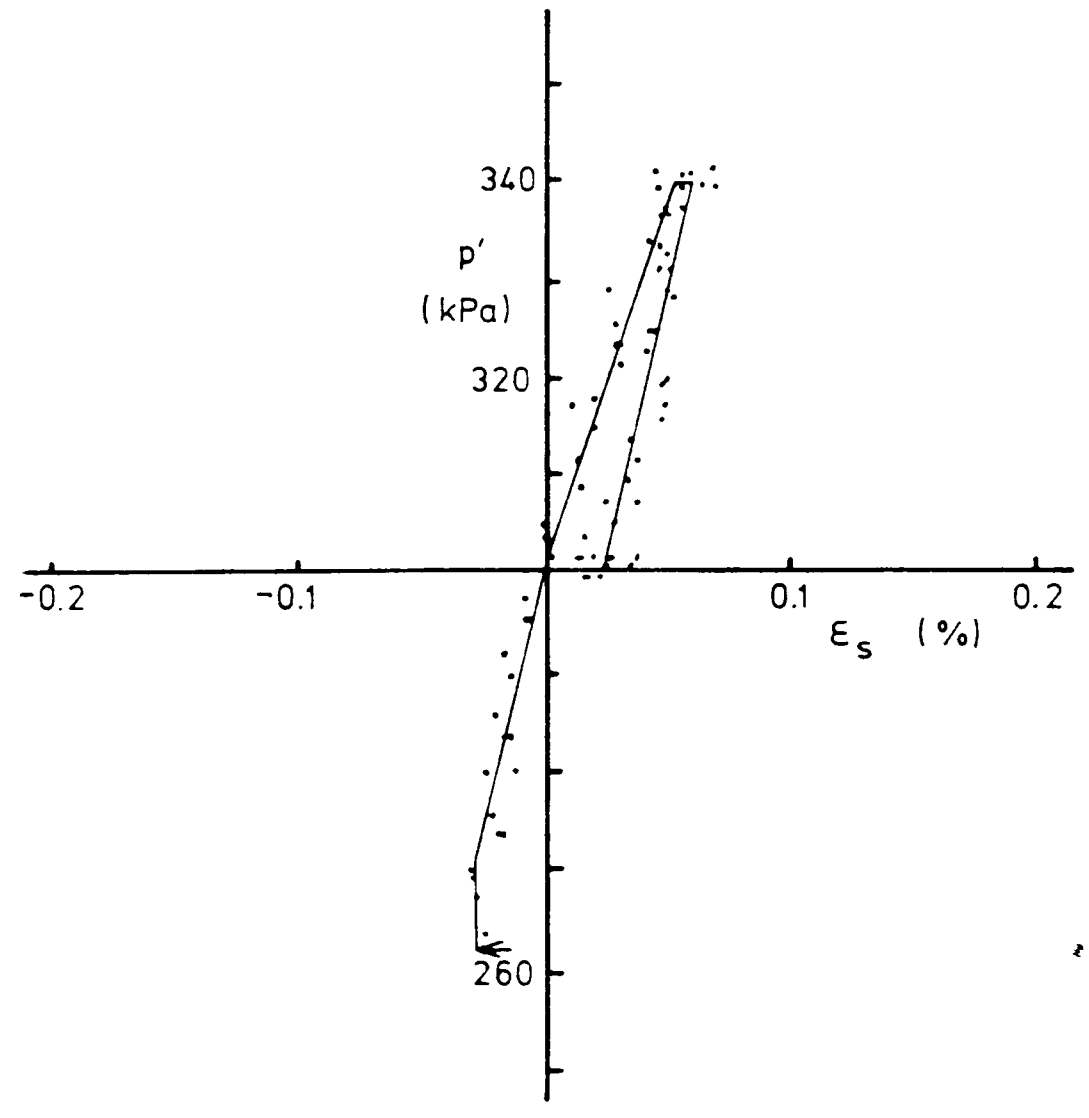

Fig 6.28 (Cont'd) Stress - strain curves for isotropic probe, Test P1 Cycle 12

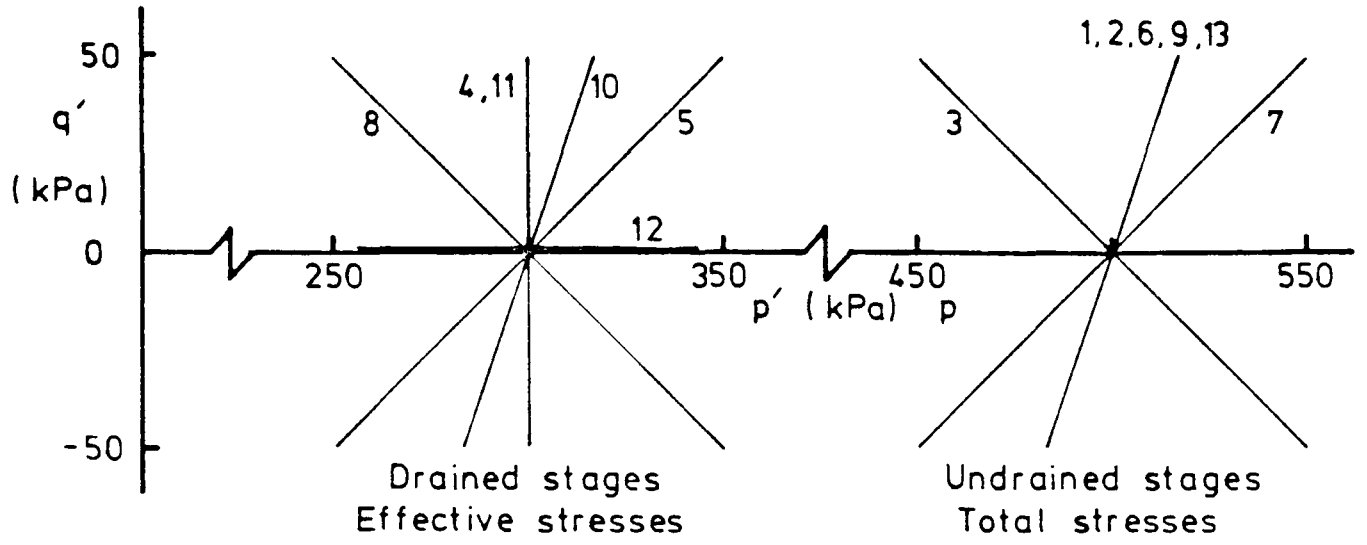

Fig 6.29 Stress path probes for Test P1

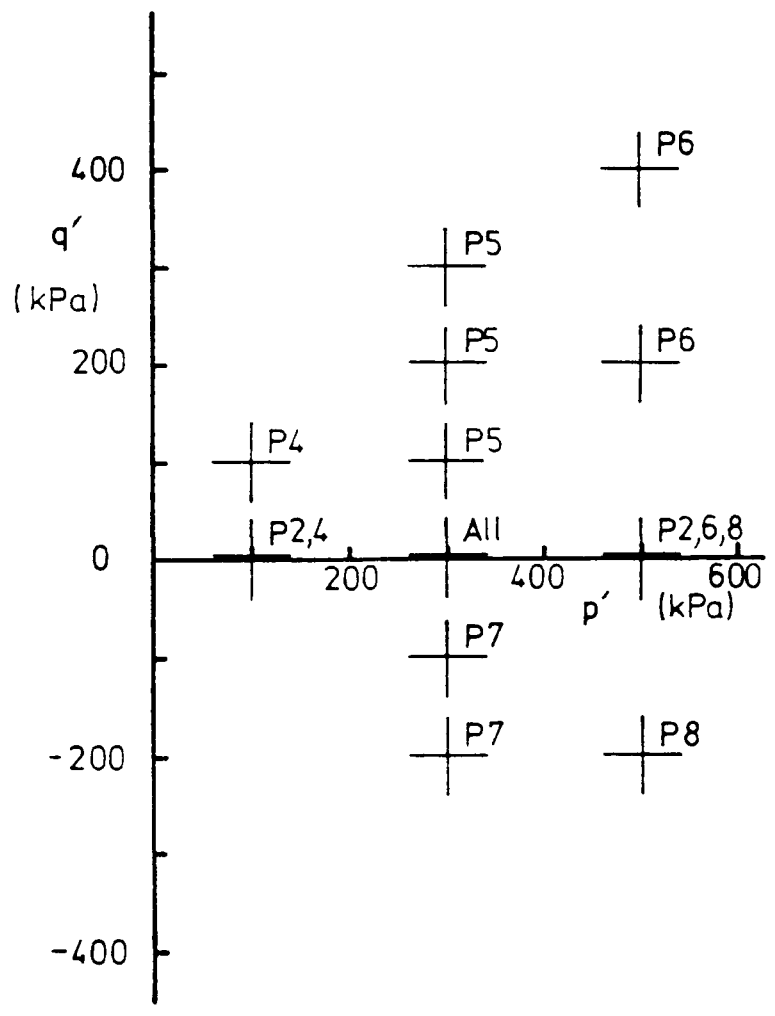

Fig 6.30 Test numbers for constant p' and constant q' probes

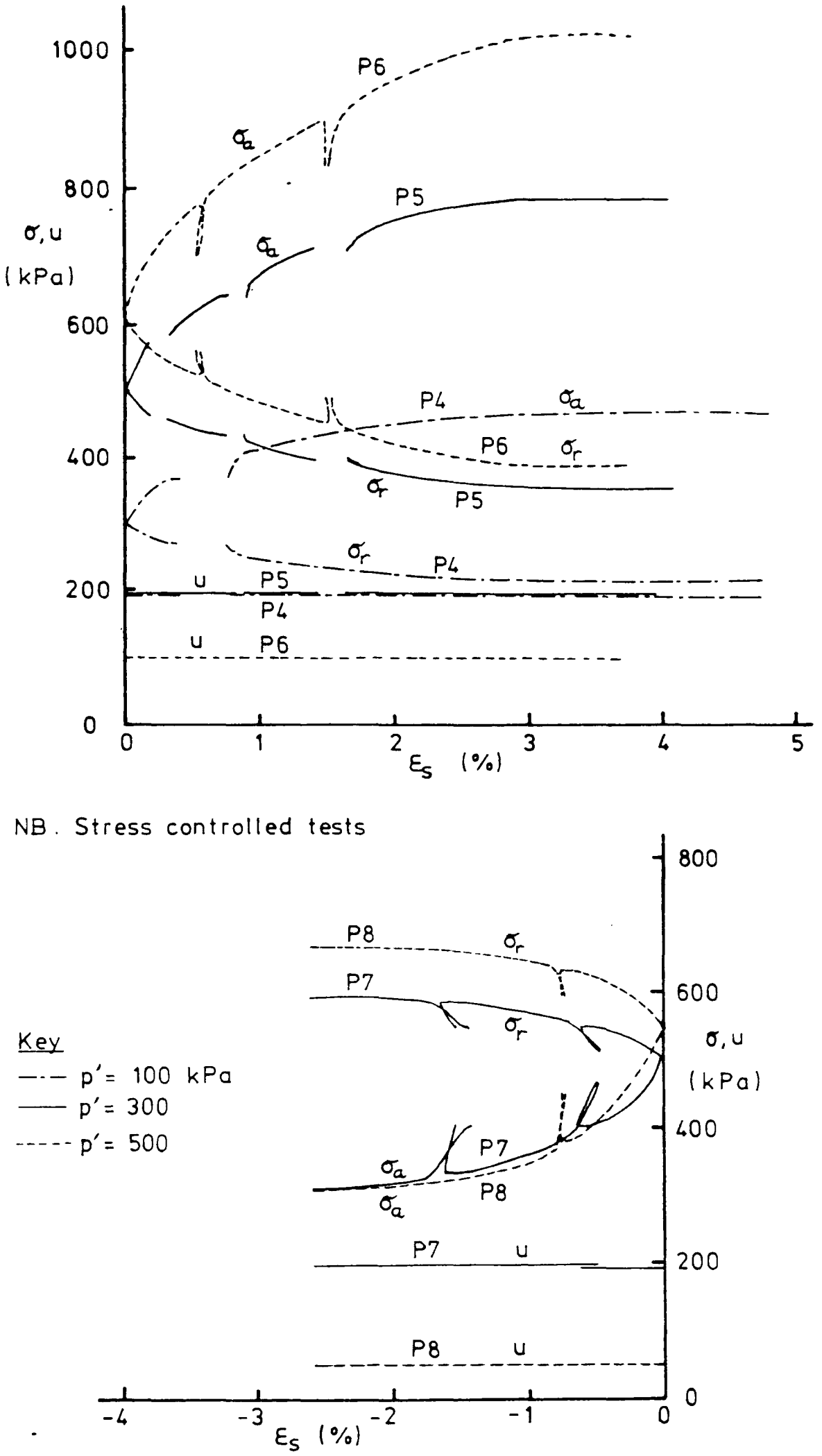

Fig 6.31 Basic test data for constant p' tests to failure

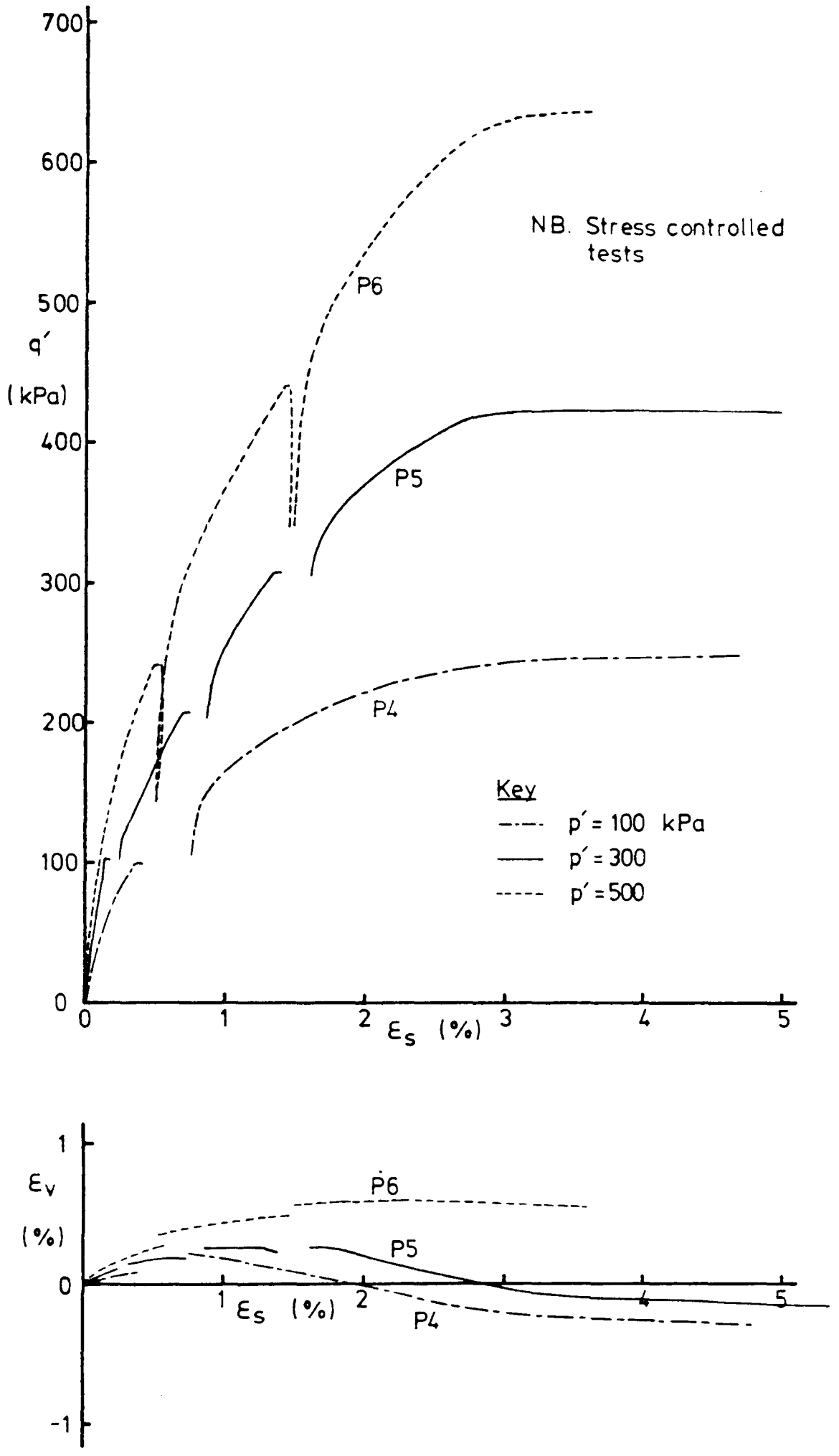

Fig 6.32 Stress - strain and volume change curves, constant p' compression tests to failure

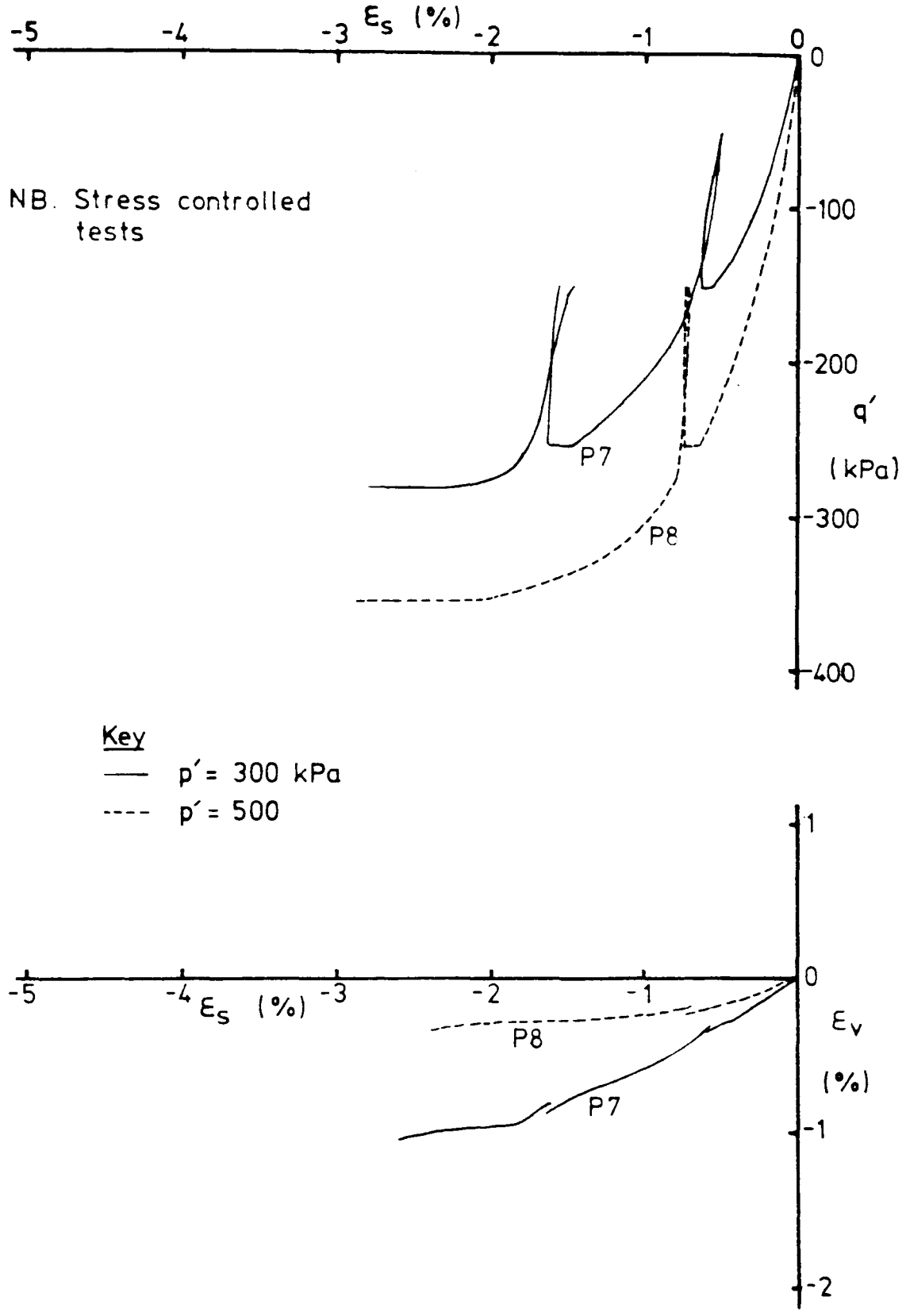

Fig 6.33 Stress - strain and volume change curves, constant p' extension tests to failure

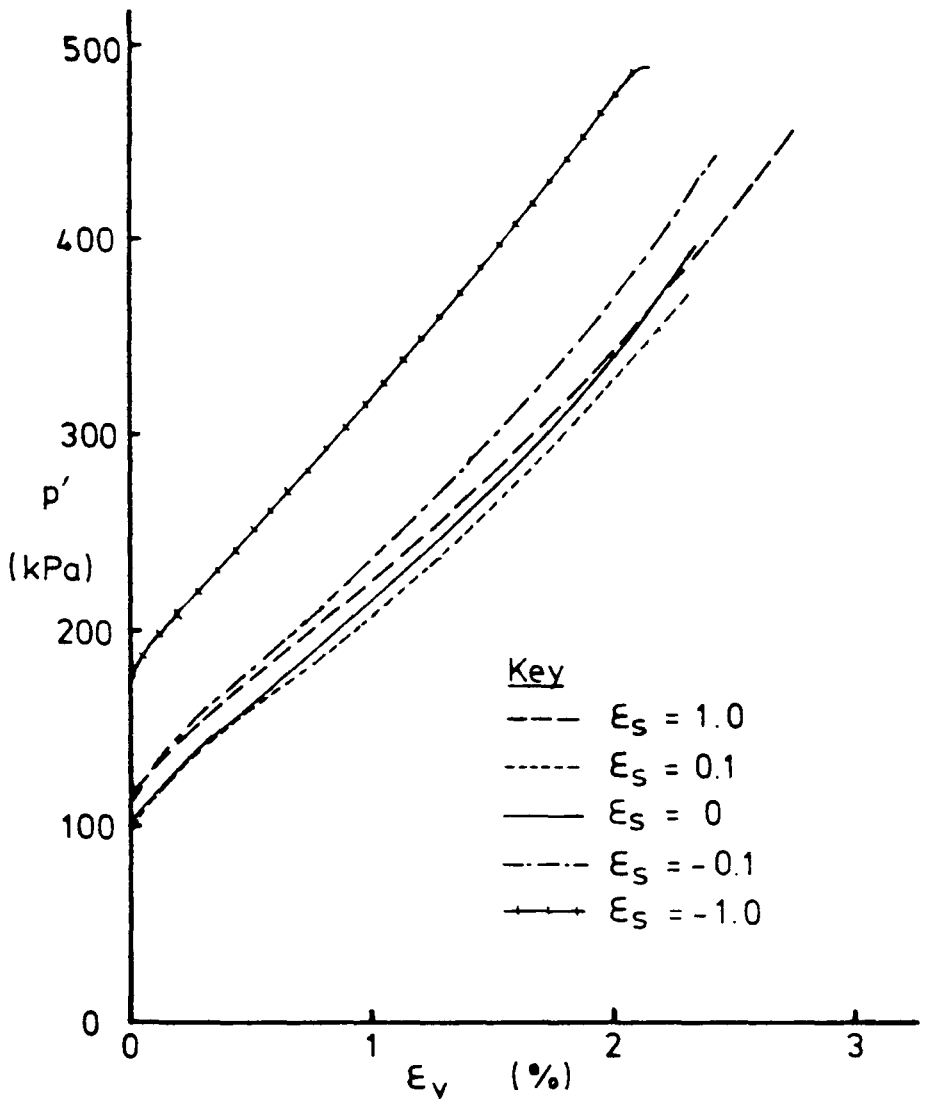

Fig 6.34 Stress - strain curves for constant shear strain test

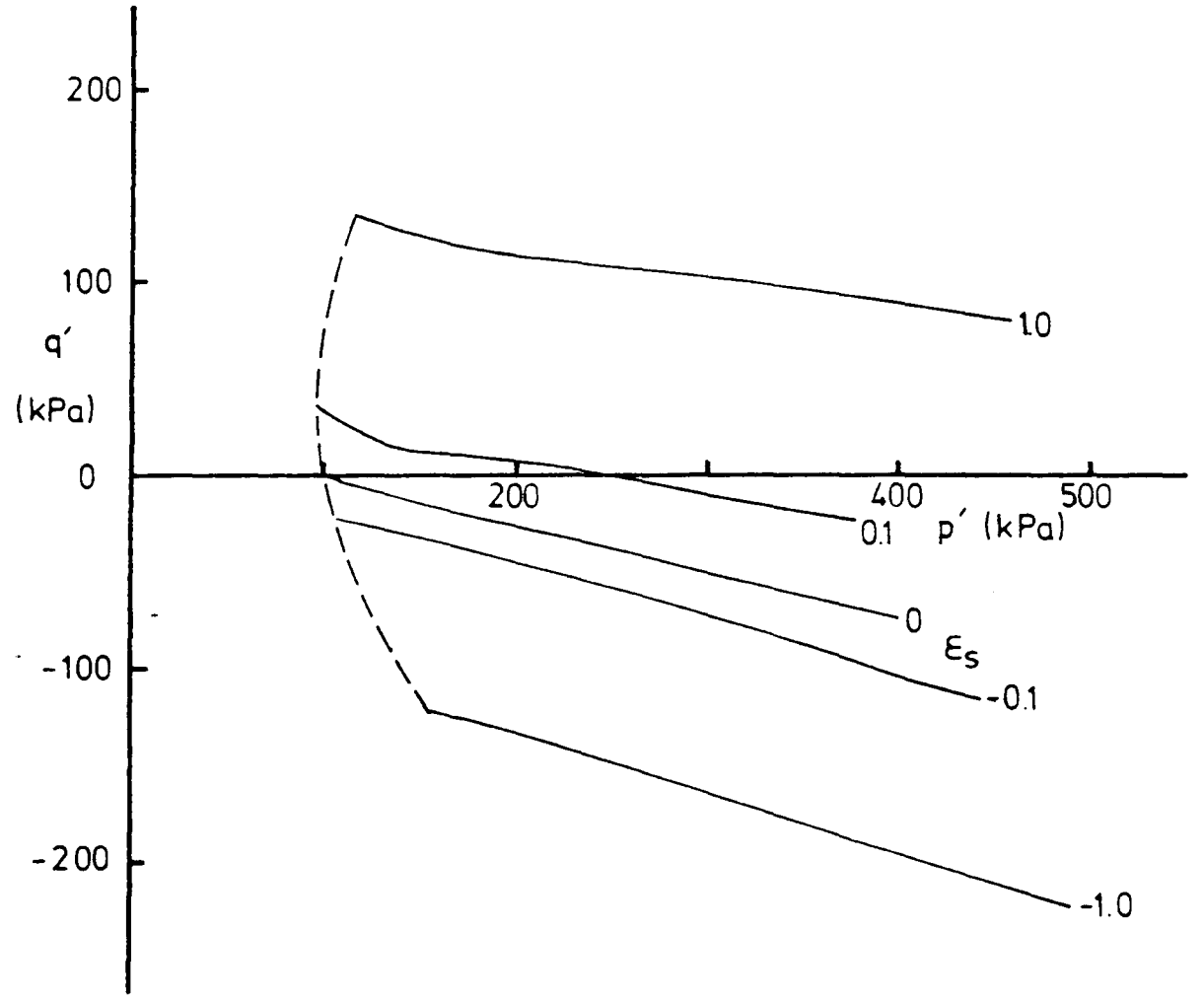

Fig 6.35 Stress paths for constant shear strain tests

CHAPTER 7

DISCUSSION

7.1 INTRODUCTION

Basic parameters are derived for the Gault Clay tested. Critical state theory is found to provide a reasonable conceptual model for the soil. The parameters are summarised in Table 7.1.

The compression law for the critical state model is examined carefully for both normal compression and overconsolidated soil. The implications for the application of elasticity theory are discussed.

Information on the stress-strain behaviour of the soil in shear is provided by three sets of compression and extension tests. These are compared using normalising procedures. The stress-strain data are discussed, and the limitations of the normalising methods are noted.

It is shown that anisotropic soil deformation parameters can be measured in the triaxial apparatus. The method is investigated by comparing results from several pairs of stress path probes.

A series of stress path probe tests provides information on the variation of elastic deformation parameters with soil state. The resulting relationships are compared with the patterns of soil behaviour found from strain path tests.

7.2 COMPRESSION AND SWELLING

7.2.1 Parameter Definitions

The critical state model assumes the isotropic normal consolidation line to be straight in v-ln(p') space, with the equation

$$v = N - \lambda \ln(p'). \qquad (7.1)$$

The swelling and recompression line is given by

$$v = v_\kappa - \kappa \ln(p') \qquad (7.2)$$

The parameter definitions are illustrated on Figure 2.3.

Butterfield (1979) proposed that the compression and swelling lines should be straight in ln(v)-ln(p') space, with the corresponding equations

$$\ln(v) = N^* - \lambda^* \ln(p') \qquad (7.3)$$

$$\ln(v) = v_\kappa^* - \kappa^* \ln(p') \qquad (7.4)$$

For an isotropic soil, compression and swelling under isotropic pressures will produce some shear deformation. This conflicts with the concept of the swelling line representing elastic volumetric compression only of the soil. However, the definition of the parameters κ and κ^* will be taken as the intersection of the elastic wall with the q'=0 plane, to be consistent with Equations 7.2 and 7.4.

7.2.2 Basic Parameters

The compression and swelling results for reconstituted and undisturbed samples have been replotted on the same graph in

Figure 7.1. The oedometer results are also included, plotting σ_v' as p'. The actual value of p' is not known because the radial stress was not measured in the oedometer tests. It is probable that the radial stress was a little lower than the applied stress, resulting in values of p' somewhat less than those plotted.

Figure 7.1 has been replotted with the axes ln(v) against ln(p') in Figure 7.2.

The normal consolidation line may be taken as the best fit to the compression test data for reconstituted samples. As shown on Figure 7.1, this is the line

$$v = 3.264 - 0.226 \ln(p') \qquad (7.5)$$

Hence, two basic parameter values are N = 3.264 and λ = 0.226.

Extrapolation of the normal consolidation line determined above is not very satisfactory, since both oedometer tests produced data which lie significantly to the right of the line. Closer examination of the reconstituted sample test data (Tests R1 to R6) shows a slight curvature. This supports the proposal by Butterfield (1979) that the normal consolidation line should be straight in a ln(v) - ln(p') plot. Less curvature can be seen in Figure 7.2 for the normal consolidation data and, possibly but less markedly, for the swelling and recompression data. The best straight line fit is shown on the figure and is given by

$$\ln(v) = 1.288 - 0.106 \ln (p') \qquad (7.6)$$

Although the oedometer data still lie very close to this new normal compression line, they do not seriously extend to the right of it. It may be concluded that this line is a better fit to the data.

The slope of the straight section of the swelling line for the isotropic reconsitituted sample in Figure 7.1 gives a value κ= 0.07. The swelling line for the K_o compressed sample is compatible with this, but curvature of this line prevents a definition of the parameter κ. The corresponding parameter in ln(v)-ln(p') space may be taken as $\kappa^* = 0.036$.

Table 7.2 gives the values of κ and κ^* for the tests on undisturbed samples (C1 to C11, O1 and O2). The linearity of the undisturbed swelling and recompression lines has been improved by replotting the specific volumes to a logarithmic scale, but there is still some curvature. This is discussed in the next section.

7.2.3 Swelling and Recompression

The linearity of the swelling line may be examined using the data for isotropic compression and swelling given in Figures 6.12 and 6.14 for Tests C1 to C11. A better view of this data can be achieved by replotting the figures. Since natural strains are used as the abscissa, the origin of the strain axis is unimportant and curves can be translated parallel to the strain axis. This has been done on Figure 7.3 making the curves coincide at p' = 300 kPa (except for the swelling curves for Tests C3 and C7 which have been fitted to the curve from Test C5 at p' = 200 kPa). Apart from one anomaly (Test C11 in compression) the results give a fairly consistent smooth curve. The average curves for compression and swelling are shown together on Figure 7.4.

The swelling and recompression behaviour of undisturbed soil may now be examined referring to the curves of Figure 7.4. Firstly, it may be noted that the curves are not identical. This could be attributed to hysteresis, involving some plastic deformation. Although plastic deformation is irrecoverable, a hysteresis loop tends to be roughly closed due to the deformation during the swelling and recompression stages being approximately equal and

opposite. There may be some tendency for progressive dilatency as loads are cycled, but this was not observed in the present series of tests. The true κ line in critical state theory represents purely elastic behaviour, and can thus be expected to fall about half way between the swelling and recompression curves. The line A-A in Figure 7.4 is suggested as a possible "true κ line".

The slope of the deduced elastic compression line from Figure 7.4 has been plotted against p' on Figure 7.5. The slope is shown to be approximately proportional to p' supporting the use of κ^* rather than κ, with a value $\kappa^* = 0.022$.

7.2.4 K_o Compression

In the critical state model the state path in v-ln(p') space for K_o compression would be expected to be parallel to the normal consolidation line and just to the left of it. The data plotted in Figure 7.1 support this, although the K_o compression line may be slightly steeper than the normal consolidation line.

From Figure 6.6 the value of K_o may be taken as 0.59. The lack of linearity in the initial part of the stress path is thought to be due to sample disturbance during installation, which would reduce the initial effective stress in the specimen leaving it in an overconsolidated state.

7.3 STATE BOUNDARY SURFACE

The state paths for the compression and extension tests may be normalised, as discussed in Section 2.2.7. The values of N and λ derived in Section 7.2 are used. The state paths are shown on Figures 7.6 and 7.7.

The Roscoe / Rendulic surface is fairly well defined by the

normalised state paths for the reconstituted samples in Figure 7.6. In Figure 7.7 there is some discrepancy between the state paths in compression for Tests R3 and R5, and this reflects the inaccuracy of measurement of specific volume in the smaller samples.

The Hvorslev surface is not well defined by the data, although the trend of the results supports the critical state model.

7.4 FAILURE STATES

7.4.1 Definition

Peak failure may be defined as the maximum deviator stress endured by the sample or as the maximum stress ratio. In the latter case, the actual point at which failure is deemed to take place will depend on the parameters chosen: maximum σ_1'/σ_3' will not in general coincide with maximum q'/p'. The definition using peak deviator stress is less prone to confusion and will be used here.

Ultimate failure is defined as continued shear deformation at an unchanging stress state.

7.4.2 Failure states

Failure states for the tests reported in Chapter 6 are plotted on Figures 7.8 to 7.10. The overall objective of the laboratory testing was to examine the stress-strain behaviour of the soil, and consequently the data for failure is limited. In particular, the constant p' tests (Tests P4 to P8) were load-controlled to failure, providing no information on post-peak behaviour.

7.4.3 The Critical State

Critical state parameters refer to the ultimate failure states of soil. In the overconsolidated undisturbed samples, failure occurred in a thin shear zone at the critical state, while the majority of the specimen was not at the critical state. Measurements made for undisturbed soil do not therefore reflect critical state failure, although the measured failure states do indicate bounds to the ultimate failure condition.

Critical state parameters should be derived from the reconstituted test results. In Figure 7.8, a suitable fit to the data in v-ln(p') space is

$$v = 3.184 - 0.226 \ln(p') \qquad (7.7)$$

The slope of the line has been chosen to correspond to that of the normal consolidation line, and the parameter Γ then takes the value 3.184.

Figure 7.10 shows the failure stress states. The data for reconstituted soil gives critical state lines

$$q' = 1.0\ p' \qquad (7.8)$$

and

$$q' = -1.0\ p' \qquad (7.9)$$

That is, $M_c = 1.0$ and $M_e = -1.0$. Data for the undisturbed soil would suggest lower values, $M_c = 0.86$ and $M_e = 0.62$. For compression, the value $M_c = 1$ corresponds to $\phi'_c = 25°$. In extension, $M_e = -1$ gives $\phi'_e = 37°$.

7.4.4 Peak Failure States

The Hvorslev surface is not well defined by the data.

The uniaxial compression and extension test results for undisturbed samples lie near the critical state line, giving the ϕ' values quoted in the previous section, with c'=0. The constant p' compression tests gave a failure line c'=60 kPa, φ'=25°.

In Figure 7.8, all the failure states for undisturbed samples lie to the left of the deduced critical state line, as would be expected.

It is interesting to note that the stress-controlled constant p' compression tests on 100mm diameter samples (Tests P4 to P6) gave consistently higher strengths than the strain-controlled drained and undrained compression tests on 38mm samples (Tests U1, U3 and U4). There is no apparent difference in extension tests. The reason for this anomaly is not clear. Stress controlled tests will tend to fail quickly as there is no constraint on the strain, which limits the development of shear zones (Atkinson and Richardson, 1986) producing a higher strength. However, the tests were suitably slow prior to failure and particularly so at the stress levels causing failure in the strain controlled tests. The stress controlled tests had all undergone stress probes at stages during compression, which may have caused some hardening effect. However, similar probing also affected the extension tests. A more likely explanation is the additional sample disturbance associated with preparing 38mm diameter samples from the U100 samples. Again, this does not appear to have affected the extension tests in the same way.

7.5 STRESS-STRAIN BEHAVIOUR

The stress-strain curves given in Figures 6.10, 6.25 and 6.32 show some variation, reflecting the differences in soil state and stress path between the tests. The exception is for Tests R4 and R6, where the drained and undrained stress paths in extension were very similar. To examine the data properly it is necessary to normalise the results. The procedure outlined in Section 2.4.4 has been used to produce the curves shown in Figures 7.11 to 7.14. These have been combined on Figure 7.15. Tangent stiffness parameters have been derived for these tests, also normalised as indicated in Section 2.4.4, and the results are plotted on Figures 7.16 to 7.18.

The normalising procedure produces a reasonable but not exact correspondence between samples at a comparable state tested with different stress paths. These groups include Tests U1, U4 and P5, Tests U2, U6 and P7, and the tests on reconstituted samples. The method may therefore be accepted as a means of comparing the results from the different tests. The normalising procedure would be modified by omitting the factor v if the Butterfield compression law was adopted. However, the dependence on specific volume is not strong, and this would not affect interpretation of the results.

The normalised results show that undisturbed soil tends to be stiffer than reconstituted soil, and that the undisturbed samples tested at lower mean effective stress tend to be stiffer than those with higher p'. This indicates an increase in normalised stiffness with overconsolidation ratio. The normalisation method can therefore only be used to compare results for soils with similar overconsolidation ratios. The parameter q'/p' does not reflect the soil's overconsolidation ratio.

It may be noted that the normalised stress-strain curves for the extension tests show much closer agreement than those for the

compression tests. The ratio q'/p' at failure in extension is much less affected by overconsolidation than it is in compression, and this is apparently true also for the stress-strain behaviour before failure. For the compression tests, if the ratio q'/p' was itself normalised by dividing by the value of q'/p' at failure for each test, it can be seen that a closer correspondence of the stress-strain curves would result. This ratio is not a very satisfactory soil parameter because of the difficulty of consistent measurement of soil strength for overconsolidated soil, where formation of a slip zone, and hence strength, is affected by test procedure. A more correct parameter could be defined by the location of the Hvorslev surface. It is suggested that a normalising parameter q'/q_h' might be investigated for heavily overconsolidated soil, where q_h' is the value of q' at the Hvorslev surface for a given p' and v. Unfortunately, the Hvorslev surface has not been well defined by the present data, and this method cannot be tested here.

7.6 CONSOLIDATION

Values for the coefficient of consolidation have been calculated from the consolidation curves shown in Figures 6.15 to 6.19 by the square root of time method. The calculation for the oedometers was in accordance with BS 1377 (1975), and for the triaxial tests the method given by Bishop and Henkel (1962) was used. The results are given on Table 7.3.

It can be seen that the c_v values found from the triaxial tests are consistently lower than those from the oedometer results. Such discrepancies are frequently found in laboratory data. Often, they are ascribed to differences in permeability in the vertical and horizontal directions. In this case, this may be a contributory factor, but the appearance of the soil does not suggest a wide difference in permeabilities. Consolidation theory (Terzaghi, 1943) gives the formula

$$c_v = k / m_v \gamma_w \qquad (7.10)$$

An alternative to suggesting that the horizontal permeability is more than the vertical is that the horizontal stiffness may be greater than the vertical stiffness. Hence, the discrepancy between oedometer and triaxial consolidation may be a further indication or result of the anisotropic stiffness of the soil.

7.7 ANISOTROPIC ELASTIC PARAMETERS

7.7.1 Introduction

An attempt has been made to measure the anisotropic elastic parameters for soil using two different stress path probes carried out on a single soil sample. This is an alternative approach to that of Graham and Houlsby (1983) who performed each stress path on a different sample, with the inherent problems of variations between samples both in soil type and in soil state.

The feasibility has been investigated using a variety of stress path probes on a single sample, returning the specimen to the same stress state after each probe. This was designated Test P1. The probes are listed in Table 6.9 and illustrated on Figure 6.29. The results of the test are given in Table 6.10.

In the following sections anisotropic elastic parameters are deduced from different pairs of stress path probes, and an assessment of the method is made.

7.7.2 Sample State, Disturbance and Consistency

The measurement of anisotropic elastic parameters from two different stress path probes will only be successful if the soil behaves consistently for both probes. This means that it must be at the same state for each probe, and that behaviour during each stress path is not affected by previous probes.

For each stress path probe, the sample was brought to the same initial stress state of p' = 300 kPa, q' = 0. By examining the values for specific volume given in Table 6.10, this appears to achieve the object of attaining almost identical soil states, with no measureable cumulative disturbance.

The latter requirement was met in Test P1 by controlling the stress history of the soil immediately prior to each probe. The target stress state was approached with a stress path approximately corresponding to the undrained reloading path from negative q'. For some probes an approach path at constant p' was accepted as very similar.

As an alternative, the stress history could be made to be continuous with the stress probe. This was the case for the unloading stages of the stress probe cycles, and for the undrained loading stages (and, approximately, for the constant p' loading). The isotropic stress probe (Test P1 Cycle 12) was most affected by change in stress path direction, so to examine this effect an additional reloading section (Cycle 12*) was added to the isotropic cycle to achieve a continuous stress history for the measurement section of the path.

The consistency between stress path probes was checked by repeating the undrained probe several times during the test (Test P1 Cycles 1,2,3,6,7,9 and 13). Although there is a fairly high scatter in the $q':\varepsilon_s$ slopes measured, this appears to be random with no progressive stiffening or weakening of the sample during

the test. For the seven undrained cycles, the standard deviation was 15 per cent of the mean value for loading, and 19 per cent for unloading.

It may be concluded that the soil can be returned to approximately the same state for each stress path probe with little disturbance. However, the scatter in undrained stress probe results shows some lack of consistency between probes.

7.7.3 Deriving Elastic Parameters

Any two different stress paths may be used to derive the three anisotropic elastic parameters, as discussed in Chapter 3, but the best definition is obtained if the stress paths are approximately at right angles to each other in stress space. Referring to Figure 6.29, suitable pairs of stress paths would be the isotropic cycle with each of the drained or undrained uniaxial cycles and the constant p' cycles, plus the pair of drained stress paths at $\Delta q' = \pm\Delta p'$.

The stress-strain data for Test P1 from Table 6.10 has been used to derive stiffness parameters following the method described in Section 3.3 and detailed in Appendix A. These parameters are given in Tables 7.4 to 7.6.

7.7.4 Discussion on Measurements

The isotropic loading following the standard stress history (Test P1 Cycle 12) gives a much stiffer response than the reloading part of the cycle (Cycle 12^*) where the stress path does not involve a change of direction. This is due to threshold effects. The greater stiffness is reflected in the derived elastic parameters, with an average value for K_a' of 39 MPa compared to 28 MPa for the continuous stress path. The average value for unloading (also with continuous stress paths) is 33 MPa. The pairs of stress paths at $\Delta q' = \pm\Delta p'$ give K_a'=33 MPa for loading

and K_a' = 28 MPa for unloading. This amplifies the importance of recent stress history in the deformation behaviour of soil.

The consistency of the measurements between the two stress paths used may be assessed by comparing the values of J'_1 and J'_2. This will be done by looking at the difference between J'_1 and J'_2 with their mean as a percentage of their mean.

For the results of Table 7.4(a) the scatter averages 38%; for Table 7.4(b) it is 16%, and for Table 7.5 it is 28%. From these three groups of measurements for undrained cycles with isotropic tests it is concluded that the most consistent data was obtained for the unloading stages. The least consistent was for undrained loading paired with the isotropic first loading, and in between came the undrained loading with isotropic reloading. This pattern was found to be typical of the results for Table 7.6 as well.

It is concluded that the most consistent results have been obtained where the soil is least affected by recent stress history in both stress probes, and that this can best be achieved by making the approach stress path continuous with the section of path to be measured.

There does not appear to be a significant difference between results for the various pairs of stress paths used.

Scatter in the values for the coupling modulus reflects that in the data from which they were derived, and is no worse than scatter for the values of G_a' measured directly. This stress probe procedure may therefore be regarded as a suitable way to measure the anisotropic elastic parameters for soil at a given state.

If anisotropy were to be ignored then values for 3G' and K' would be taken as the stress-strain slopes in constant p' and isotropic

tests respectively. However, these apparent moduli are about 25% lower than the values calculated from the same data but taking anisotropy into account. This value is comparable to the scatter in the data, but unlike the scatter the error is constant in direction. There is therefore a significant benefit in recognising the anisotropy of soils if deformation parameters are needed.

7.8 VARIATION OF DEFORMATION PARAMETERS WITH SOIL STATE

7.8.1 Introduction

The variation of anistropic elastic parameters is investigated using all the stress probe data for Tests P1 to P8 given in Tables 6.10 to 6.19. The stiffness parameters have been derived using the methods given in Appendix A, and the results are presented in Tables 7.4 to 7.15.

The data from the isotropic compression tests are used to provide further information on the bulk modulus, and the critical state parameter κ is examined.

Finally, a strain pattern diagram similar to that of Wroth and Loudon (1967) is produced, and this approach is extended by a similar diagram based on stress paths for constant shear strain. The strain pattern is related to the parameter varation found from the stress probe tests.

7.8.2 Bulk Modulus

The values of the basic critical state parameter κ were discussed in Section 7.2 and it was concluded that the parameter κ^* (the slope of a straight swelling line in ln(v) - ln(p') space) was preferred. This parameter represents the intersection of the elastic wall with the q'=0 plane.

The bulk modulus K' is defined as $dp'/d\varepsilon_v$ for isotropic soil, and for anisotropy the equivalent K_a' is defined by

$$\begin{Bmatrix} \delta q' \\ \delta p' \end{Bmatrix} = \begin{bmatrix} 3G_a' & J' \\ J' & K_a' \end{bmatrix} \cdot \begin{Bmatrix} \delta\varepsilon_s \\ \delta\varepsilon_v \end{Bmatrix} \qquad (7.11)$$

Thus, for isotropic soil

$$K' = vp'/\kappa \qquad (7.12)$$

or

$$K' = p'/\kappa^* \qquad (7.13)$$

However, for anisotropic soil the swelling line is defined by

$$\begin{Bmatrix} 0 \\ \delta p' \end{Bmatrix} = \begin{bmatrix} 3G_a' & J' \\ J' & K_a' \end{bmatrix} \cdot \begin{Bmatrix} \delta\varepsilon_s \\ \delta\varepsilon_v \end{Bmatrix} \qquad (7.14)$$

giving

$$\delta p'/\delta\varepsilon_v = K_a' - J'^2/3G_a' = p'/\kappa^* \qquad (7.15)$$

and K'_a cannot be related directly to κ or κ^*. However the variation of the two parameters with soil state may be expected to be similar.

Variation of the bulk modulus K_a' may be examined from the results of the stress probe tests. The data for Tests P1 to P8 were given in Tables 6.10 to 6.19, and the anisotropic stiffness parameters derived using the procedure contained in Appendix A are presented in Tables 7.4 to 7.15.

The discussion will initially be confined to soil at an isotropic

stress state q'=0. The two remaining state parameters are p' and v.

In the Cam Clay model the bulk modulus is assumed to vary with the specific volume. This seems wrong intuitively since denser soil may be expected to be stiffer. This is complicated by a difference in the overconsolidation ratio R between soils at the same p' but with different specific volumes. The three parameters are linked by the equation

$$v = N - (\lambda - \kappa)\ln(R) - \lambda \ln(p') \qquad (7.16)$$

For Butterfield's (1979) compression law K' is independent of v.

These relationships have been tested in Figure 7.19 by plotting K_a' against v for all the samples tested at p' = 300 kPa. The results are not particularly conclusive due to scatter and the relatively narrow range of volumes, but they do not support $K_a' \propto v$. The trend is for some inverse variation of K_a' with v, but a lack of dependence would also be an acceptable interpretation.

In the critical state model, a soil parameter κ or κ^* leads to a direct variation of the bulk modulus with the mean effective stress. Accepting that variations in specific volume may be neglected, this may be tested by plotting K_a' against p' for all the results from Tables 7.4 to 7.15 for Tests P1 to P8 at q' = 0. This is given on Figure 7.20. The graph indicates that a straight line relationship is reasonable, but with an intercept on the p'=0 axis. This is consistent with the equation

$$K_a' - J'^2/3G_a' = p'/\kappa^* \qquad (7.15 \text{ bis})$$

with the ratio $J'^2/3G_a'$ roughly constant (≈10MPa) over the range of p' tested.

In the critical state model the bulk modulus is not expected to vary with deviator stress, and for isotropic soil the elastic wall is a vertical plane cutting the q' = 0 plane along the swelling line. Anisotropy simply inclines the elastic wall. K_a' has been plotted against q' on Figure 7.21 for Tests P4 to P8. For the tests at p' = 100 and 300 kPa the values for K_a' are not greatly affected by q'. At p' = 500 kPa the compression stiffness was found to increase significantly as q' increased. The reason for this is not clear, but may be due to threshold effects. This would be in line with Simpson's (1986) observation that threshold limits increase in size at higher effective pressures.

7.8.3 Shear Modulus

Variation of the shear modulus with specific volume has seldom been investigated. As with the bulk modulus, the shear stiffness of soil might be expected intuitively to increase as the specific volume decreases. The anisotropic shear moduli given in Table 7.15 (for p' = 300 kPa, q' = 0) have been plotted against v in Figure 7.22(a), and the anticipated trend is evident. Replotting the data against 1/v in Figure 7.22(b), the tentative conclusion is that G_a' is inversely proportional to the specific volume.

In investigating the variation of G_a' with p' and q' the results will be normalised by multiplying G_a' by the specific volume.

The shear modulus normalised with respect to specific volume has been plotted against p' on Figure 7.23. The values are for q'=0 and have been taken from Tables 7.4 to 7.15. There is quite a wide scatter in the data. An increase of $v.G_a'$ with p' is evident but the relationship does not appear to be linear. A power law presents a reasonable fit to the data with

$$v.Ga' = a\ p'^{0.6} \qquad (7.17)$$

where the value of a lies between about 0.6 and 1.4. This agrees well with the results of Houlsby (1981). The shear stiffness in loading is noticeably higher than in unloading. The reason for this is not clear.

The effect of overconsolidation ratio on shear stiffness has not been investigated directly in the present series of tests. An indication of the probable effect was noted in Section 7.5.

Variation of the shear modulus with deviator stress is evident from the curvature of the stress-strain curve for undrained tests. Figure 7.17 shows a variation in tangent stiffness that is typical of many heavily overconsolidated clays.

Figures 6.32 and 6.33 are interesting in that they show the integration of unloading/reloading sections into the stress-strain curves. The usual interpretation for curves of this type is that the amount of plastic shearing gradually increases as the deviator stress increases, and this adds to the elastic (recoverable) shear deformation. The unloading/reloading deformation is assumed to represent the elastic part of the shear strain, and this has been measured in the stress probe tests.

The variation of the shear modulus with deviator stress is shown on Figure 7.24. The modulus has been normalised with respect to specific volume, but the results for each value of p' should be regarded separately. As may be expected, at p'=100 and 300 kPa the shear stiffness was found to decrease as q' increased. It is interesting to note that in the corresponding extension tests the stiffness tends to increase as the deviator stess increases. It is not clear why this should be so, but more data would be needed to confirm this observation. The shear stiffnesses for p'=500 kPa show some very high values. As for the bulk modulus, it is thought that these results are affected by threshold effects.

As for the bulk modulus, the value of the shear modulus is

significantly larger than the measured value of $\delta q'/\delta \varepsilon_s$ in constant p' tests because of the anisotropy of the soil.

The overall assessment of the shear modulus data is that there is a lot of scatter in the results. This is caused by a combination of soil variability and measurement inaccuracies. The latter is probably a consequence of the relatively high stiffnesses being measured, where small variations in strain measurements can cause an appreciable change in the computed modulus.

7.8.4 Patterns of Strain

Undrained stress paths represent lines of constant volumetric strain in q':p' space. Following the method used by Wroth and Loudon (1967) contours of equal shear strain may be plotted on the undrained stress paths, as shown in Figure 7.25. The results are similar to those of Wroth and Loudon, and the effect of anisotropy is to incline the undrained stress paths.

The contours of shear strain have been drawn as straight lines, but it can be seen that they do not pass through the origin of the axes. Soil with zero mean effective stress would be expected to have no stiffness. This would suggest that the lines should be curved. For soil near the isotropic stress axis this would agree with the findings of the previous section, with $G' \propto p'^{0.6}$ approximately.

The spacing of the contours of shear strain are related to the curvature of the stress-strain curves for the undrained tests. No comparison can be made with the unloading/reloading moduli discussed in the previous section. It may be noted that there is no symmetry about the p' axis. The shear modulus is lower for the extension tests than for compression tests.

The computer controlled triaxial apparatus has enabled constant shear strain paths to be followed, as shown on Figure 6.35.

Values for volumetric strain from Figure 6.34 may be used to draw the contours shown on Figure 7.26. This may be seen as a complementary diagram to that of Figure 7.25.

The stress paths for constant shear strain are inclined which is a measure of the anistropy. The slope in q':p' space is given by the ratio J'/K_a'. There is a slight divergence of the lines, indicating that the soil anisotropy is more pronounced in extension, and diminishes with increased positive deviator stress. This may be an indication that the anisotropy is substantially stress-induced for this soil.

For all the constant shear strain paths the $p':\varepsilon_v$ lines shown in Figure 6.32 have just a slight curvature which is less than the curvature for the compression tests under isotropic stresses. The $p':\varepsilon_v$ lines all show very similar behaviour, with the consequence that the ε_v contours sketched on Figure 7.26 are roughly parallel to each other and to the undrained path representing $\varepsilon_v=0$.

The slopes of the curves on Figure 6.34 give K_a' directly. Figure 7.27 shows the derived bulk modulus plotted against p'. For the test at $\varepsilon_s=0$, $K_a' \propto p'$ fits the data well for the later stages of the test. For the tests at other values of shear strain, the bulk modulus was found to vary roughly linearly with mean effective stress, but with a small intercept on the p'=0 axis. This probably indicates that there would be some curvature at the lower stress levels.

Critical State		Other	
Reconstituted Samples		**Reconstituted Samples**	
N	3.264	K_o	0.59
λ	0.226	ϕ'_c	25°
κ	0.070	ϕ'_e	37°
Γ	3.184		
M_c	1.0	**Undisturbed Samples**	
M_e	-1.0		
λ^*	0.106	m_v	0.08 m^2/MN
κ^*	0.036	c_v	0.1 to 0.5 m^2/yr
N^*	1.288		

Table 7.1 Summary of Basic Soil Parameters

Test	Stage	Compression or swelling	κ	κ*
C1	1	s	0.023	0.015
C2	1-3	c	0.056	0.033
	4-6	s	0.035	0.021
C3	1	s	0.046	0.025
C4	1	c	0.037	0.021
C5	1	c	0.044	0.026
	2,3	s	0.032	0.019
C6	1	c	0.047	0.027
	2	cK_o	0.070	0.041
	3	sK_o	0.035	0.021
C7	1	s	0.039	0.022
C8	1	c	0.043	0.025
C9	1	c	0.041	0.024
	2	s	0.022	0.013
C10	1	s	0.028	0.017
C11	2	c	0.033	0.021
	1	s	0.029	0.018
01	1-4	c	0.049	0.029
02	1-4	c	0.043	0.027

Table 7.2 Slopes of v-ln(p') and ln(v)-ln(p') Lines for Compression and Swelling Tests on Undisturbed Samples

Test	Stage	Pressure Range (kPa)	v	c_v (m^2/yr)
D1	1	212 - 400	1.682	0.28
D2	1	128 - 200	1.679	0.19
	2	200 - 300	1.666	0.17
	3	300 - 500	1.649	0.17
D3	1	300 - 400	1.658	0.14
	2	400 - 600	1.643	0.09

(a) Triaxial

Test	Stage	Pressure Range (kPa)	v	c_v (m^2/yr)
01	1	320 - 428	1.673	0.45
	2	428 - 856	1.654	0.45
	3	856 -1712	1.620	0.50
	4	1712 -3424	1.574	0.50
02	1	320 - 428	1.628	0.70
	2	428 - 856	1.614	0.45
	3	856 -1712	1.585	0.47
	4	1712 -3424	1.541	0.57

(b) Oedometers

Table 7.3 Measurements of the Coefficient of Consolidation

Pairs of cycles	$3G_a'$ (MPa)	J_1' (MPa)	J_2' (MPa)	K_a' (MPa)
1 + 12	76	-35	-18	40
2 + 12	82	-38	-14	38
3 + 12	78	-36	-16	39
6 + 12	64	-30	-17	40
7 + 12	61	-28	-13	38
9 + 12	67	-31	-10	37
13 + 12	97	-45	-18	40

(a) Loading

Pairs of cycles	$3G_a'$ (MPa)	J_1' (MPa)	J_2' (MPa)	K_a' (MPa)
1 + 12	66	-23	-17	32
2 + 12	58	-20	-16	32
3 + 12	74	-26	-19	33
6 + 12	87	-30	-24	34
7 + 12	100	-35	-18	32
9 + 12	105	-36	-26	35
13 + 12	89	-31	-25	35

(b) Unloading

Table 7.4 Stiffness Parameters Using Undrained and Isotropic Cycles
Test P1

Pairs of cycles	$3G_a'$ (MPa)	J_1' (MPa)	J_2' (MPa)	K_a' (MPa)
1 + 12*	76	-27	-18	29
2 + 12*	82	-29	-14	28
3 + 12*	78	-28	-16	29
6 + 12*	64	-23	-17	29
7 + 12*	61	-22	-13	28
9 + 12*	67	-24	-10	27
13 + 12*	97	-35	-18	29

Table 7.5 Stiffness Parameters Using Undrained Cycles with Isotropic Reloading
Test P1

Pairs of cycles	$3G_a'$ (MPa)	J_1' (MPa)	J_2' (MPa)	K_a' (MPa)
Const p' (4) + Isot.(12)	70	-12	-33	37
Const p' (11) + Isot.(12)	79	-30	-37	46
Drained (10) + Isot.(12)	80	-37	-8	36
Const p' (4) + Isot.(12*)	68	-8	-24	26
Const p' (11) + Isot.(12*)	72	-20	-26	30
Drained (10) + Isot.(12*)	72	-26	+1	23
$\Delta q'=\Delta p'$ (5) + $\Delta q'=-\Delta p'$ (8)	54	-15	-16	33

(a) Loading

Pairs of cycles	$3G_a'$ (MPa)	J_1' (MPa)	J_2' (MPa)	K_a' (MPa)
Const p' (4) + Isot.(12)	61	-17	-21	32
Const p' (11) + Isot.(12)	75	-22	-26	34
Drained (10) + Isot.(12)	57	-20	-18	32
$\Delta q'=\Delta p'$ (5) + $\Delta q'=-\Delta p'$ (8)	58	-22	-16	28

(b) Unloading

Table 7.6 Stiffness Parameters Derived Using Various Pairs of Stress Probes
Test P1

Cycles	p_o' (kPa)	q_o' (kPa)	v_o	$3G_a'$ (MPa)	J_1' (MPa)	J_2' (MPa)	K_a' (MPa)
12,14	100	0	1.675	39	-5	-11	16
7,9	300	0	1.607	58	+6	-21	36
2,4	500	0	1.596	68	-24	-16	49

(a) Loading

Cycles	p_o' (kPa)	q_o' (kPa)	v_o	$3G_a'$ (MPa)	J_1' (MPa)	J_2' (MPa)	K_a' (MPa)
12,14	100	0	1.675	17	-4	-4	17
-	300	0	1.607	-	-	-	-
2,4	500	0	1.596	43	-12	-13	38

(b) Unloading

Table 7.7 Stiffness Parameters
Test P2
Constant p' and Constant q' Probes

Cycles	p_o' (kPa)	q_o' (kPa)	v_o	$3G_a'$ (MPa)	J_1' (MPa)	J_2' (MPa)	K_a' (MPa)
13,14	100	0	1.676	39	-11	-4	15
8,9	300	0	1.608	96	-35	-16	44
3,4	500	0	1.595	150	-36	-27	49

(a) Loading

Cycles	p_o' (kPa)	q_o' (kPa)	v_o	$3G_a'$ (MPa)	J_1' (MPa)	J_2' (MPa)	K_a' (MPa)
13,14	100	0	1.676	18	-4	-8	18
8,9	300	0	1.608	40	-	-12	-
3,4	500	0	1.595	68	-21	-14	38

(b) Unloading

Table 7.8 Stiffness Parameters
Test P2
Undrained and Isotropic Cycles

Cycle	p_o' (kPa)	q_o' (kPa)	v_o	$3G_a'$ (MPa)	J_2' (MPa)
8	200	0	1.694	57	-5
6	300	0	1.677	59	-11
4	400	0	1.666	140	-14
2	500	0	1.661	70	-25

(a) Loading

Cycle	p_o' (kPa)	q_o' (kPa)	v_o	$3G_a'$ (MPa)	J_2' (MPa)
8	200	0	1.694	31	-8
6	300	0	1.677	34	-11
4	400	0	1.666	36	-13
2	500	0	1.661	41	-10

(b) Unloading

Table 7.9 Stiffness Parameters
Test P3
Undrained Cycles

Cycles	p_o' (kPa)	q_o' (kPa)	v_o	$3G_a'$ (MPa)	J_1' (MPa)	J_2' (MPa)	K_a' (MPa)
2,4	100	0	1.675	37	-5	-10	15
7,8	100	100	1.677	28	-4	-10	15

(a) Loading

Cycles	p_o' (kPa)	q_o' (kPa)	v_o	$3G_a'$ (MPa)	J_1' (MPa)	J_2' (MPa)	K_a' (MPa)
2,4	100	0	1.675	28	-6	-7	19
-	100	100	1.677	-	-	-	-

(b) Unloading

Table 7.10 Stiffness Parameters
Test P4
Constant p' and Constant q' Probes

Cycles	p_o' (kPa)	q_o' (kPa)	v_o	$3G_a'$ (MPa)	J_1' (MPa)	J_2' (MPa)	K_a' (MPa)
1,2	300	0	1.577	68	-8	-24	26
5,6	300	100	1.575	32	-4	-21	35
7,8	300	200	1.574	45	+3	-31	30
9,10	300	300	1.573	14	+8	-16	28

(a) Loading

Cycles	p_o' (kPa)	q_o' (kPa)	v_o	$3G_a'$ (MPa)	J_1' (MPa)	J_2' (MPa)	K_a' (MPa)
1,2	300	0	1.577	61	-17	-21	32
-	300	100	1.575	-	-	-	-
-	300	200	1.574	-	-	-	-
-	300	300	1.573	-	-	-	-

(b) Unloading

Table 7.11 Stiffness Parameters
Test P5
Constant p' and Constant q' Probes

Cycles	p_o' (kPa)	q_o' (kPa)	v_o	$3G_a'$ (MPa)	J_1' (MPa)	J_2' (MPa)	K_a' (MPa)
5,6	500	0	1.579	132	-25	-36	34
8,9	500	200	1.575	141	-30	-44	62
11,12	500	400	1.571	55	-10	-39	91

(a) Loading

Cycles	p_o' (kPa)	q_o' (kPa)	v_o	$3G_a'$ (MPa)	J_1' (MPa)	J_2' (MPa)	K_a' (MPa)
5,6	500	0	1.579	80	-10	-24	47
8,9	500	200	1.575	201	-13	-69	72
11,12	500	400	1.571	220	0	-83	105

(b) Unloading

Table 7.12 Stiffness Parameters
Test P6
Constant p' and Constant q' Probes

Cycles	p_o' (kPa)	q_o' (kPa)	v_o	$3G_a'$ (MPa)	J_1' (MPa)	J_2' (MPa)	K_a' (MPa)
1,3	300	0	1.643	77	-20	-27	27
5,6	300	-100	1.647	87	-35	-33	31
8,9	300	-200	1.656	69	-24	-24	24

(a) Loading

Cycles	p_o' (kPa)	q_o' (kPa)	v_o	$3G_a'$ (MPa)	J_1' (MPa)	J_2' (MPa)	K_a' (MPa)
1,3	300	0	1.643	52	-13	-19	20
5,6	300	-100	1.647	66	-19	-23	24
8,9	300	-200	1.656	80	-21	-28	25

(b) Unloading

Table 7.13 Stiffness Parameters
Test P7
Constant p' and Constant q' Probes

Cycles	p_o' (kPa)	q_o' (kPa)	v_o	$3G_a'$ (MPa)	J_1' (MPa)	J_2' (MPa)	K_a' (MPa)
4,5	500	0	1.631	45	-13	-17	41
7,8	500	-200	1.633	407	-407	-187	63

(a) Loading

Cycles	p_o' (kPa)	q_o' (kPa)	v_o	$3G_a'$ (MPa)	J_1' (MPa)	J_2' (MPa)	K_a' (MPa)
4,5	500	0	1.631	83	-22	-33	51
7,8	500	-200	1.633	111	-18	-45	49

(b) Unloading

Table 7.14 Stiffness Parameters
Test P8
Constant p' and Constant q' Probes

Test	Cycles	v_o	$3G_a'$ (MPa)	J_1' (MPa)	J_2' (MPa)	K_a' (MPa)
1	4,12*	1.577	68	-8	-24	26
2	7,9	1.607	58	+6	-21	36
3$	6,7	1.677	59	-	-11	-
4			As Test 2			
5			As Test 1			
6	1,3	1.594	73	-21	-20	34
7	1,3	1.643	77	-20	-27	27
8	1,2	1.645	57	-18	-20	29

$ Using undrained cycles

(a) Loading

Test	Cycles	v_o	$3G_a'$ (MPa)	J_1' (MPa)	J_2' (MPa)	K_a' (MPa)
1	4,12*	1.577	61	-17	-21	32
2	7,9	1.607	40	-	-12	-
3$	6,7	1.677	34	-	-11	-
4			As Test 2			
5			As Test 1			
6	1,3	1.594	60	-9	-14	17
7	1,3	1.643	52	-13	-19	20
8	1,2	1.645	40	-10	-15	24

$ Using undrained cycles

(b) Unloading

Table 7.15 Stiffness Parameters
All Tests at p_o'=300, q_o'=0

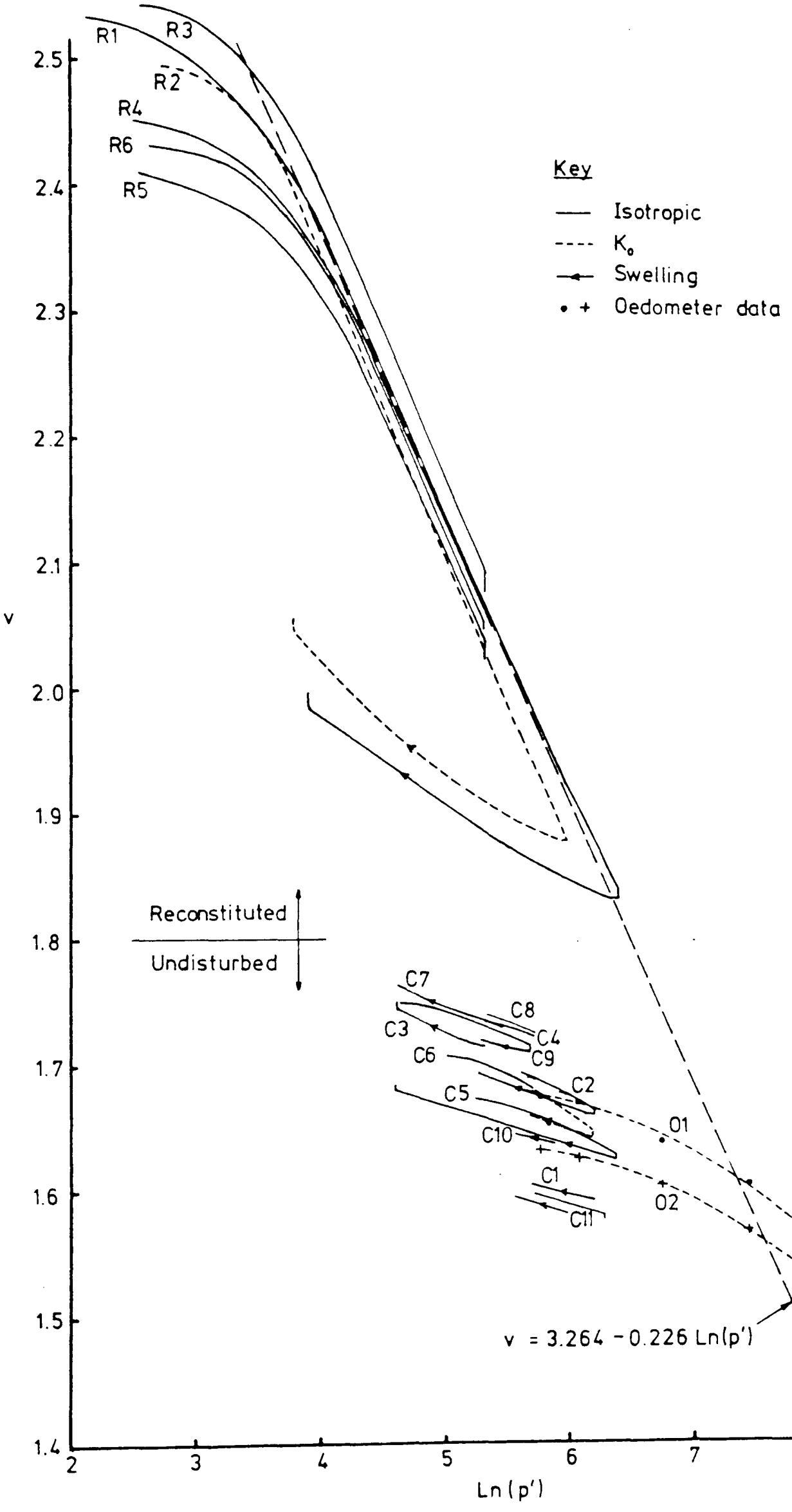

Fig 7.1 Compression and swelling test results

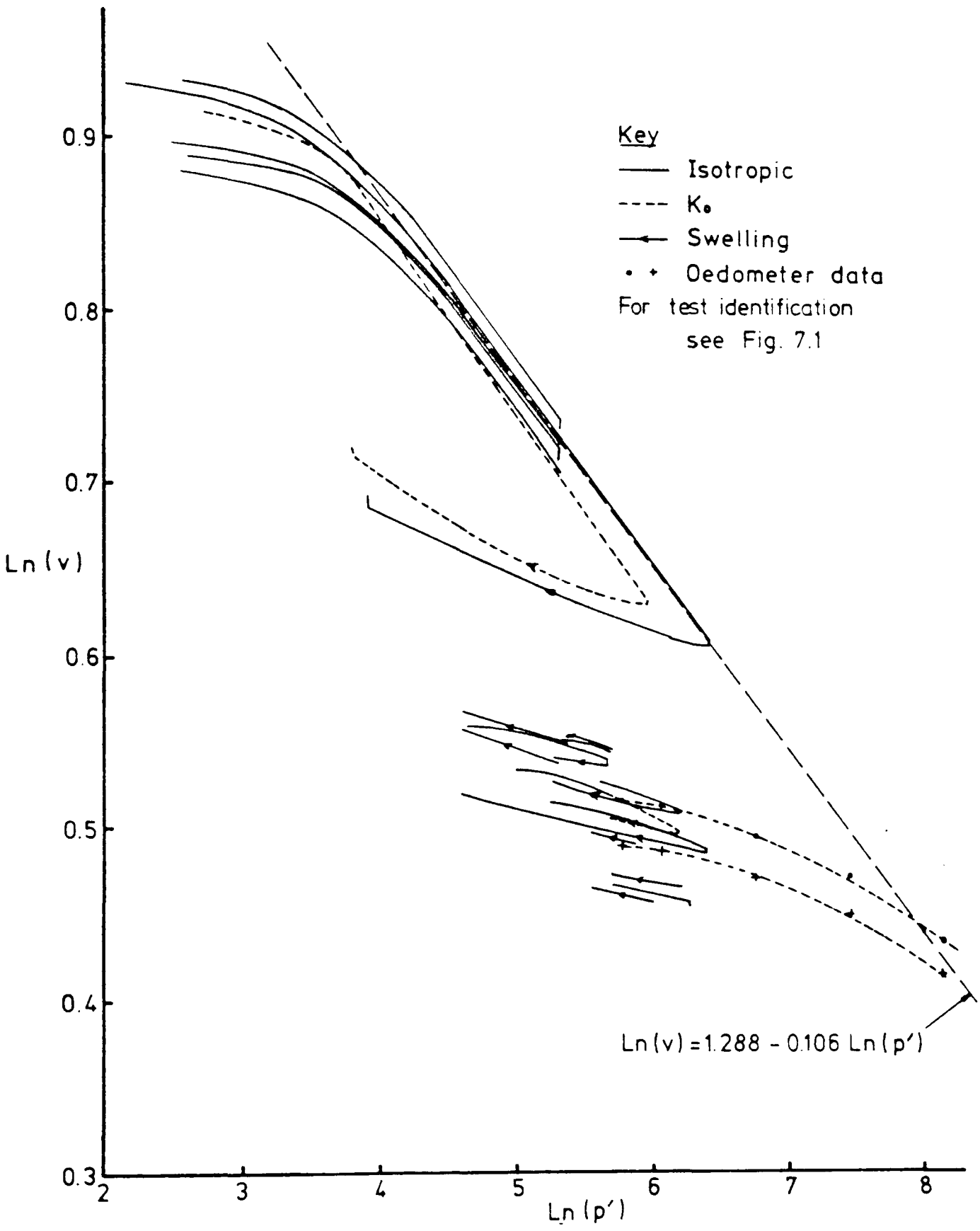

Fig 7.2 Compression and swelling test results

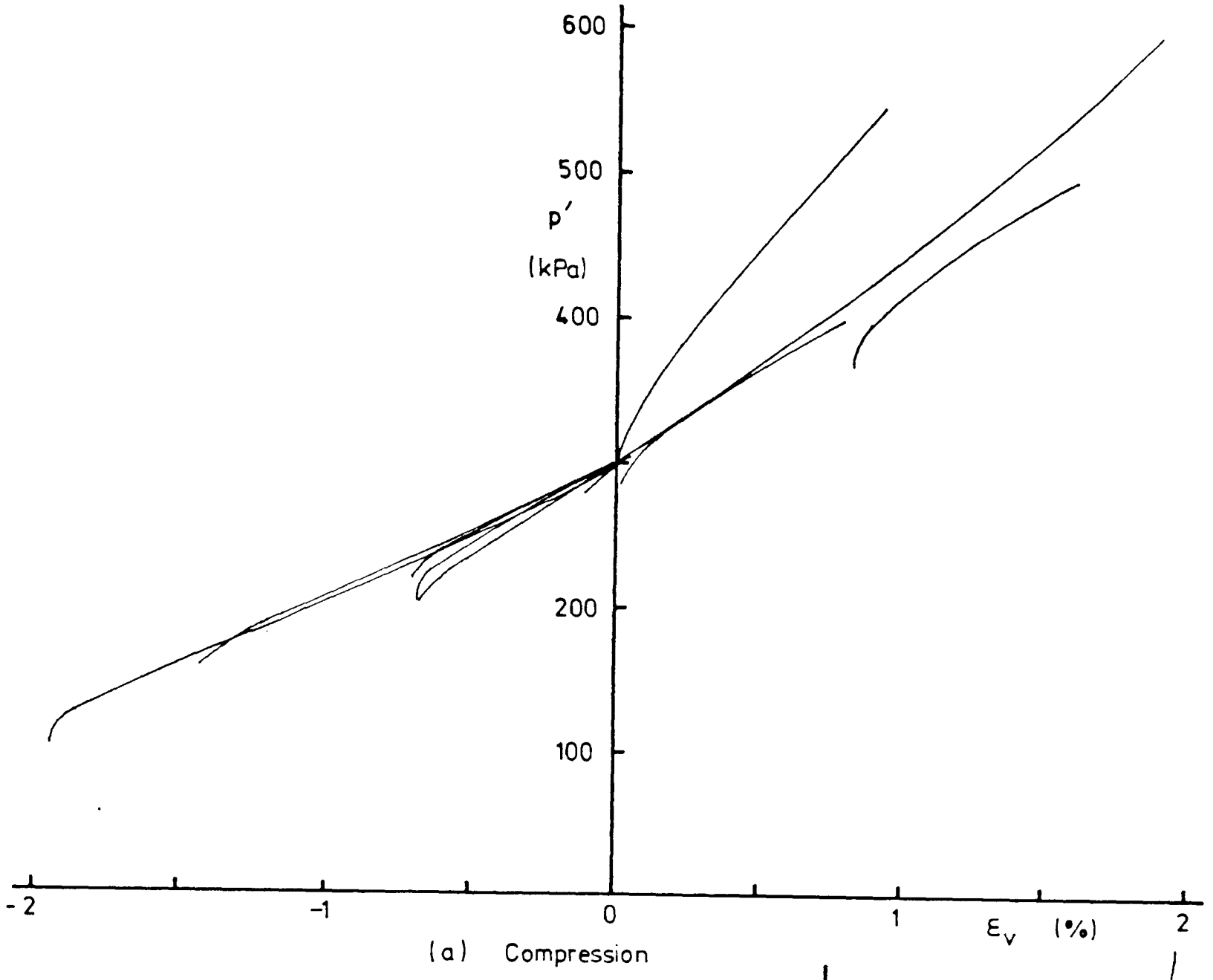

(a) Compression

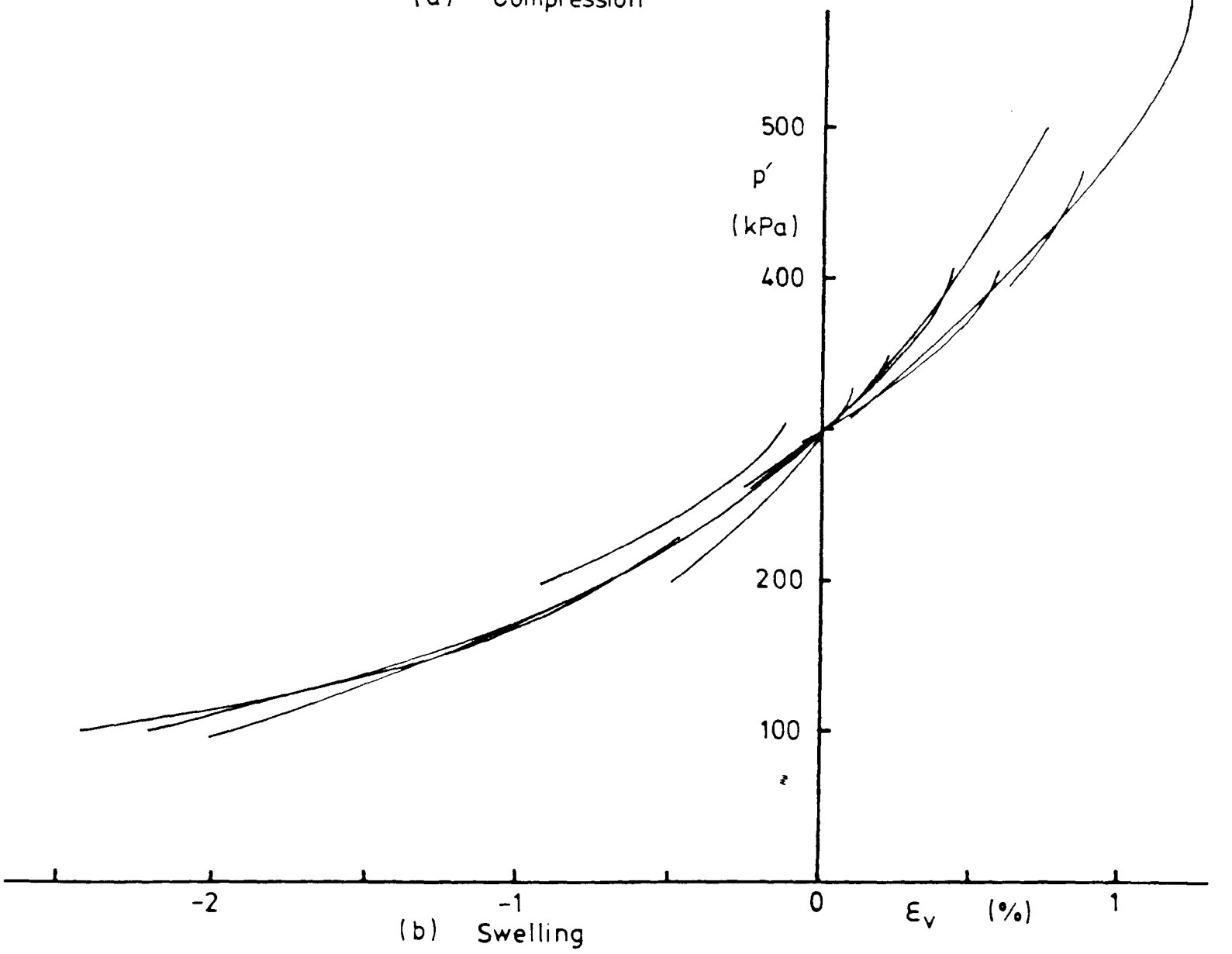

(b) Swelling

Fig 7.3 Combined stress - strain curves for isotropic compression and swelling tests

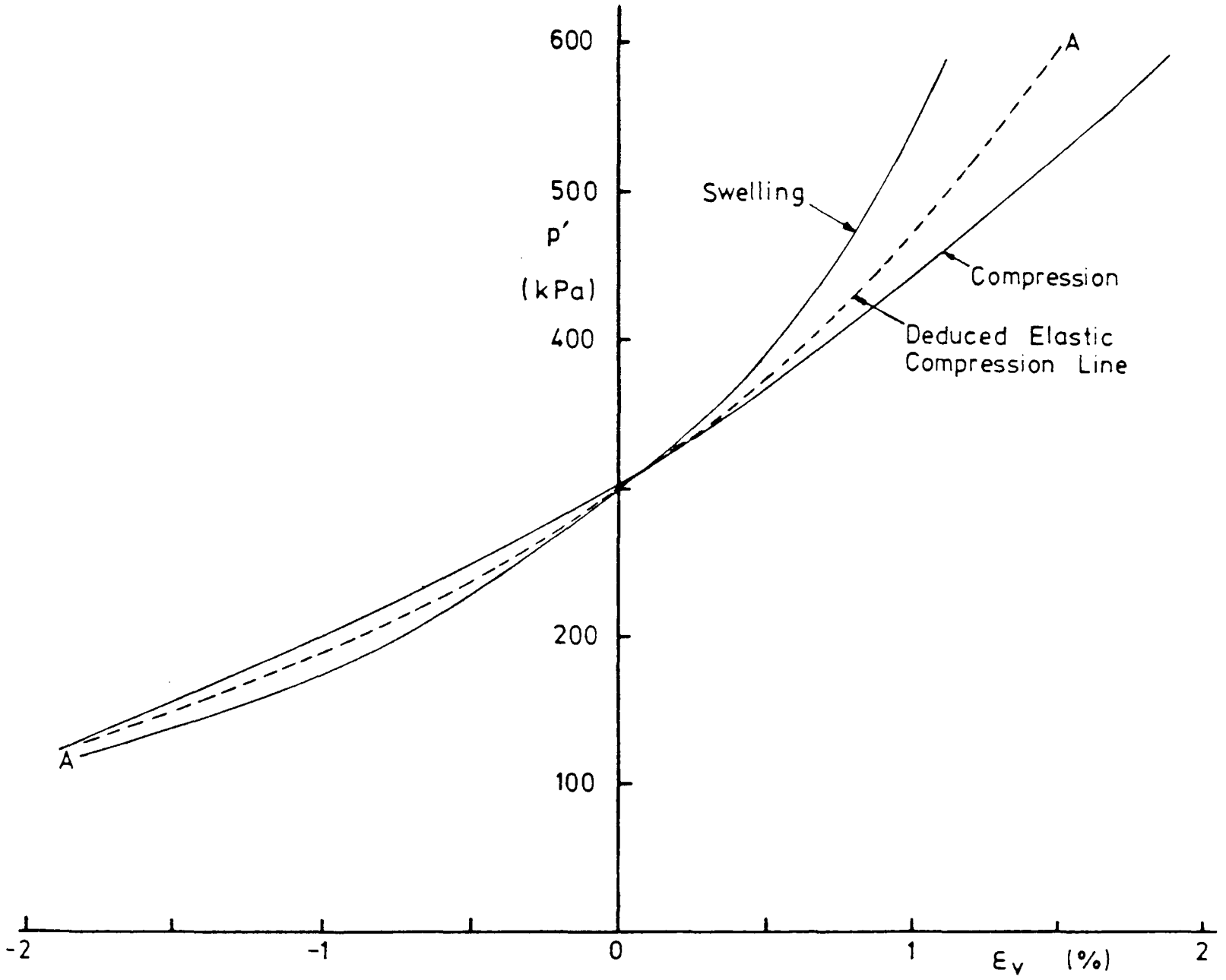

Fig 7.4 'Average' compression and swelling curves with deduced elastic compression line

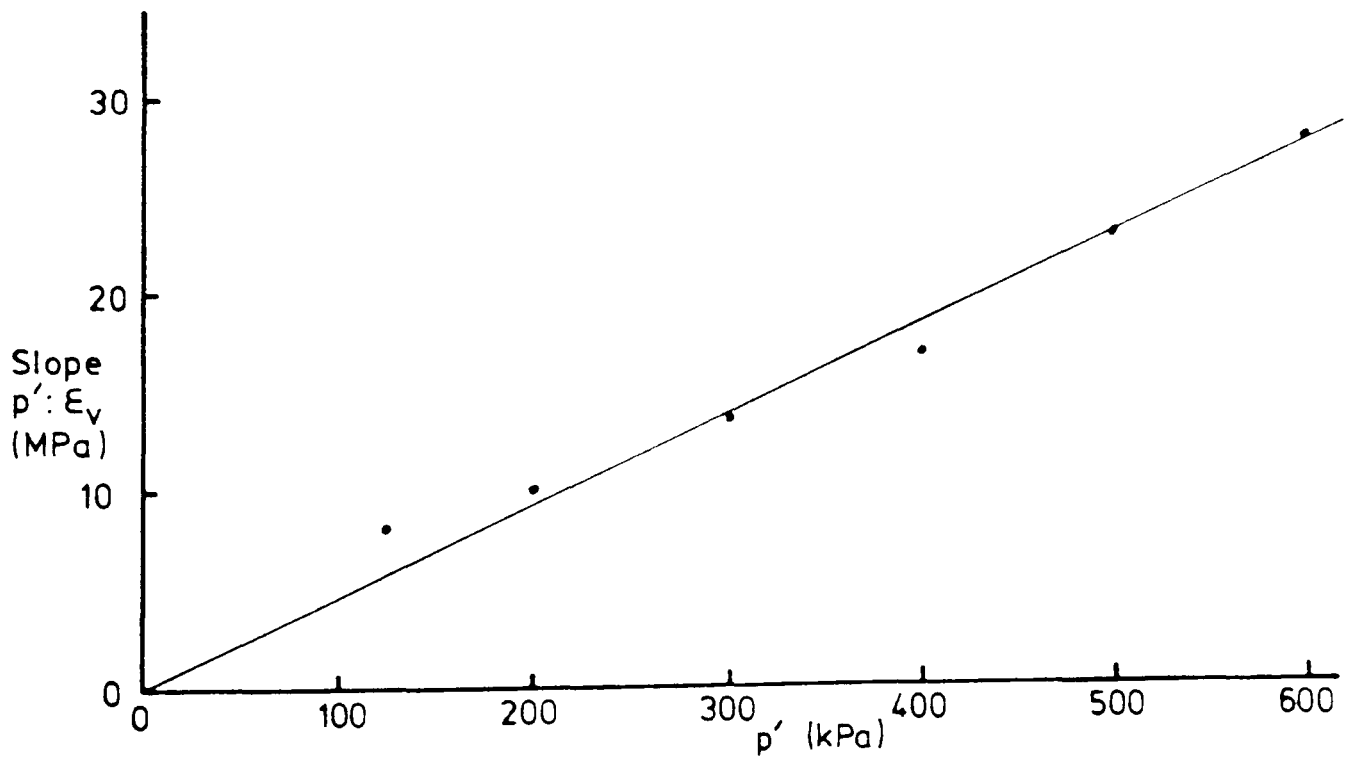

Fig 7.5 Slope of elastic compression line against mean effective stress

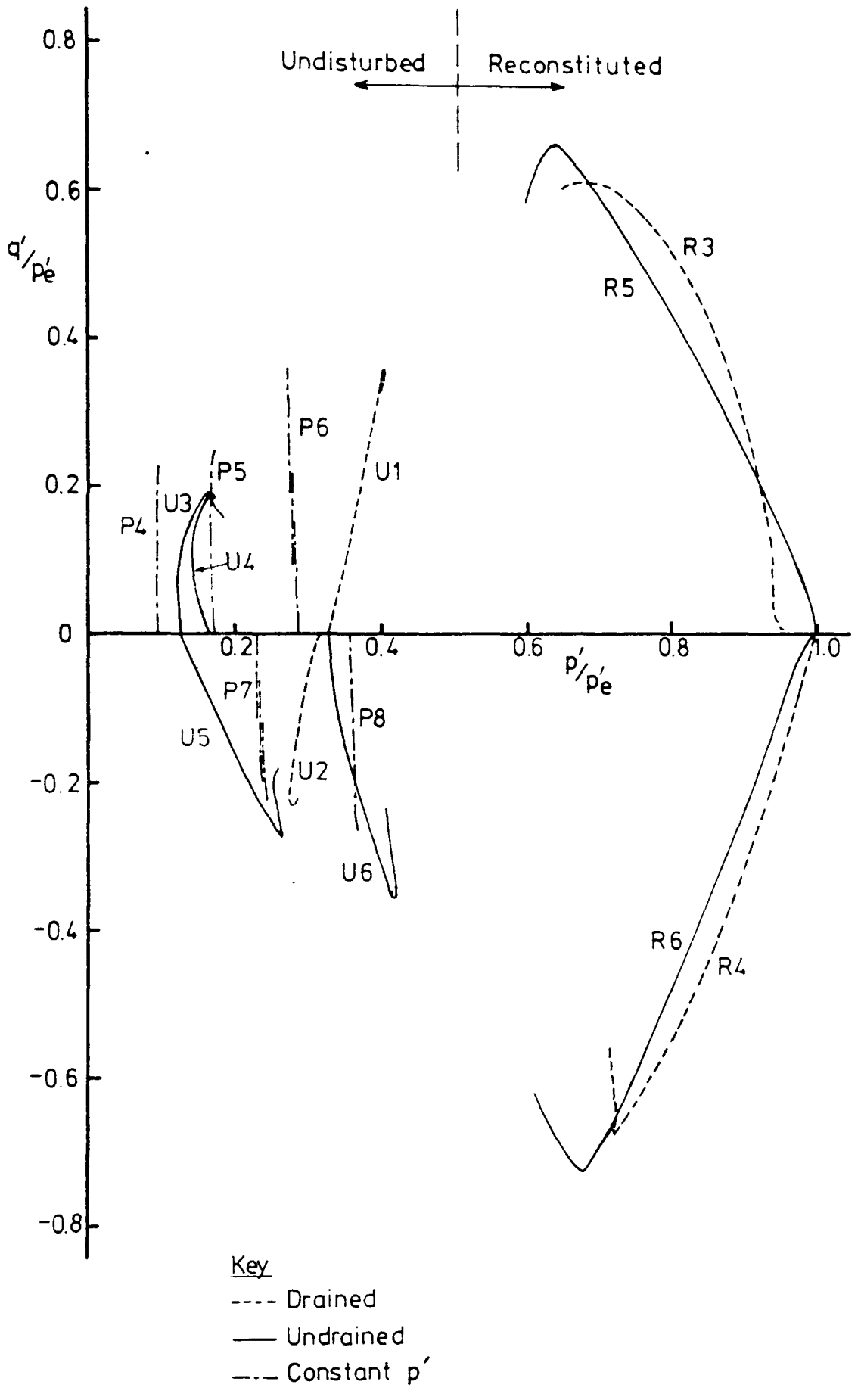

Fig 7.6 Normalised stress paths

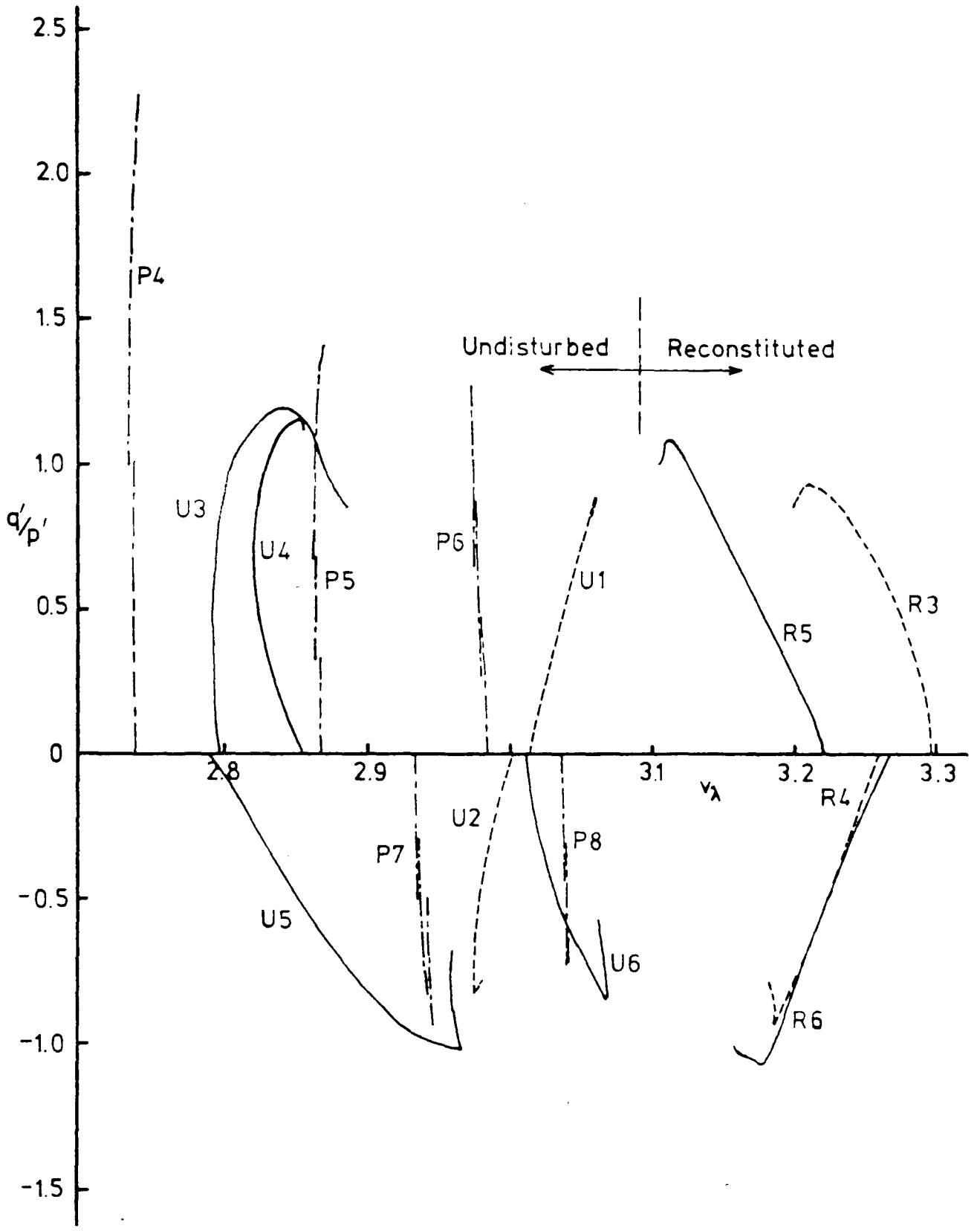

Key

---- Drained

—— Undrained

—·— Constant p′

Fig 7.7 Normalised state paths

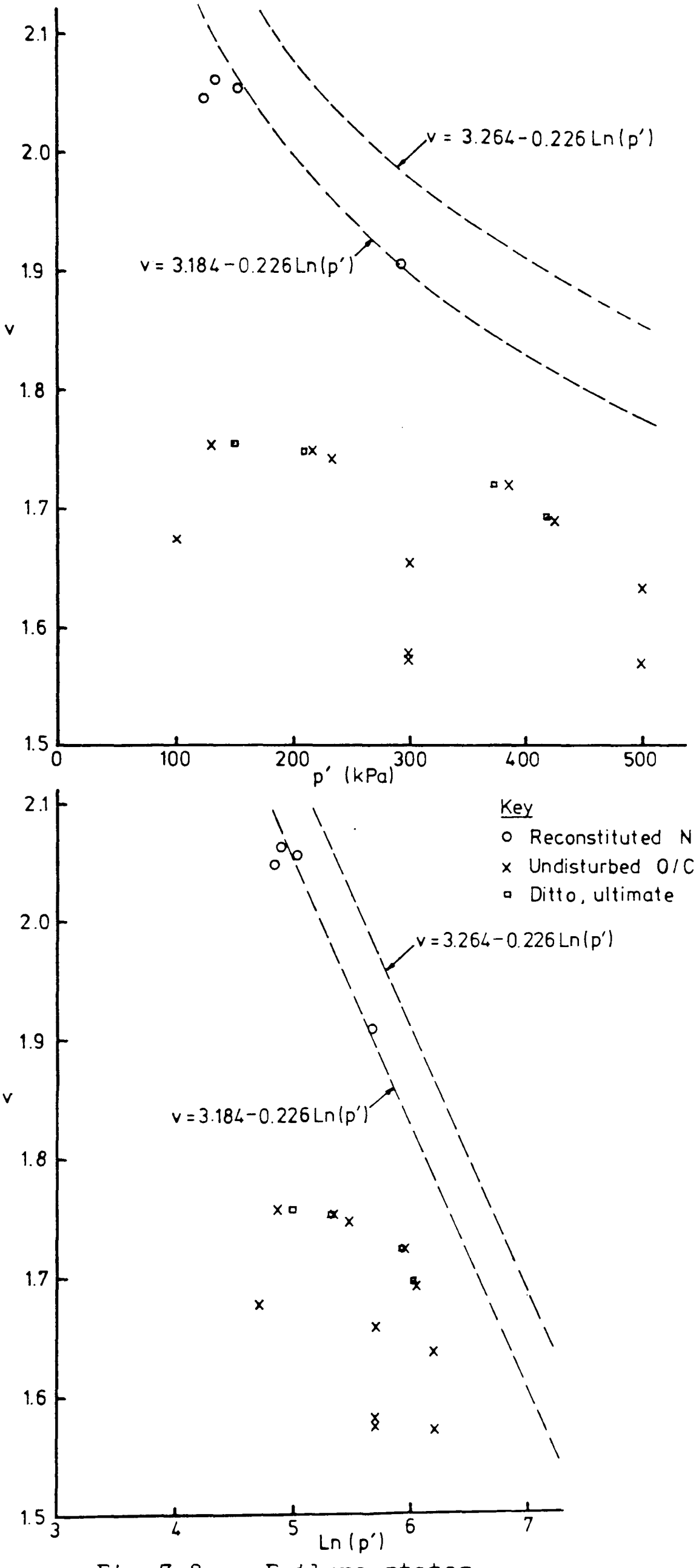

Fig 7.8 Failure states

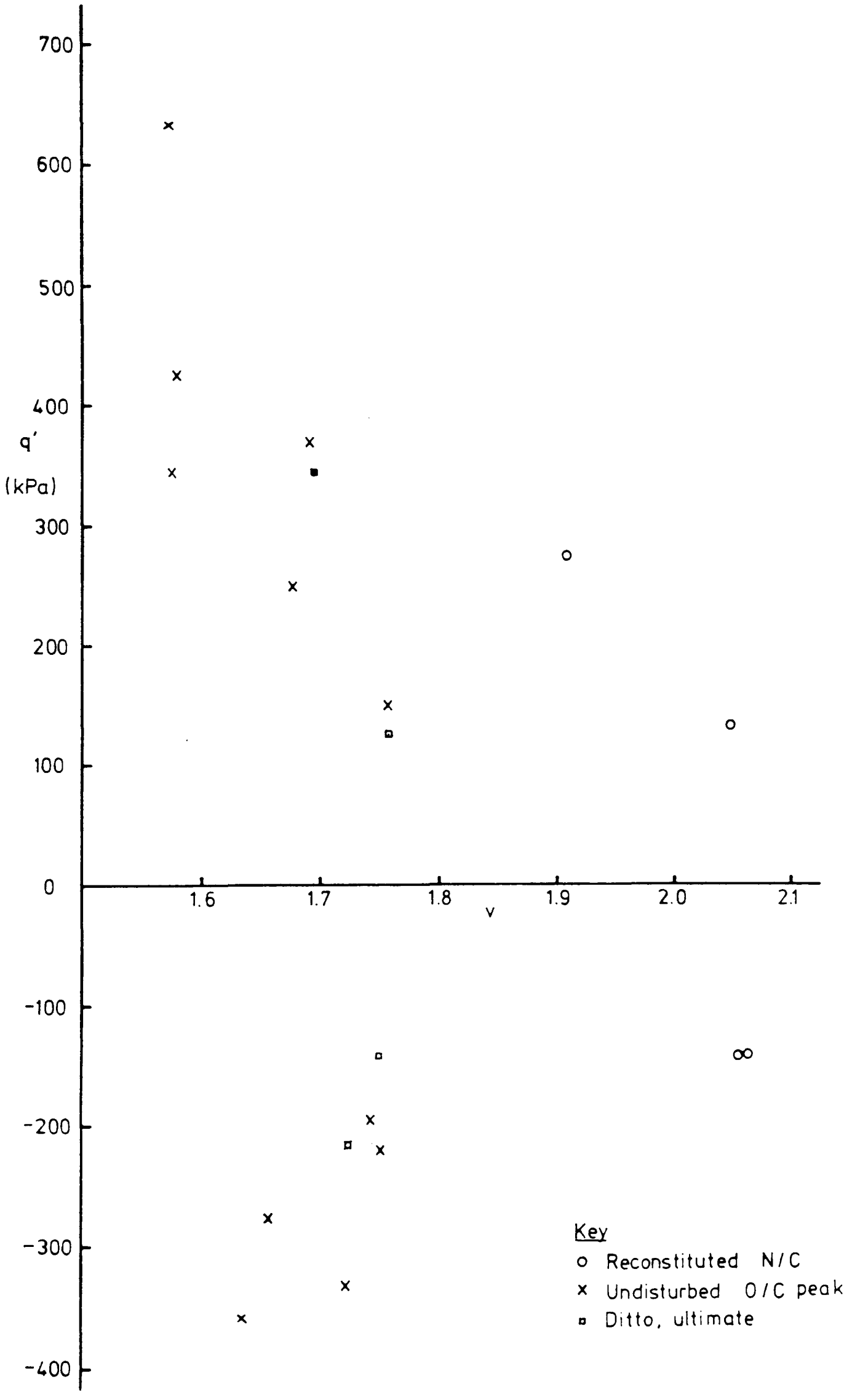

Fig 7.9 Failure states

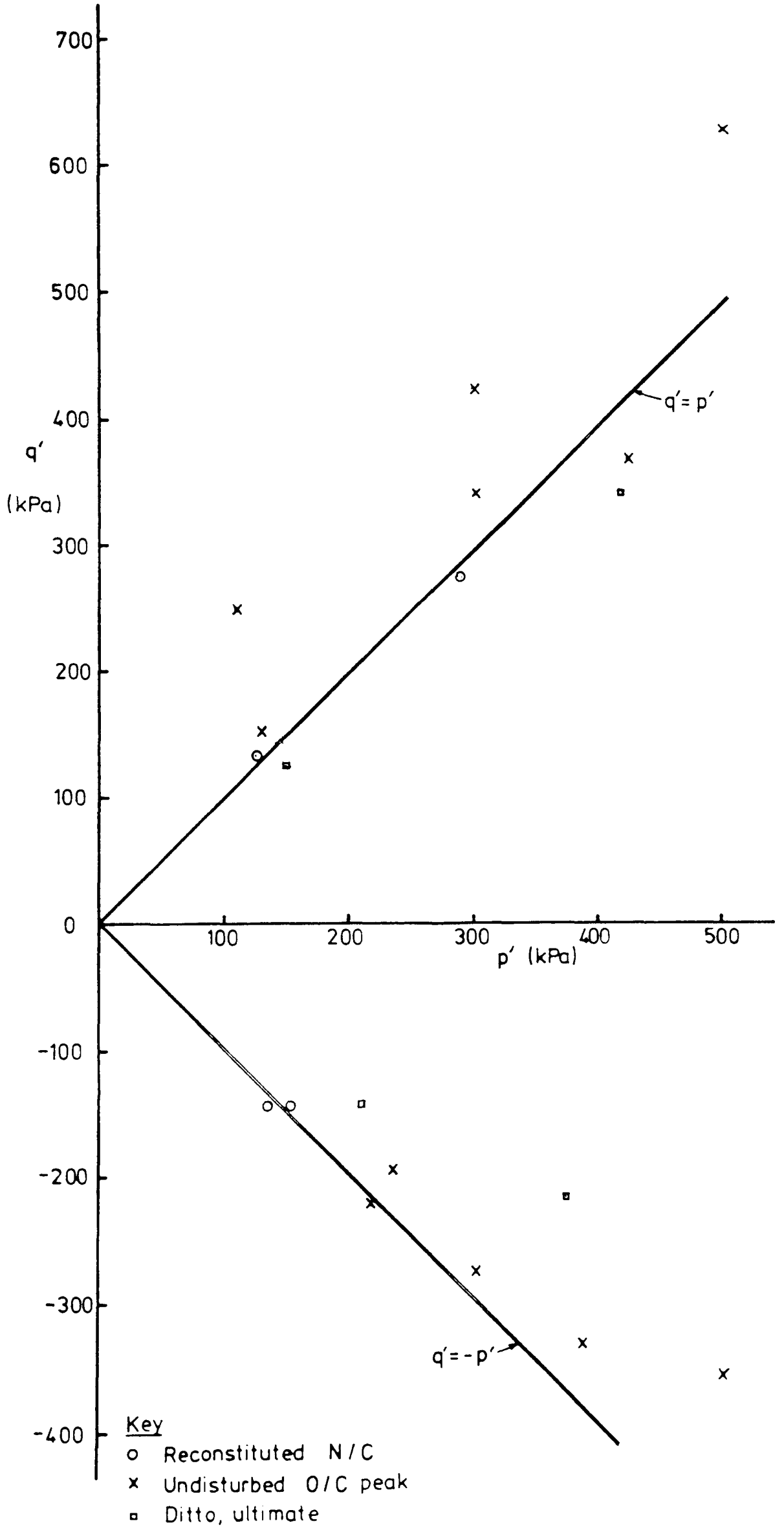

Fig 7.10 Failure stress states

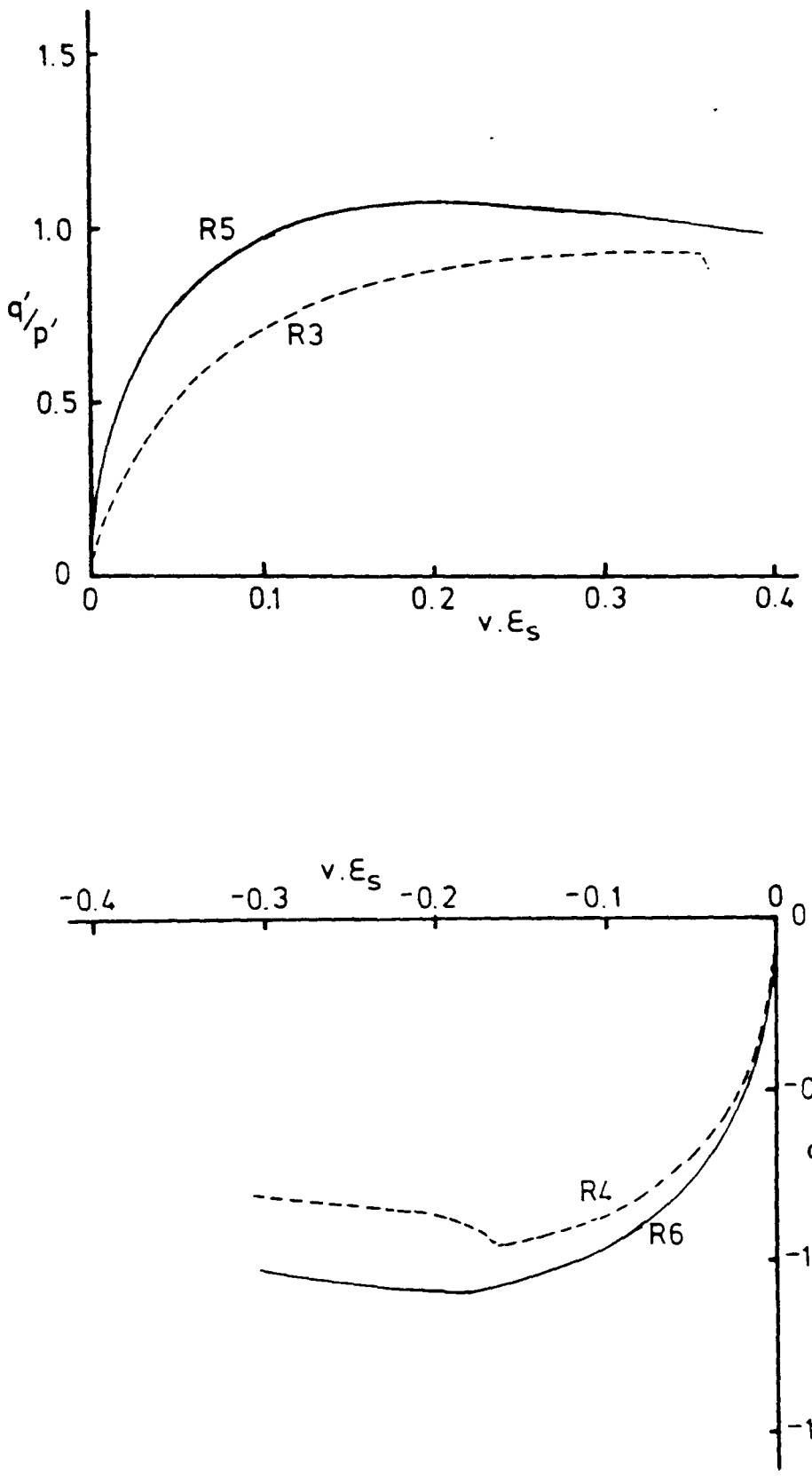

Fig 7.11 Normalised stress - strain curves, reconstituted samples

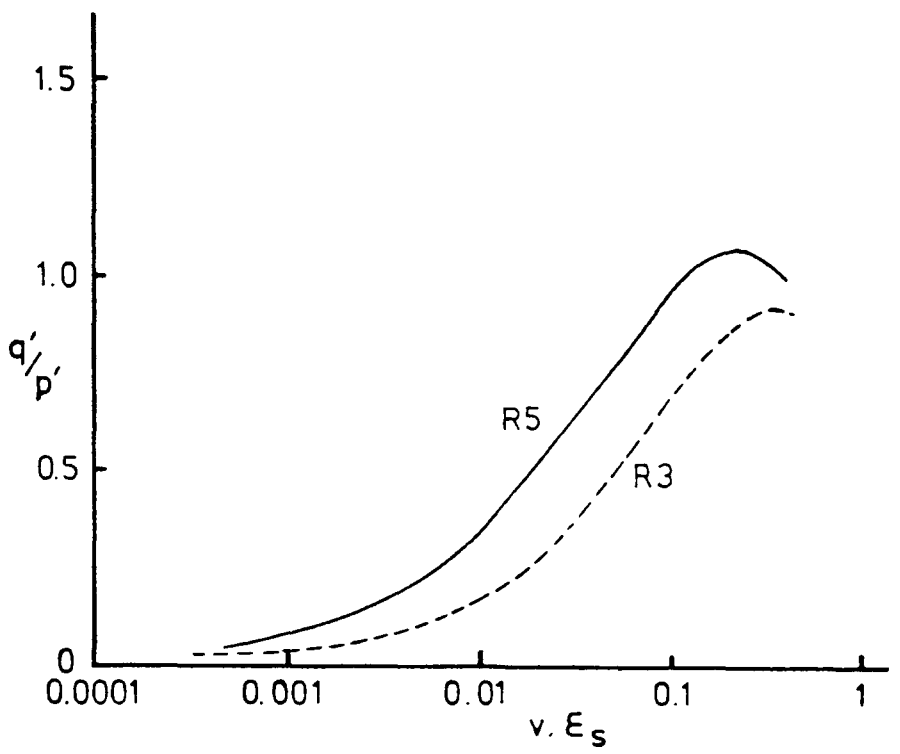

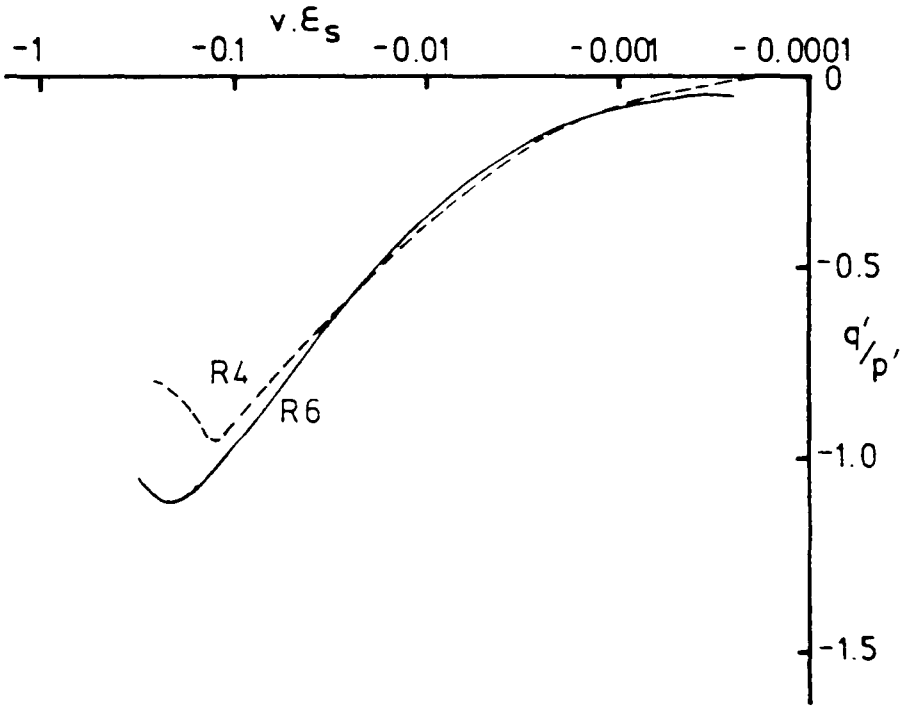

Key
---- Drained
—— Undrained

Fig 7.12 Normalised stress - strain curves, reconstituted samples

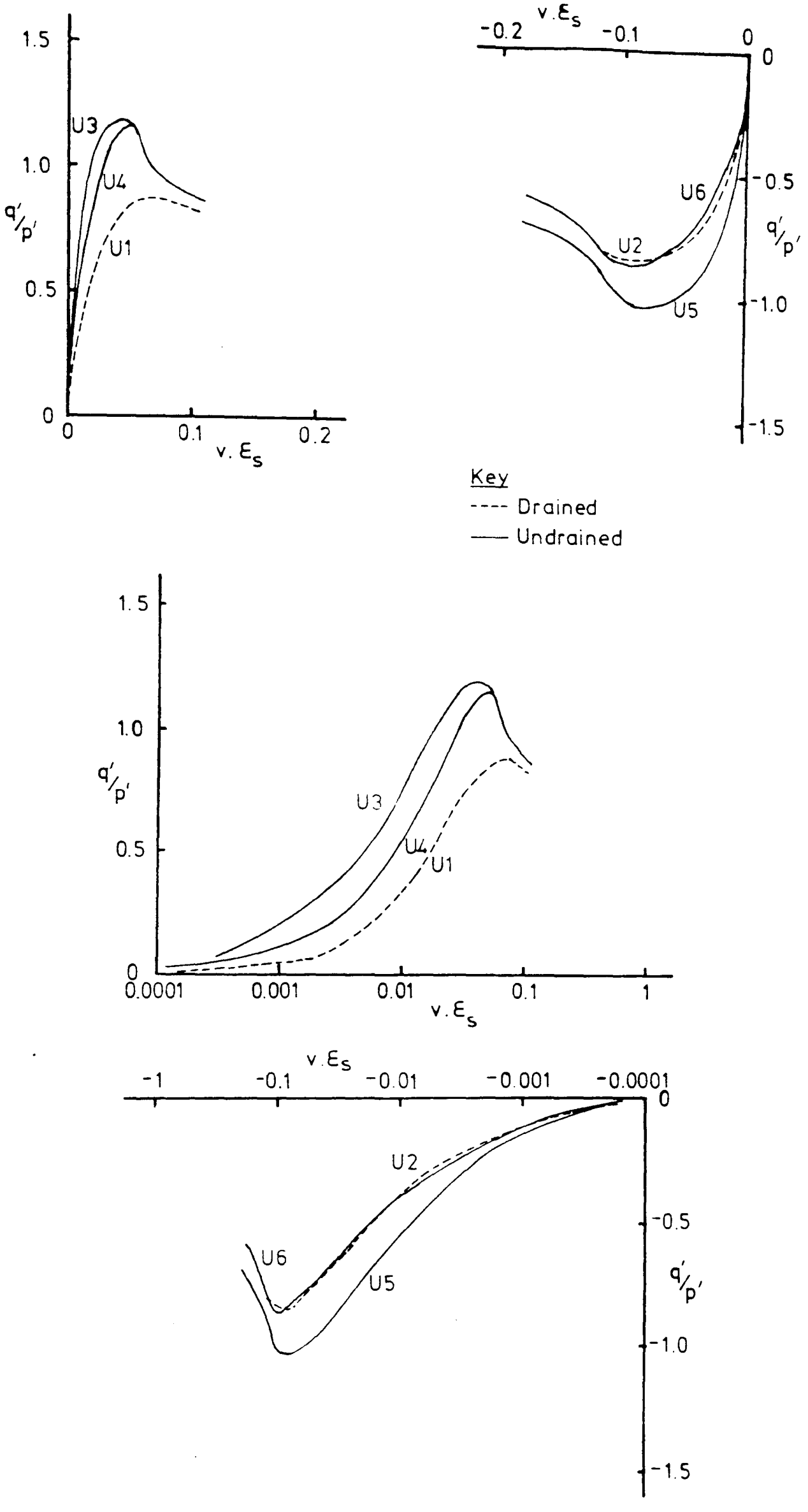

Fig 7.13 Normalised stress - strain curves, undisturbed samples

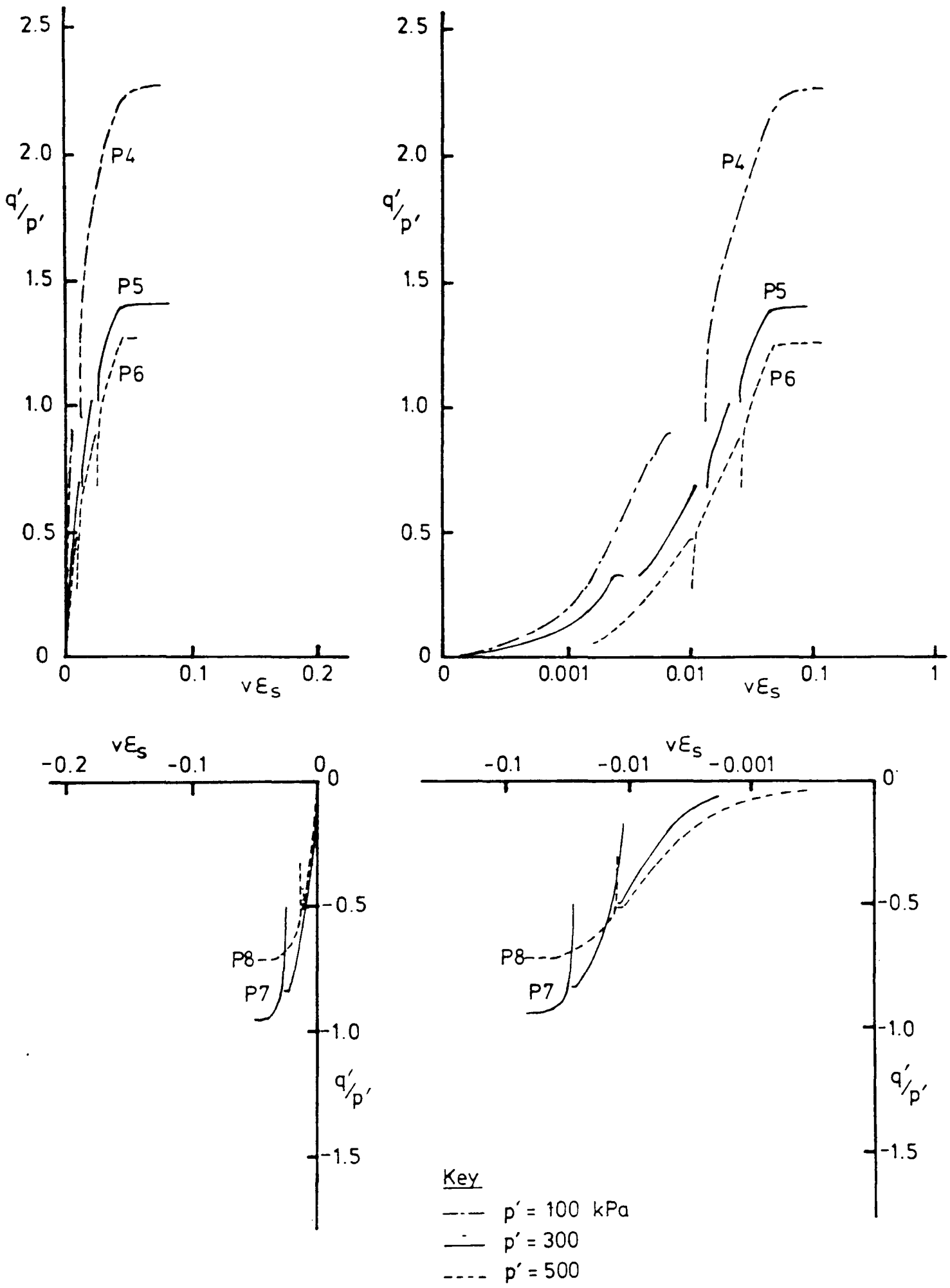

Fig 7.14 Normalised stress - strain curves, constant p' tests

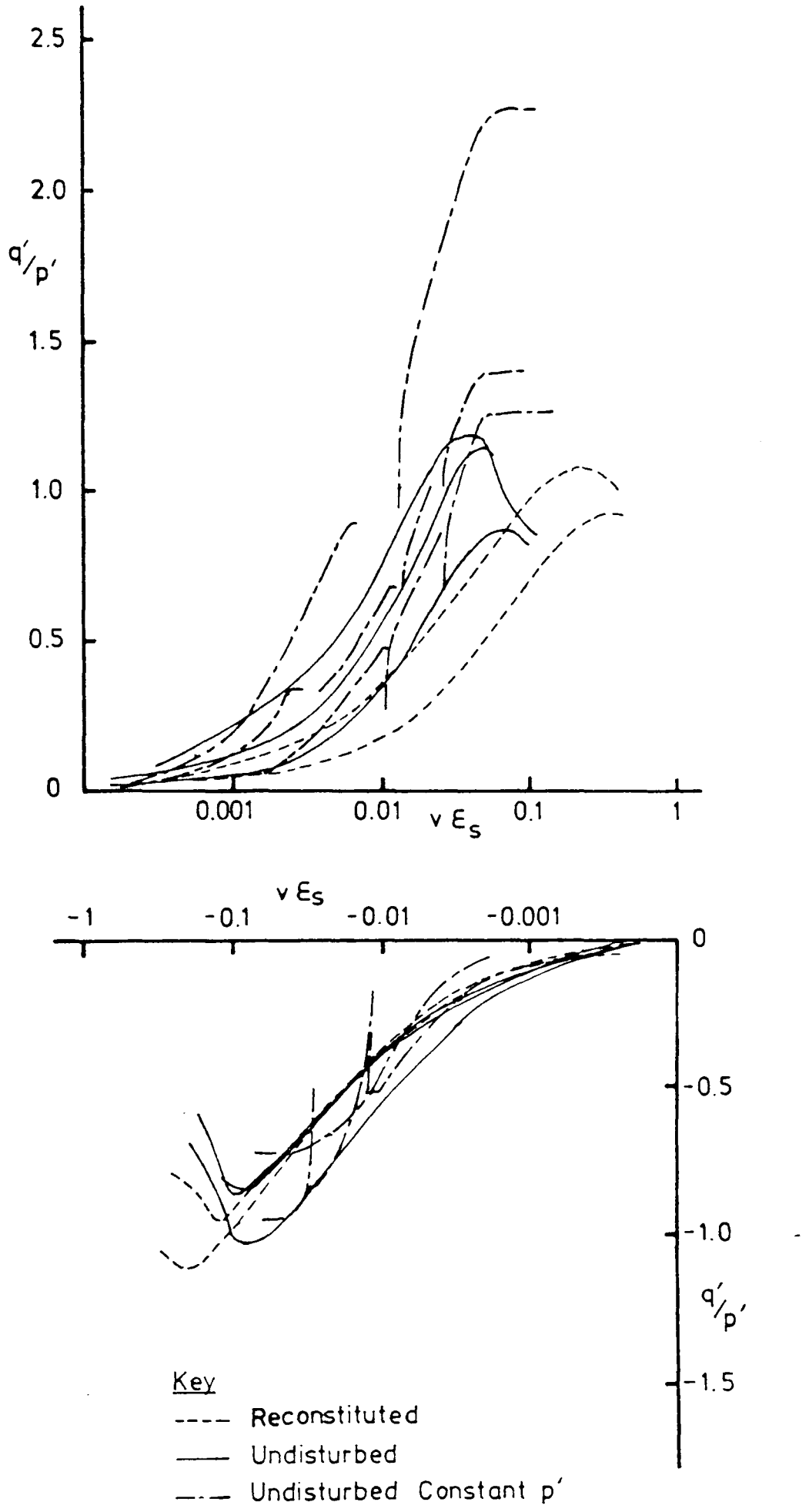

Fig 7.15 Combined normalised stress - strain curves

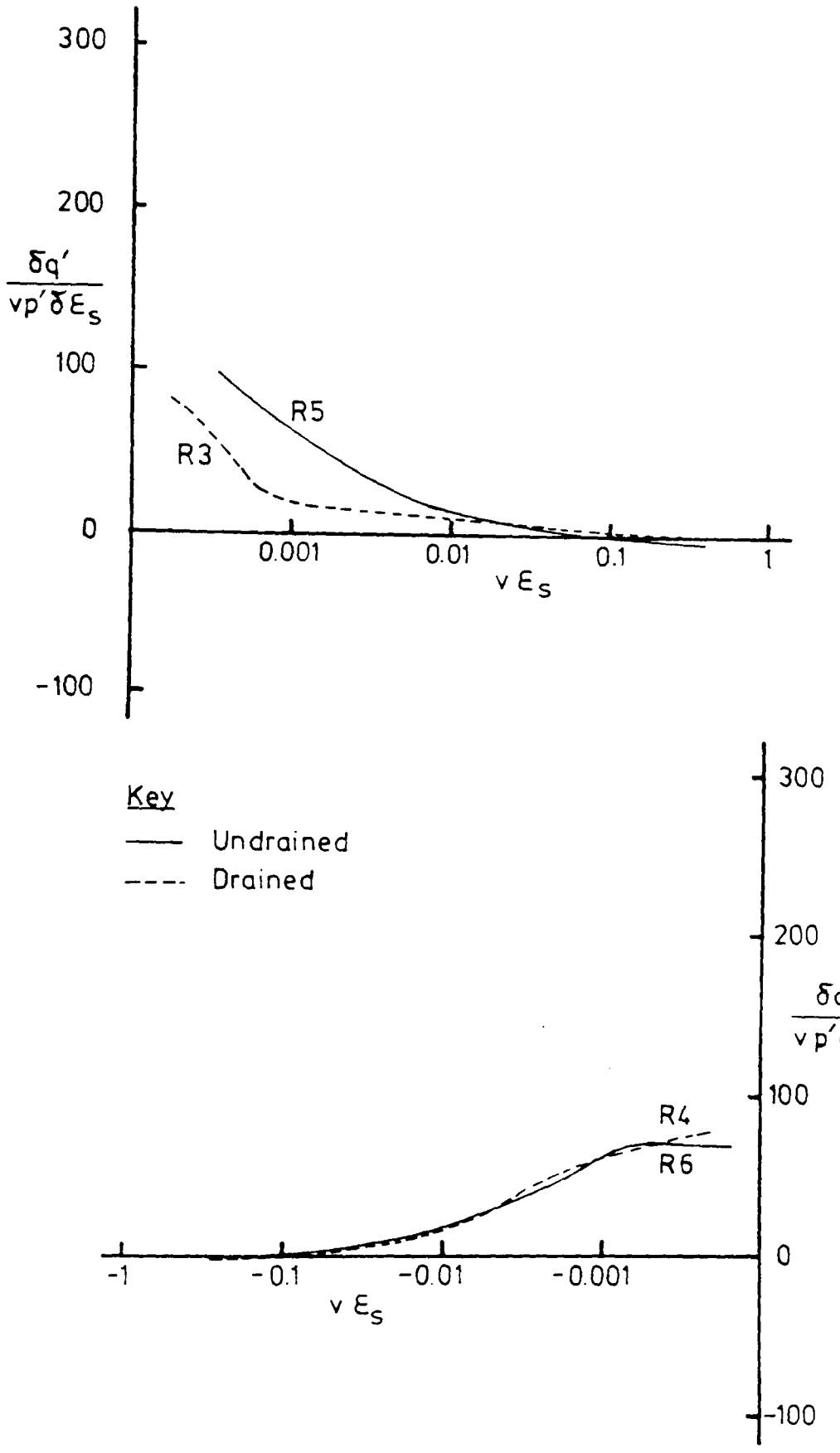

Fig 7.16 Normalised tangent stiffness parameters, reconstituted samples

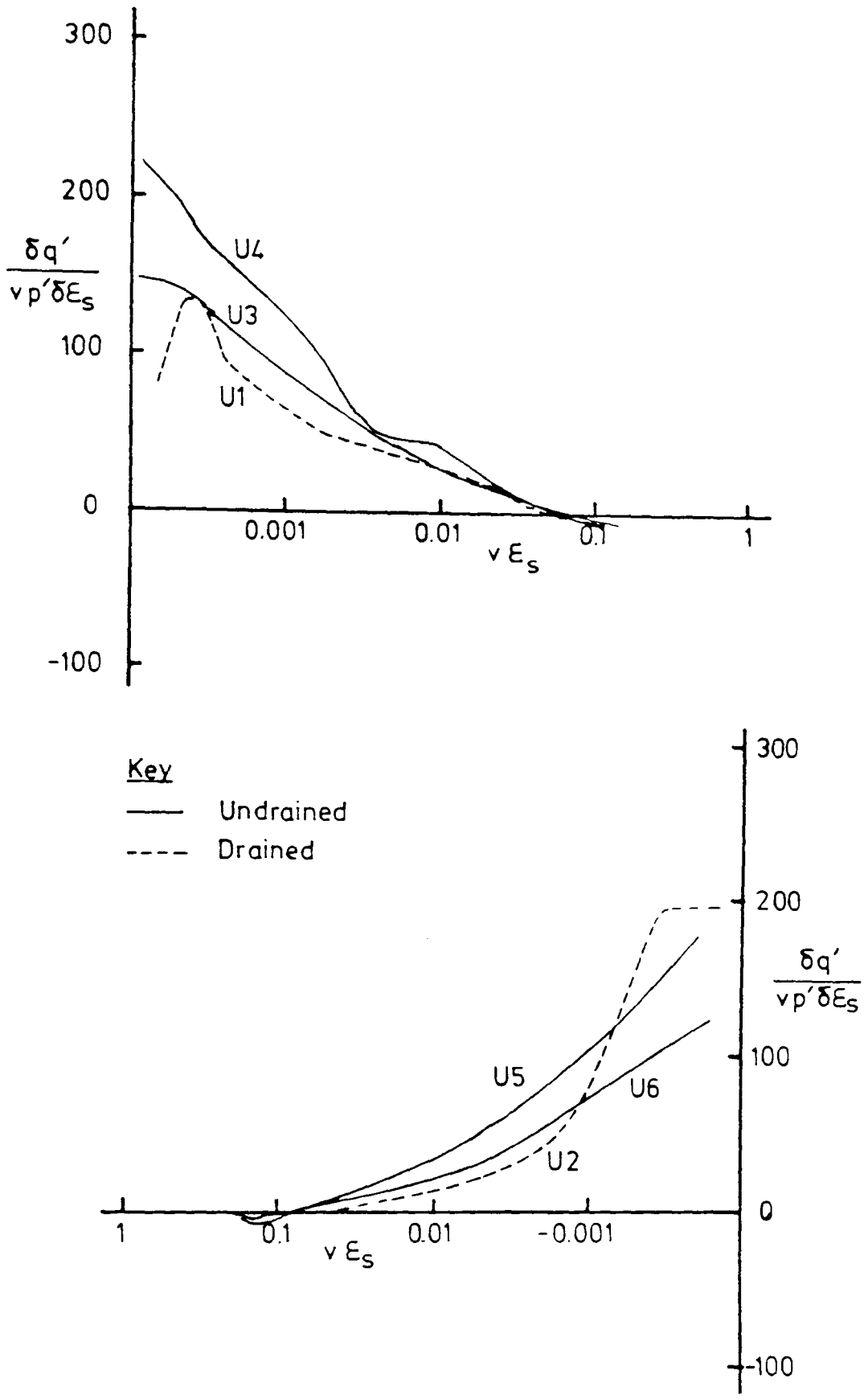

Fig 7.17 Normalised tangent stiffness parameters, undisturbed samples

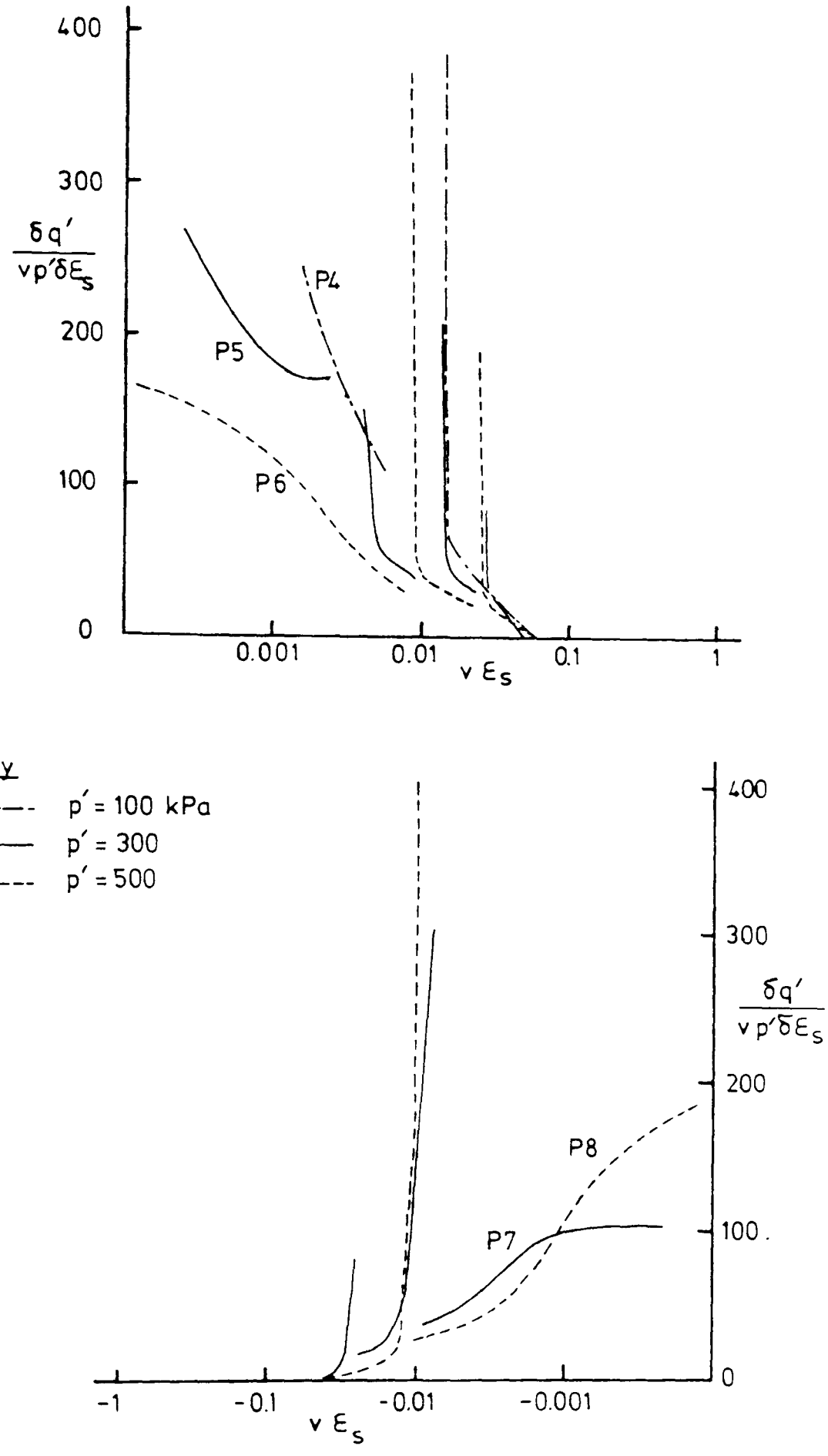

Fig 7.18 Normalised tangent stiffness parameters, constant p' tests

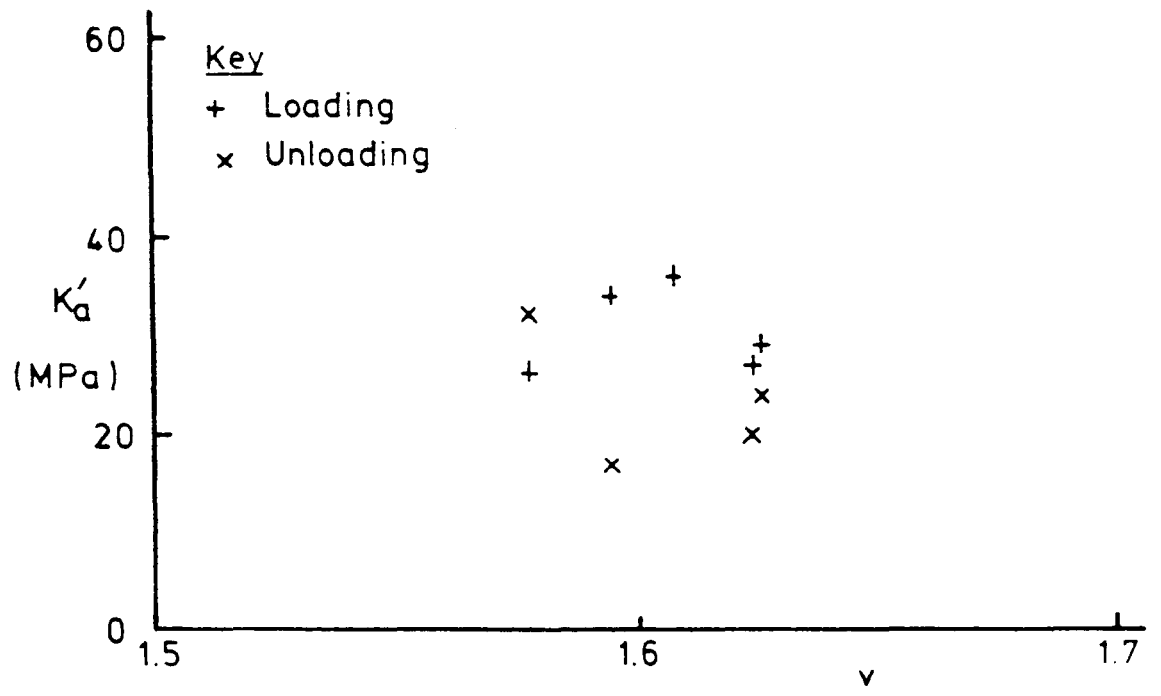

Fig 7.19 Variation of bulk modulus with specific volume for p'=300 kPa, q'=0

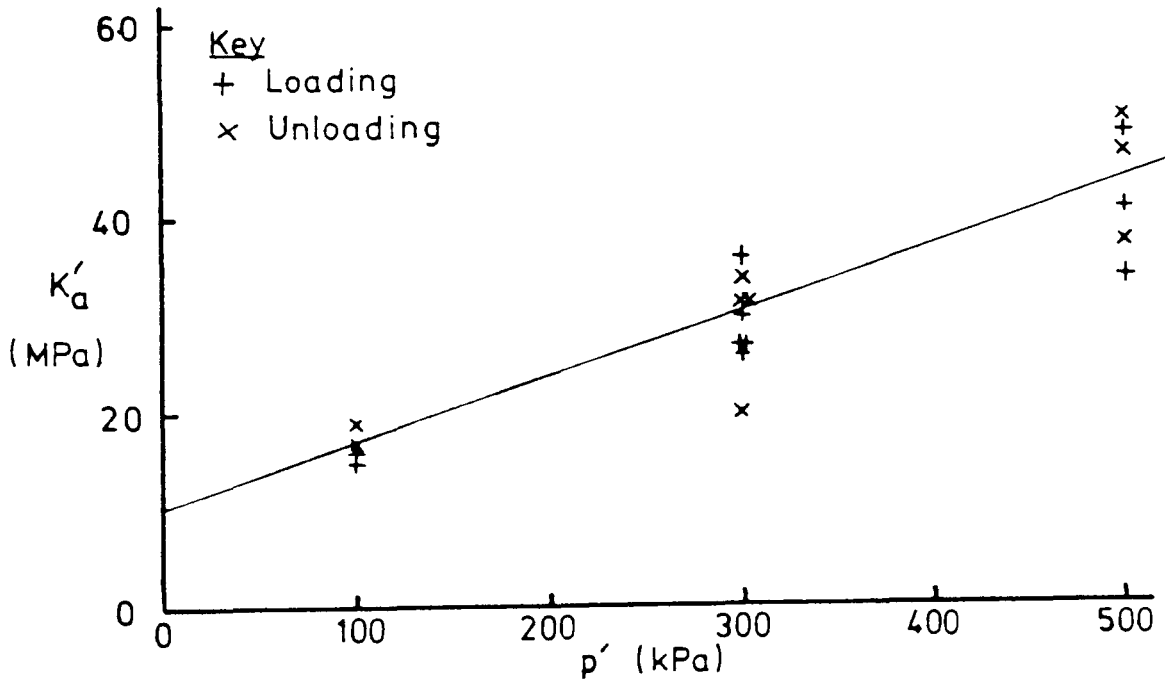

Fig 7.20 Variation of bulk modulus with mean effective stress

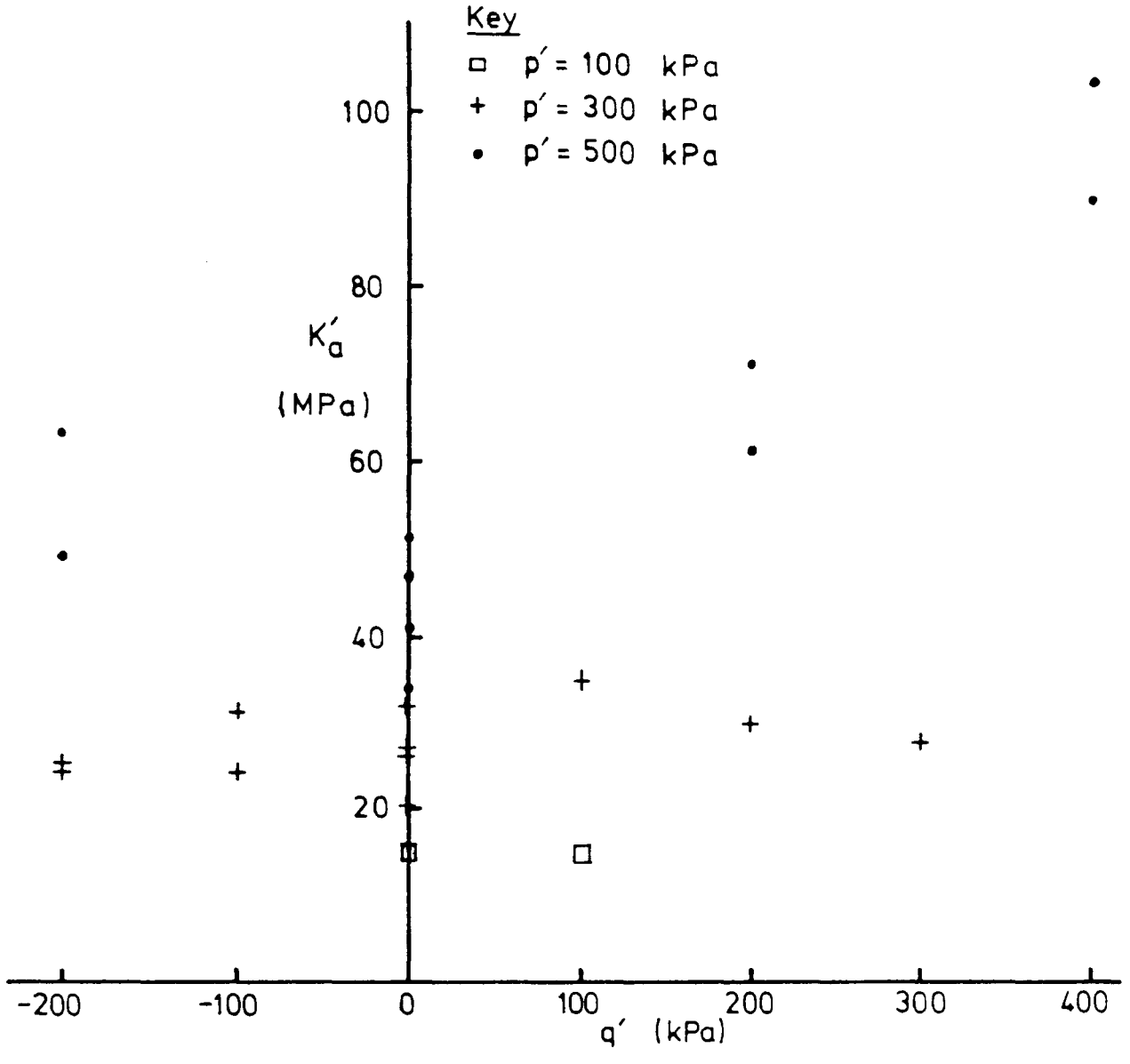

Fig 7.21 Variation of bulk modulus with deviator stress

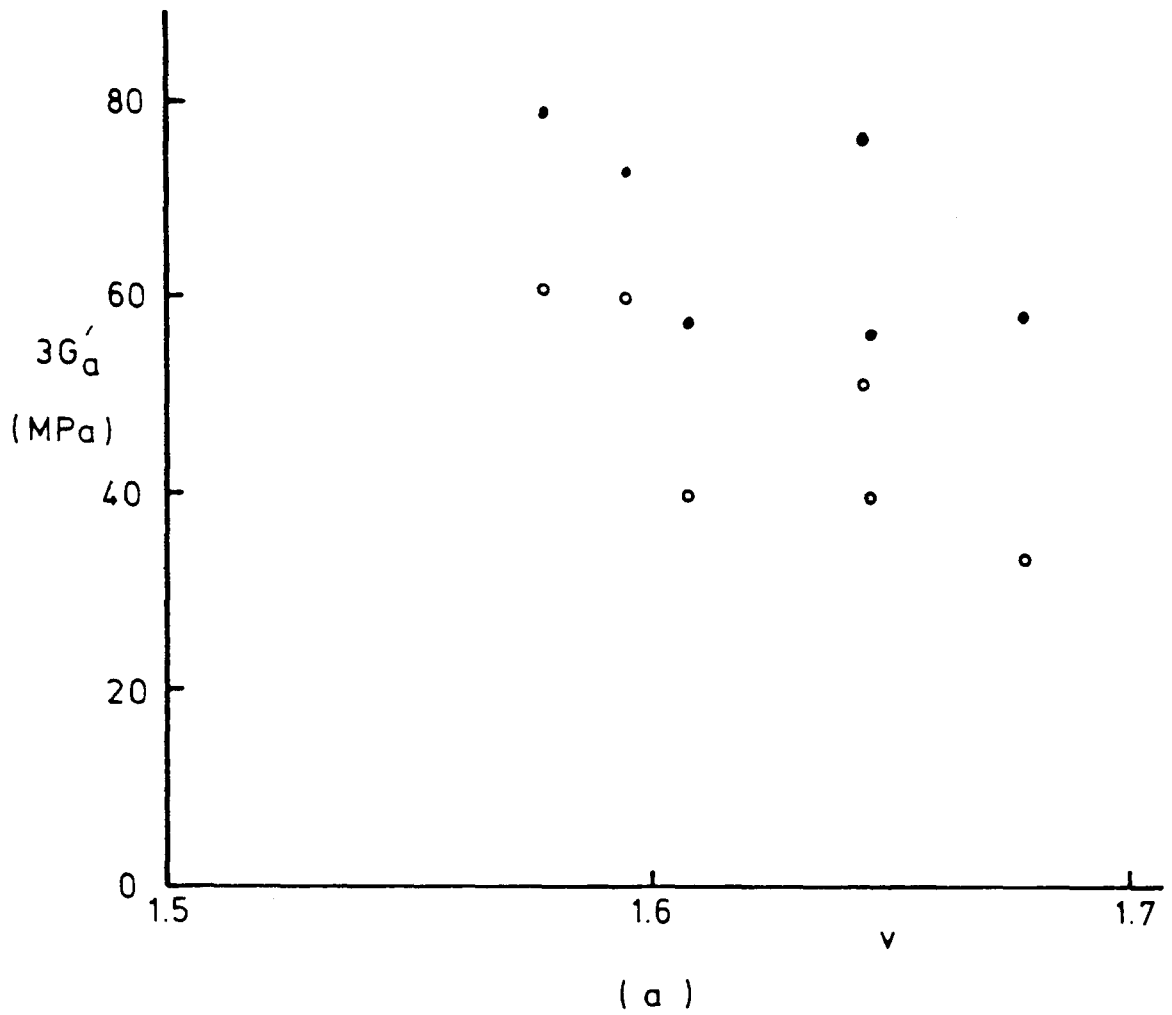

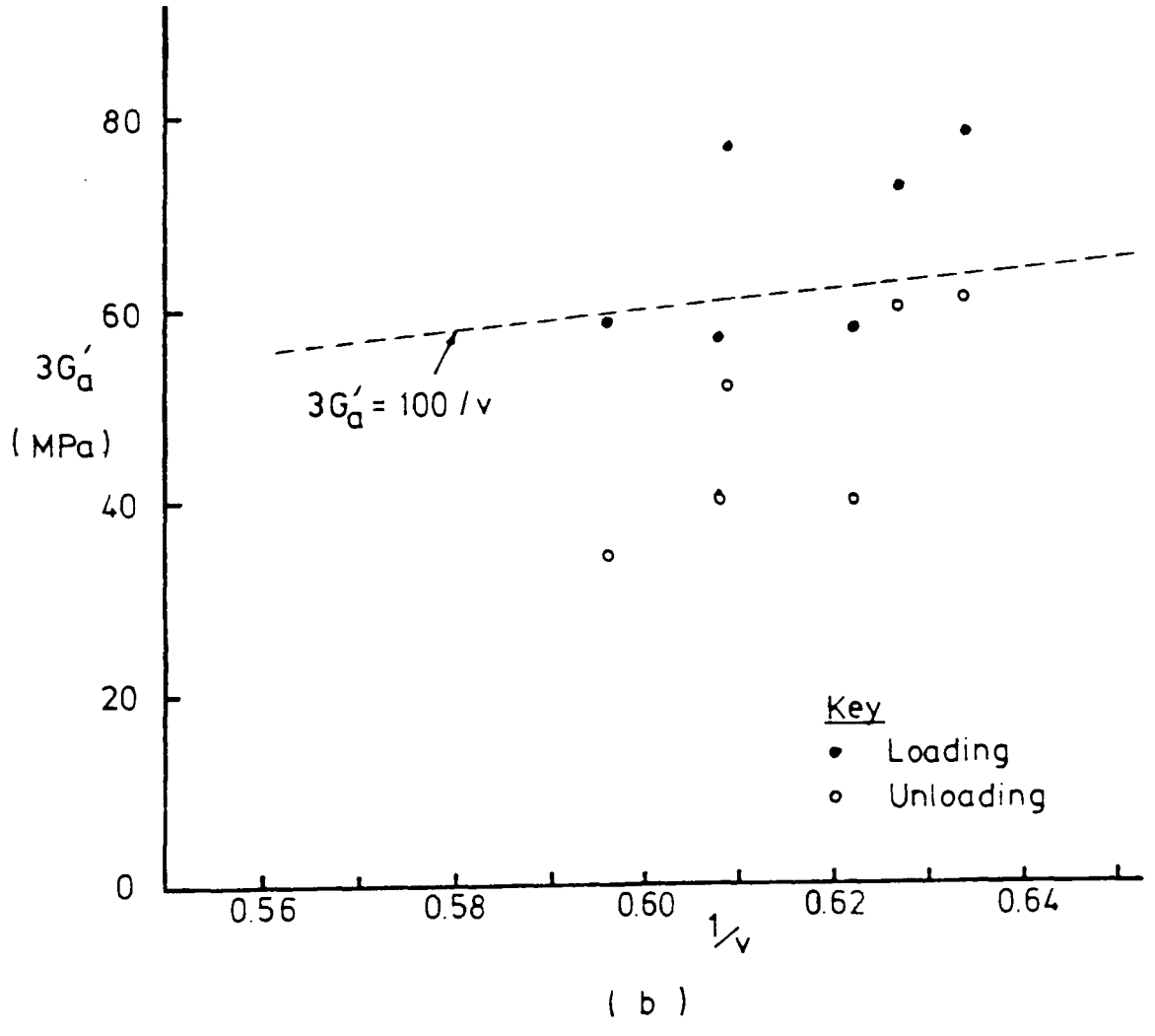

Fig 7.22 Variation of shear modulus with specific volume

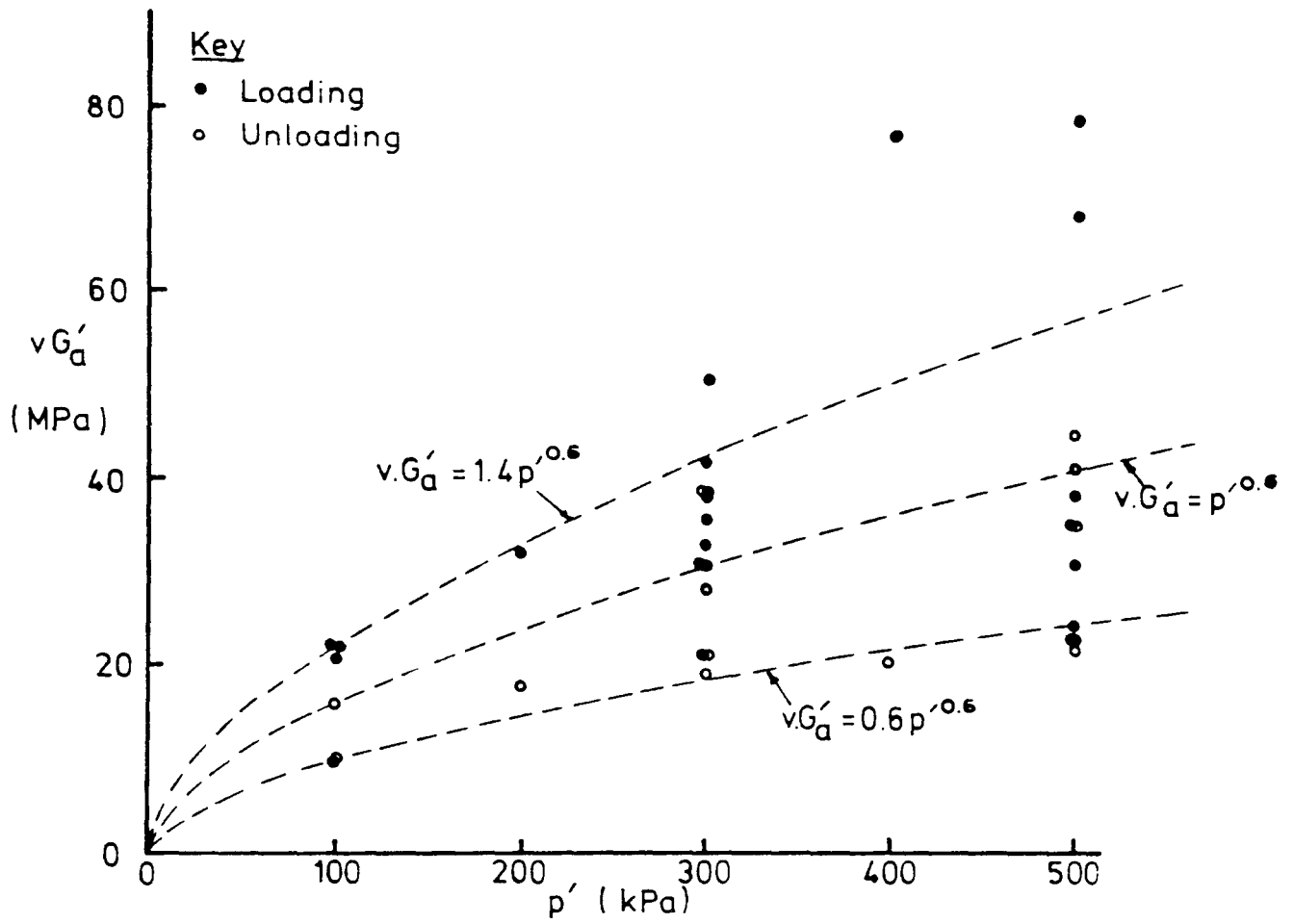

Fig 7.23 Variation of normalised shear modulus with mean effective stress

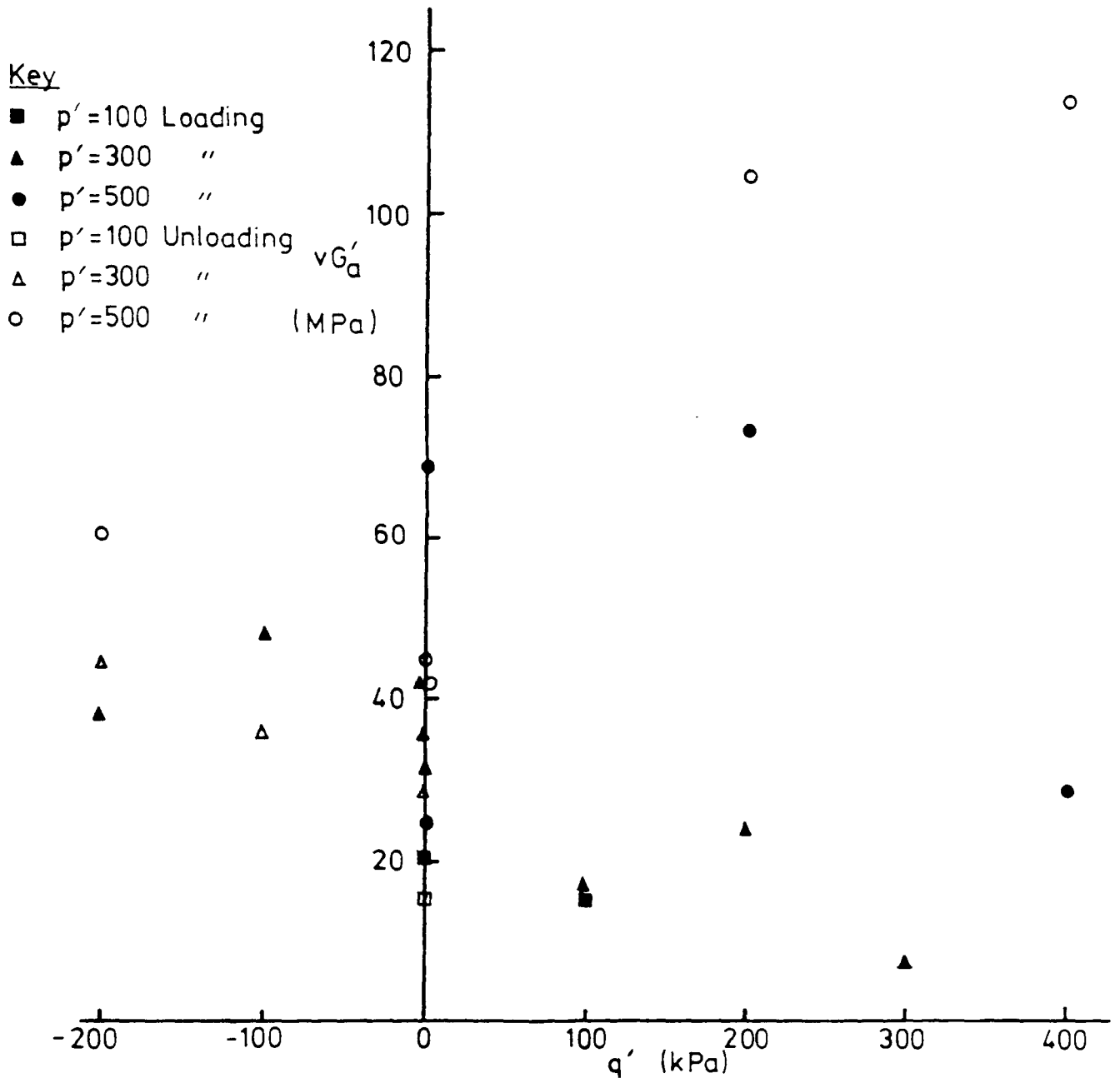

Fig 7.24 Variation of normalised shear modulus with deviator stress

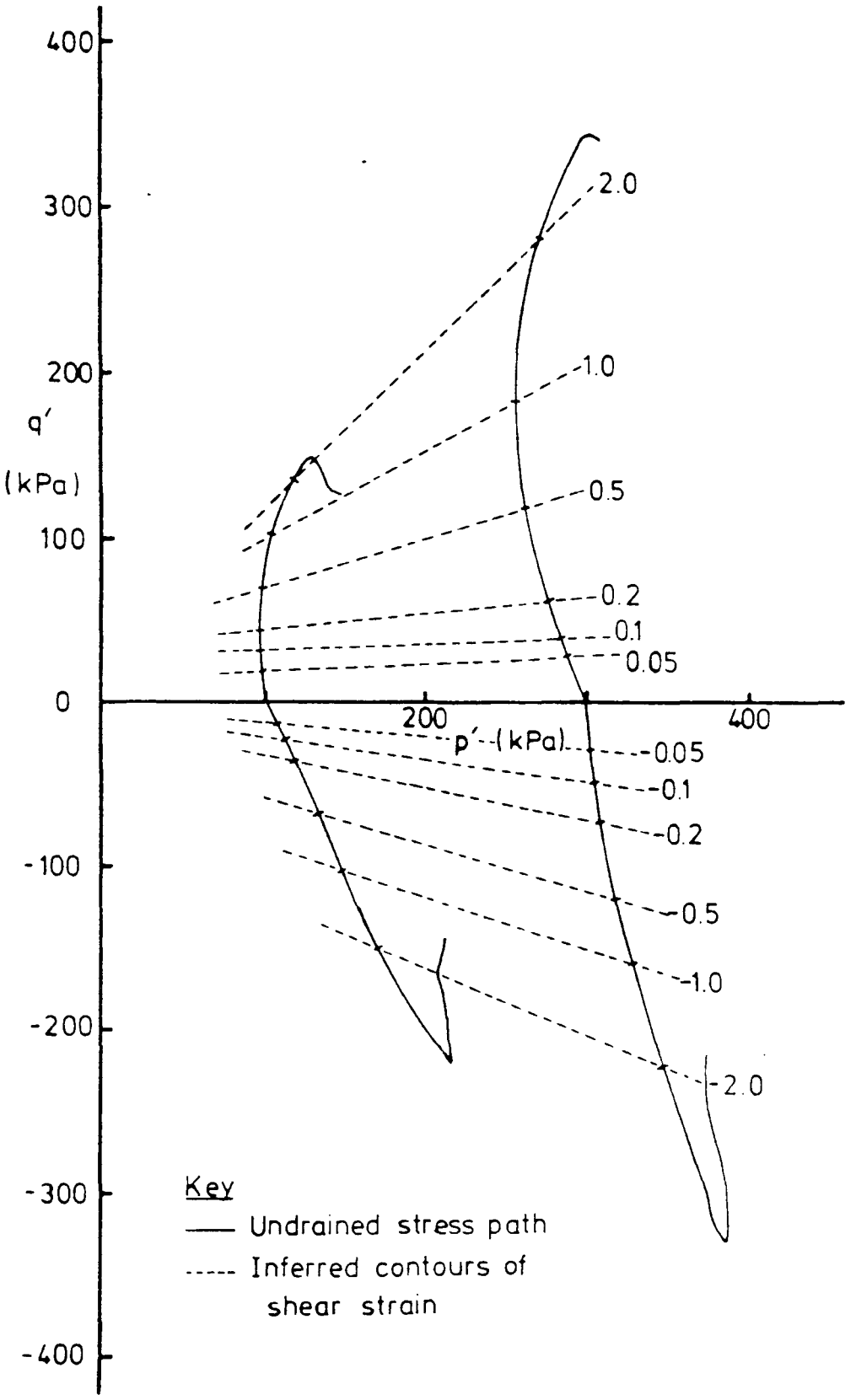

Fig 7.25 Contours of shear strain for undrained tests

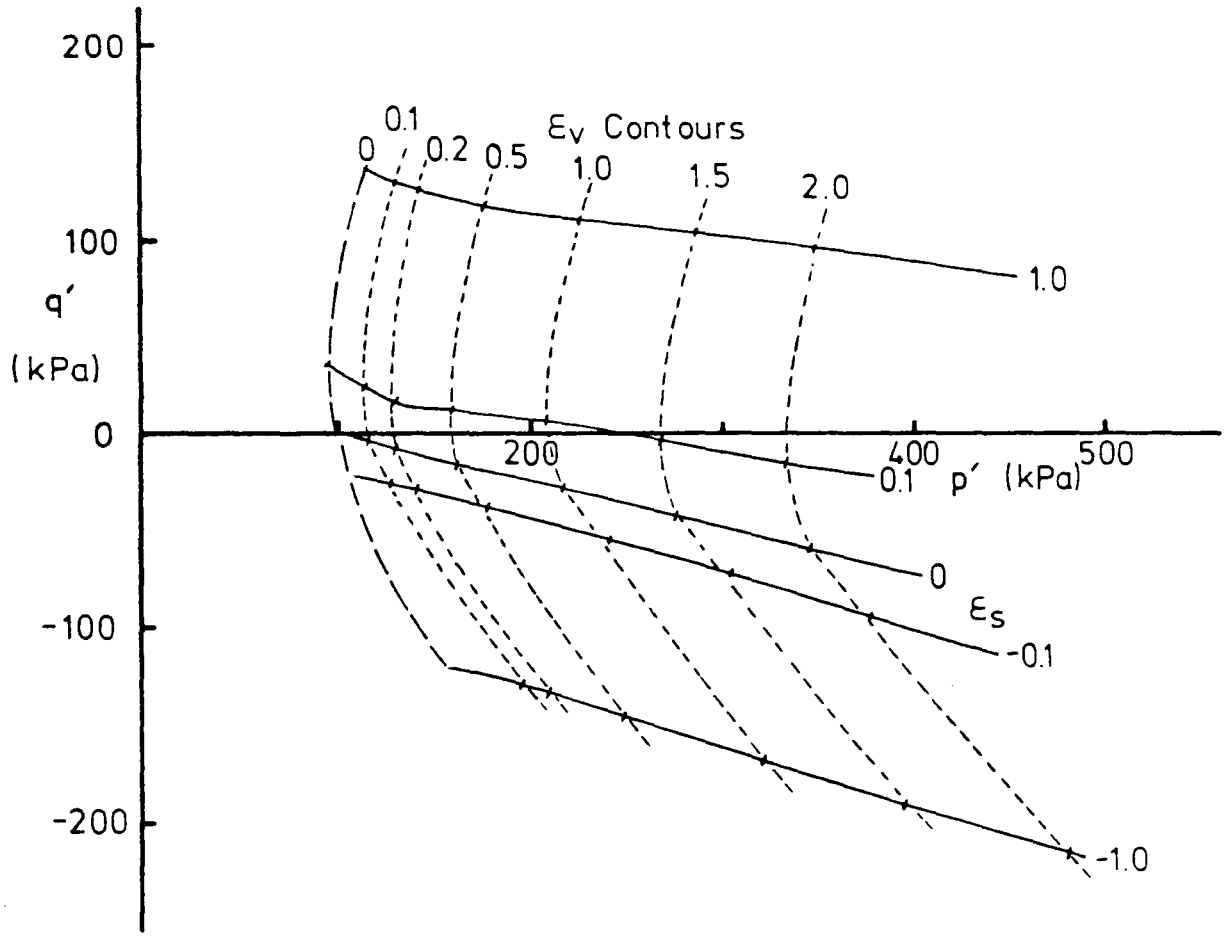

Fig 7.26 Contours of volumetric strain for constant shear strain tests

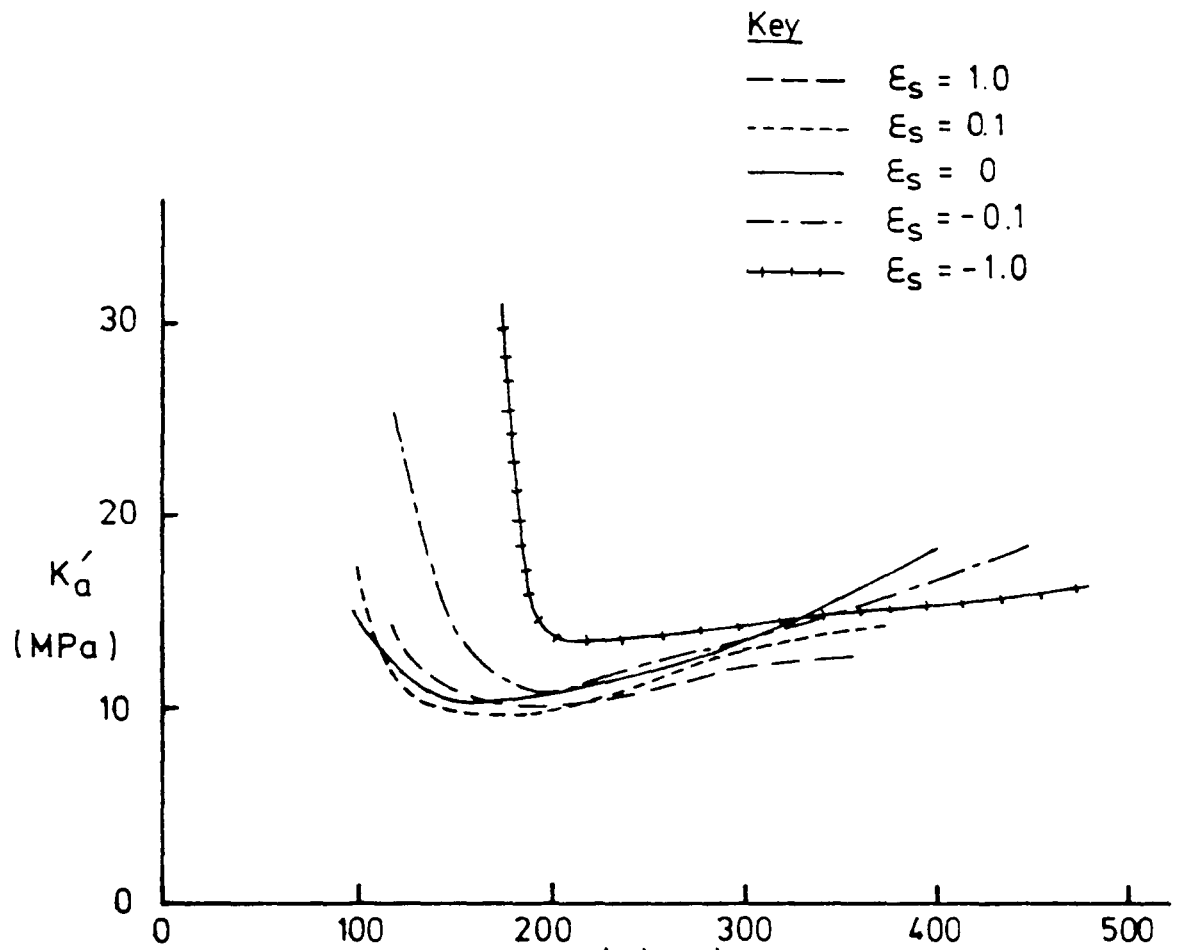

Fig 7.27 Bulk modulus measured by constant shear strain tests

CHAPTER 8

CONCLUSIONS

8.1 CRITICAL STATE MODEL

Critical state theory provides a reasonable conceptual model for the behaviour of the Gault Clay tested.

In the critical state model the equation for the normal consolidation line is given as

$$v = N - \lambda \ln(p') \qquad (8.1)$$

This is found to be a reasonable fit to the data, but a better fit may be obtained using Butterfield's (1979) compression law

$$\ln(v) = N^* - \lambda^* \ln(p') \qquad (8.2)$$

For overconsolidated soil, the swelling line is defined as

$$v = v_K - \kappa \ln(p') \qquad (8.3)$$

This requires the bulk modulus to be proportional to the product vp'. For $K' \propto p'$ there are several theoretical problems in formulating a consistent elastic model (Zytynski et al., 1978). $K' \propto v$ is wrong intuitively. Linearity of the swellng line in ln(v)-ln(p') space is preferred (after Butterfield, 1979), but some other compression law producing an inverse relationship between K' and the specific volume would also be acceptable.

Normalisation of elastic stiffness parameters for heavily overconsolidated clays using the critical state model is not entirely adequate. Some account must be taken of the overconsolidation ratio of the soil.

8.2 ANISOTROPY

Anisotropy in stress-strain behaviour may be caused by the structure of the soil or induced by stress changes if the stress-strain behaviour of the soil is not linear. Divergence of the stress paths for constant shear strain tests suggests that at least part of the anisotropy seen in the soil tested is stress induced.

Anisotropic stress-strain behaviour is evident in many of the test results for undisturbed Gault Clay. In undrained tests the stress path is inclined in q':p' space; in isotropic compression tests some shear strain is measured.

Differences in the values for the coefficient of consolidation measured in the oedometer and the triaxial cell can be attributed to anisotropic stiffness of the soil.

For isotropic soil the shear and bulk moduli may be measured directly in undrained and isotropic tests respectively. If this was attempted for the anisotropic soil used in the present tests, the measured values would be about 25 per cent in error through neglecting anisotropy.

8.3 TRIAXIAL MEASUREMENTS

Three of the five independent elastic parameters for cross-anisotropic soil may be measured using pairs of stress paths in the triaxial apparatus. Those which cannot be measured are the independent shear modulus G_v' and Poisson's ratio in the plane of symmetry.

The method of using successive stress path probes on single soil samples is reasonably successful for heavily overconsolidated

clay. The best results are obtained using pairs of stress paths approximately at right angles to each other in stress space. Reasonably consistent results can be obtained. There is some scatter in results due to inaccuracies in measurements for the small values of strain encountered.

Particular attention must be paid to threshold and stress history effects when conducting stress probe tests. The best results can be obtained if changes in stress path direction can be avoided.

8.4 VARIATION OF ELASTIC STIFFNESS PARAMETERS

The variation of the anisotropic elastic parameters was investigated using stress path probes on soil samples at several stress states. The results include some scatter, but some trends are evident.

The bulk modulus is found to be approximately proportional to the mean effective stress. In a plot of K_a' against p' the straight line fit to the data has an intercept on the K_a' axis which is attributable to the coupling factor $J'^2/3G_a'$.

The shear modulus is approximately proportional to the mean effective stress raised to the power 0.6. This relationship may be more directly controlled by the overconsolidation ratio, which has not been investigated here.

The requirements of the critical state model that the moduli be proportional to the specific volume are not supported by the data. Such a variation is not in any case intuitively correct. The data for variation of the bulk modulus with specific volume are inconclusive. For the shear modulus the data suggest $G_a' \propto 1/v$.

8.5 .FURTHER RESEARCH

The compression law used in the critical state model has been questioned. The present results do not define the changes needed in the compression law since they contain the additional complication of anisotropic soil behaviour. A further series of isotropic swelling and compression tests on isotropic soil using the larger triaxial apparatus (for better volume strain measurement) would provide some interesting results. It may then be possible to review the way in which the elastic parameters vary with soil state, and to develop a theoretically more consistent elastic soil model.

In measuring the variation of stiffness parameters with soil state, the present testing has concentrated on varying the state parameters q', p' and v. The strong influence of over-consolidation ratio has been noted. A further series of tests to investigate the effect of overconsolidation ratio on soil stiffness would provide useful information.

APPENDIX A

METHODS OF DEDUCING STIFFNESS PARAMETERS

(a) Constant p' and Constant q' Tests

$$\begin{Bmatrix} \delta\varepsilon_s \\ \delta\varepsilon_v \end{Bmatrix} = \begin{bmatrix} A & B \\ C & D \end{bmatrix} \cdot \begin{Bmatrix} \delta q' \\ \delta p' \end{Bmatrix}$$

Const. p' test: $1/A = \delta q'/\delta\varepsilon_s$ $\quad 1/C = \delta q'/\delta\varepsilon_v$

Const. q' test: $1/B = \delta p'/\delta\varepsilon_s$ $\quad 1/D = \delta p'/\delta\varepsilon_v$

Invert matrix:
$$3G_a' = D / (AD - BC)$$
$$J_1' = -B / (AD - BC)$$
$$J_2' = -C / (AD - BC)$$
$$K_a' = A / (AD - BC)$$

(b) Undrained and Isotropic Tests

$$\begin{Bmatrix} \delta q' \\ \delta p' \end{Bmatrix} = \begin{bmatrix} 3G_a' & J_1' \\ J_2' & K_a' \end{bmatrix} \cdot \begin{Bmatrix} \delta\varepsilon_s \\ \delta\varepsilon_v \end{Bmatrix}$$

Undrained: $\delta\varepsilon_v = 0$ $\quad 3G_a' = \delta q'/\delta\varepsilon_s$, $J_2' = \delta p'/\delta\varepsilon_s$

Isotropic: $\delta q' = 0$ $\quad J_1' = -3G_a' (\delta\varepsilon_s/\delta\varepsilon_v) = -3G_a' (\delta p'/\delta\varepsilon_v)/(\delta p'/\delta\varepsilon_s)$

$$K_a' = (\delta p'/\delta\varepsilon_v) - J_2' (\delta\varepsilon_s/\delta\varepsilon_v) = (\delta p'/\delta\varepsilon_v) - J_2' (\delta p'/\delta\varepsilon_v)/(\delta p'/\delta\varepsilon_s)$$

(c) Drained and Isotropic Tests

$$\begin{Bmatrix} \delta\varepsilon_s \\ \delta\varepsilon_v \end{Bmatrix} = \begin{bmatrix} A & B \\ C & D \end{bmatrix} \cdot \begin{Bmatrix} \delta q' \\ \delta p' \end{Bmatrix}$$

Isotropic test: $\delta q' = 0$ $\quad 1/C = \delta p'/\delta\varepsilon_s$, $1/D = \delta p'/\delta\varepsilon_v$

Drained test: $\delta q'/\delta p' = 3$ $\quad A = 1/(\delta q'/\delta\varepsilon_s) - B/3$, $C = 1/(\delta q'/\delta\varepsilon_v) - D/3$

Invert Matrix as in (a) above to get stiffness parameters.

(d) <u>$\Delta q'=\Delta p'$ and $\Delta q'=-\Delta p'$ Stress Paths</u>

$$\begin{Bmatrix} \delta\varepsilon_s \\ \delta\varepsilon_v \end{Bmatrix} = \begin{bmatrix} A & B \\ C & D \end{bmatrix} \cdot \begin{Bmatrix} \delta q' \\ \delta p' \end{Bmatrix}$$

$\Delta q'=\Delta p'$: $\quad A + B = 1/(\delta q'/\delta\varepsilon_s)_a \qquad D + C = 1/(\delta p'/\delta\varepsilon_v)_a$

$\Delta q'=-\Delta p'$: $\quad A - B = 1/(\delta q'/\delta\varepsilon_s)_b \qquad D - C = 1/(\delta p'/\delta\varepsilon_v)_b$

Solving:

$$A = [\ 1/(\delta q'/\delta\varepsilon_s)_a + 1/(\delta q'/\delta\varepsilon_s)_b\ ] / 2$$

$$B = [\ 1/(\delta q'/\delta\varepsilon_s)_a - 1/(\delta q'/\delta\varepsilon_s)_b\ ] / 2$$

$$C = [\ 1/(\delta p'/\delta\varepsilon_v)_a - 1/(\delta p'/\delta\varepsilon_v)_b\ ] / 2$$

$$D = [\ 1/(\delta p'/\delta\varepsilon_v)_a + 1/(\delta p'/\delta\varepsilon_v)_b\ ] / 2$$

Invert Matrix as in (a) above to get stiffness parameters.

APPENDIX B

DETAILS OF STRESS PROBE TESTS

Test	Stage	Start			End		
		p' (kPa)	q' (kPa)	v	p' (kPa)	q' (kPa)	v
P1	1a	300	0	1.576	296	50	1.576
	b	296	50	1.576	317	-50	1.576
	c	317	-50	1.576	305	0	1.576
	2a	300	0	1.577	290	50	1.577
	b	290	50	1.577	312	-50	1.577
	c	312	-50	1.577	300	0	1.577
	3a	300	0	1.577	289	50	1.577
	b	289	50	1.577	315	-50	1.577
	c	315	-50	1.577	300	0	1.577
	4a	300	0	1.577	300	50	1.576
	b	300	50	1.576	300	-50	1.578
	c	300	-50	1.578	300	0	1.577
	5a	300	0	1.577	350	50	1.573
	b	350	50	1.573	250	-50	1.582
	c	250	-50	1.582	300	0	1.578
	6a	300	0	1.578	284	50	1.578
	b	284	50	1.578	307	-50	1.578
	c	307	-50	1.578	294	0	1.578
	7a	300	0	1.578	286	48	1.578
	b	286	48	1.578	312	-48	1.578
	c	312	-48	1.578	300	0	1.578
	8a	300	0	1.578	250	50	1.580
	b	250	50	1.580	350	-50	1.575
	c	350	-50	1.575	300	0	1.577
	9a	300	0	1.577	289	50	1.577
	b	289	50	1.577	311	-50	1.577
	c	311	-50	1.577	299	0	1.577
	10a	299	0	1.577	317	50	1.576
	b	317	50	1.576	283	-50	1.579
	11a	300	0	1.577	300	50	1.576
	b	300	50	1.576	300	-50	1.578
	c	300	-50	1.578	300	0	1.577
	12a	300	0	1.577	340	0	1.575
	b	340	0	1.575	260	0	1.580
	c	260	0	1.580	340	0	1.575
	d	340	0	1.575	300	0	1.577
	13a	300	0	1.577	290	50	1.577
	b	290	50	1.577	311	-50	1.577
	c	311	-50	1.577	303	0	1.577

Cont'd/-

Test	Stage	Start			End		
		p' (kPa)	q' (kPa)	v	p' (kPa)	q' (kPa)	v
P2	1a	500	0	1.596	485	50	1.596
	b	485	50	1.596	503	-50	1.596
	c	503	-50	1.596	495	0	1.596
	2a	495	0	1.596	495	90	1.595
	b	495	90	1.595	495	-90	1.596
	c	495	-90	1.596	495	90	1.594
	d	495	90	1.594	495	0	1.595
	3a	495	0	1.595	475	100	1.595
	b	475	100	1.595	520	-100	1.595
	c	520	-100	1.595	501	0	1.595
	4a	501	0	1.595	600	0	1.590
	b	600	0	1.590	500	0	1.593
	5	500	0	1.593	300	0	1.606
	6a	300	0	1.606	298	50	1.606
	b	298	50	1.606	319	-50	1.606
	c	319	-50	1.606	313	0	1.606
	7a	300	0	1.607	300	50	1.607
	b	300	50	1.607	300	-50	1.608
	c	300	-50	1.608	300	0	1.608
	8a	300	0	1.608	288	50	1.608
	b	288	50	1.608	321	-100	1.608
	c	321	-100	1.608	303	0	1.608
	9	303	0	1.608	350	0	1.606
	10	Data Lost					
	11a	100	0	1.675	106	50	1.675
	b	106	50	1.675	118	-50	1.675
	c	118	-50	1.675	112	0	1.675
	12a	112	0	1.675	112	50	1.674
	b	112	50	1.674	112	-50	1.677
	c	112	-50	1.677	112	0	1.676
	13a	112	0	1.676	106	50	1.676
	b	106	50	1.676	118	-50	1.676
	c	118	-50	1.676	112	0	1.676
	14a	112	0	1.676	152	0	1.673
	b	152	0	1.673	72	0	1.680
	c	72	0	1.680	152	0	1.673
	d	152	0	1.673	100	0	1.677

Cont'd/-

Test	Stage	Start			End		
		p' (kPa)	q' (kPa)	v	p' (kPa)	q' (kPa)	v
P3	1	374	0	1.677	500	0	1.661
	2a	500	0	1.661	474	50	1.661
	b	474	50	1.661	493	-50	1.661
	c	493	-50	1.661	477	0	1.661
	3	477	0	1.661	400	0	1.666
	4a	400	0	1.666	393	44	1.666
	b	393	44	1.666	425	-50	1.666
	c	425	-50	1.666	413	0	1.666
	5	413	0	1.666	300	0	1.677
	6a	300	0	1.677	291	50	1.677
	b	291	50	1.677	325	-50	1.677
	c	325	-50	1.677	312	0	1.677
	7	312	0	1.677	200	0	1.694
	8a	200	0	1.694	195	50	1.694
	b	195	50	1.694	224	-50	1.694
	c	224	-50	1.694	213	0	1.694
P4	1a	100	0	1.675	106	50	1.675
	b	106	50	1.675	118	-50	1.675
	c	118	-50	1.675	112	0	1.675
	2a	112	0	1.675	112	50	1.674
	b	112	50	1.674	112	-50	1.677
	c	112	-50	1.677	112	0	1.676
	3a	112	0	1.676	106	50	1.676
	b	106	50	1.676	118	-50	1.676
	c	118	-50	1.676	112	0	1.676
	4a	112	0	1.676	152	0	1.673
	b	152	0	1.673	72	0	1.680
	c	72	0	1.680	152	0	1.673
	d	152	0	1.673	100	0	1.677
	5a	100	0	1.677	100	50	1.677
	b	100	50	1.677	115	-50	1.677
	c	115	-50	1.677	110	0	1.677
	6	110	0	1.677	110	100	1.675
	7a	110	100	1.675	150	100	1.670
	b	150	100	1.670	110	100	1.672
	8	110	100	1.673	110	250	1.682

Cont'd/-

Test	Stage	Start			End		
		p' (kPa)	q' (kPa)	v	p' (kPa)	q' (kPa)	v
P5	1a	300	0	1.577	300	50	1.576
	b	300	50	1.576	300	-50	1.578
	c	300	-50	1.578	300	0	1.577
	2a	300	0	1.577	340	0	1.575
	b	340	0	1.575	260	0	1.580
	c	260	0	1.580	340	0	1.575
	d	340	0	1.575	300	0	1.577
	3a	300	0	1.577	290	50	1.577
	b	290	50	1.577	311	-50	1.577
	c	311	-50	1.577	303	0	1.577
	4	303	0	1.577	303	100	1.575
	5a	303	100	1.575	330	100	1.574
	b	330	100	1.574	300	100	1.575
	6	300	100	1.575	300	200	1.574
	7a	300	200	1.574	330	200	1.572
	b	330	200	1.572	300	200	1.573
	8	300	200	1.573	300	300	1.573
	9a	300	300	1.573	330	300	1.571
	b	330	300	1.571	300	300	1.573
	10	300	300	1.573	300	425	1.573
P6	1a	405	0	1.582	260	0	1.595
	b	260	0	1.595	340	0	1.592
	c	340	0	1.592	300	0	1.593
	2a	300	0	1.593	314	-50	1.593
	b	314	-50	1.593	293	50	1.593
	c	293	50	1.593	313	-50	1.593
	d	313	-50	1.593	305	0	1.593
	3a	305	0	1.593	305	50	1.593
	b	305	50	1.593	305	-50	1.594
	c	305	-50	1.594	305	50	1.593
	d	305	50	1.593	305	0	1.594
	4	305	0	1.594	540	0	1.578
	5a	460	0	1.582	540	0	1.577
	b	540	0	1.577	460	0	1.580
	6a	500	50	1.578	500	-50	1.578
	6b,7	500	-50	1.578	500	250	1.574
	8a	460	200	1.574	540	200	1.572
	b	540	200	1.572	460	200	1.573
	9a	500	250	1.574	500	150	1.574
	9b,10	500	150	1.574	500	450	1.571
	11a	460	400	1.572	540	400	1.570
	b	540	400	1.570	460	400	1.570
	12a	500	450	1.571	500	350	1.571
	12b,13	500	350	1.571	500	645	1.573

Cont'd/-

Test	Stage	Start			End		
		p' (kPa)	q' (kPa)	v	p' (kPa)	q' (kPa)	v
P7	1a	310	0	1.639	260	0	1.645
	b	260	0	1.645	340	0	1.640
	2a	300	-50	1.643	276	50	1.643
	b	276	50	1.643	305	-50	1.643
	3a	305	-50	1.643	305	50	1.641
	3b,4	305	50	1.641	305	-150	1.648
	5a	260	-100	1.651	340	-100	1.644
	b	340	-100	1.644	260	-100	1.651
	6a	305	-150	1.648	305	-50	1.645
	6b,7	300	-50	1.646	300	-250	1.656
	8a	260	-200	1.658	340	-200	1.652
	b	240	-200	1.652	260	-200	1.659
	9a	300	-250	1.656	300	-150	1.653
	9b,10	300	-150	1.655	300	-279	1.658
P8	1a	260	0	1.645	340	0	1.641
	b	340	0	1.641	260	0	1.647
	2a	300	50	1.643	300	-50	1.645
	b	300	-50	1.645	300	50	1.643
	3	350	0	1.641	450	0	1.635
	4a	540	0	1.629	460	0	1.632
	b	460	0	1.632	540	0	1.629
	5a	500	-50	1.630	500	50	1.629
	5b,6	500	50	1.629	500	-250	1.634
	7a	460	-200	1.635	540	-200	1.632
	b	540	-200	1.632	460	-200	1.634
	8a	500	-250	1.634	500	-150	1.634
	8b,9	500	-150	1.633	500	-353	1.635

REFERENCES

APTED, J.P. (1977). Effect of weathering on some geotechnical properties of London Clay. PhD Thesis: London University.

ATKINSON, J.H. (1973). The deformation of undisturbed London Clay. PhD Thesis: University of London.

ATKINSON, J.H. (1975). Anisotropic elastic deformations in laboratory tests on undisturbed London Clay. Géotechnique 25 No. 2: 357 - 374.

ATKINSON, J.H. (1984a). Rate of loading in drained and undrained stress path and triaxial tests. Research Report GE/84/1: The City University, Geotechnical Engineering Research Centre.

ATKINSON, J.H. (1984b). Some procedures for normalising soil test results. Research Report GE/84/3: The City University, Geotechnical Engineering Research Centre.

ATKINSON, J.H. and BRANSBY, P.L. (1978). The Mechanics of Soils. (McGraw-Hill, London).

ATKINSON, J.H. and CLINTON, D.B. (1984). Stress path tests on 100mm diameter samples. In: CONFERENCE ON SITE INVESTIGATION PRACTICE, Guildford. Proceedings. (Geological Society).

ATKINSON, J.H. and RICHARDSON, D. (1986). The effect of local drainage in rupture zones on the undrained strength of overconsolidated clay. Research Report GE/86/7: The City University, Geotechnical Engineering Research Centre.

ATKINSON, J.H., EVANS, J.S. and HO, E.W.L. (1985). Non-uniformity of triaxial samples due to consolidation with radial drainage. Géotechnique 35: 353-355.

ATKINSON, J.H., EVANS, J.S. and SCOTT, C.R. (1985). Developments in microcomputer controlled stress path testing equipment for measurement of soil parameters. Ground Engineering: 15 - 22.

BALASUBRAMANIAM, A.S. (1969). Some factors influencing the stress-strain behaviour of clays. PhD Thesis: University of Cambridge.

BALIGH, M.M. (1984). The strain path method in geotechnical engineering. Report No. R84 - 01: Massachusetts Institute of Technology.

BALLESTER, F. and SAGASETA, C. (1979). Anisotropic elastoplastic undrained analysis of soft clays. Géotechnique 29 No. 3: 323-340.

BARDEN, L. (1963). Stresses and displacements in a cross-anisotropic soil. Géotechnique 13 No. 3: 198 - 210.

BISHOP, A.W. (1971). Shear strength parameters for undisturbed and remoulded soil specimens. In: SYMPOSIUM ON STRESS-STRAIN BEHAVIOUR OF SOILS, Cambridge. Proceedings. (Foulis): 3-58.

BISHOP, A.W. and HENKEL, D.J. (1962). The Measurement of Soil Properties in the Triaxial Test. 2nd Ed. (Edward Arnold).

BISHOP, A.W., KUMAPLEY, N.K. and EL-RUWAYIH, A. (1975). The influence of pore-water tension on the strength of clay. Royal Society Philosophical Transactions Vol 278: 511 - 554.

BISHOP, A.W. and WESLEY, L.D. (1975). A hydraulic triaxial apparatus for controlled stress path testing. Géotechnique 24 No. 4: 657 - 670.

BJERRUM, L. (1967). Engineering geology of Norwegian normally consolidated marine clays as related to settlements of buildings. Géotechnique 17 No. 2: 81 - 118.

BOUSSINESQ, J. (1885). Applications des potentials a l'étude de l'équilibre et du mouvement des solides élastiques. (Paris, Gauthier-Villard).

BRITISH STANDARDS INSTITUTION (1975). Methods of Test for Soils for Civil Engineering Purposes. BS1377. (HMSO).

BURLAND, J.B., BROMS, B.B. and DE MELLO, V.F.B. (1977). Behaviour of foundations and structures. In: INTERNATIONAL CONFERENCE SOIL MECHANICS AND FOUNDATION ENGINEERING, 9th Tokyo. Proceedings. Vol 2: 495 - 546.

BURMINSTER, D.M. (1945). The general theory of stresses and displacements in layered soil systems. Journal of Applied Physics, Vol 16, No.2: 89-96; No.3: 126-127; No.5: 296-302.

BUTLER, F.G. (1975). Heavily over-consolidated clays. In: CONFERENCE ON SETTLEMENT OF STRUCTURES. Cambridge. Proceedings: 531-578.

BUTTERFIELD, R (1979). A natural compression law for soils (an advance on e - log p'). Géotechnique 29 No. 4: 469 - 480.

CALLADINE, C.R. (1963). Correspondence. Géotechnique 13: 250-255.

CAMPANELLA, R.G. and VAID, Y.P. (1972). A simple K_o triaxial cell. Canadian Geotechnical Journal: 249 - 260.

CLINTON, D.B. (1986). User manual for TRIAX and TRIAX.+, programs for computer control of triaxial stress path tests. Research Report GE/86/14: The City University, Geotechnical Engineering Research Centre.

CLINTON, D.B., and NG, C.L. (1984). Dovercourt Bypass Stage 2 - preliminary site investigation special soil testing. Research Report GE/84/16: The City University, Geotechnical Engineering Research Centre.

COOPER, M.R. (1986). Report on an investigation of the suitability of a proposed geotechnical test-bed site at Selborne, Hants. SERC Research Contract Report GR/D02799, Southampton University.

COSTA FILHO, L.M. (1985). Measurement of axial strains in triaxial tests on London Clay. Geotechnical Testing Journal, 8 No. 1 (ASTM): 3 - 13.

D'APPOLONIA, D.J. and LAMBE, T.W. (1970). Method for predicting initial settlement. American Society of Civil Engineers, Proceedings, SM2: 523 - 544.

DAVIS, E.H. and POULOS, H.G. (1963). Triaxial testing and three-dimensional settlement analysis. In: AUSTRALIA/NEW ZEALAND CONFERENCE ON SOIL MECHANICS AND FOUNDATION ENGINEERING, 4th Proceedings: 233 - 243.

DAVIS, E.H. and POULOS, H.G. (1968). The use of elastic theory for settlement prediction under three-dimensional conditions. Géotechnique 18 No.1: 67 - 91.

DE URENA, R, PIQUER, J.S., MUZAS, F. and SANZ SARACHO, J.M. (1966). Stress distribution in cross-anisotropic media. In: CONGRESS INTERNATIONAL SOCIETY ROCK MECHANICS, 1st, Lisbon. Proceedings. Vol 1: 313 - 317.

DEVEAUX, D., VUEZ, A., AMOROS, D., MIEUSSENS, C. and DUCASSE, P. (1981). Essais triaxiaux à chargement controlé. In: INTERNATIONAL CONFERENCE ON SOIL MECHANICS AND FOUNDATION ENGINEERING, 10th, Stockholm. Proceedings. Vol.1: 581-586.

FOSTER, C.R. and AHLVIN, R.G. (1954). Stresses and deflections induced by a uniform circular load. Proc. Highway Research Board, Vol. 33: 467 - 470.

GENS, A. (1982). Stress-strain and strength characteristics of a low-plasticity clay. PhD. Thesis: London University.

GENS, A. and HIGHT, D.W. (1979). The laboratory measurement of design parameters for a glacial till. In: EUROPEAN CONFERENCE ON SOIL MECHANICS AND FOUNDATION ENGINEERING, 7th, Brighton. Proceedings. Vol 2: 57 - 65.

GEOTECHNICAL DIGITAL SYSTEMS LTD. (1982). Microprocessor enables computer automated triaxial testing. Ground Engineering, 15 No.3: 37 - 38.

GERRARD, C.M. and HARRISON, W.J. (1970 a). Circular loads applied to a cross-anisotropic half-space. Technical Paper No. 8: CSIRO Australia, Division of Applied Geomechanics. Reproduced in Poulos and Davis (1974).

GERRARD, C.M. and HARRISON, W.J..(1970 b). Stresses and displacements in a loaded orthorhombic half-space. Technical Paper No. 9: CSIRO Australia, Division of Applied Geomechanics. Reproduced in Poulos and Davis (1974).

GIBSON, R.E. (1967). Some results concerning displacements and stresses in a non-homogeneous elastic half-space. Géotechnique 17, No. 1: 58 - 67.

GIBSON, R.E. (1974). The analytical method in soil mechanics. Géotechnique 24, No. 2: 115 - 140.

GRAHAM, J. and HOULSBY, G.T. (1983). Anisotropic elasticity of a natural clay. Géotechnique 33 No. 2: 165 - 180.

HEARMON, R.F.S. (1961). An Introduction to Applied Anisotropic Elasticity. (Oxford University Press).

HENKEL, D.J. (1971). The relevance of laboratory-measured parameters in field studies. In: SYMPOSIUM ON THE STRESS-STRAIN BEHAVIOUR OF SOILS, Cambridge. Proceedings: (Foulis): 669 - 675.

HENKEL, D.J. and GILBERT, G.D. (1952). The effect of the rubber membrane on the measured triaxial compression strength of clay samples. Géotechnique, 12 No.3: 20 - 29.

HIGHT, D.W. (1983). Laboratory investigations of sea-bed clays. PhD Thesis: University of London.

HIGHT, D.W. (1986). Personal communication.

HIGHT, D.W., GENS, A. and JARDINE, R.J. (1985). Evaluation of geotechnical parameters from triaxial tests on offshore clay. In: INTERNATIONAL CONFERENCE ON OFFSHORE SITE INVESTIGATION, London. Proceedings: 253 - 268.

HOULSBY, G.T. (1981). A study of plasticity theories and their applicability to soils. PhD Thesis: University of Cambridge, Engineering Department.

HOULSBY, G.T. (1985). The use of a variable shear modulus in elastic-plastic models for clays. Computers and Geotechnics 1: 3 - 13.

HVORSLEV, M.J. (1949). Subsurface Exploration and Sampling of Soils for Civil Engineering Purposes. (US Waterways Experiment Station).

INTERCOLE SYSTEMS LTD. (1985). User manual, Spectra Micro-ms.

JARDINE, R.J., SYMES, M.J. and BURLAND, J.B. (1984). The measurement of soil stiffness in the triaxial apparatus. Géotechnique, 34 No. 3: 323 - 340.

JURGENSEN, L. (1934). The application of theories of elasticity and plasticity to foundation problems. In: Contributions to Soil Mechanics 1925 - 1940. (Boston Society of Civil Engineers).

KIRKPATRICK, W.M. and KHAN, A.J. (1984). The reaction of clays to sampling stress relief. Géotechnique 34 No.1 : 29 - 42.

KO, H.Y. and STURE, S., (1980). Data reduction and application for analytical modelling. State of Art Paper, ASTM Symposium, Chicago.

KONING, H. (1957). Stress distribution in a homogeneous, anisotropic, elastic semi-infinite solid. In: INTERNATIONAL CONFERENCE ON SOIL MECHANICS AND FOUNDATION ENGINEERING, 4th London 1957. Proceedings. Vol 1: 335 - 338.

LADD, C.C., FOOTT, R. ISHIHARA, K, SCHLOSSER, F. and POULOS, H.G. (1977). Stress-deformation and strength characteristics. In: INTERNATIONAL CONFERENCE ON SOIL MECHANICS AND FOUNDATION ENGINEERING. 9th, Tokyo. Proceedings. Vol.2: 421-494.

LAMBE, T.W. (1964). Methods of estimating settlement. American Society of Civil Engineers, Proceedings. SM5: 43-67.

LAMBE, T.W. (1967). Stress path method. American Society of Civil Engineers, Proceedings, SM6: 309 - 332.

LEKHNITSKII, S.G. (1963). Theory of Elasticity of an Anisotropic Elastic Body. (Holden-Day).

LEWIN, P.I. (1978). The deformation of soft clay under generalised stress conditions. PhD Thesis: London University.

LEWIN, P.I. and BURLAND, J.B. (1970). Stress-probe experiments on saturated normally consolidated clay. Géotechnique 20 No. 1: 38 - 56.

LEWIN, P.I. and POWELL, J.J.M. (1985). Patterns of stress strain behaviour for a clay till. In: INTERNATIONAL CONFERENCE ON SOIL MECHANICS AND FOUNDATION ENGINEERING, 11th, Los Angeles Proceedings.

LOVE, A.E.H. (1927). A Treatise on the Mathematical Theory of Elasticity. (Cambridge University Press).

MAGUIRE, W.M. (1975). The undrained strength and stress-strain behaviour of brecciated Upper Lias Clay. DIC Thesis: London University.

MAJID, K.I. and CRAIG J.S. (1971). An incremental finite element analysis of structural interaction with soil of non-linear properties. In: SYMPOSIUM ON INTERACTION OF STRUCTURE AND FOUNDATION, Birmingham, Proceedings: 131 - 145.

MARSLAND, A. (1971). Laboratory and in-situ measurements of the deformation moduli of London Clay. In: SYMPOSIUM ON THE INTERACTION OF STRUCTURE AND FOUNDATION, Birmingham. Proceedings: 7 - 15.

McGOWN, A., BARDEN, L., LEE, S.H. and WILBY, P. (1974). Sample disturbance in soft alluvial Clyde Estuary Clay. Canadian Geotechnical Journal: 651 - 660.

MENZIES, B.K., SUTTON, H., and DAVIES, R.E. (1977). A new system for automatically simulating K_o consolidation and K_o swelling in the conventional triaxial cell. Géotechnique, 27 No.4: 593 - 596.

MINDLIN, R.D. (1936). Force at a point in the interior of a semi-infinite solid. Journal of Applied Physics, Vol.7 No.5: 195 - 202.

MORGENSTERN, N.N. and PHUKAN A.L.T. (1968). Stresses and displacements in a homogeneous non-linear foundation. In: INTERNATIONAL SYMPOSIUM OF ROCK MECHANICS, Madrid. Proceedings. 313 -320.

NAYLOR, D.J., PANDE, G.N., SIMPSON, B. and TABB, R. (1981). Finite Elements in Geotechnical Engineering. (Pineridge Press, Swansea).

NEWMARK, N.M. (1942). Influence charts for computation of stresses in elastic soils. Bulletin 338: University of Illinois, Engineering Experimental Station.

PARRY, R.H.G and AMERASINGHE, S.F. (1973). Plastic deformations in clay at high overconsolidation ratio and low stress level. In: SYMPOSIUM ON PLASTICITY IN SOIL MECHANICS, Cambridge. Proceedings: 108-126.

PARRY, R.H.G. and NADARAJAH, V. (1974). Observations on laboratory prepared, lightly overconsolidated specimens of kaolin. Géotechnique 24 No.3: 345 - 358.

PERLOFF, W.H., BALADI, G.Y. and HARR, M.E. (1967). Stress distribution within and under long elastic embankments. Highway Research Record 181: 12 - 40.

PICKERING, D.J. (1970). Anisotropic elastic parameters for soil. Géotechnique 20 No.3 : 271 - 276.

POULOS, H.G. and DAVIS, E.H. (1974). Elastic Solutions for Soil and Rock Mechanics. (Wiley).

RAYMOND, G.P. (1970). Discussion. Géotechnique 20 No.4: 456 - 458.

RAYMOND, G.P. (1972). Prediction of undrained deformations and pore pressures in weak clay under two embankments. Géotechnique 22 No.3 : 381 - 401.

RICHARDSON, D. (1986). Investigations of threshold effects in soil deformations. PhD Thesis: The City University, Civil Engineering Department.

RIVARD, P.J. and LU, Y. (1978). Shear strength of soft fissured clays. Canadian Geotechnical Journal: 382 - 390.

ROSCOE, K.H. and SCHOFIELD, A.N. (1963). Mechanical behaviour of an idealised wet clay. In: EUROPEAN CONFERENCE ON SOIL MECHANICS, 2nd. Proceedings: 47-54

ROWE, P.W. and BARDEN, L. (1964). Importance of free ends in triaxial testing. American Society of Civil Engineers, Proceedings SM1: 1-27.

SCHOFIELD, A.N. and WROTH, C.P. (1968). Critical State Soil Mechanics. (McGraw-Hill, London).

SIMONS, N.E. (1967). Discussion. In: GEOTECHNICAL CONFERENCE, Oslo. Proceedings. Vol 2. : 159 - 160.

SIMONS, N.E. (1971). The stress path method of settlement analysis applied to London Clay. In: SYMPOSIUM ON STRESS STRAIN BEHAVIOUR OF SOILS, Cambridge, Proceedings. (Foulis): 241 - 252.

SIMONS, N.E. and SOM, N.N. (1970). Settlement of structures on clay with particular emphasis on London Clay. CIRIA Report 22. (HMSO).

SIMPSON, B. (1986). Implementing a stress-strain model for London Clay. Seminar given at The City University.

SIMPSON, B., CALABRESI, G., SOMMER, H. and WALLEYS, M. (1979). Design parameters for stiff clays: General Report. In: EUROPEAN CONFERENCE ON SOIL MECHANICS AND FOUNDATION ENGINEERING, 7th, Brighton. Proceedings Vol 5: 91 - 125.

SKEMPTON, A.W. and BJERRUM, L. (1957). A contribution to the settlement analysis of foundations on clay. Géotechnique 7 No.4 : 168 - 178.

SKEMPTON, A.W., SCHUSTER, R.L. and PETLEY, D.J. (1969). Joints and fissures in the London Clay at Wraysbury and Edgware. Géotechnique 19 No. 2.: 205 - 217.

SKEMPTON, A.W., and SOWA, V.A. (1963). The behaviour of saturated clays during sampling and testing. Géotechnique 13: 269 - 290.

SOM, N.N. (1968). The effect of stress path on the deformation and consolidation of London Clay. PhD Thesis: University of London.

ST. JOHN, H.D. (1980). A review of current practice in the design and installation of piles for offshore structures. Offshore Technology Paper 5, OT-R-8002. (Department of Energy).

TAN, T-K. (1961). Consolidation and secondary time effect of homogeneous anisotropic saturated clay strata. In: INTERNATIONAL CONFERENCE ON SOIL MECHANICS AND FOUNDATION ENGINEERING, 5th, Paris. Proceedings, Vol 1: 367 - 379.

TAVENAS, F. and LEROUEIL, S. (1979). Clay behaviour and the selection of design parameters. In: EUROPEAN CONFERENCE ON SOIL MECHANICS AND FOUNDATION ENGINEERING, 7th Brighton, Proceedings. Vol 1: 281 - 291.

TAYLOR, D.W. (1948). Fundamentals of Soil Mechanics. (John Wiley).

TERZAGHI, K. (1943). Theoretical Soil Mechanics. (Wiley).

WARD, W.H., SAMUELS, S.G. and BUTLER, M.E. (1959). Further studies of the properties of London Clay. Géotechnique 9 No.2: 33 - 58.

WROTH, C.P. (1971). Some aspects of the elastic behaviour of overconsolidated clay. In: SYMPOSIUM ON STRESS-STRAIN BEHAVIOUR OF SOILS, Cambridge. Proceedings. (Foulis): 347 - 361.

WROTH, C.P. and LOUDON, P.A. (1967). The correlation of strains within a family of triaxial tests on overconsolidated samples of kaolin. In: GEOTECHNICAL CONFERENCE, Oslo. Proceedings. Vol 1: 159 - 163.

WROTH, C.P., RANDOLPH, M.F., HOULSBY, G.T. and FAHEY, M. (1979). A review of the engineering properties of soils with particular reference to the shear modulus. Report CUED/D-SOILS TR75: Cambridge University.

ZYTYNSKI, M., RANDOLPH, M.F., NOVA, R. and WROTH, C.P. (1978). On modelling the unloading - reloading behaviour of soils. Int. J. Numerical and Analytical Methods in Geomechanics 2: 87 - 93.